Continuous Screening using Mesoscale Oscillatory Baffled Reactors

A thesis submitted to the Newcastle University
for the Degree of Doctor of Philosophy in Chemical Engineering

By

FATIMAH RUBAIZAH BINTI MOHD RASDI

School Of Chemical Engineering & Advanced Materials
Newcastle University
June 2014

CONFIDENTIAL

Abstract

A mesoscale Oscillatory Baffled Reactor ("mesoscale-OBR") is a laboratory-scale reactor (5mm inner diameter) with a total volume of approximately 5.5mL containing equally spaced baffles. Due to its small volume, it is suitable as a platform technology for process screening or investigating reaction kinetics. Traditionally, these are conducted in batch; however, continous screening can be performed in the mesoscale-OBR, with flexible adjustment of the input and reduced reagent usage. In this project, continuous dynamic and "steady state" screening was demonstrated in the mesoscale-OBR. These techniques can be used to rapidly and logically obtain process data and kinetics of any liquid-liquid reactions. Exothermic reactions of several aldehydes (benzaldehyde, *o*-tolualdehyde, *m*-tolualdehyde and *p*-tolualdehyde) with *n*-butylamine to form imines were chosen as the case studies to demonstrate the ability of the mesoscale-OBR. Online FTIR was used to monitor reactions. The mesoscale-OBR exhibited a high degree of consistency in experimental results: the uncertainty in the rate constant for benzaldehyde and *n*-butylamine imination was three times lower than in a conventional batch beaker method. MATLAB was used to model reaction kinetics and validated using experimental data. Both experiments and modelling demonstrated that the rate constant for 1-butanamine, N-(phenylmethylene)-synthesis was $2.1 \times 10^{-1} mol^{-0.9} L^{0.9} s^{-1}$ with total reaction order of 1.9 (1.7 for benzaldehyde and 0.22 for n-butylamine). The process development time when using "dynamic screening" (i.e continuous variation of one of the input parameters) was reduced by 50% compared to batch screening using beakers. A higher area to volume ratio of the mesoscale-OBR (than the beaker) allowed exothermic reactions to be screened safely and quickly e.g. temperature for solvent free imination was at ~40^{o}C in a jacketed mesoscale-OBR, whereas ~90^{o}C (above the boiling point of n-butylamine) for a jacketed beaker. To passively improve the temperature distribution along the length of the reactor, the centrally baffled mesoscale-OBR was constructed *inside* a thermosyphon: the temperature difference along the reactor length at residence times of 60s and 90s was reduced to 2^{o}C, rendering the reaction safer and more amenable to determination of exothermic reaction kinetic parameters.

Acknowledgement

I would like to express my special appreciation and thanks to the following for their tremendous help and support in completing this journey:-

- Professor Adam Harvey and Dr Anh Phan for their supervision and guidance. Your encouragement, feedback and comments are greatly appreciated.
- The workshop team (Steward Latimer, Simon Daley, Ian Ditchburn, Ian Strong and Brian Grover) for their advice and support on the technical matter related to the project.
- Rob Dixon and Paul Sterling for their help on laboratory related matters.
- Process Intensification Group for their critics and motivation.
- Malaysian Rubber Board (MRB) for their financial support.
- My beloved husband (Azizul Haqim) and daughter (Fatimah Arissa Qurratuain) for their understanding, love and patience throughout this years.
- My parents, in-laws and families for their sacrifices and prayers that reminds me to always push myself forward each and everyday
- All my friends (BBGS, MRSM, AIM, KFK, NU) for their encouragement and supports.

This journey will be impossible without all these supports. Again, from the bottom of my heart, thank you very much. God bless all of you.

Table of Contents

List of Figures

List of Figures

List of Figures

List of Tables

Nomenclature and Abbreviations

Symbols		Units
A	absorbance	-
A($\tilde{v}$)	wavenumber dependent absorbance	-
[A]	concentration of a reagant	mol dm^{-3}
b	path length of the sample	m
C	concentration of the compound in solution	mol dm^{-3}
c	speed of light	m s^{-1}
C_i	existing tracer concentration	mol dm^{-3}
Ci_e	experimental concentration	mol dm^{-3}
Ci_m	simulated concentration	mol dm^{-3}
D	tube internal diameter	m
d_o	baffled diameter	m
E	energy of a charged electrons	J
E(θ)	tracer distribution curve of a dimensionless time	-
E(t)	tracer distribution curve	
f	frequency	Hz

k	rate constant	$M^{-0.9}\ s^{-1}$
K	equilibrium constant	-
k_{obs} / k’	pseudo first order rate constant	-
k_m	mixing coefficient	s^{-1}
L	baffle spacing	m
L_e	evaporator length	m
l	absorption path	m
N	number of tank in series	-
Nu_t	Nusselt number	-
OD	Outside diameter of a tube	m
Re_n	net flow Reynolds number	-
Re_o	oscillatory Reynolds number	-
s	skewness	-
S	fractional open area of baffle	-
St	Strouhal number	-
t_i	time	s

u	superficial velocity	$m\ s^{-1}$
V	volume of the reactor	m^3
x_o	oscillation amplitude	m
ψ	velocity ratio	-
ρ	fluid density	$kg\ m^{-3}$
μ	viscosity	m^2s^{-1}
ε	molar absorptivity	$dm^3\ mol^{-1}cm^{-1}$
θ	dimensionless time	-
σ^2	variance	-
Δt_i	interval time	s
τ	residence times	s
λ	wavelength	m
ω	wavenumber	m^{-1}
$\alpha(\tilde{\nu})$	wavenumber dependent absorption coefficient	-

Abbreviations

AHP	annular heat pipe
CFD	computational fluid dynamics
IR	infrared Spectroscopy
NMR	nuclear magnetic resonance
ODE	ordinary differential equations
OBR	oscillatory baffle reactor
PIV	particle image velocimetry
PTC	phase transfer catalysis
RTD	residence time distribution
SNR	signal to noise ratio
SPC	smooth periodic baffles column
SSE	sum square of error
ST	stirred tank
TG	triglyceride concentration

Chapter 1 Introduction

1.1 Research background

In general, most processes in the chemical industry use batch reactors or continuous stirred tank reactors (CSTRs) as they are well-understood technologies. Mixing is conducted using a mechanical agitator in batch processes and CSTRs or by operating conventional tubular continuous reactor systems in turbulent conditions thereby achieving plug flow. However, before scaling up chemical processes, laboratory screening of the process and condition parameters needs to be conducted. Conventionally, such investigations are conducted at laboratory-scale in batch mode using standardized glassware (Jas and Kirschning, 2003; Wiles and Watts, 2007). Other than this platform, higher multiple batch screening is also available such as the 96-well plates to obtain high through-put screening. The mixing in this batch screening platforms use apparatus such as magnetic stirrers or upright impeller mixers, leading to variations in mass transfer, energy transfer and mixing speed (Ehly *et al.,* 2007). Furthermore, common un-baffled laboratory vessels produce different mixing profiles than pilot plant or industrial baffled reactor system. It also leads to substantial reagent usage and waste generation with screening in typical laboratory vessels (50-500mm diameter) (Hall *et al.*, 2005). Even though high through-put screening are achieved with the multiple batch platforms, the changes in the difference apparatus use for the batch operation from the screening (96-ell plate), synthesis (beaker or conical flaks) to pilot plant (CSTR) might leads to inconsistencies outcome and necessitating time-consuming for re-optimisation. The results from laboratory and pilot plant scale can also be very different, due to the changes in surface to volume ratio for instance (heat transfer).

Continuous screening, also known as the flow chemistry approach, has motivated the re-evaluation of the laboratory chemical reaction screening and synthesis (Figure 1-1). The continuous method means performing the chemical reaction, screening and synthesis in a tube or pipe, through which the reagents are pumped together and mixed in the same apparatus platform.

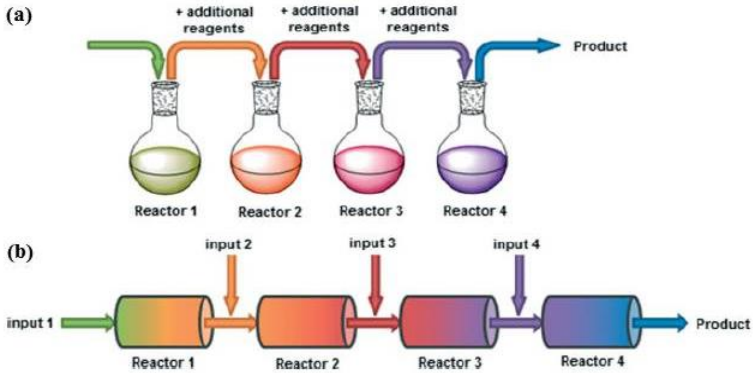

Figure 1-1: Chemical reaction conducted via (a) batch and (b) continuous flow screening (Baxendale, 2013a)

The continuous flow chemistry can also be viewed as an approach in which chemical optimization and process intensification (Figure 1-2) (Baxendale, 2013a) are combined. This can be an important route towards sustainable manufacturing. This agrees with the roundtable discussion in 2007 by the Green Chemistry Institute (GCI) (a part of American Chemical Society (ACS)) as described by Wiles and Watts (2012).

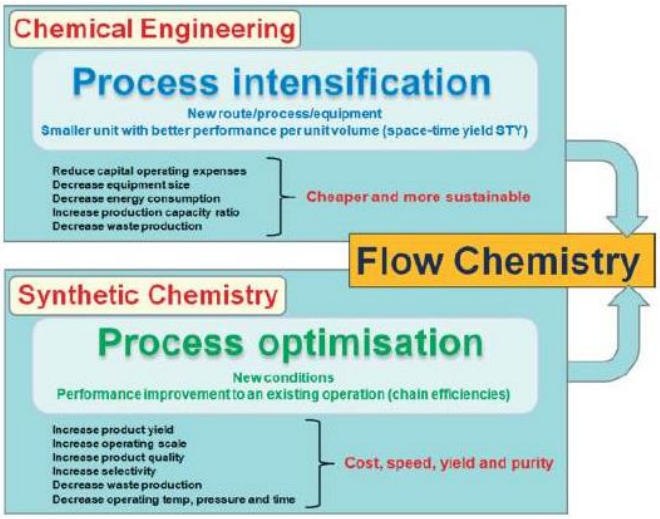

Figure 1-2: Cross disciplinary interaction in continuous flow chemistry (Baxendale, 2013a).

The advantages of flow chemistry are, in principle, faster and safer reaction platforms, rapid reaction optimisation screening and predictable scale-up. It also allows flexible adjustment of the input and output processes, renders monitoring and minimizes reactor downtime due to cleaning (Calabrese and Pissavini, 2011; Baxendale, 2013a). Furthermore, small-scale laboratory flow reactors offer considerable advantages with small quantities of reagent and minimizing waste during preliminary or screening laboratory work than the conventional glassware such as beaker and conical flasks.

With the continuous approach, it also uses similar apparatus and mixing characteristic from starting the screening to synthesis work, follow by optimisation and lastly producing the industrial volume of the product desire. Example of this approach was proven with the continuous reactor platform of microreactor (Watts, 2010).

The use of continuous flow reactors for laboratory-scale process screening has rapidly grown in the last 10-20 years. This continuous flow approach has changed synthesis and screening chemical reactions both in the laboratory and at industrial scale. Chemical synthesis such as fine chemical or pharmaceutical products often involves multiple reaction steps. Continuous screening, can offer advantages in terms of reducing process development time, safety and space. For example, continuous screening in multiphase biodiesel production at four molar ratios of methanol to rapeseed oil (4:1, 5:1, 8:1 and 12:1) was conducted in a sharp-edge helical mesoscale-OBR at 10% of the total time (40min) used in the conventional bench-scale stirred tank reactor (Phan *et al.*, 2011). Several different designs ranging from micro to macro size are being developed and tested for different reaction mechanisms. The laboratory-scale "Mesoscale Oscillatory Baffled Reactor" (mesoscale-OBR) is one of the reactor platforms developed and is suitable for this continuous screening approach. The reactor platform have been used extensively in many types of application such as in biodiesel(Zheng *et al.*, 2007; Phan *et al.*, 2011; Phan *et al.*, 2012) and bioprocessing(Reis *et al.*, 2006a; Reis *et al.*, 2006b) applications. However the capabilities as a laboratory screening platform not yet extensively explored. Therefore, the purpose of this work is to manipulate the advantages of the oscillation mixing with the continuous screening approach in obtaining screening data by exploiting the reaction experimental space.

1.2 Layout of the thesis

The thesis will be divided into 5 chapters. Following this chapter, background and previous literature related to the study is reviewed in Chapter 2. This covers the development of OBR technology, investigation of mesoscale-OBR for screening and understanding the synthesis and kinetics of imine synthesis.

The materials and method involved in the mesoscale-OBR characterization, aldehydes and *n*-butylamine reaction and screening via batch and continous, development of the new thermosyhphon mesoscale-OBR and numerical modelling is listed in Chapter 3.

Chapter 4 describes the results obtained from experiments using the centrally baffled mesoscale-OBR, including characterization of the reactor, and imine synthesis with and without solvent in a continuous mode. Modelling validation on the reaction mechanisms and kinetic parameters obtain experimentally were also reported and discussed. Development and evaluation of the "heat pipe OBR" is also reported.

Lastly, the conclusions and future work are summarized in Chapter 5.

Chapter 2 Literature Review

This literature survey begins with an introduction to the Oscillatory Baffled Reactor (OBR) concept and its mixing mechanism. This is followed by a review of the scaled down OBR (the "mesoscale-OBR") development and applications. Different types of laboratory screening platforms are also reviewed and discussed for comparison with the mesoscale-OBR reactor. Operation and advantages of the heat pipe and thermosyphon system as a chemical reactor are reviewed for further understanding on its isothermal capabilities. Lastly, the imine synthesis reaction reviewed on the details of the reaction and common analytical instrument used in monitoring the process.

2.1 Oscillatory Baffled Reactor

An Oscillatory Baffled Reactor (OBR) is a reactor containing periodically-spaced orifice baffles along supporting rods in a cylindrical tube (Figure 2-1).

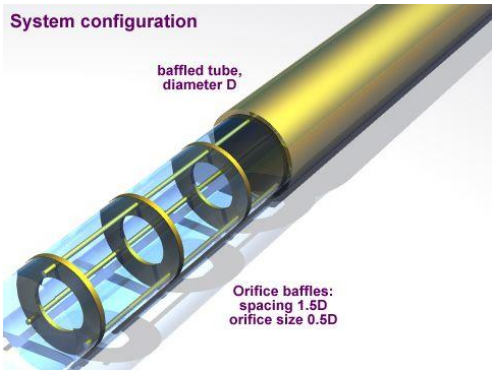

Figure 2-1: Conventional OBR with spaced orifice baffles (Zheng *et al.*, 2007).

The fluid inside the system is oscillated by an oscillator placed at the base of the column. There are two different types of mechanisms: pulsing fluid and oscillating baffle (Figure 2-2). The oscillation by the former mechanism is generated using either a diaphragm, piston or bellows, whereas the latter involves oscillating the baffles using mechanical, hydraulic, pneumatic or electro-mechanical devices (Mackley, 1991; Ni *et al.*, 1998). The reactor can be operated vertically, horizontally or at any angle (Ni *et al.*, 2001b).

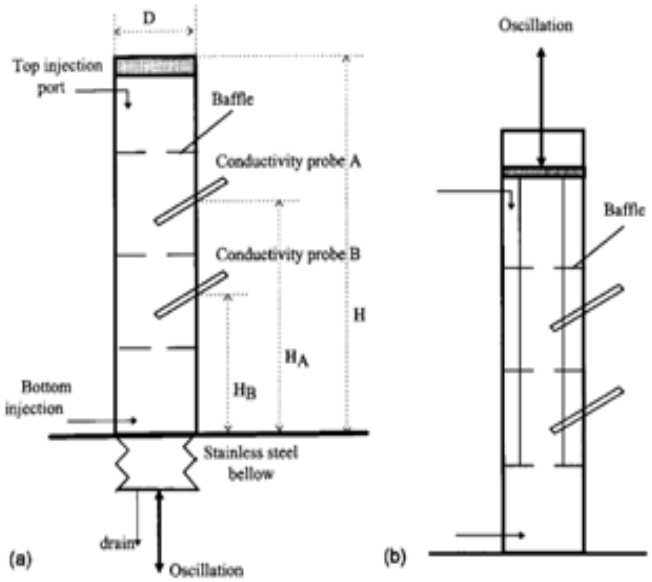

Figure 2-2: Different Oscillation mechanisms for the OBR (a) Pulsing fluid mechanism and (b) Oscillating baffles mechanism (Ni *et al.*, 1998).

The reactor can also be operated in different configurations depending on its applications: in batch, continuous single tube, multi-pass or multi-tube as shown in Figure 2-3 (Mackley (1991).

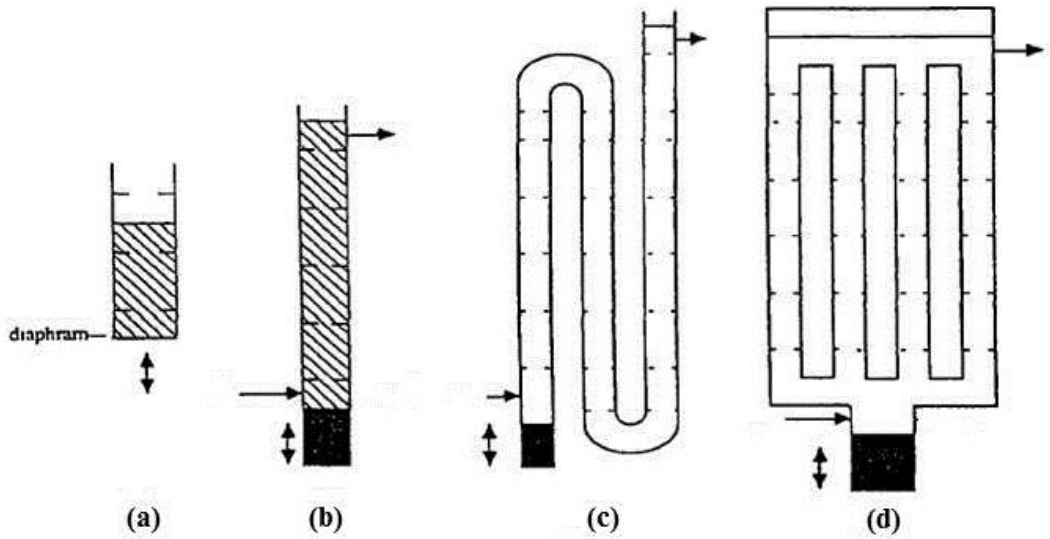

Figure 2-3: Different orientations of OBR (a) batch, (b) continuous, (c) continuous multi-pass and (d) continuous multi-tube (Mackley, 1991)

During oscillatory motion, the fluid accelerates and decelerates according to a sinusoidal velocity time function (Stonestreet and Van Der Veeken, 1999). As shown in Figure 2-4, when the flow accelerates, the vortices are formed downstream of the baffles. When the flow decelerates, these vortices are swept into the bulk fluid and subsequently unravelled as flow accelerates in the opposite direction. As this motion repeats, effective and uniform mixing can be obtained in the reactor (Mackley and Ni, 1991; Ni and Mackley, 1993).

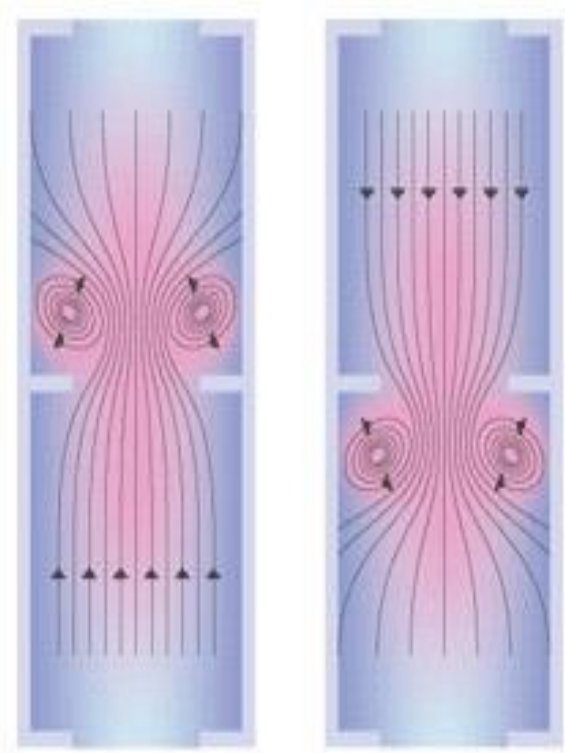

Figure 2-4: Schematic eddy motion in baffles tube

Studies comparing the mixing profiles between unbaffled and baffled smooth tube with or without oscillation flow imposed provided a clear perspective on the advantages of the oscillation mixing (Mackley and Ni, 1993). With no baffles at a net flow of Re_n=212, a similar degree in axial mixing was observed without (Figure 2-5 (a)) and with (Figure 2-5(b)) oscillatory mixing. This profile was also seen in the baffled tube without oscillation mixing (Figure 2-5(c)). However, when combining oscillation with periodic baffles as shown in Figure 2-5(d), uniform mixing was obtained in each baffle cavity due to the formation of vortices. When there is uniform mixing in each of the baffle cavities, the tube is essentially a series of well mixed stirred tanks (Stonestreet and Harvey, 2002; Vilar *et al.*, 2008).

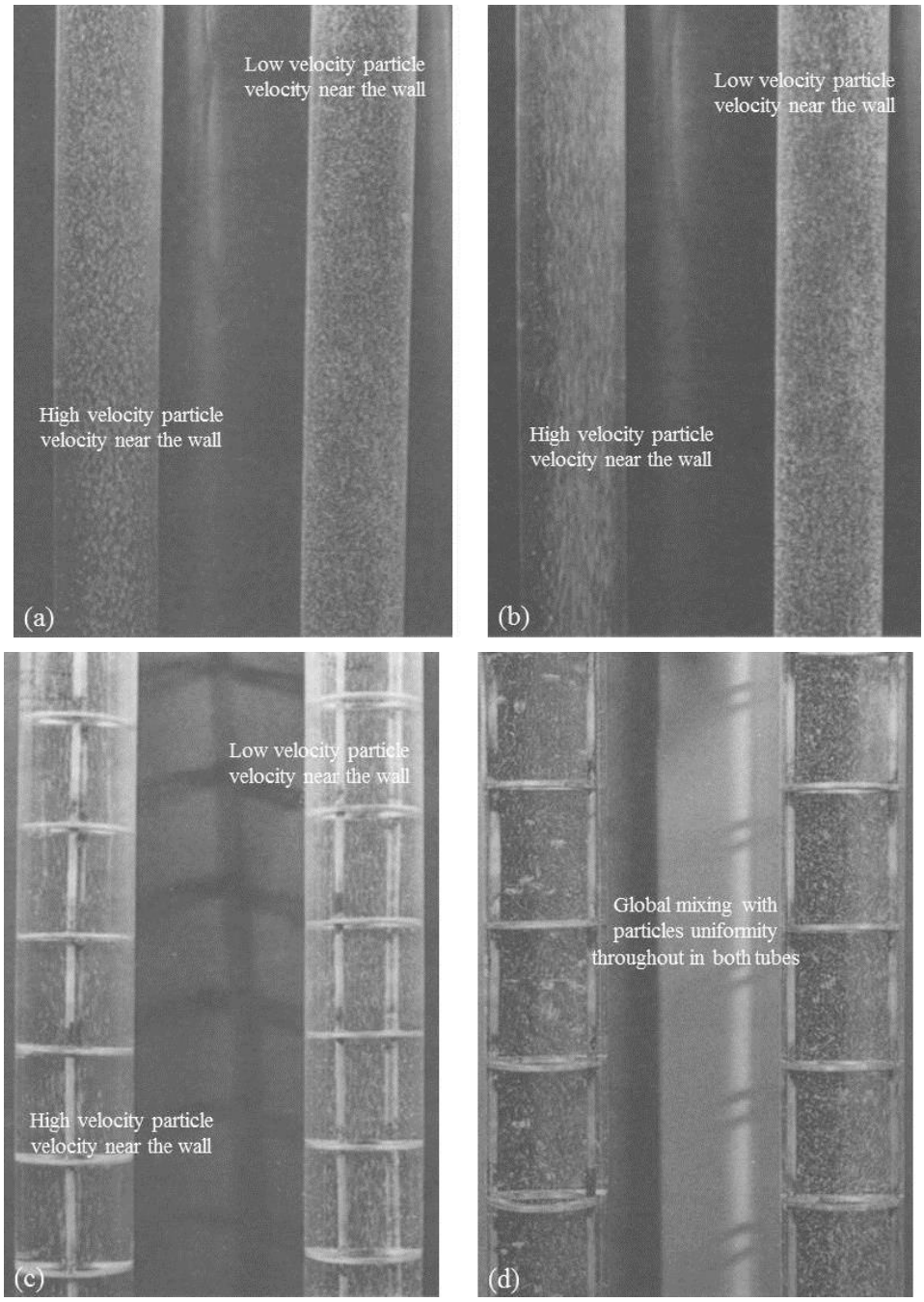

Figure 2-5: Flow profiles at net flow Reynolds Re_n=212 for (a) no baffles and oscillation (b) no baffles with oscillation at Re_o=2324, (c) with baffles and no oscillation and (d) with baffles and oscillation at Re_o=378 (Mackley and Ni, 1993)

The oscillatory mixing was found through the work by Binnie (1945), involving the liquid turbelence flowed through a long horizontal glass pipe. However, the concept evolved to the development of the OBR only in the late 1980's. Unlike conventional tubular reactors, in which mixing is due to turbulence (net flow Reynolds>2000), the mixing inside OBRs is independent of net flow and controlled by oscillation conditions, leading to a greatly reduced ratio of length to diameter. The OBRs can provide plug flow at low net flow rates (in the laminar regime), leading to a niche application which

allows to convert long reactions from batch to continuous mode. This was shown through a saponification study by which the reactor volume was reduced 100-fold from the stirred tank batch method through converting the process to the continuous OBR system (Harvey *et al.*, 2001). Safety aspects of the saponification process were improved due to the smaller reactor volume. Furthermore, the operating temperature was able to be lowered from 115ºC to 85ºC in the OBR for the ester saponification reaction (Harvey *et al.*, 2001). This further improves the safety aspect of the process.

This uniform mixing in each of the baffled cavity leads to a plug flow behaviour in the OBR. Plug flow refers to a fluid movement with a flat velocity profile as shown in Figure 2-6(a). It is different to laminar flow where the velocity is nearly zero at the wall and maximum at the centre region of the tube (Figure 1-6(b)).

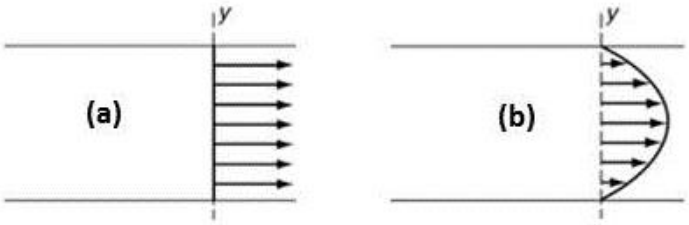

Figure 2-6: Velocity profiles of (a) plug flow and (b) laminar flow

Plug flow behaviour is desirable as it provides consistent product quality. Plug flow can be achieved using a conventional tubular reactor in which the superficial velocity is sufficiently high to obtain good mixing (turbulent mixing, $Re_n \approx 2100$) or through a series of continuous stirred tanks (normally number of tanks are above 10). However, in the OBRs, plug flow behaviour can be achieved at very low net flow rates (which represent a laminar regime in steady state) as the mixing in the OBR are govered by the baffle and oscillation motion (Stonestreet and Harvey, 2002). With that, discussion on the fluid mechanics of the OBR are discussed below.

2.1.1 Fluid Mechanics

The fluid mechanics in OBRs are governed by geometrical and dynamic parameters (Ni and Gough, 1997). The geometrical parameters are the distance between baffles (baffle spacing, L) and the ratio of baffle open area (S) as described in eqs.2-1 and 2-2.

$$L = 1.5D \quad \text{eq. 2-1}$$

$$S = \frac{d_o^2}{D^2} \text{ (Typically in the range of 0.2-0.4)} \quad \text{eq. 2-2}$$

…where d_o is the orifice diameter (m) and D is the tube internal diameter (m).

The baffle spacing (L) parameter and the ratio of baffle open area (S) influence the shape of the eddies and the width of the vortices generated in a baffle cavity (Ni and Gough, 1997). The effect of baffle spacing ranging from 1.0-2.0 times the tube diameter on the mixing inside the tube were investigated. It was found that the optimum baffle spacing was 1.5 for the pulsing oscillation mechanism (Brunold *et al.*, 1989) and 2.0 times the tube diameter for the oscillating baffle mechanism (Ni *et al.*, 1998). Ni *et al.* (1998) found that decreasing the ratio of baffle open area (S) from 0.5 to 0.1 decreased the mixing time at different oscillation frequency (1-5Hz) and amplitude (2.5-10mm). However, the optimal ratio of baffle open area of around 0.2 gave the shortest mixing time. The effect of the gap size between the baffles and tube on the fluid mixing was also investigated (Ni and Stevenson, 1999). Increasing the gap size increased the mixing time regardless of the frequency or amplitude. This was due to the vortex split phenomenon between the baffle and the gap that reduces the intensity of eddy formation. A typical range of S was between 0.2 and 0.4, e.g. S=0.34 was used for a study related to energy dissipation and heat transfer (Baird and Stonestreet, 1995; Mackley and Stonestreet, 1995) whilst S=0.21 was used for a bioreactor application (Gaidhani *et al.*, 2003)

The dynamic dimensionless groups governing the fluid mechanics are the oscillatory Reynolds number (Re_o), net flow Reynolds number (Re_n) and Strouhal number (St) as described in eq.2-3 to 2-5 below respectively. The oscillatory Reynolds number describes the intensity of the mixing. It is similar to Re_n but the superficial velocity (u) is replaced by the maximum oscillatory velocity ($2\pi fx_o$). Strouhal number (St), which is inversely proportional to the oscillation amplitude, measures the effectiveness of the eddy propagation in relation to tube geometry. In describing the interdependence of the Re_o and Re_n, the "velocity ratio" (ψ) (eq.2-6) is used. The oscillatory Reynolds number (Re_o) was higher than the net flow Reynold number (Re_n) to maintain the effect of the periodically reversing motion within each baffle cavity (Stonestreet and Harvey, 2002; Ni *et al.*, 2003) or the velocity ratio ψ needs to be above 1. Stonestreet and Harvey

(2002) suggested that the maximum oscillatory velocity needs to be at least twice the value of the net flow, but Mackley (1991) found that the Re_n need to be 5 times lower than the Re_o. Stonestreet and Van Der Veeken (1999) found that that the velocity ratio should be maintained in the range of $2 \leq \psi \leq 6$ for net flows Re_n of 95-252 to obtain a high degree of plug flow (high number of tanks-in-series, N) as shown in Figure 2-7.

$$Re_o = \frac{2\pi f x_o \rho D}{\mu} \qquad \text{eq. 2-3}$$

$$Re_n = \frac{\rho D u}{\mu} \qquad \text{eq. 2-4}$$

$$St = \frac{D}{4\pi x_o} \qquad \text{eq. 2-5}$$

$$\psi = Re_o / Re_n \qquad \text{eq. 2-6}$$

…where u (m/s) is the superficial velocity; D (m) is the tube diameter; μ (m^2s^{-1}) is the viscosity; x_o (m) is the centre to peak amplitude of oscillation; f (Hz) is the oscillation frequency and ρ (kg m^{-3}) is fluid density.

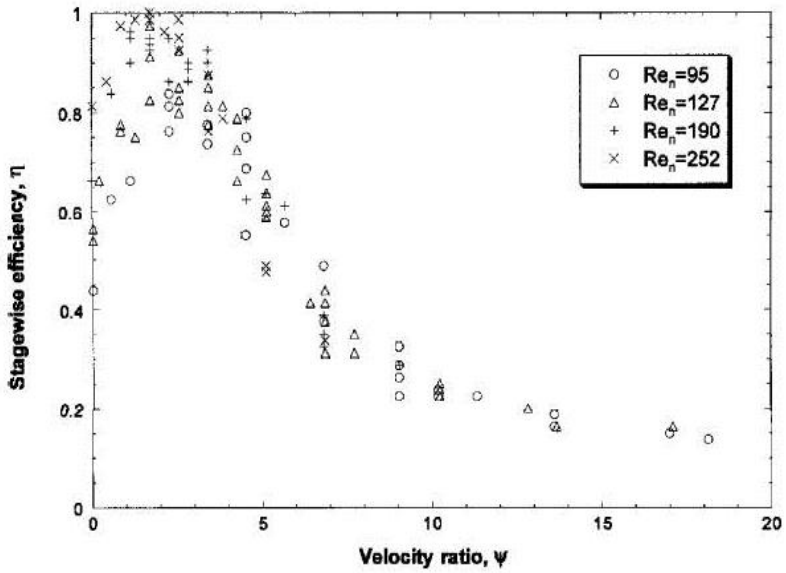

Figure 2-7: The dependency of stage-wise efficiency on the velocity ratio at different net flow rate value. (stagewise efficiency relates the actual number (N) of stirred tank-in-series with the theoretical number of ideal stirred tank.) (Stonestreet and Van Der Veeken, 1999)

The effect of dynamic parameters (Re_o, Re_n and St) on the mixing has been studied intensively (Stonestreet and Van Der Veeken, 1999). Different mixing regimes depending on Re_o were identified as shown in Table 2-1. Howes et al. (1991) also found that at Re_o=100 the vortices remained steady and symmetrical. At Re_o above 300, the fluid mixing becomes more complex with the broken symmetry similar to turbulence.

Table 2-1: Flow behavior for different Re_o (Stonestreet and Van Der Veeken, 1999)

Oscillatory Reynolds Number (Re_o)	**Flow behavior**
<250	Laminar flow (low intensity)
250-2000	Turbulent
>2000	Fully turbulent

Manipulation of this dynamics parameter have shown effects on the process properties. In using the OBR as a flocculator (Ni *et al.*, 2001a) have shown significantly increased of the percentage of bentonite flocculated with increasing oscillation amplitude, while it remained constant with various oscillation frequencies, as shown in Figure 2-8, e.g. the flocculation percentage increased from 2% to 9% when increasing x_o from 2mm to 8mm.

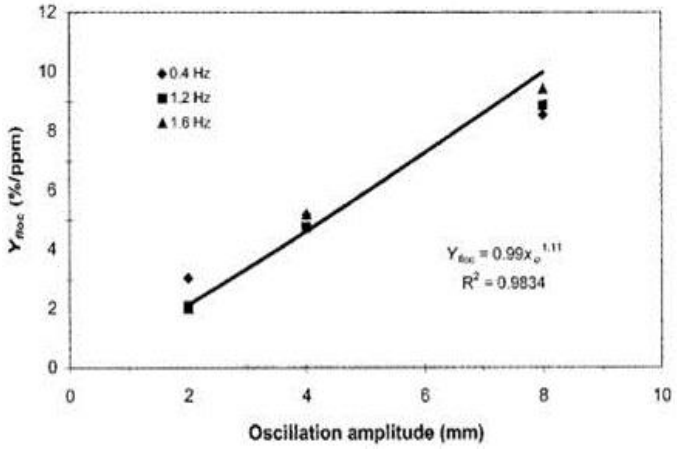

Figure 2-8: Effect of oscillation amplitude and frequency on the flocculation percentage of bentonite (Ni *et al.*, 2001a).

When the OBR was used as a fermenter (Gaidhani *et al.*, 2003), the yield of a polysaccharide was increased (~50%) by increasing both the oscillation amplitude and frequency. It was found there was an optimum condition for both parameters (x_o=20mm and f=2 Hz) to achieve the highest yield. This demonstrates the flexibility of the OBR

in changing the mixing intensity via the amplitude and frequency parameter to obtain a desired output. On plug flow characterisation behaviour of the OBR, there are extensive studies conducted related to this matter. Review on the studies are discussed below.

2.1.2 OBR characterisation

The conditions required to obtain a degree of plug-flow in the OBR was quantified by evaluating axial dispersion (D) or the number of tank-in-series parameter (N). The axial dispersion method has been performed by Dickens *et al.* (1989) to investigate the effect of oscillation amplitude on the fluid mixing in a 24mm diameter OBR at a fixed net flow Re_n=110 and oscillation frequency of 3.5Hz. The results showed that the dispersion coefficient increased with oscillation amplitude. For example, the dispersion coefficient was $0.025m^2s^{-1}$ at 1mm oscillation amplitude, but $0.135m^2s^{-1}$ at 4mm oscillation amplitude. Howes and Mackley (1990) also used an axial dispersion (D) method for a 51mm diameter OBR. At a fixed amplitude of x_o=4mm and Re_n=106, the oscillation frequency had little effect on the dispersion coefficient at $200 \leq Re_o \leq 800$. This study also showed the effect of varying Re_n (Re_n=40 and 106) on the axial dispersion value. At Re_n=40, the minimum dispersion was in a range of Re_o=200-300 for both tested St=0.8 and 2.0. However, at Re_n=106, the minimum dispersion was in a range of Re_o=500-700 for St=0.8 and at Re_o=320 for St=2.0.

Stonestreet and Van Der Veeken (1999) characterised the plug flow behaviour of a 24mm ID OBR using the number of tank-in-series (N) approach. In this study, the baffle spacing and open area were 1.5 times the tube diameter and 0.25 respectively. Over the range Re_n=95-250, increasing the net flow increased the Re_o at which the number of tanks-in-series (N) was at its maximum. For instance, the maximum N at Re_n=95 was at Re_o=200-300, whereas it was at Re_o=300-600 for Re_n=252. Plug flow behavior can be achieved with any net flow (Re_n) by altering the oscillation condition (Re_o).

Generally, the mixing in the OBR is independent of the net flow. Plug flow behaviour can easily be achieved in a "operating window", e.g. ψ=2-6.

2.1.3 OBR application

The enhanced processing aspects which related to the mass and energy transfer, efficient mixing, narrow RTD profile and wide range of operating (amplitude and frequency) window have leads to various applications using the OBR. This are briefly summarizes in Table 2-2 below.

Table 2-2: Main applications of the Oscillatory Baffled Reactor (OBR)

Application	Mode	References
Biodiesel production	Continuous	(Ghazi *et al.*, 2008)
Bioprocessing	Batch Batch	(Abbott *et al.*, 2014) (Ni *et al.*, 1995)
Chemical reaction	Batch	(Ni and Mackley, 1993)
Crystallisation	Batch Continuous	(Ni *et al.*, 2004) (Lawton *et al.*, 2009)
Fermentation	Batch	(Gaidhani *et al.*, 2003)
Flocculator	Batch	(Ni *et al.*, 2001a)
Heat exchanger	Continuous Batch	(Mackley and Stonestreet, 1995) (Stephens and Mackley, 2002)
Phase transfer reaction	Batch	(Wilson *et al.*, 2005)
Photocatalytic	Batch	(Fabiyi and Skelton, 1999)
Polymerisation	Batch	(Ni *et al.*, 1999)
Saponifications	Continuous	(Harvey *et al.*, 2001)

Superimposing oscillatory flow upon a net flow in the OBRs significantly enhances the mass transfer in an air-yeast culture application (Ni *et al.* (1995). The OBRs exhibited 75% higher volumetric oxygen mass transfer coefficient than stirred tank bioreactors. In a fermentation process, the OBR demonstrated 2-fold higher levels of polysaccharide and biomass concentration compared to a stirred tank reactor (STR) with 50% reduction in reaction time (Gaidhani *et al.*, 2003). Nusselt number (Nu_t) in a continuous OBR increased 30-fold compared to a smooth walled tube in a heat exchanger application (Mackley and Stonestreet, 1995). For a batch OBR (Stephens and Mackley, 2002) the Nu_t value was similar to that obtained from the continuous OBR system at zero net flow rates.

Using OBRs can also reduce power consumption. 90.0% flocculation was achieved in the OBRs at $13.1s^{-1}$ shear compared to $300s^{-1}$ shear in a stirred tank (Ni *et al.*, 2001a). Beside this, the mixing conditions in the OBRs can easily be manipulated from "soft" to intense mixed regime by varying either the frequency or/and amplitude of the oscillation mixing (Ni *et al.*, 2003). For example, in a liquid-liquid phase-transfer (PTC) reaction, the final fractional conversion of phenyl-acetonitrile ($PhCH_2CN$) increased from 0.1 to 0.9 when changing the oscillatory velocity ($x_o f$) from 10 mm/s to 70 mm/s (Wilson *et al.*, 2005).

2.1.4 OBR Scale-up

Scale-up of OBRs is predictable through maintaining geometric parameters (baffle spacing and baffle open area) and dynamic parameters (Re_o St, and Re_n). Smith and Mackley (2006) studied the scale-up from 24mm, 54mm and 150mm inner diameter tube in continuous mode. A near pulse injection tracer was used and its concentration at two points downstream was measured, but the position (distance) of the sensors was not mentioned. The results showed that a similar axial dispersion value (D) was obtained in these tube diameters over a wide range of oscillation conditions ($80 \leq Re_o \leq 800$) at a fixed Re_n=107. Ni *et al.* (2001b) investigated the scale-up OBR with diameters ranging from 40mm to 150mm in both batch and continuous modes. Regardless of the differences in operation modes and baffle designs (close and loose fits), the axial dispersion coefficient (D) was linear with the mixing characteristic (x_o and f) and the tube size. Numerical studies (Jian and Ni, 2005) showed that the flow patterns were similar for all tested diameters of the OBR (50mm, 100mm and 200mm). The fluids mechanics in terms of the velocity ratios value were found to be independent of the scale-up by maintaining the average surfaces mean velocity. Here the average surfaces mean velocity is referred to the sum of three instantaneous velocities on a plane (V_r, V_θ and V_z) and divided by the number of points. The OBRs can also be scaled up using multi-tube rig configurations (Mackley and Ni, 1993).

Generally, the OBRs provide significant processing advantages with flexible operating windows and net flow conditions. This was illustrated with the various applications such as in heat transfer (Mackley and Stonestreet, 1995; Stephens and Mackley, 2002), mass transfer (Ni *et al.*, 2001a; Gaidhani *et al.*, 2003), and organic synthesis (Harvey *et al.*, 2001; Wilson *et al.*, 2005). Furthermore, the scaling up of OBRs is also predictable.

However, for the purposes of screening operating conditions, these scales require a significant amount of reagents and consequently generate large amount of waste. Due to this, mesoscale-OBRs (~350mm length and ~5mm internal diameter) were developed to cover more potential applications, such as process condition screening and laboratory synthesis in applications such as biodiesel (Zheng *et al.*, 2007), bioprocessing (Reis *et al.*, 2006b), and organic reactions (Reis *et al.*, 2008; Mohd Rasdi *et al.*, 2013) by manipulating the advantages of the oscillatory mixing.

2.2 Mesoscale-OBR

A mesoscale-OBR is a millimetre scale reactor of typical ~350mm length and ~5mm internal diameter. Glass tubes were used at this scale to allow observation along the reactor length during the screening or synthesis applications

2.2.1 Smooth Periodic Baffled Column (SPC)

The smooth periodical baffled column (SPC) is a mesoscale-OBR reactor consisting of smooth baffles. The smooth design was used to reduce shear rate compared to the sharp-edged orifice baffles in OBRs. As shown in Figure 2-9, the SPC reactor was a glass tube of 350mm length and 4.4mm internal diameter. The baffle spacing was at 3.0 times the tube diameter and baffle open-cross section (S) of 0.13. These differ to the conventional OBRs described in section 2.1.1 (the baffle spacing of 1.5 times the tube diameter and baffle open-cross sectional area between 0.2-0.4).

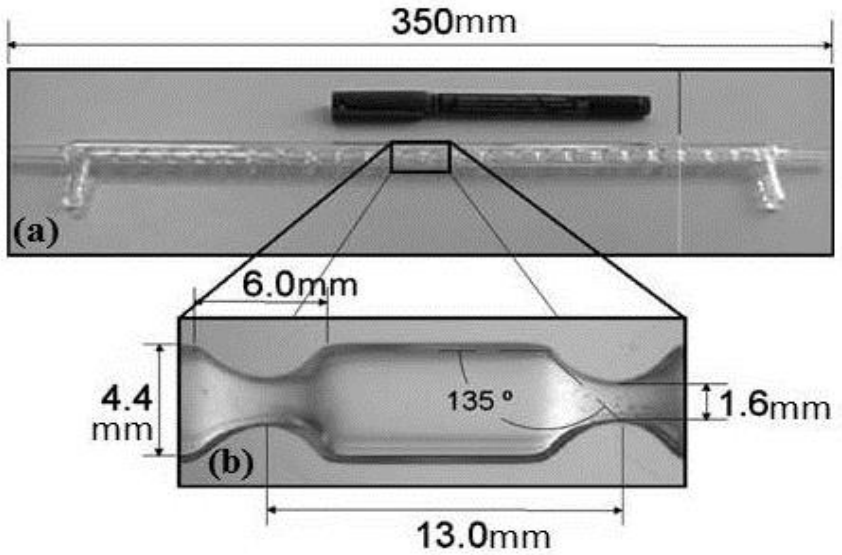

Figure 2-9: SPC tube configuration (a) the length of single tube (b) the dimension of single baffles cavity (Reis *et al.*, 2006a)

Due to the new geometric design, the flow patterns in the SPC flow were studied in detail using particle image velocimetry (PIV) and computational fluid dynamics (CFD) on single-pass tubes operating in batch mode (Reis *et al.*, 2005). Although the mixing profile obtained from PIV was similar to that in the conventional OBRs, the critical Re_os (at which vortex rings were formed symmetrically and non-symmetrically) were lower in SPCs than in OBRs. In SPCs, the symmetric and non-symmetric flows occurred at Re_o>10 and at Re_o>100, respectively whereas they were at Re_o >50 and >300 for the OBRs (Howes *et al.*, 1991; Mackley and Ni, 1991). Furthermore, the fluid mixing behaved differently depending on the oscillation frequency and amplitude even at a similar Re_o condition (Reis *et al.*, 2005). For example, at Re_o=117 the flow symmetry was observed at oscillation conditions of 4Hz and 1.0mm, but broke at oscillation condition of 1.1 Hz and 3.8mm in the SPC.

The SPC was also characterised by evaluating its residence time distribution (RTD) by tracer injection and response technique (Reis *et al.*, 2004; Reis *et al.*, 2010). The mixing coefficient (k_m) calculated for batch reactors showed that oscillation amplitude had a more pronounced effect on the mixing time than the oscillation frequency (f) (Reis *et al.*, 2004). This was also observed in the continuous flow, where the oscillation frequency ($0Hz \leq f \leq 15Hz$) had a relatively small influence on the back mixing (g) compared to the oscillation amplitude ($0mm \leq x_o \leq 3.0mm$). The axial dispersion (D) in a batch SPC increased with an increase of Re_o (Zheng and Mackley (2008)). However, a lower D was observed when using a higher St (lower amplitude) for the same Re_o conditions at 300. In the continuous system, it shows a minimal dispersion coefficient value ($\leq$0.01) for all the tested Re_n of 10, 19 and 58 at various Re_o conditions (50-900). However it also shows that the oscillation amplitude affects the D value significantly compared to the oscillation frequency. For example, at fixed Re_n=58 and f=2Hz, the D value changes from $6x10^{-3}$ to $3x10^{-3}$ for x_o of 0.5mm and 1.0mm respectively.

2.2.1.1 SPC applications

The SPC was applied for biodiesel screening in batch and continuous modes (Zheng *et al.* (2007)) at various oscillation conditions to determine the optimal operating conditions in terms of enhancing mass transfer through droplet breakage and emulsion formation. Both in batch and continuous modes (τ=49min), high oscillation frequencies

($f \geq 8$Hz) and amplitudes ($x_o \geq 2.0$mm) were required to achieve the level of triglyceride (TG) at ≤ 0.2% after 40 min of reactions.

Reis *et al.* (2006a) used the SPC for bioprocessing in the production of γ-decalactone in batch and showed an increase in the production rate of γ-decalactone from $1x10^{-8}$ $mg.cells^{-1}.h^{-1}$ to $16x10^{-8}$ $mg.cells^{-1}.h^{-1}$when increasing Re_o from 500 to1500. The time to obtain the maximum concentration of γ-decalactone was reduced by approximately 50% compared to a traditional ST bioreactor or shake flasks. The SPC only required a minimal aeration rate of 0.064vvm compared to 1vvm aeration rate used in a ST bioreactor to obtain similar γ-decalactone concentration. .

Evidence on the benefits of oscillatory mixing was also observed in gas-liquid systems, such as in fermentation, photosynthesis and gas-liquid catalytic reactions. The oscillatory mixing facilitates bubbles breaking to form smaller and more uniform bubbles than in conventional bubble columns, thereby increasing the bubble residence time inside the SPC or increasing the mass transfer (Reis *et al.*, 2007; Reis *et al.*, 2008). Biomass production increased from 83% and 214% when using the SPC as an aerobic fermenter compared to a stirred tank (ST) bioreactor and a shake flask (Reis *et al.* (2006b)).

Generally, the SPC provides better and uniform mixing at a smaller volume than conventional shake flasks and ST bioreactors. It allows screening to be conducted through the effective oscillation mixing and follows the process intensification concept, increasing space-time yields. Due to its small volume reactor, the SPC increases the safety of processes as it reduces the hazardous inventory in conducting any chemical reactions.

2.2.2 New Baffle Designs (central, integral and helical baffles)

Three different types of baffle designs, namely central baffle (Figure 2-10(a)), integral baffle (Figure 2-10(b)) and helical baffle (Figure 2-10(c)) were constructed by Phan and Harvey (2010). They are millimeter-scale glass jacketed tubes of 350mm long and 5mm internal diameter.

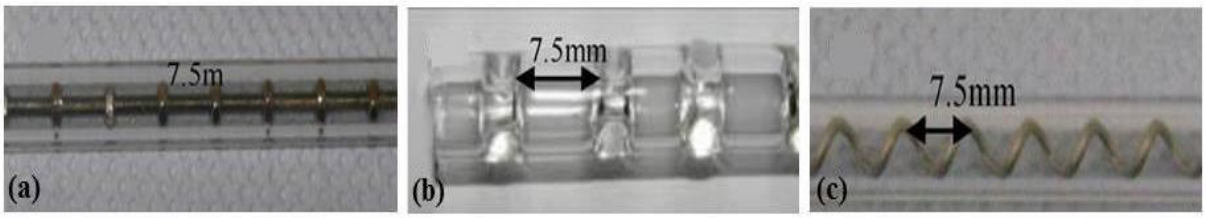

Figure 2-10: New designs of mesoscale-OBR baffles (a) Central, (b) Integral and (c) Helical (Phan and Harvey 2010)

The baffle patterns vary from smooth to sharp-edge designs to provide different mixing intensities. The baffle geometries were similar to those in conventional OBRs in terms of baffle spacing (1.5 times the reactor tube diameter) and ratio of open cross-sectional area (0.2-0.4). The central baffled design consisted of hexagonal stainless steel solid discs (approximately 4mm diameter) placed periodically at a distance of 1.5 tube diameters along a 2 mm narrow rod, providing 0.36 open cross seactional-area. With the integral baffled design, the baffle spacing was 7.5mm, with an orifice diameter of 2.5mm diameter, providing an open cross sectional area of 0.25. As for the helical baffled design, it consisted of 1.1mm stainless steel wire coiled at a pitch of 7.5mm with the open area at each turn around 0.26. Summaries of the designs are listed in Table 2-3.

Table 2-3: Different designs of baffles for mesoscale-OBRs (Phan and Harvey 2010).

Design		**Central Baffles**	**Integral Baffles**	**Helical Baffles**
Parameters	**Baffle spacing (L), mm**	7.5	7.5	7.5
	Ratio of open cross-sectional area (S)	0.36	0.25	0.26
	Diameter (D), mm	5	5	5

Generally, the three types of baffles designs cover a wide range of applications. With the integral baffled design, it is suitable for shear-sensitive applications, such as bioprocessing applications (Reis *et al.*, 2005; Reis *et al.*, 2006a) whereas the sharp-edged centrally baffled design provides high shear, which aids mixing in 2-phase liquid-liquid systems such as biodiesel production. The helical baffled design has advantages for solid-liquid reactions, as the main flow is less constricted, thereby reducing particle clogging.

Residence Time Distribution (RTD) investigation for the integral, central and helical baffled designs was conducted at Re_n ranging from 4.3 to 34.0 over various oscillation conditions (x_o=0.5-4mm and *f*=1-6Hz) (Phan and Harvey, 2010). Plug flow behaviour for the central and integral baffled designs was significantly affected by oscillation amplitude compared to oscillation frequency. For example, for the integral baffled design, at a fixed frequency (*f*=3Hz), variances increased significantly from 0.068, 0.132 and 0.223 when oscillation amplitude increased from 0.5mm, 2mm to 4mm. The change in variances from one condition to another was significant compared to the data obtained at a fixed oscillation amplitude, e.g. 0.087, 0.082 and 0.101 for oscillation frequency of 2Hz, 4Hz and 6Hz respectively at x_o=2.0mm. The study also established that the suitable oscillation amplitude conditions were 0.5-1.0mm for the integral and central baffled design. Outside this range, the obtained RTD profiles were similar to those in a well-mixed ST, indicating that axial mixing was dominant. At different Re_n (Re_n=4-35), the variance increased significantly at Re_n<10 for the various oscillation condition applied (Re_o=10-500) and minimum variance changes (~0.1 difference) with Re_n>25 for the both system design of central and integral baffled. Apart from that, in order to obtain a number of tank-in-series (N) above 10, the velocity ratio (ψ) had to be in the range 4-10 for the central and integral baffled designs.

However, at low net flow Reynolds number, e.g. Re_n<5, the two designs exhibited different behaviour (Phan *et al.*, 2011a). In the central baffled design, at x_o=0.25-0.5mm (St=1.59-0.8) (Figure 2-11(a)) and x_o=2-3mm (Figure 2-11(b)) the number of tank-in-series (N) was around 10 (or normalised variance $\sigma(\theta)^2$=0.10) and 25 for oscillation condition range of 10 ≤Re_o ≤120 and 150 ≤Re_o ≤500, respectively.

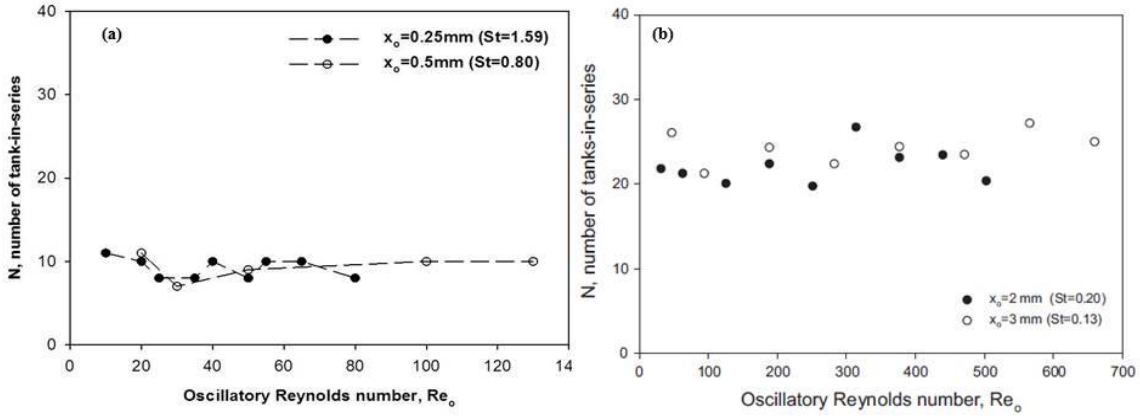

Figure 2-11: Dependency of the number of tank in series at (a) x_o=0.25-0.5mm and (b) x_o=2-3mm onto the Re_o at Re_n=1.27 for central baffled mesoscale-OBR. (Phan *et al.*, 2011a).

However at x_o=1.0-1.5mm (St=0.4-0.27), it exhibited an increase to an optimum value (N≈30) at the Re_o range of 100-125 before decreasing to its minimum value of 10 (Figure 2-12)

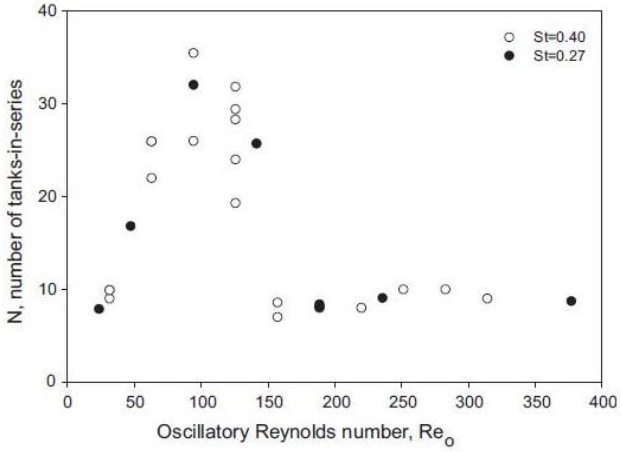

Figure 2-12: Dependency of the number of tank-in-series at St=0.27-0.40 onto the Re_o at Re_n=2.55 for central baffled mesoscale-OBR. (Phan *et al.*, 2011a).

This trend was also observed at x_o=4mm with maximum N=30 obtained at Re_o≈50. However, regardless of tested Re_n (1.27 or 2.55) and Re_o, the minimum N for the central design was above 10. At Re_n=2.55 (Figure 2-13(a)), the integral baffled design behaved as a well-mixed ST (N<10) at oscillation amplitudes of 0.25mm (St=1.59), 0.5mm (St=0.8), 1.0mm (St=0.4) and 2.0mm (St=0.20) regardless of tested Re_o. At x_o=1.5mm, N reached its maximum (N=18) at Re_o=50 (Figure 2-13 (b)).

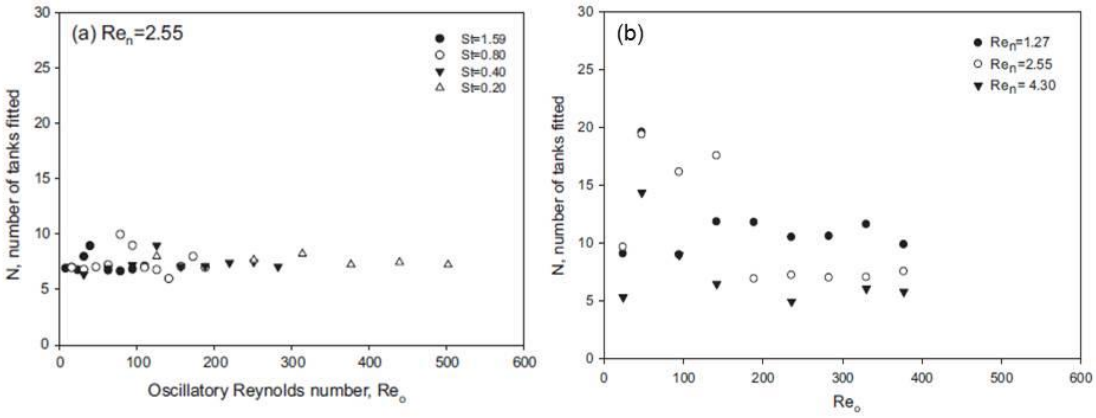

Figure 2-13: Dependency of the number of tank in series at (a) Re_n=2.55 for various St = 0.20-1.59 and (b) x_o=1.5mm for various Re_n=1.27-4.30 for integral baffled mesoscale-OBR (Phan *et al.*, 2011a).

It can be concluded that the central baffled design had a wider operating window (i.e. high degree of plug flow over a wider range of oscillation conditions and net flows) than the integral baffle design.

For the helical design, the more significant effect of oscillation amplitude on the plug flow behaviour than oscillation frequency was also observed (Phan and Harvey, 2010; Phan and Harvey, 2012). However, the oscillation amplitude (x_o) was higher than (x_o=2-4mm) those obtained for the central and integral baffled designs (0.5-1.0mm). For example, tested at Re_n=7.2 and *f*=3Hz the variance was 0.03-0.07 for x_o=2-4mm in the helical design compared to 0.09-0.10at x_o=0.5-1.0mm for the others. At different net flow conditions (Re_n=1.25-10), N≥10 was established at a wider Re_o operating window when using x_o=4mm compared to x_o=2mm with Re_o range of 100-500 and 50-300 respectively.

The effect of oscillation conditions on mesoscale-OBRs with varying helical pitches was also investigated (Phan and Harvey, 2011b). The study examined five different helical pitches of 2.5mm, 5.0mm, 7.5mm, 10.0mm and 15.0mm. Different optimum Re_o ranges were found for individual helical pitches in order to obtained high plug flow behaviour. For example, at x_o=4mm and Re_n=7.2, Re_o range was 100-300 and 100-700 for the helical pitches of 2.5mm and 15.0mm respectively. The degree of plug flow was found to be a function of the ratio of the oscillation amplitude and the helical pitch, e.g. the optimal ratio of oscillation amplitude to the helical pitch was in the range of 0.2-0.6. For example, variance decreased from 0.1 to 0.05 when decreasing amplitude from 4.0mm to 1.0mm for 2.5mm helical pitch at Re_n=7.2. The mixing inside the helical baffled design was achieved not only from the vortex formation but also from the swirling flow. This swirling flow was generated due to the effects of the helical design with the centre flow. Two distinct regions were observed on the dependency plots of the variance on different Re_o conditions with x_o=4mm: the effect of vortex flow (region I) and effect of swirling flow (region II) as shown in Figure 2-14 (Phan and Harvey, 2012). This agreed with the study by Solano *et al.* (2012) using a numerical simulation. From the flow pattern assessment, the swirled flow was formed at the centre of the helical pitch and its rotation depended on the reversing effects of the oscillation motion. The radial mixing was also promoted by increasing Re_o due to the formation of eddies downstream of the baffles.

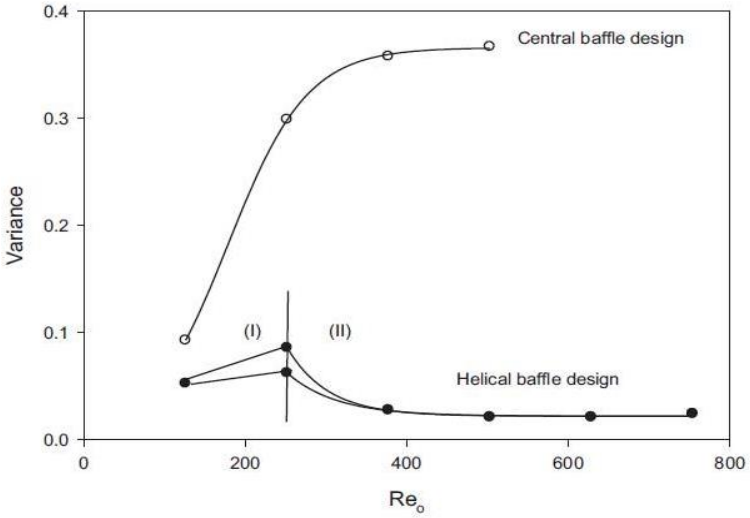

Figure 2-14: Dependency of the fluid mixing (variance) on the oscillation Reynolds number (Re_o) at Re_n=7.2 with x_o=4mm

So far, these baffles (central, helical and integral) were used in biodiesel production. Continuous screening biodiesel at total flowrate of 1.98ml/min (Phan *et al.*, 2011) showed that indistinct step changes between different ratio of methanol to oil were observed for both central and helical baffle designs. This was due to the immiscibility of the reactants (oil and methanol), indicating that the designs were not suitable to be used with a two-phase reaction system for screening purposes. Hence, modification was conducted by changing the smooth edge to a sharp edge helical wire and inserting a 1mm rod in the helical design. This resulted in a clear step change in the methyl ester content when changing the ratio of methanol and oil from 4:1 to 12:1 (Phan *et al.*, 2011). Similar sharp-edged helical baffles with a central rod were used to compare the methyl ester content obtained from the integral baffles and wire wool baffles (Phan *et al.*, 2012). A Clear steady-state screening was observed for all the baffled designs at $Re_o \geq 107$. However, the highest methyl ester was obtained in the integral design (82%) at Re_n=1.74 and Re_o=160. Eze *et al.* (2013) used the integral baffled design for the heterogeneously catalysed esterification of hexanoic acid in a continuous mode. A clear step change in hexanoic acid conversion was observed when changing the residence times from τ=30min to 60min. The catalyst suspended in mesoscale-OBR also exhibited a higher turnover frequency (TOF) of $57h^{-1}$ than in a conventional stirred tank TOF of $31h^{-1}$. This was due to the reduction of water poisoning of the catalyst in the continous method compared to a conventional stirred tank method. From these applications, it is proven that the mesoscale-OBR allows a wide range of screening conditions to be explored easily and rapidly at a continuous mode. The mesoscale OBRs also decrease significantly reaction times compared to continuous or batch stirred tank for biodiesel

production. For example, the time to achieve steady-state operation in a continuous stirred tank was 300min compared to 15min in the continuous mesoscale-OBR (Phan *et al.*, 2012). In addition, the mesoscale-OBR have the flexibility in changing the baffled designs to suit a given application compared to the fixed baffles and impeller designs in conventional stirred tank reactors.

2.3 Other screening reactors platform

Rapid screening, and use of a minimal amount of reagent and waste generated coupled with an increase in overall process safety are key drivers for the new approach to conduct preliminary screening and synthesis at laboratory scale. Here, various laboratory-scale screening reactors are reviewed to compare with the present work conducted using the mesoscale-OBRs. However the surveys are limited to reactors that are able to perform liquid phase reactions.

2.3.1 Multiple batch screening reactor

Multiple batch screening reactors are designed to screen reactions rapidly at various experimental conditions simultaneously. Raposo *et al.* (2009) demonstrated the influence of inoculum to substrate ratio on the anaerobic biodegradability of sunflower oil cake using this multiple batch reactor. Six different experimental conditions were screened simultaneously using 250 mL flasks with a magnetic stirrer for mixing. This method only took about 7 days to obtain the screening data from 6 different experiments compared to 42 days if conducted individually. In kinetic determination of the inactivation of broth and fruit juice (Parton *et al.*, 2007), 6 of 2mL cylindrical steel reactors with screw caps (Figure 2-15) were used. Here, the mixing was achieved using a magnetic stirrer bar inside each reactor chamber. Apart from the 6 simultaneous data sets collected at different treatment times, this reactor set-up allowed more controllable conditions for each data point. For example, once the treatment time was reached, a reactor was removed and the number of microorganisms was counted and analysed without disturbing other reactor chambers with different treatment times. Furthermore, this reactors set up avoid a reduction in volume due to sample taken for analysis.

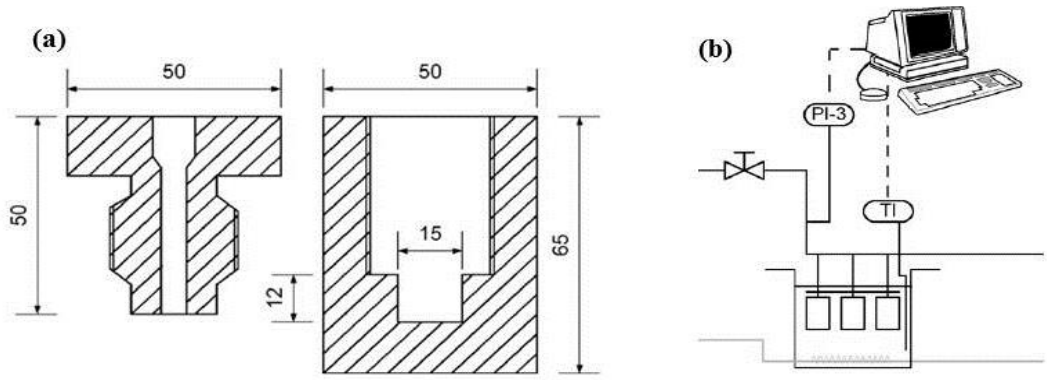

Figure 2-15: The (a) dimension of one of the six reactor in the multi batch system and (b) schematic diagram of the multi-batch reactor submerged in a thermostatic water bath (Parton *et al.*, 2007).

2.3.2 Microreactors

A microreactor consists of microchannels etched on substrates such as metal, glass or silicon with diameter < 1 mm. The design of the channel varies from straight channels to a novel sine-wave pattern. The microreactor is associated with the steady growth on the flow chemistry concepts and explored to various chemical synthesis and kinetics studies (McMullen and Jensen, 2010; Calabrese and Pissavini, 2011; Baxendale, 2013a). Several pumping methods such as hydrodynamic pumping, electrokinetic pumping or capillary flow is used with the reactor system to move the fluid through the channels (Geyer *et al.*, 2006). The hydrodynamic pumping involved with the usage of either a syringe or a high performance liquid chromatography (HPLC) pump that allows broad variation of flow speed from μL min^{-1} to L min^{-1}. With the electrokinetic pumping, known as electroosmotic flow (EOF), the fluid movement inside the channel occurs as a result of an applied external electric field which causes to the formation of the electric double layer (EDL) (Figure 2-16) (Hisham, 2012).

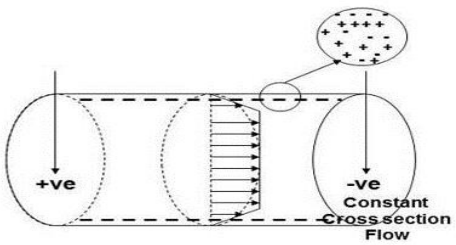

Figure 2-16: Schematic of velocity distribution in electroosmotic flow (EOF) (Hisham, 2012)

The EDL consists of immobile charges adjacent to the channel surface and mobile ions as a diffuse layer. Under the electric field, movement of these mobile ions also pulled

surrounding molecules through the viscous effect. However this pumping method requires polar solvent and can only be applied to analytical scale reactor (Geyer *et al.*, 2006). In capillary flow, the fluid moves through the channels without any external assistance such as pumps. This fluid movement significantly depends on the channel aspect ratio (channel depth / channel width) (Mukhopadhyay *et al.*, 2010). Regardless of the pumping methods, the flow inside a microreactor is laminar with mixing caused by diffusion and convection effects (Wirth, 2008). The enhancement of the diffusion and convection are commonly conducted through side-by-side flow or segmented flow. The side-by-side flow exploit two fluid streams in parallel inside the mixing channel which causes diffusion interactions across the stream (Hartman *et al.*, 2011). With the segmented flow, the recirculation patterns of fluid packets or slug are created inside the microreactor channel. This created an internal fluid vortex which caused rapid mixing within each segments. However the cross-section of the channel needs to be smaller than the length of the fluid plugs to avoid the formation of emulsion (Ahmed *et al.*, 2006).

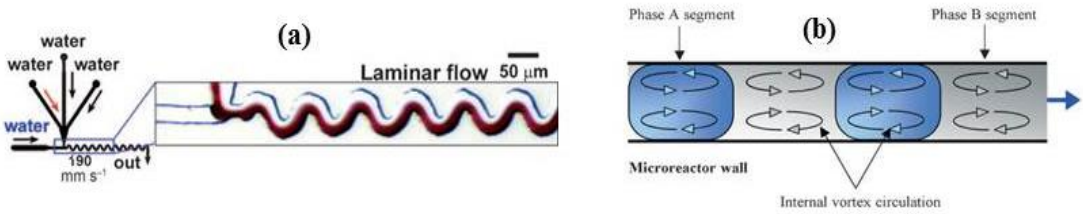

Figure 2-17: Schematic (a) side-by-side (Hartman *et al.*, 2011) and (b) segmented flow(Ahmed *et al.*, 2006) in microreactor channel.

There are two basic principles used to generate mixing inside the microreactor. The first involves an active mixing, which is achieved by applying external forces onto the reactor system (Hessel *et al.*, 2005; Hartman *et al.*, 2011). The external forces can vary from ultrasound irradiation (Zhang *et al.*, 2012b), periodical variation of pumping (Bottausci *et al.*, 2007), magnetic microimpellers (Zhang *et al.*, 2006), piecoelectrically vibrating membrane (Feth *et al.*, 2013) etc. A microbioreactor was used in cultivating *Escherichia coli* cell growth using a magnetic microimpeller at 180rpm (Zhang *et al.*, 2006). A cell growth rate of $1.5hr^{-1}$ was comparable with Sixfors reactor system ($1.55hr^{-1}$) at 500rpm.

The second means of mixing is known as passive mixing, generated through the pumping power or the designs of the microstructure channels (Hessel *et al.*, 2005).

Various ways of achieving this passive mixing are listed in Table 2-4. The mixing behaviour can be chaotic eddy-based flow, multi-lamellae flow or turbulence depending on the types of methods used. Advantages of this passive mixing was demonstrated in biodiesel synthesis, exhibiting an increase in the biodiesel yield from 60% to 94% for 10 and 350 curves respectively of the microreactor channel (Wen *et al.*, 2009).

Table 2-4: Various methods in generating passive mixing in microreactors (Hessel *et al.*, 2005)

Passive Mixing	
Pumping power energy input method	**Microstructure design method**
• Interdigital multi-lamellae • Split-and-Recombine concepts (SAR) • Chaotic mixing by eddy formation and folding • Nozzle injection in flow • Collision of jets	• T- and Y-flow configurations • Interdigital- and bifurcation flow distribution structures • Multi-holes plates • Meander-like or zig-zag channels • Tiny nozzles

Conventionally, scale-up approach was used in increasing the production output from the laboratory to pilot plant and lastly the industrial scale. This method can be challenging due to the changes of the surface to volume ratio leading to the variation in effect on the mixing and heat and mass transfer properties of a reaction (Geyer *et al.*, 2006; Watts, 2010). Therefore it required re-optimisation on the operating conditions of the process thereby causing delays to achieve the commercial volume. For microreactors, increasing the output of the production, can be done by scaling out or *'numbering up'* approach (Mettler *et al.*, 2010) as shown in Figure 2-18.

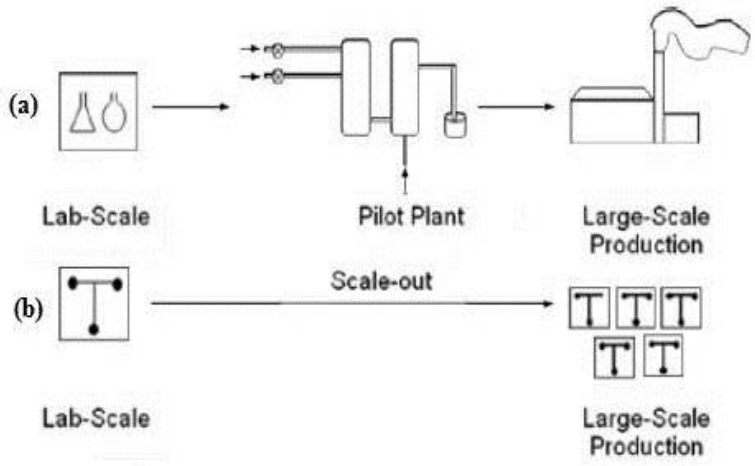

Figure 2-18: Schematic comparing the (a) scale-up and (b) scale-out approach to commercial scale production

Scaling out or numbering out method was seen as a more sensible and less risky as it used similar optimal laboratory conditions with each of the reactor sets, producing similar product conversions and yields every time (Wiles and Watts (2007) (Watts, 2010) (Geyer *et al.*, 2006)). However, to scale-out multiple miniaturise system is costly.

2.3.2.1 Microreactor applications

The microreactor can be used for various types of reaction: e.g. liquid-liquid, liquid-gas or liquid-solid (Geyer *et al.*, 2006). Due to small dimension, microreactors reduce the use of reagents, efficient process control (heat and mass transfer), provide rapid screening conditions and enhance process safety (Jas and Kirschning, 2003; Benito-Lopez *et al.*, 2005). For example, 85% of 1, 3- dehydrochlorination of dichloropropanol (DCP) conversion was obtained when using a microreactor compared to 10% when using the conventional batch method Zhang *et al.* (2012a). This was due to the excellent mass transfer and mixing properties in the microreactor. 80% yield in a lithium−halogen exchange reaction was obtained over a wide range of temperatures (-40 to 10^{o}C) using a microreactor but only 50% when using 100mL round bottom flasks (Liu *et al.*, 2013). In pharmaceutical applications, synthesis of an alcohol base compound increased the yield from 52% to 71% for batch and microreactor respectively (Wheeler *et al.*, 2007). Using the microflow operation also reduced the process time by 100% compared to a batch system. With liquid-gas reactions, Ehrich *et al.* (2002) showed that the photochemical chlorination of toluene-2,4-diisocyanate resulted with 55% conversion and 80% selectivity of the desired product using microreactor system. Even though

higher conversion (65%) was achieved with the traditional batch glassware, the selectivity was reduced to 45%.

On the applications as a screening reactor, esterification reaction between formic acid and methanol were screened based on the Central Composite Face-centered (CCF) experimental design (Naef *et al.*, 2010). Different flowrates were adjusted to give different residence time. The output concentration profile was than analyse using FTIR spectrophotometer with the aim to determine the kinetics parameter. It resulted with forward (k_1) and backward (k_{-1}) rate constant at $2x10^{-4}$ and $5x10^{-4}$ $mol.L^{-1}.s^{-1}$ respectively. It was also claimed that the method requires minimal personnel and material resources. Rapid screening for carbon dot (CD) reaction using microreactor also allow hundreds of reaction condition (various precursor, solvents and additive) to be screened at approximately 15min per condition in order to achieve the desired photoluminescence (PL) properties (Lu *et al.*, 2014).Through this continuous screening it allows precise controlling of the reaction time that resulted with consistent PL properties of the CD. Other than that, the input into the reactor system can easily be adjusted with the continuous manner (Figure 2-19).

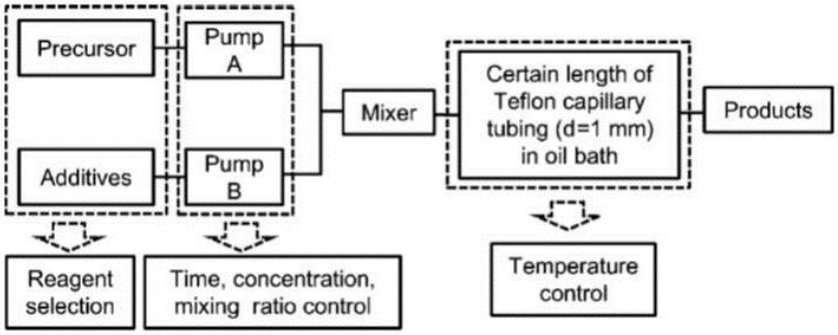

Figure 2-19: Schematic illustration for the rapid screening of carbon dot reaction using microreactor platform (Lu *et al.*, 2014).

Manipulation of the segmented flow method in the development of microfluidic cartridges preloaded with nanoliter plugs of reagents highlights the advantage over the common 96-well plates screening platform(Chen and Ismagilov, 2006). The methods involve in 3 steps. First, nanoliters of reagants were dispensed in arrays of plugs in a capillary. Secondly, the plugs of reagants were merge in a merging junction with a substrate resulted with a spontaneous mixing due to diffusions. Lastly, the receiving capillary was detached from the merging junction for analysis. As the reagents were reacted and stored in a capillary, evaporation occurrence was reduced than the 96-well

plates screening platforms. Schematic flow of the method is illustrated in Figure 2-20. This approach also had been applied to screen reaction of bicyclo[3.2.1]octanoid scaffolds for pharmaceutical application(Goodell *et al.*, 2009).

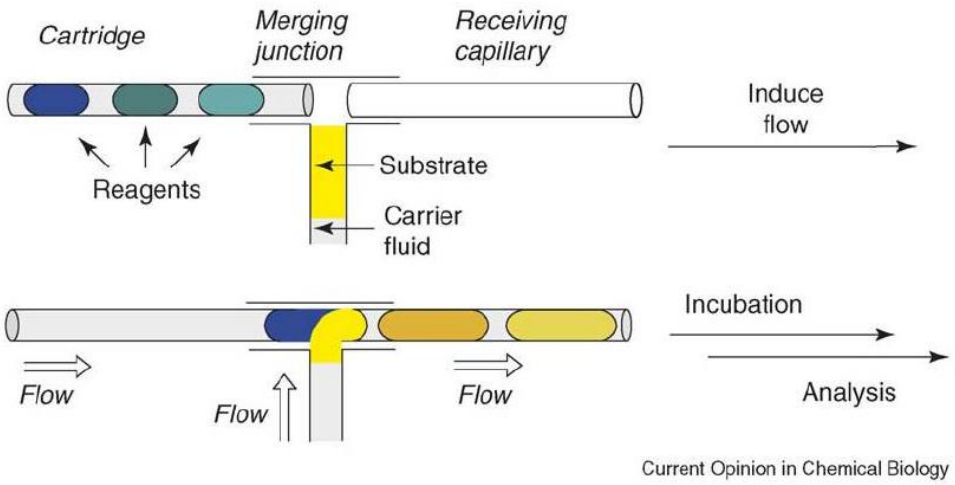

Figure 2-20: Schematic process of the preloaded cartridges method screening using microfluidic platform (Chen and Ismagilov, 2006).

However, microreactors are of limited use for liquid-solid systems. The solids may clog the narrow channel of the reactors and obstruct the continuous flow. With that, the solid, for example a catalyst, is restricted to use either by coating onto the inner wall of the reactor or pre-packing in a reaction cartridge. This was demonstrated by Snyder *et al.* (2005) with a reaction of phenyl-iodide and ethyl acrylate passed through a solid-phase catalyst cartridge of 10% palladium on charcoal. It yields 99% of the ethyl cinnamate in 30min but at lower temperature of 130^{o}C with the microreactor than 140^{o}C with the conventional batch system.

2.4 Heat pipe and thermosyphon

Conventionally, a jacketed system is used with a reactor system to obtain an isothermal condition. However this requires external pumping system and also large amount of cooling or heating material to remove or supply heat to the reactor. This involves with additional operating and capital cost. On that note, a heat pipe or thermosyphon system was chosen as a platform to create a passive jacketed reactor system.

2.4.1 Operating mechanism of heat pipe and thermosyphon

Generally, thermosyphons or heat pipes consist of 3 main parts: a condenser section, an evaporator section and an adiabatic section (Figure 2-21). When the liquid at the

evaporator side is heated, it vaporizes. This vapor then moves to the cold end of the condensation side. The condensate then returns to the hot end (evaporator side) by gravity. As mentioned by Reay and Kew (2006), even though a large heat quantity were transported from the evaporator to the condenser side, the temperature difference along the heat pipe is small. Thermosyphons (Figure 2-21(a)) must be vertical with the evaporator at the bottom. The condensate returns to the evaporator side through gravity flow. The limitation for the orientation position can be overcome by introducing a wick inside the system. When there is also a wick, the system is known as heat pipe (Figure 2-21 (b)). The wick facilitates the return of the condensate to the evaporator through capillary effects. This therefore does not restrict the tube orientation.

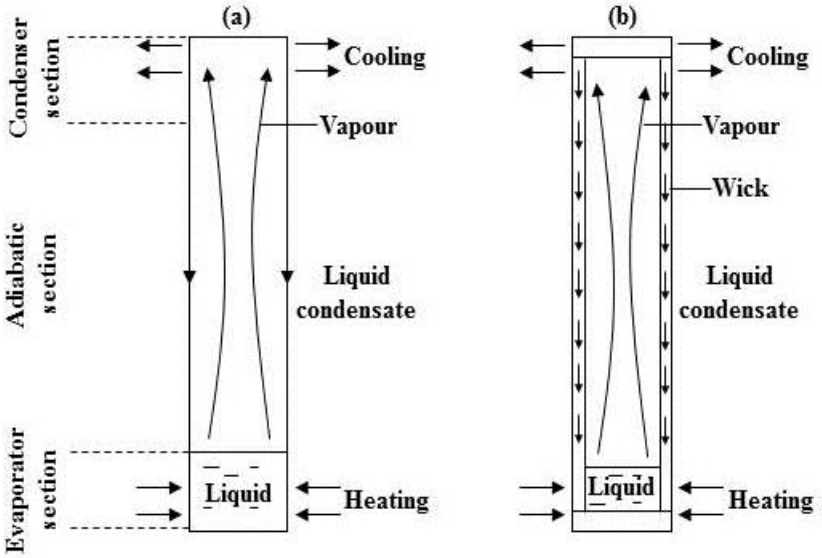

Figure 2-21: Schematic diagram of a (a) thermosyphon and (b) heat pipe (Reay and Kew, 2006)

Various studies have shown that the heat transfer from the evaporator and condenser is limited. One of the reasons is that the restriction of the vapor flow in the internal space (Parent *et al.*, 1983). The filling ratio of the evaporator is critical in terms of reducing such limitations. An investigation by Kang *et al.* (2010) of a thermosyphon loop system showed that the optimal filling ratio was 10% with methanol and 30% with water. The system consisted of a 25mm inner diameter and 25mm long evaporator and 7 vertical smooth copper tubes of 4mm outer diameter and 80mm in length (Figure 2-22). Noie (2005) found that the maximum heat transfer rate was obtained at filling ratios of 90%, 60% and 30% for aspect ratio (L_e/OD) of 7.45, 11.8 and 9.8 for a two-phase closed thermosyphon system. This demonstrates that the filling ratio is not a linear function of the system dimension. Here it show that, determination of the optimum filling ratio is

important before any work is conducted using the heat pipe or thermosyphon system. This is because the parameter reflects the occurrence of drying out or over-filling phenomena inside the heat pipe or thermosyphon systems. The latter phenomena prevent condensate to returns due to large volume of liquid in the evaporator side.

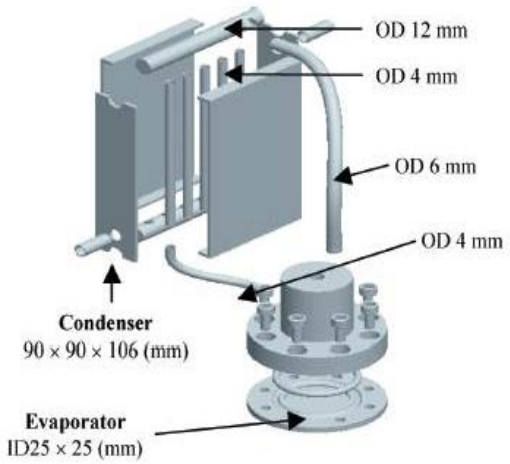

Figure 2-22: Schematic diagram of a loop thermosyphon system (Kang *et al.*, 2010)

Other parameters, such as the working fluid and material of construction also play an important role in enhancing heat pipe or thermosyphon efficiency (Reay and Kew, 2006). The main consideration in selection of working fluid is related to the operation working temperature range desire for the work conducted. Table 2-5 listed several working fluid used with the heat pipe and thermosyphon system (Reay and Kew, 2006).

Table 2-5: Selection of working fluid use with the heat pipe or thermosyphon system (Reay and Kew, 2006)

Working fluid	**Melting point (ºC)**	**Boiling point at atmospheric pressure (ºC)**	**Useful range (ºC)**
Helium	-271	-261	-271 to -269
Nitrogen	-210	-196	-203 to -160
Ethanol	-112	78	0 to 130
Heptane	-90	98	0 to 150
Water	0	100	30 to 200
Toluene	-95	110	50 to 200
Sodium	98	892	600 to 1200
Silver	960	2212	1800 to 2300

Other concerns related to the working fluid determination are related to the fluid compatibility, latent heat, thermal conductivity, surface tension and vapour pressure properties (Reay and Kew, 2006). Merit number (*M'*) (e.q.) value is also used to obtain optimum performance of the heat pipe or thermosyphon system in the range of the working temperature desired. However, this *M'* is relatively insensitive to temperature difference (Reay and Kew, 2006).

$$M' = \left(\frac{Lk_1^3\rho_1^2}{\mu_1}\right)^{\frac{1}{4}} \qquad \text{eq. 2-7}$$

As with the selection of the material of construction for the heat pipe or thermosyphon container, it depends on several factors such as the compatibility (both with the working fluid and the external environment), strength-to-weight ratio, thermal conductivity, and ease of fabrication, porosity and wettability (Reay and Kew, 2006 212).

2.4.2 Heat pipe or thermosyhphon application as a reactor

The heat pipe or thermosyphon system have proven to provide high isothermal conductivity in several application such as spacecraft (Swanson and Birur, 2003), solar cells (Armijo and Carey, 2013), chemical reactors (Parent *et al.*, 1983; Richardson *et al.*, 1988), heat exchangers (Vasiliev, 2005) and electronics cooling activities (Reay and Kew, 2006). In this section, only the applications related to chemical reactors are reviewed.

The use of heat pipe in reactor applications was reported by Parent *et al.* (1983) and Richardson *et al.* (1988). Parent *et al.* (1983) used an annular heat pipe (AHP) for a tube wall reactor for an exothermic reaction in which naphthalene was oxidised to phthalic anhydride. This was compared to the conventional liquid cooled reactor system. At similar conversion of 96% of naphthalene, the AHP system only requires a shorter reactor length (1.6m) at a lower temperature (750K) than the conventional cooling fluid system (2.0m in length and 770K). The design consisted of 4 annular crescent-shaped channels joined together to form a heat pipe (Figure 2-23(a)). The tube wall reactor was then inserted inside this channel with the dimension at ~1.7m long. Richardson *et al.* (1988) used a heat pipe for an endothermic reaction of steam reforming of methane. The heat pipe exhibited a highly isothermal level along its length but severe temperature

gradients were observed in the catalyst bed. This was due to low flow rates of the feed into the reactor. The heat pipe was inserted in the center of the reactor with the evaporator side outside the length of the reactor (Figure 2-23(b)). This serves as a preheated region. This reactor is 2.13m long with a diameter of 15.2cm.

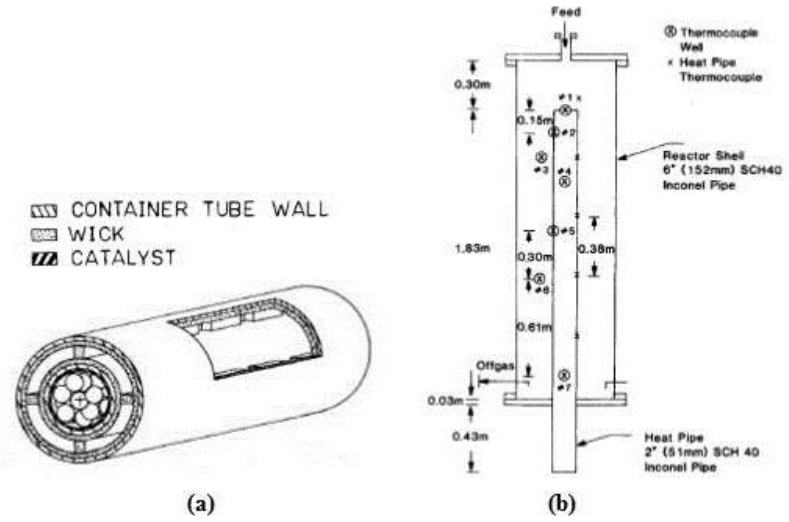

Figure 2-23: Schematic diagram of heat pipe reactor for (a) exothermic naphthalene oxidation reaction (Parent *et al.*, 1983) and (b) endothermic reaction of methane reforming (Richardson *et al.*, 1988).

As there were no external mixing apparatus attached to the system, it resulted in relatively long reactors for both systems in order to allow adequate length for heat transfer or mixing to occur (Figure 2-23).

2.5 Imine Synthesis

Single-phase liquid-liquid reactions of several aldehydes with primary amines to form imines were chosen to demonstrate the ability of the mesoscale-OBR as a screening reactor platform. Imines known as Schiff bases, are produced through an addition-elimination reaction between aldehyde or ketone with amine. The reaction is exothermic and reported mostly to be reversible (Naqvi *et al.*, 2009). As shown in Figure 2-24, the mechanisms involve a nitrogen base attacking a carbonyl compound to form an intermediate, followed by dehydration steps to form an imine (Anderson and Jencks, 1960). This is a 2-step process involving bond breaking and formation, including protonations and deprotonation (Page, 1983). The tetrahedral intermediate formed during the first step of the reaction is known to be reactive and unstable (Layer, 1963; Iwasawa *et al.*, 2007). Hence, in practice, it is not possible to monitor the carbinolamine intermediate directly due to its vanishingly small concentration.

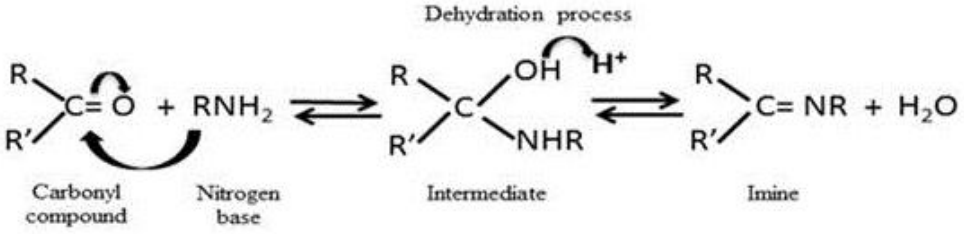

Figure 2-24: Imine reaction mechanisms of carbonyl and nitrogen compound

Similar reaction mechanisms are also involved in the production of oxime, hydrazone and semicarbazone. The difference in the product was due to the type of amine used during this addition elimination reactions, as illustrated in Figure 2-25.

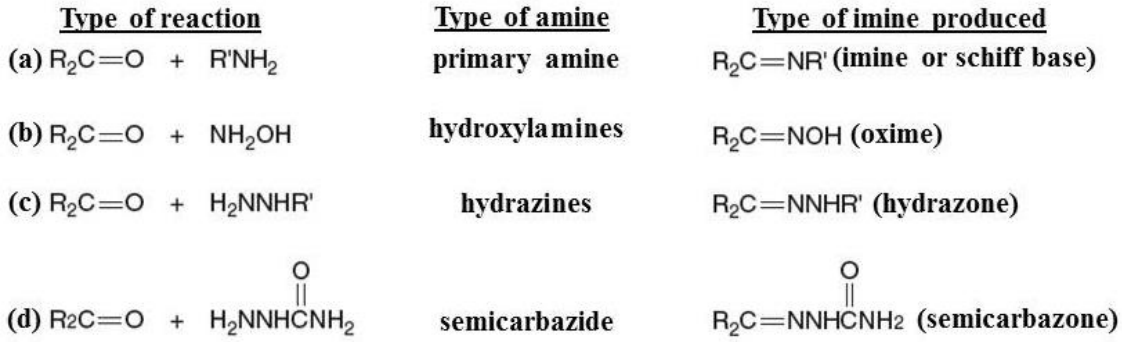

Figure 2-25: Different types of addition-elimination reactions between aldehyde and different types of amines (Carey and Sundberg, 2007)

The rate determining step in this two-step mechanism depends upon the pH of the reaction mixture. At neutral and alkaline pHs, the dehydration path was identified as the rate determining step, whereas the attack of the amine becomes rate determining in acidic conditions because of the conversion to its conjugate acid (Cordes and Jencks, 1962). In order to facilitate the detection of imine formation, water removal via azeotropic distillation technique or reagents can be used (Reusch, 1999). Because the aromatic aldehydes are so reactive, the imines formed using this type of reagent can be detected quantitatively without the need for water removal (Layer, 1963).

Imine has several applications such as in biological processes, polymer synthesis and dynamic combinatorial chemistry (Cordes and Jencks, 1963; De Carvalho Alcântara *et al.*, 1996; Saggiomo and Lüning, 2009). In the enzymatic reaction, the imine reaction involves carbon nitrogen double bond formation between a substrate and enzyme; i.e. reaction of a lysine amino group from a protein with a carbonyl substrate (Page, 1983). Aromatic imines have also been found to be useful in applications as hydrogen sulphide

and mercaptan scavengers in the water and petroleum sectors (Westlund and Weller, 2011). These initiated interest in its reaction kinetics. Currently, most of the imine reaction studies (synthesis, screening, kinetic studies) was conducted via batch reactions. Work by Jencks (1959) reported the rate constant (k) of benzaldehyde and hydroxylamine in aqueous solvent was $7.0x10^6$ $l.mol^{-1}min^{-1}$. In aqueous solvent, the rate constant for the synthesis of benzaldehyde and t-butylamine was a function of pH (Cordes and Jencks, 1963). For instance, at pH <4, an average k_{obs} (pseudo first order rate constant) was 0.01 min^{-1} and increased to approximately at $1.0min^{-1}$ at pH >8. Reaction kinetic studies related to imine synthesis to obtain parameters such as the reaction order, reaction rate and rate constant are normally conducted using the pseudo-first-order method using a large excess of nitrogen base (samicarbazide, t-butylamine, n-butylamine, ethylamine, cycloexylamine, s-butylamine) (Anderson and Jencks, 1960; Cordes and Jencks, 1962; Rotondo *et al.*, 1976).

Apart from determination of kinetic parameters, there has also been interest in the effect of other reaction parameters such as temperature, solvent and reagents on the imine yield. De Carvalho Alcântara *et al.* (1996) found that the yield of imine increased with increasing temperature, 0.06% at 0^{o}C but 2.0% at 36^{o}C using 0.05M butyraldehyde and 0.05M primary aliphatic amine. The results also showed that there was no correlation between polar and non-polar solvents in the yield of the imine. This was supported by other studies (Simion *et al.*, 2001; Saggiomo and Lüning, 2009) in water/aqueous medium. Comparisons of different steric effects of amine groups resulted in the equlibrium constant (K) at $156M^{-1}$ for t-butylamine and $K=1008.3M^{-1}$ for adamantylamine (De Carvalho Alcântara *et al.*, 1996). This indicated that less the steric effect (such as in adamantylamine) produced a higher yield of imine (higher K value). Similar findings was reported by Godoy-Alcántar *et al.* (2005). Here it shows that the types of aldehyde and amine used in imine synthesis are important to obtain high conversions of the imine products. Layer (1963) reported that aromatic aldehyde produced stable and quantitative imines. However, low reaction rates were obtained when using weak amines regardless of the type of aldehydes

A "green chemistry route" has also been developed for imine synthesis. Instead of using organic solvents, water was used due to its lower environmental impact (Simion *et al.*, 2001; Saggiomo and Lüning, 2009; Chu and Li, 2010). Although several studies stated that water pushed the reaction backward (Layer, 1963), 80% yield of imines have been

obtained. Other methods, such as microwave irradiation, were also used, with the aim of conducting the imine synthesis without solvent. Paquin *et al.* (2006) demonstrated the imine synthesis without catalyst, whereas Varma and Dahiya (1997) used catalysts combined with microwaves with imine yields ≥80%. However, the microwave irradiation method was limited to non-volatile amines.

On the basis of continuous synthesis of the imine, Smith *et al.* (2011) used a microfluidic flow reactor to produce imine with a high yield for various amine and aldehyde compounds, e.g. a 93% yield was obtained for the reaction between benzaldehyde and benzyl azide. However there are still limited works on continuous manner for these reactions.

With regards of analysis, monitoring and quantifying the imine reaction, various instruments were used such as the spectrophotometer, Raman spectroscopy, nuclear magnetic resonance (NMR) and infrared spectroscopy (IR). Generally, the data collected through this analytical instument was used to determine reaction kinetic parameters (rate constant or reaction rate) or evaluating the product qualitatively or/and quantitatively. For example, Lee *et al.* (2003) used Raman spectroscopy to monitor qualitatively and quantitavely the imine synthesis from acetophenone and aniline through off-line analysis. The rate constant for this reaction was $1.06x10^{-2}$ M^{-1} min^{-1} at 25ºC, which was calculated through the disappearance data of C=O stretching at $1684cm^{-1}$. Another example by Holsey (2006) used NMR to determine the imination kinetics between 5-methylfurfurylamine and piperonal conducted stoichiometrically in a vigorously shaken vial. The rate constant was $0.07M^{-1}$ min^{-1} NMR spectra were taken at several interval times for up to 22 hours also via the off-line method. Namli and Turhan (2006) and (2007) followed the imine synthesis using the *in situ* infrared spectroscopy (IR) at a carbonyl peak of $1702cm^{-1}$. The studies shows that the reaction was reversible with the reaction order of 2.0.

With this findings, it can be concluded that imine reaction path can either go through a irreversible or reversible mechanism. This was proven with the calculated rate constant (k) and equilibrium constant (K) listed above depending on the types of aldehyde and amine reactions. Furthermore, quantitative imine (80%) was also detected when using water as a solvent that discard the claim of the reaction being pushed backward in an

imine reaction. The reasons of these difference are due to many factors such as the types of aldehyde and amine, solvents and catalyst used.

2.6 Infrared Spectroscopy (IR) technique

Infrared spectroscopy (IR) is a tool to determine any organic substances that covers both qualitative and quantitative aspects (Conley, 1972). The nondestructiveness of IR is an advantage when dealing with an expensive material. The infrared region can be divided into three segments; near-, mid- and far-infrared as shown in Table 2-6.

Table 2-6: Common subdivision of the infrared regions

Region	Frequency Range (cm^{-1})	Wavelength Range(μm)
Near-infrared	14000-4000	0.8-2.5
Mid-infrared	4000-400	2.5-25
Far-infrared	400-10	25-1000

Different regions of the IR spectrum excite different types of vibration (Conley, 1972). Overtone vibration is excited at high frequency energies of near-IR (14000-4000 cm^{-1}), whereas skeletal vibration is excited at low frequency region of far-IR (400-10 cm^{-1}). The most useful region in reaction monitoring is the mid-IR, which gives information on the fundamental vibration-rotation structure. Once the IR energy is absorbed by the molecule and matches the specific molecular vibrational energy, the photon is excited from the ground energy state to the vibrational energy state (Figure 2-26) (Betteridge and Hallam, 1972). Through this, a sample can be characterised to determine different chemical bonds.

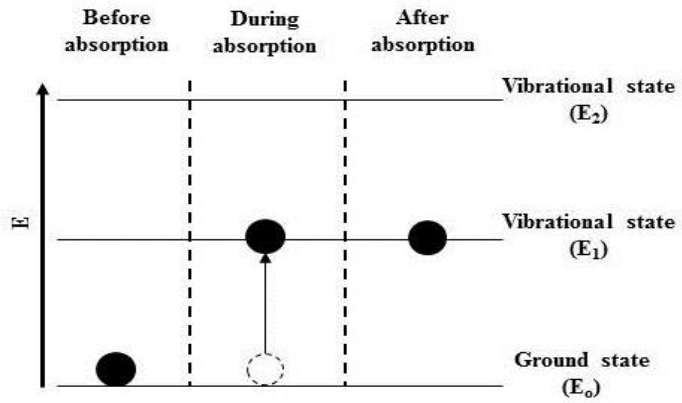

Figure 2-26: Schematic presentation of molecule absorption process (Betteridge and Hallam, 1972)

The molecule frequency arises from such energy transition are related through the Bohr frequency condition (eq.2-7).

$$E = h\nu = \frac{hc}{\lambda} \qquad \text{eq. 2-8}$$

...where h is Planck's constant: 6.6×10^{-34} J.s

The relationship can also be expressed in terms of wavelenghts (λ). The wavelengths have an inverse relationship with the frequency (*f*) as the infrared radiation travels at the speed of light (c) (Conley, 1972). The relationship between the two is expressed as:

$$\nu = {}^{c}/_{\lambda} \qquad \text{eq. 2-9}$$

...where $c = 3 \times 10^{10}$ cm s^{-1}, the speed of light.

IR spectra are also often reported in terms of wavenumber (ω), which this is a reciprocal of the wavelength (eq.2-9).

$$\lambda = {}^{1}/_{\omega} \qquad \text{eq. 2-10}$$

Information from the IR is obtained by monitoring the changes in the intensity or formation of the unique absorption band for each functional group. Regarding qualitative analysis, spectral interpretation is conducted by either comparing the collected spectra with known reference material spectra or by peak assignment (Conley, 1972; International, 2002). The latter is conducted through step-by-step procedure, which starts with the peak identification related to the solvent used (if any). This is followed by identification of the common functional group absorption band (C=O, O-H, N-H, C=C) and lastly to the fingerprint region (1430-625 cm^{-1}). The summary of characterisation of different functional group bands is easily accessed from literature (Conley, 1972; Socrates, 1994). For quantitative analysis, a calibration curve is needed for the conversion of the absorbance data to the concentration value according to the Beer-Lambert law relationship (eq.2-10). According to this law, the absorbance (A) has a linear relationship towards the molar absorptivity (ε), path length (b) and compound concentration (c).

$$A=\varepsilon bc \qquad \text{eq. 2-11}$$

The molar absorptivity and path length are constant; hence, concentration data can be obtained directly from the constructed calibration curve of absorbance data with several known concentrations. However, this linear relationship is not obeyed at high substance concentrations as shown in Figure 2-27 for cyclohexanone in cyclohexane solution.

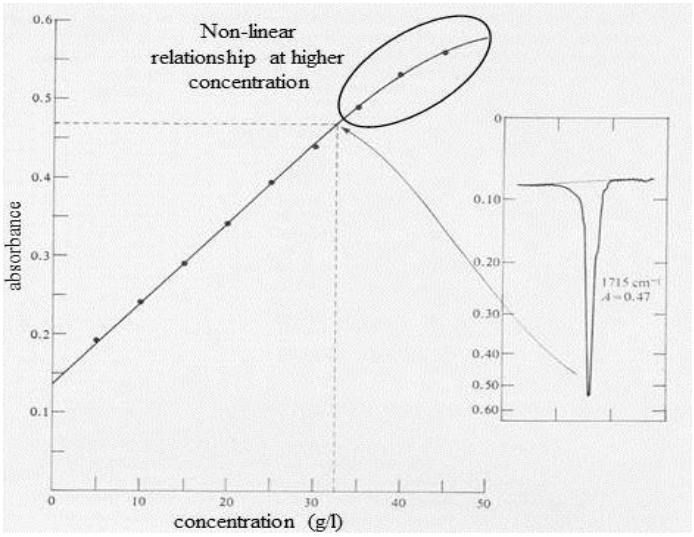

Figure 2-27: Calibration curve of cyclohexanone in cyclohexane solution at various concentration (Conley, 1972)

Measurement of the absorbance data can be conducted either through the peak height or peak area methods. Regardless of the methods, the baseline position is important to avoid any deviation during data collection. There are various ways to construct a baseline during the analysis, as shown in Figure 2-28. The peak-zero (Figure 2-28(a) method involves constructing the baseline at zero wavenumber. In the tangent method (Figure 2-28(b)), the baseline is formed by joining the two lowest points at the peak of interest. The peak-peak (Figure 2-28(c)) method uses the baseline developing from the lowest peak beside the peak of interest. However, the peak-zero method reduces error compared to the tangent and peak-peak methods because the baseline is fixed at zero absorbance. However, the tangent and peak-peak methods can be used for qualitative or quantitative analysis of single substance as this does not involve any reaction that will change the position of the peaks.

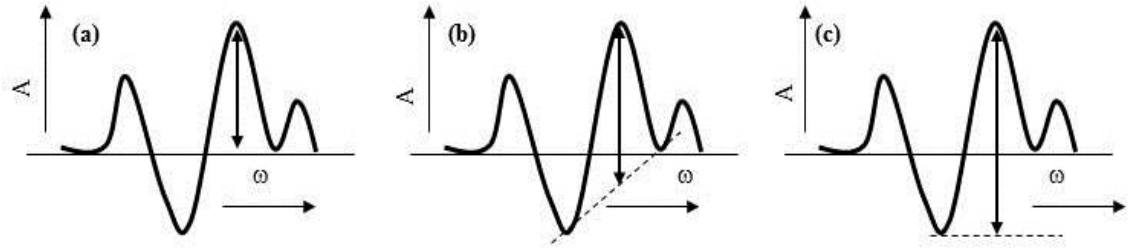

Figure 2-28: Baseline construction through (a) peak-zero method, (b) tangent method and (c) peak-peak method (Conley, 1972; K. Laqua, 1988)

Data treatment can improve experimental results. A second derivative treatment is the most common choice (Pierce and Wehling, 1994; A. L. Woodhead, 1997; Rieppo *et al.*, 2012) in treating data. Differentiating the Beer-Lambert law twice (eq.2-11) reduces the signal to noise ratio and improves the detectability of small and overlapping peaks (K. Laqua, 1988; Rieppo *et al.*, 2012). This method also eliminates baseline shift and reduces systematic error in the analysis.

$$A(\tilde{\nu}) = \alpha(\tilde{\nu}) l c$$

$$\frac{dA^2(\tilde{\nu})}{d(\tilde{\nu})^2} = \frac{d^2\alpha(\tilde{\nu})}{d(\tilde{\nu})^2}$$

eq. 2-12

…where $A(\tilde{\nu})$ is the wavenumber dependent absorbance, $\alpha(\tilde{\nu})$ wavenumber dependent absorption coefficient, l is the absorption path and c is the concentration.

2.6.1 Analysis of reaction kinetic parameters with quantitative data

Data obtained from the IR was used to determine the reaction parameters of the process, e.g. rate constant, reaction rate and reaction order. Conley (1972) stated that reaction kinetics can be measured if a functional band of the reacting molecules significantly decreased. This quantitative approach was reviewed through an investigation of several reaction routes. For example, the reaction of benzaldehyde with aniline was monitored using the peak at 1702cm^{-1} for the C=O of benzaldehyde and 1619 cm^{-1} and 1499cm^{-1} for H-N-H and C-N of the aromatic aniline, respectively (Namli and Turhan, 2007). The disappearance of the C=O peak data collected *in situ* was converted to its concentration profile using the constructed calibration curve (correlation coefficient of 0.996). With the calculated concentration data, it was found that the benzaldehyde reached its

equilibrium reaction at approximately 0.07M. Another example of this quantitative approach was in homogeneously catalysed liquid-phase sucrose hydrolysis (Pintar *et al.*, 2002). A calibration curve was constructed using data collected in the 1200-900 cm^{-1}region to cover the high absorbance profiles of sucrose, fructose and glucose. The calculated concentration data obtained was fitted to the pseudo-first order equation, giving a rate constant of 0.01224 l mol^{-1} min^{-1} for sucrose inversion.

Generally, the reaction parameters (rate constant, rate of reaction and reaction order) of a reaction were determined by integrating differential equations of the rate expression (Capellos and Bielski, 1980; Wright, 2004). As shown in Figure 2-29, linear plots are obtained through the integration results.

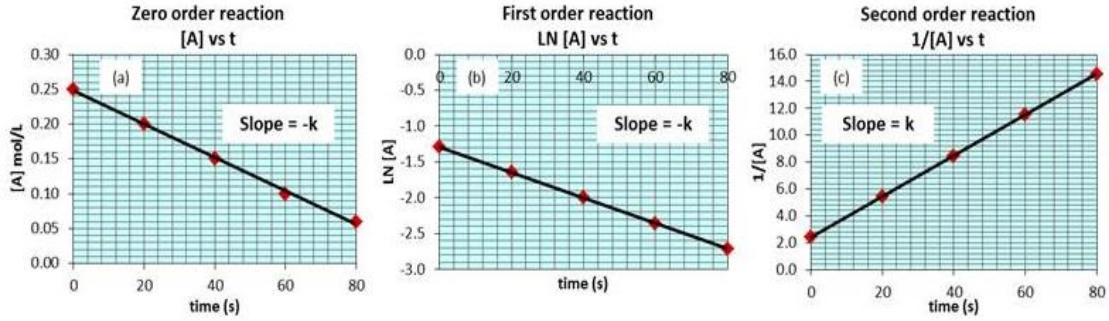

Figure 2-29: Integrated rate expression of (a) zero order reaction; (b) first order reaction and (c) second order reaction. ([A] is the concentration of a reagent) (Capellos and Bielski, 1980; Wright, 2004)

The rate constant value was determined from the slope of the plots. The reaction order was measured through various fittings, i.e [A] vs time (zero order), ln [A] vs time (first order) and lastly 1/ [A] vs time (s order). As for reaction order >2, the integrated form in eq. 2-12 was used (Laidler, 1987).

$$k = {}^{1}/_{t(n-1)} \left[{}^{1}/_{(A_o - x)^{n-1}} - {}^{1}/_{{A_o}^{n-1}} \right] \qquad \text{eq. 2-13}$$

However, the determination of reaction order was valid only for the overall reaction order not for the individual reactant reaction order. This integrated rate expression was also applied when using the pseudo-order reaction method. The pseudo-order reaction method involves conducting reactions with one of the reactants in large excess (a minimum of a 20-fold stoichiometric excess). The changes in concentration of the reagent in excess are minor. Hence, a second order reaction will behave like a first order

reaction but the rate constant obtain from the plots is known as pseudo-rate constant (k′). The true rate constant can then be obtained through the plots of ln (k′) and various concentrations of the excess reactant.

The determination or validation of the reaction kinetic parameters (rate constant, rate of reaction and reaction order) can also be conducted through kinetic modelling using the quantitative data collected with the IR. This has been conducted through multivariate fitting of absorption data with the kinetics model and reaction mechanisms (de Juan *et al.*, 2000). Minimal sum of square of errors (SSE) is used to determine the fit between the experimental and the modelling data (de Juan *et al.*, 2000; Abdallah, 2010). This SSE method was used to investigate many chemical reactions such as cyclometallation reactions between imines and palladium acetate (de Juan *et al.*, 2000), hydrosilylation (Imlinger *et al.*, 2007) and acetylsalicylic acid synthesis (Imlinger *et al.*, 2008). A software package (MATLAB) or computer programming (FORTRAN) can be used in modelling the process. Although the simulation platforms are different, the approach to determinate or validate the reaction kinetic parameters are similar (Abdallah, 2010; Seoud and Abdallah, 2010). Generally, the procedure begins by determining a reaction path, leading to a differential equation to be modelled (example see in Figure 2-30 for the reaction of saponification of di-esters).

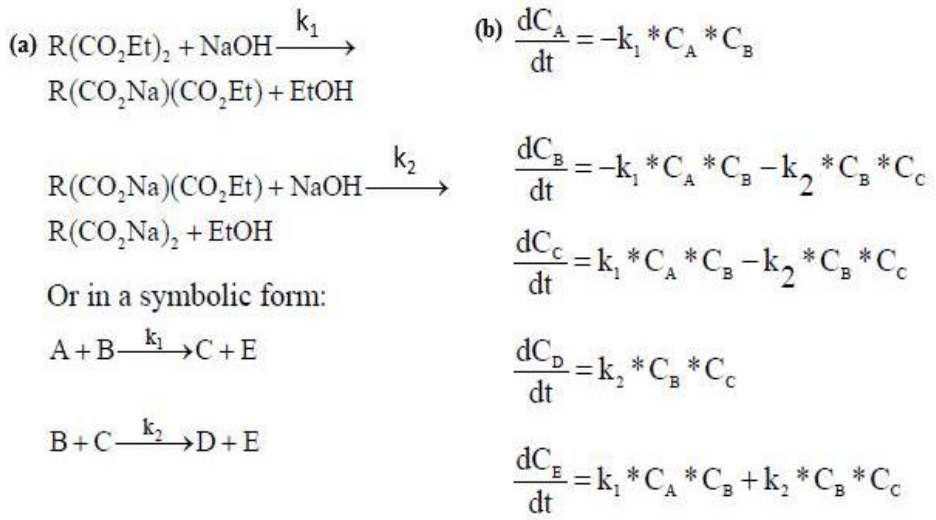

Figure 2-30: Saponification of di-esters (a) reaction path and (b) its derivative equations (Seoud and Abdallah, 2010)

Then the experimental concentration-time data of the reaction is collected at any desired reaction conditions. In order to obtain the modelling concentration-time data for

comparison with the experimental concentration data, a rate constant and/or reaction order is required. This can be obtained by referring to previous published work or calculating through the integrated rate expression, initial rate method or by the differential method (Abdallah, 2010; Seoud and Abdallah, 2010). Once the entire requirement is met, the ordinary differential equations (ODE) can be solved numerically using the Runge-Kutta method to get the modelling concentration-time data. The data were compared to the experimental value with the aim to obtain minimal SSE. When this is reached, the rate constant and/or reaction order value used is the results for the reaction under study. This kinetic modelling allows iterative process by setting a range value of rate constant and/or reaction order based on the calculated value. Apart from that, it can also be used to deduce different reaction mechanisms easily by changing the initial setting of the reaction kinetic path.

2.7 Summary

This chapter reviews the development, design and process advantages of the OBRs. This reactor allows long residence time reactions to be conducted in a continuous mode with a significant reduction in length to diameter ratio. Scale-up in OBRs is linear by maintaining geometric (baffle spacing and baffle open area) and dynamic (Re_o, Re_n, St and ψ) for reactor diameters $\geq$ 25mm. Recently, OBRs have been scaled down to "mesoscale" (~5mm diameter). Different baffle designs allow a wide range of applications from shear-sensitive applications to multiphase to high-shear mixing applications. Plug flow is easily achieved in these reactors; meaning that rapid screening of reactions with residence times varying from several min to several hours is possible.

However, there is limited work on rapid and dynamic screening capabilities using the mesoscale-OBR. In this study, the mesoscale-OBR was used to screen and manipulate experimental parameters to rapidly obtain reaction data in a continuous mode. The advantages of continuous processes have often been reported (Calabrese and Pissavini, 2011; Baxendale, 2013b). Recently, micro- and macro-reactor systems have been used as flow channels in providing a new method of conducting chemical reaction, synthesis ans screening (Benito-Lopez *et al.*, 2005; Stojkovič and Žnidaršič-Plazl, 2012). As for the "mesoscale" size, it bridges the gap between micro- and macroscale systems, and broadens the selection of laboratory or small-scale reaction analysis (Wheeler et al., 2007). Table 2-7 illustrates the advantages and disadvantages of the microreactor and

mesoscale-OBR as a continuous screening and synthesis reactor platform. The microreactor only need reagent at microliter volume in conducting screening or preliminary laboratory work than the mesoscale-OBR (millimetre). However, the mesoscale-OBR provides the flexibility with the operation modes either at batch or continuous manner which is restricted with the microreactor system. Furthermore, the baffle types in mesoscale-OBRs can easily be changed as they are not embedded in the reactor. Other than that, mesoscale-OBR systems allow solid catalysts to be used without clogging based on (Eze *et al.*, 2013) work that uses propylsulfonic acid derivatised SBA-15($PrSO_3H$-SBA-15) silica powder catalyst. Hence it is more flexible to be used as a laboratory screening platform.

Table 2-7: Comparison between mesoscale-OBRs and microreactors

	Volume	**Mixing**	**Operation mode**	**Mixing channel or baffled**	**Increased production size**
Mesoscale-OBR	milimeter	oscillation and diffusion	Batch and continuous	Different baffled design (central, integral and helical)	Scale-up
Microreactor	microliter	diffusion	continuous	straight to a novel sine-wave pattern channels	Scale-out

Even though the multiple batch reactors screening platforms provide rapid screening data especially related to kinetics study, its design limits its application. The magnetic stirrer without baffles to break up the mixing flow leads to inconsistencies in mass, energy transfer and agitation that could lead to misleading data. Using a magnetic bar (Halász *et al.*, 2007) also show to create a cylindrical dye curtain developed around the vortex axis when the dye was injected at the centre of the system, indicating insufficient mixing within the system (Figure 2-31).

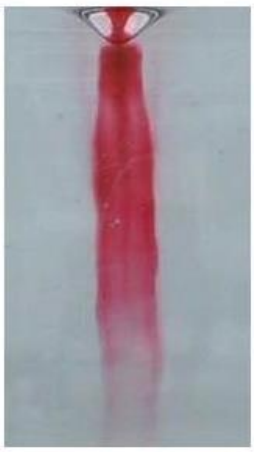

Figure 2-31: Developing cylindrical dye curtain below the vortex using a magnetic bar stirrer (Halász *et al.*, 2007)

Heat distribution in a continuous reactor is more rapid, leading to a smaller temperature gradient inside and along the reactor than that in batch reactor (Junkers, 2014). This reduces the occurrence of hot spots that may promote the formation of undesirable products. Due to that, the mesoscale-OBR was combined with a heat pipe or thermosyphon system to create a passive jacketed reactor system. Generally, review on the heat pipe and thermosyphon showed that the filling ratio of the evaporator section plays an important role as one of the factors affecting the heat distribution within system. A good temperature control for either exothermic or endothermic reactions was observed when applying the heat pipes and thermosyphon systems as a chemical reactor shows. Yet it resulted in relatively long reactors due to high feed flow rates required to achieve adequate mixing.

Imine synthesis reviewed shows that the reaction has several applications in biological processes, polymer synthesis and dynamic combinatorial chemistry (Cordes and Jencks, 1963; De Carvalho Alcântara *et al.*, 1996; Saggiomo and Lüning, 2009; Murugesan *et al.*, 2012). Previous studies shows that types of aldehyde (aromatic) and amine (primary) used in imine synthesis are important to obtain high conversions of the imine products. Other than that, the findings show that the imine reaction path can either go through a irreversible or reversible mechanism due to many factors such as the types of aldehyde and amine, solvents and catalyst used. However, almost of the imine reaction studies (synthesis, screening, kinetic studies) were conducted via batch reactions using conventional glassware set-up (beaker and conical flaks). Apart of performing the imine reaction screening continuously using the mesoscale-OBR in the present study, the reason imine reaction was used is due to its simple reaction as it do not involve any

competitive reactions path. This eased the reaction monitoring process to established the fundamental platform in conducting continous screening using the mesoscale-OBR.

Any type of analytical instrument can be used for collecting and analysing the data by the continuous method to obtain representative information with the reaction under study such as Raman and Infrared (IR) Spectroscopy (Lee *et al.*, 2003; Namli and Turhan, 2006; Namli and Turhan, 2007).Outcome from the data collected with this various analytical instrument resulted with different information related to the reaction understudy such as the kinetic parameters, product yield and selectivity. Choosing analysis method depends upon the reaction conducted and the detection limitation with the system (solvent and reagent used). In this study the *in situ* infrared spectroscopy (IR) was used as the analytical instrument in assisting the imine screening determination The IR determination involves a non-destructive sampling process, which is an advantage when dealing with small volumes or expensive samples. Furthermore, *in situ*, real-time data collection is faster and more efficient than off-line techniques, because it eliminates the possibility of any further reactions and removes the need for sample preparations (Pintar *et al.*, 2002).

2.8 Research objectives

The main aim of this research was to demonstrate the ability of the mesoscale-OBR to rapidly and logically screen and manipulate the experimental reaction space (residence time, chemical ratio or temperature) continuously for liquid-liquid phase reactions. The data collected was then used to determine kinetic parameters, such as rate constant and reaction order. *In situ* IR was used to monitor real-time quantitative and qualitative characteristics of the reaction system.

To achieve the objective of the study, five research tasks were identified:-

1. To characterize the modified central baffle mesoscale-OBR (enlarged from 5mm to 20mm at the outlet to accommodate the 16mm diameter IR probe) at different net flow rates, corresponding to $6.0 \leq Re_n \leq 120$ over a range of oscillation conditions $62<Re_o<246$ to determine its operating window for plug flow behaviour.

2. To screen reactions and determine kinetic parameters using the mesoscale-OBR in batch, continuous multi steady-state and continuous dynamic modes (continuous variation of the residence time), and to validate the techniques against one another, and against conventional batch (beaker) screening.

3. To model the reaction kinetic parameters (rate constants, reaction order) and reaction mechanism, and validate it using experimental data.

4. To characterise the performance of the jacketed and non-jacketed mesoscale-OBR system for an exothermic reaction in batch and continuous multi steady-state, and to compare the results to conventional jacketed and unjacketed beakers in batch mode.

5. To develop and evaluate a thermosyphon mesoscale-OBR for a highly exothermic reaction.

Chapter 3 Materials and methods

The methods and instruments used in reactor characterization and continuous screening of imine synthesis in a centrally baffled mesoscale oscillatory baffled reactor (mesoscale-OBR) are described in this chapter. The mesoscale-OBR was characterized over a wide range of net flows and oscillatory conditions to determine its residence time distribution behaviour, and associated degree of plug flow. The results were used to investigate the kinetics of an imine reaction in a continous mode using a typical reagent-solvent mixture to suppress the exotherm generated during the reaction. This was conducted through continous multi-steady state and dynamic screening, varying one or more parameters (residence time and molar ratio of benzaldehyde to n-butylamine). Dynamic screening through multiple sets of different types of imine reactions was also conducted to obtain data without having to refill and discharge. This demonstrates the flexibility and advantages of the mesoscale-OBR system as a screening platform for obtaining data rapidly and logically. Comparison to batch mesoscale OBRs and standardized laboratory beakers was also carried out. The data was collected *in situ* using infrared spectroscopy (IR) with second derivative data treatment applied.

The imine reaction was also conducted solvent-free using the mesoscale-OBR to exhibit the heat transfer advantages of the system. The screening was carried out using a jacketed mesoscale-OBR and a mesoscale-OBR coupled with a thermosyphon heat pipe system. This was compared to the non-jacketed mesoscale-OBR system to evaluate the effects of imposing greater isothermality during the synthesis.

3.1 Chemicals

The reactants used in this study were *n*-butylamine ($C_4H_{11}N$), benzaldehyde (C_7H_5O), *o*-tolualdehyde (C_8H_8O), *p*-tolualdehyde(C_8H_8O) and *m*-tolualdehyde(C_8H_8O). All were >98% pure and were supplied by Sigma-Aldrich. *N*-hexane (*n*-C_6H_{14}) with >95% purity was used as a solvent in the kinetics experiments. Benzaldehyde was diluted in n-hexane to 0.25 mol dm^{-3} whilst *n*-butylamine was prepared at a set of various concentrations of 0.25, 0.50, 1.00 and 1.50 mol dm^{-3}. For *o*-tolualdehyde, *p*-tolualdehyde and *m*-tolualdehyde, the reactions were conducted at a molar ratio of 1:1 of the aldehyde to amine at the concentration of 0.25 mol dm^{-3}.

3.2 Experimentation Methods

Each "mesoreactor" consisted of a glass tube of 360mm length and 5.0mm inner diameter inserted with central baffles, giving a total working volume of 7mL (Figure 3-1a). The central baffles (axial baffles) were hexagonal stainless steel solid discs (approximately 4mm diameter) periodically spaced 1.5 tube diameters apart along a 2 mm rod as presented in Figure 3-1b (Phan and Harvey, 2010; Phan *et al.*, 2011a). The outlet of the reactor was modified from the 5mm diameter to 20mm diameter to accommodate the IR probe for analysis purpose (Figure 3-2).

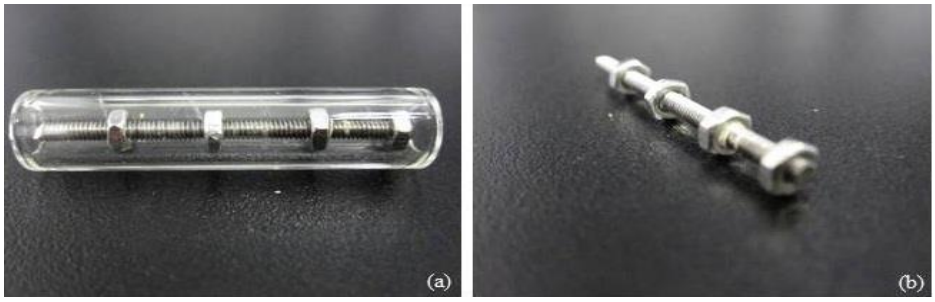

Figure 3-1: (a) Mesoscale-OBR glass tube inserted with central baffle and (b) central baffle with hexagonal stainless steel solid disc along a 2mm rod.

Figure 3-2: (a) Modified mesoscale-OBR for in-situ analysis using IR spectroscopy and (b) normal mesoscale-OBR

The central baffles design was used in the present work as it is suitable for the continuous single phase liquid-liquid imine reaction screening understudy. Apart from

that, the design has not been tested with the reaction system conducted (single phase liquid-liquid). Compared to the integral baffled design, the number of tank-in-series (N) of the central baffles at different Re_o (10 to 700) and Re_n (1.27 to 34) was always at minimum of 10 which reflects to a plug flow behaviour(Phan and Harvey, 2010; Phan *et al.*, 2011a). This gives wider operation window in changing the residence time (flowrates) during the screening process while maintaining the plug flow condition. With the imine reaction understudy in the present work (i.e. benzaldehyde with n-butylamine), it does not involved any usage of solid catalyst, with that the less constricted baffles design (helical baffles) was not used.

3.2.1 Characterisation of the Modified Mesoscale-OBR

The experimental set-up and diagram used to characterise the reactor is shown in Figure 3-3. Figure 3-4 is the schematic of the same equipment. A similar experimental set-up was used in the imine screening using the mesoscale-OBR. This is later described in section 3.2.3. Three PVM Confluent syringe pumps (Eurodyne Ltd.) were used to provide net flows, inject the tracer (benzaldehyde 98% purity) and oscillate the fluid (hexane was used as the working fluid).

Prior to an experiment, the pump systems and reactor must be air-free by filling the system with the working fluid (hexane). The pumps were set to the desired oscillation condition by adjusting frequency and amplitude and net flow (Re_n). The oscillation frequency was determined by the speed of piston movement whilst the oscillation amplitude was obtained by the amount of liquid dispensed. Approximately 0.5mL of benzaldehyde was injected at the highest flowrate of ~3400 mL/hr (Re_n=470) to obtain a sharp pulse injection (Phan and Harvey, 2010). At the outlet of the reactor, the IR probe was immersed to monitor the reaction progress. The C=O peak at 1714cm^{-1} was measured and monitored until the peak height was zero. The conversion of the peak height-time data to tracer concentration-time was conducted directly due to the linear relationship of the both parameter according to Beer-Lambert law (Conley, 1972).

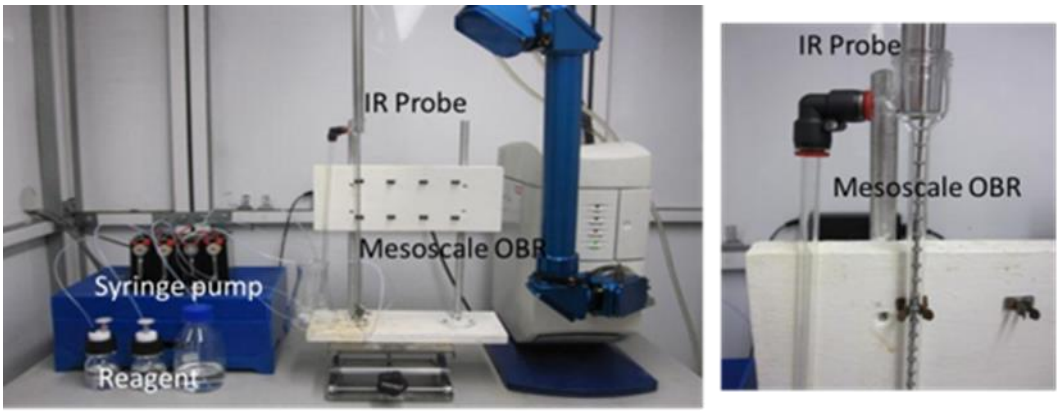

Figure 3-3: Experimental set-up for plug flow determination using a mesoscale-OBR

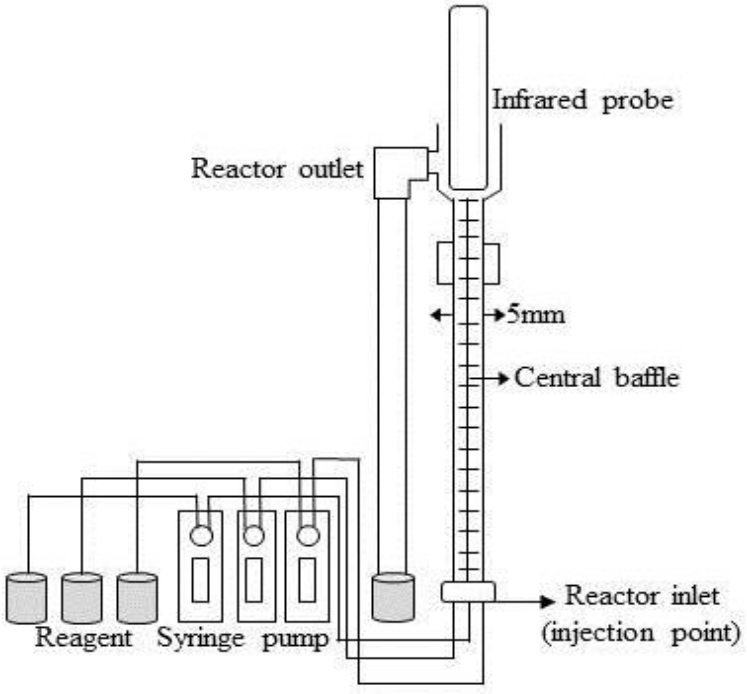

Figure 3-4: Schematic for experimental set-up for characterisation of the mesoscale-OBR

3.2.2 Characterisation of the Multi-tube Mesoscale-OBR

Three different designs of baffles were characterised: central (Figure 3-5 (a)), integral (Figure 3-5(b) and helical baffles (Figure 3-5(c)). All the baffles have similar baffle spacing of 1.5 times the tube diameter (7.5mm). The central design consisted of evenly spaced 4mm hexagonal stainless steel solid discs with 36% open cross sectional area (S). This baffle was known as a "sharp edged" baffle. As for the integral design, the baffle open-cross sectional area was 25% and consisted of smooth baffles. Lastly, the

design of the helical baffle was constructed with baffle open-cross sectional area at 26%.

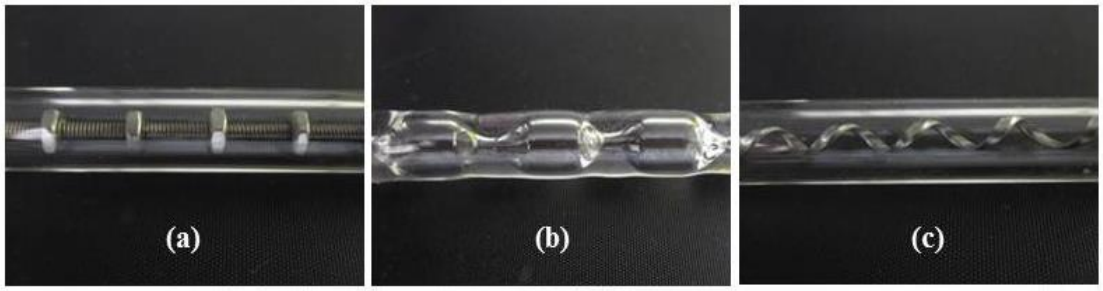

Figure 3-5: Different types of baffled designs; (a) Central baffles; (b) Integral baffles and (c) Helical baffles

The experimental set-up for the multi-tube RTD analysis is shown in Figure 3-6.

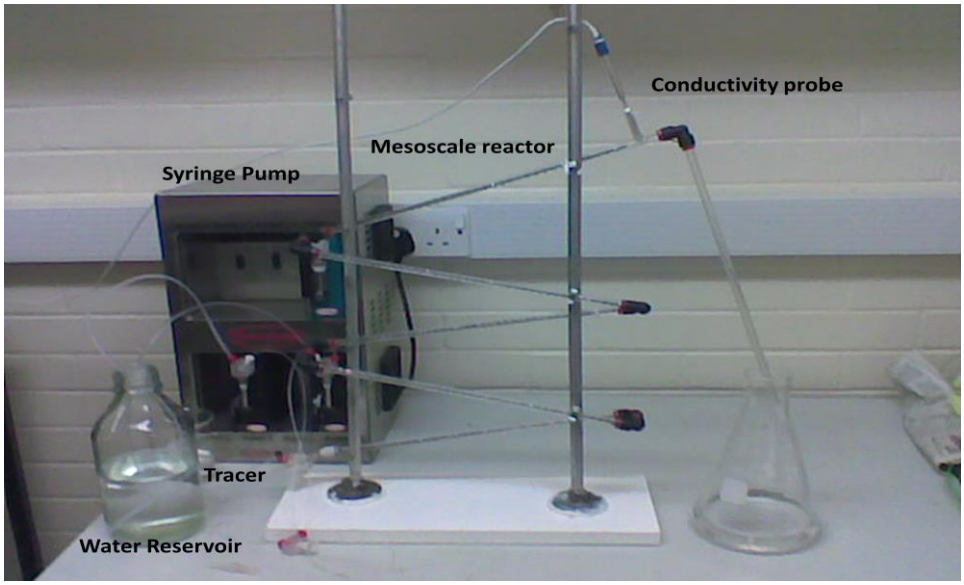

Figure 3-6: Experimental set-up for RTD analysis for multi-tube mesoscale OBR

Three PVM Confluent syringe pumps (Eurodyne Ltd) were used to provide the net flow (water was used in this case), inject the tracer (potassium chloride (KCl)) and oscillate the fluid. Five mesoscale-OBR reactor tubes were used in this characterisation. This is equivalent to approximately 1.4m length with a total volume of 25ml. Before starting the experiment, the pump system and reactor must be air-free. The pumps were set to the desired oscillation condition (frequency and amplitude) and net flow (Re_n). The oscillation conditions were manipulated via the piston movement. The frequency of the oscillation was controlled by the speed of the piston, whereas the amount of water dispensed determined the amplitude. The determination started by injecting 0.5 ml of 3.0 mol dm^{-3} potassium chloride (KCl) tracer at the inlet. This was conducted at the highest flowrate (~3400mL/hr) possible to obtain a sharp pulse in the concentration.

Together with this, the system was continously filled with water dispensed from the reservoir. At the outlet, the conductivity was measured using a 4mm diameter of 2-pole conductivity probe (E61014) connected to a CDM210 conductivity meter (Hach-Lange Ltd). This measurement was conducted until the reading returned to zero following the pulse. The data was collected using a "Picolog" recorder and analysed using a spreadsheet package (Excel). This process was repeated for various different baffle designs and Re_ns. However, Phan *et al.* (2011a) showed that the RTD (E(θ) was independent of the injection pulse volume and the tracer concentration (Figure 3-7) in the same conditions.

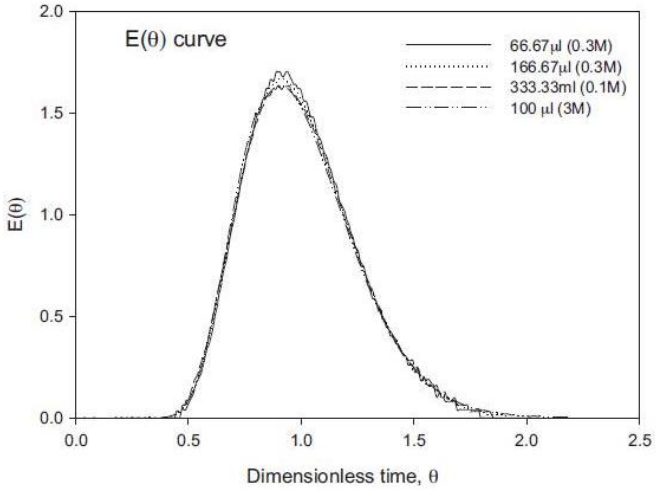

Figure 3-7: E curves for different tracer concentration and flow at 2mm and 6Hz

However this characterisation will be discussed in Appendix G. This is because the outcome of this determination is not related with the main objective of the main results and discussion chapter.

3.2.3 Reaction in a Mesoscale-OBR

The experimental set-up for the imine synthesis was similar to the characterisation experiment shown in section 3.2.1. Two syringe pumps (Eurodyne Ltd.) were used for providing reagent net flows (benzaldehyde and n-butylamine) and the other was used for oscillating the reaction mixture. The oscillation conditions (via frequency and amplitude) and net flow of the reagents (Re_n) were adjusted to the desired value via a computer.

3.2.3.1 Solvent Reaction of Imine Synthesis

3.2.3.1.1 Batch Reactions Screening

At a temperature of approximately 25^{o}C, reactions in batch were performed by dispensing *n*-butylamine and benzaldehyde into the reactor at the same flow rate (stoichiometric molar ratio of 1:1) until the reactor was filled and the tip of the IR probe was covered with the reaction mixture. The mixing conditions (oscillatory Reynolds numbers, Re_o) were in the range 35- 400, which represents mixing regimes from "low" to "high" intensity. The highest flow rate of the syringe pump was used (~3400 mL/hr) for individual reagents to minimise the filling time. As soon as the reaction mixture reached the tip of the IR probe (about 15s), the IR started recording the spectra of the reaction. Each spectrum was taken at 15s intervals for 60 min. The 15s interval period was used as it was the quickest interval available with the IR data collection system in monitoring the reaction trend *in situ* visually. The same procedure was applied to investigate the reaction at various molar ratios of benzaldehyde to n-butylamine, e.g. 1:2, 1:4 and 1:6 at the oscillation condition Re_o=62.

3.2.3.1.2 Continuous Steady-state and Dynamic Screening

The mixing condition of Re_o = 62, corresponding to an oscillation amplitude of 1mm and frequency of 1Hz, was chosen because it provided a high degree of plug flow (N~13) for the central baffle design (Phan and Harvey, 2010). Various residence times, corresponding to different flow rates as shown in Table 3-1, were tested at a molar ratio of *n*-butylamine to benzaldehyde of 1:1 of which each residence time was maintained for approximately 4 min. IR data/spectra were collected as soon as the reactor was filled and the IR probe tip was covered. Each spectrum was taken at 15s intervals for 60 min.

Table 3-1: Flow rates at each residence time in steady-state flow reaction using the mesoscale-OBR

Flow rates, mL/hr	**Net flow Reynolds Number (Re_n)**	**Residence time (τ), s**
840	117	30
420	58	60
280	38	90
210	29	120
168	23	150
140	19	180
105	15	240
53	7	480
42	5	600

In "dynamic" screening, the first step (screening at τ=30s) was maintained for approximately 4 min to obtain a steady state whilst each subsequent step change in the residence time lasted for only ~15s. The rapid step changes from one set of conditions to another were conducted to provide a fast ramp input to the system. This was conducted by adding smaller step change between each residence time performed at steady state condition (i.e. between 30s and 60s) which was schematic illustrated in Figure 3-8 and numerically in Table 3-2. The targeted residence time in dynamic screening is referred to the similar residence time conducted in the steady-state screening.

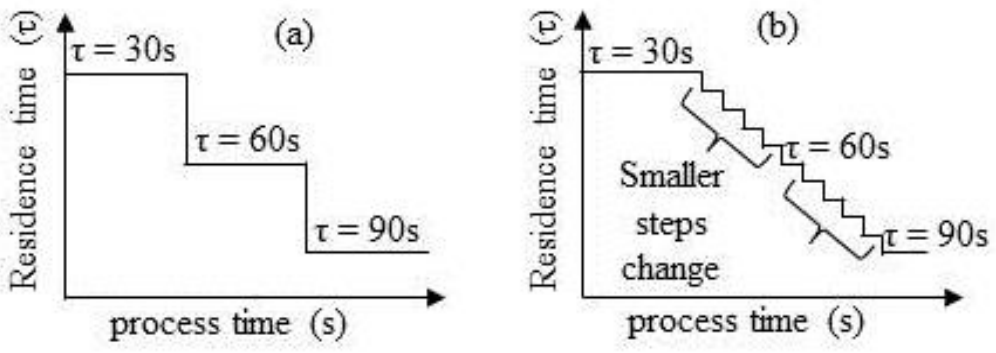

Figure 3-8: Schematic diagram of (a) steady step change and (b) dynamic step change screening conducted using PVM Confluent syringe pumps (Eurodyne Ltd.).

Table 3-2: Smaller step changes between two targeted residence time in dynamic flow reaction using the mesoscale-OBR

Flow rates, mL/hr	**Residence time (τ), s**
840	30 (targeted)
720	35
630	40
560	45
504	50
458	55
420	60 (targeted)

The same procedure for steady-state and dynamic screening was applied for molar ratios of 1:1.5 and 1:2 of benzaldehyde to n-butylamine.

3.2.3.1.3 Continuous Dynamic Multiple Variable Screening

Two variables (residence time and molar ratio of benzaldehyde to n-butylamine) were varied by changing the flow rate of each reagent at an oscillation condition Re_o of 62 as illustrated in Table 3-3 for a residence time from 210 to 240 s. The initial condition of the screening (τ=30s, 1:1 ratio of benzaldehyde to *n*-butylamine) was maintained at 4 min to obtained a steady-state profile. A similar subsequent procedure for dynamic screening as in section 3.2.3.1.2 was used with about ~15 s for each of the residence time steps.

Table 3-3: Flow rates at two targeted residence times in a dynamic flow reaction for multivariable screening using the mesoscale-OBR

Flow rates, mL/hr (Benzaldehyde)	**Flow rates, mL/hr (N-butylamine)**	**Residence time (τ), s**	**Molar ratio of Benzaldehyde to N-butylamine)**
94	121	210 (targeted)	1:1.3
84	113	215	1:1.3
75	104	220	1:1.4
65	95	225	1:1.5
55	86	230	1:1.6
46	77	235	1:1.8
35	69	240 (targeted)	1:2.0

3.2.3.1.4 Continuous Dynamic Screening of Different Imine Synthesis

A schematic of the experimental set-up for screening different imine synthesis is shown in Figure 3-9.

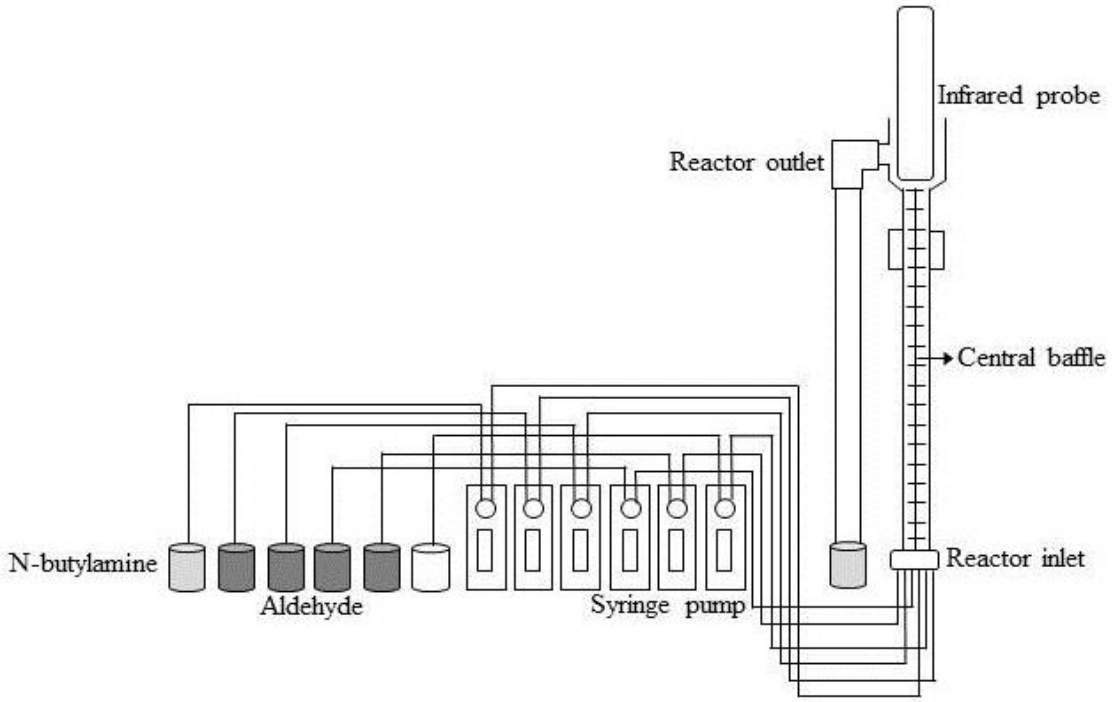

Figure 3-9: Schematic diagram for experimental set-up for dynamic screening of different imine using mesoscale-OBR

Six pumps were allocated to conduct the reaction screening continuously. Four syringe pumps (Eurodyne Ltd.) were used for providing aldehyde net flows (*p*-tolualdehyde, *o*-tolualdehyde, *m*-tolualdehyde and benzaldehyde), one for providing *n*-butylamine net flow and one was used for oscillating the reaction mixture. This screening involved repeated cycling of the dynamic screening procedure for reaction of *n*-butylamine with *p*-tolualdehyde followed by *o*-tolualdehyde, *m*-tolualdehyde and benzaldehyde respectively. This sequence was used due to the similar absorption peak of C=O stretching for p-tolualdehyde and m-tolualdehyde at 1711cm^{-1} (Figure 3-10) using IR analysis.

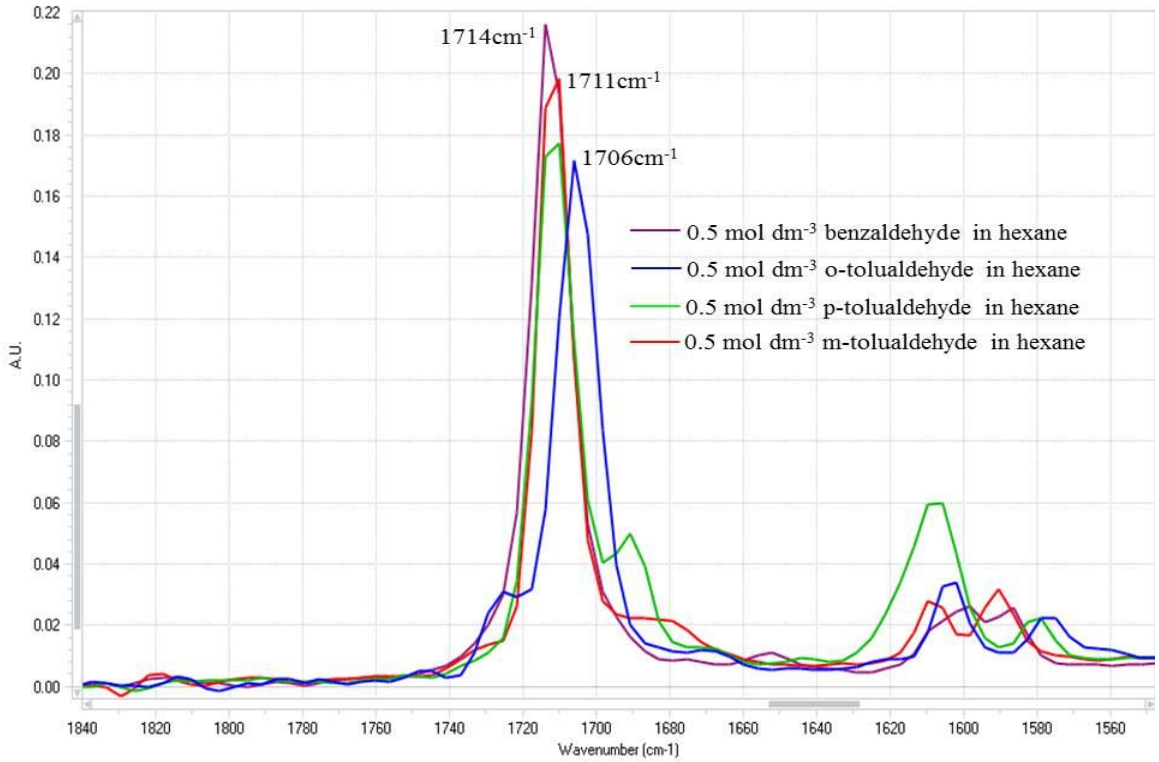

Figure 3-10: Infrared Spectra for C=O streching of benzaldehyde, o-tolualdehyde, p-tolualdehyde and m-tolualdehyde in hexane.

This allowed clear determination and observation during the screening process without overlapping peak occurrence. Each cycle was screened from 30s to 600s residence time at a stoichiometric ratio of 1:1 with oscillation condition (Re_o) of 62. Similar detailed dynamic screening procedure was used, as mentioned in section 3.2.3.1.2, which involved maintaining the initial screening condition (30s) at approximately 4 min to obtain a steady state profile. Once this was completed, the conditions were altered rapidly in small steps, one every 15 s, for every residence time. Screening IR data/spectrum was collected at intervals of 15 s.

3.2.3.2 Non-Solvent Reaction of Imine Synthesis

3.2.3.2.1 Thermosyphon Mesoscale-OBR Reactor

The thermosyphon reactor system was a copper tube of 360mm length, consisting of two main units: a 5mm inner diameter mesoscale-OBR reactor placed inside a 20mm outer diameter copper thermosyphon tube (Figure 3-11). The thermosyphon tube was tightened at both ends using end caps to create a sealed tube shown in Figure 3-11 (a). A steam valve was welded near the outlet of the reactor at the side of the thermosyphon to release steam during the outgassing process. Water was used as a working fluid as it covers operating temperatures in the range 30 - 200ºC (Reay and Kew, 2006). For the

mesoscale-OBR, three inlets were welded onto the end cap for the reactor tube, of which two were used to provide net flows into the reactor system and the third to oscillate the reaction mixture. The outlet of the reactor was expanded to 20mm diameter to insert the IR probe for analysis purposes (Figure 3-11(b)).

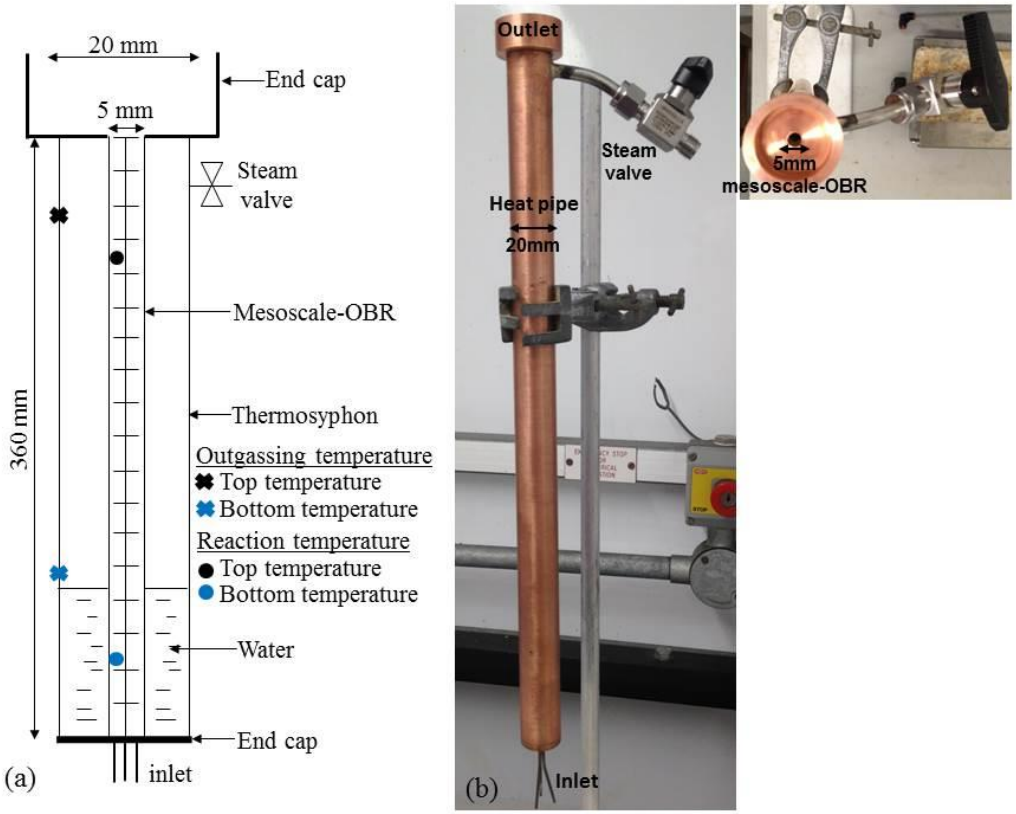

Figure 3-11: Dimension of (a) schematic diagram and (b) photograph of the thermosyphon reactor system for non-solvent imine reaction screening.

3.2.3.2.1.1 Outgassing Process

The outgassing for the thermosyphon mesoscale-OBR was conducted to release trapped gas inside the thermosyphon tube system. Two methods were applied and evaluated for this determination as shown in Table 3-4.

Table 3-4: Outgassing methods conducted in the thermosyphon meso-OBR system to obtain isothermal condition along the system

Method A	50mL water (50% volume of the thermosyphon) was pumped into the system. The reactor was heated (direct contact with fire) and steam was condensed at the steam-valve outlet. The process was stopped and the steam valve was closed after 20mL water was collected.
Method B	30mL water was pumped into the system. The reactor was heated (direct contact with fire) with a valve closed. Once the temperature of the top and bottom for the annular section (5cm and 28cm from the outlet, respectively) reached ≥100^{o}C, the valve was opened and closed immediately to release a small portion of the steam formed inside the reactor.

3.2.3.2.1.2 Imine Reaction Screening

A similar procedure as that described in sections 3.2.3.1 (for batch) and 3.2.3.1.2 (for the steady-state screening) at a stoichiometric ratio of 1:1 of benzaldehyde to *n*-butylamine but without solvent was used for imine reaction screening. Two thermocouples were inserted inside the mesoscale-OBR at the distances of 10cm and 30cm from the outlet to measure the temperature inside the system.

3.2.3.2.2 Jacketed Mesoscale-OBR

The modified mesoscale-OBR reactor system was jacketed to perform non-solvent imine reactions (Figure 3-12). Cool water (~13^{o}C) at 186 mL/min flow rate was used as the cooling fluid during the imine screening process. Two thermocouples were inserted at a distance of 10cm and 30cm from the outlet. Similar procedures described for the imine synthesis in sections 3.2.3.1 (for batch) and 3.2.3.1.2 (for steady-state continuous screening) were also applied for this work.

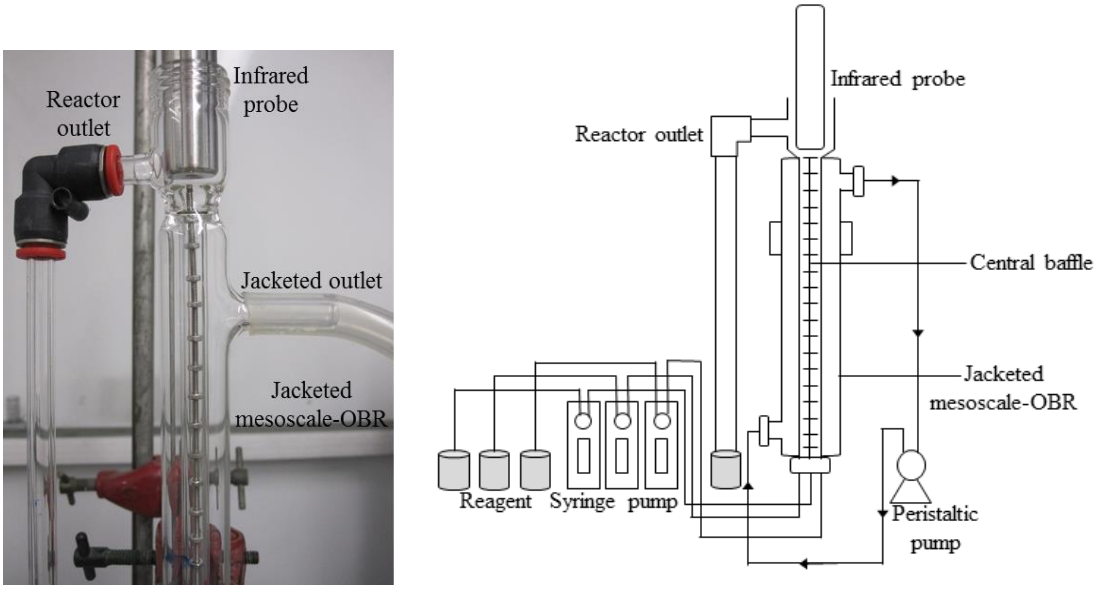

Figure 3-12: Jacketed modified mesoscale-OBR experimental set-up for non-solvent imine synthesis.

3.2.4 Reaction in Beakers

3.2.4.1 Batch Reactions in Beakers

The 1-butanamine, N-(phenylmethylene) reaction was also carried out in a beaker at a temperature of 25^{o}C for comparison as shown in Figure 3-13. Approximately 40 mL of n-butylamine (0.25mol dm^{-3}) and 40mL benzaldehyde (0.25mol dm^{-3}) were added into a 100mL beaker. The reaction mixture was agitated using a magnetic stirrer set at a speed range of 200rpm – 1200rpm, equivalent to an impeller Reynolds number (Re_{imp}) from 3000-14700 (Raju *et al.*, 2005). The reaction spectra were continuously taken at 15 s interval for 60 min by immersing the IR probe at the middle of the beaker.

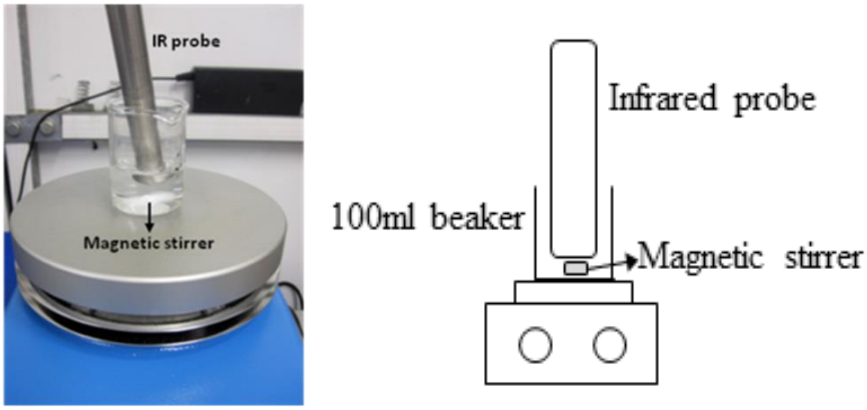

Figure 3-13: Experimental set-up for imine synthesis using a 100 mL beaker

This same process was applied for *o*-tolualdehyde, *m*-tolualdehyde and *p*-tolualdehyde at a mixing speed of 537rpm. This mixing speed was used as it gives moderate mixing

vortex. Apart from that, it was shown that there are no effects on the apparent reaction kinetics at different mixing speed (Mohd Rasdi *et al.*, 2013). Similar set-up and procedure was also used for the solvent free reaction of benzaldehyde with n-butylamine at the ratio of 1:1 for the non-jacketed beaker. Similar mixing speed at 5737rpm was used.

3.2.4.2 Batch Non-Solvent Reaction in Jacketed beaker

The non-solvent imine reaction was also conducted in a jacketed beaker for comparison as shown in Figure 3-14. Cool water (~13^{o}C) at 186 mL/min flow rate was used as the cooling fluid during the imine reaction screening. Temperature was recorded by using a thermocouple immersed at the centre of the reaction mixture. Similar procedure as describe in section 3.2.4.1 was also applied for this determination.

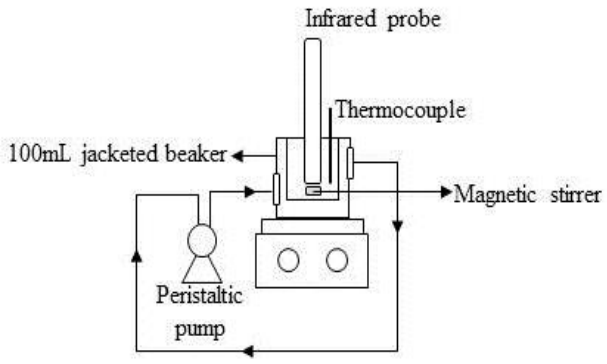

Figure 3-14: Schematic set-up for non-solvent imine synthesis using a 100mL jacketed beaker

3.3 Analytical and characterisation methods

3.3.1 Infrared Spectroscopy (IR)

The IR used was a Mettler Toledo ReactIR 4000 equipped with DiComp (diamond) probe with a mercury cadmium telluride (MCT) band detector. The diamond probe was used due to its resistance in any acidic or alkaline solution ranging from pH 1-14 with temperature tolerance from -80 to 200^{o}C. The range of detected functional wavenumber of the diamond probe is 4000-2250cm^{-1} and 1950-650cm^{-1}. The blind spot in the region of 2250-1950cm^{-1} was due to diamond absorption of the infrared energy, which masks a few functional group frequencies, such as the isocyanate and azide. The consistency and accuracy of the spectrum/data collected with the IR instrument was assured through the determination of the signal to noise ratio (SNR) together with the collection of

background spectrum prior to each experiment. The SNR for the instrument was maintained at the range of 2500-3500 to give better detection of the sample (Toledo, 2010) and to minimise variation between the experiments conducted. To eliminate any instrument response in the desired spectrum, a background spectrum of air was collected.

The experiments spectrum and data for peak heights were recorded using an iC-IR vers. 4.2.26 software at a resolution of 8cm^{-1}. All collected spectrum data were treated using a second derivative method (refer to section 2.6) to improve the detectability of small and/or overlapping peaks on a main band. Peak-zero method (refer to section 2.6) was used for the quantitative analysis prior to this second derivative method. Through this peak-zero method it fixed the baseline at zero regardless of any changes or movement on the peak under study (C=O stretching). As shown in Figure 3-15(a) below, the reduction of benzaldehyde (peak at 1714cm^{-1}) and the formation of imine (peak at 1652cm^{-1}) obtained during the reaction was difficult to determine without a derivative treatment. The baseline shifts between measurements and the peaks of benzaldehyde and imine overlap with other peaks. However, when using the second derivative data treatment as shown in Figure 3-15(b), these peaks were isolated, with a clear, sharp peak on the same baseline.

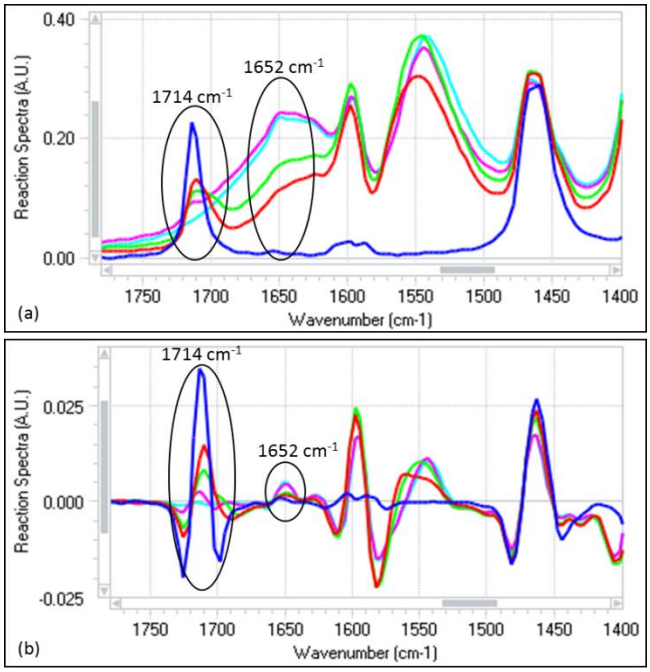

Figure 3-15: Reaction spectrum of imine synthesis (a) without second derivative treatment (b) with s derivative treatment.

3.3.2 Syringe Pumps

A syringe pump (Eurodyne Ltd.) was coupled to a flexible plunger and driven by a stepper motor with a speed moving from 1.2 s to 20 min for each full stroke. Different sizes of glass syringes were used together with the pump, which range from 1mL to 5mL. Glass material was chosen to eliminate any side reactions occurring during its application. The pumps were controlled via a computer using "Sapphire" software. List of common commands used for the system are listed in Appendix D. The syringe was calibrated by measuring the volume dispensed using graduated cylinder.

3.3.3 Calibration Curve

3.3.3.1 Aldehyde Calibration

A set of various concentrations (0.0-1.0 mol dm^{-3}) of benzaldehyde solutions were prepared at room temperature (approximately 25^{o}C) using hexane as a solvent. The set chosen covered the concentration range of the experiments. A spectrum for each solution was taken at 15s intervals for 3 min to provide 12 data points for every analysis conducted. A peak height at a wavenumber of 1714cm-1 was extracted from the spectrum. This represents the carbonyl stretch in aldehyde species. The average value from 12 data points for each solution was plotted to establish a relationship between the peak height and benzaldehyde concentration. The same procedure was applied for o-tolualdehyde, p-tolualdehyde and m-tolualdehyde.

3.3.3.2 1-butanamine, N-(phenylmethylene) Calibration

As the imine product of 1-butanamine, N-(phenylmethylene) from benzaldehyde and n-butylamine is not available in the market, the product was synthesised via batch method using mesoscale-OBR. This was conducted at the concentration of 0.25 mol dm^{-3} for each reagent at the molar ratio of 1:1 of the benzaldehyde and n-butylamine in hexane as the solvent. The reaction was completed once the C=O peak at 1714cm^{-1} reached zero peak height. Next the solvent (hexane) was removed from the mixture through rotary evaporator. Finally, the sample obtained after the rotary evaporation was analyse using the IR and NMR before being used in preparing the calibration curve.

The calibration curve were constructed at a set of various concentrations (0.0-0.6 mol dm^{-3}) using hexane as the solvent. This was prepared at room temperature

(approximately 25°C). Similar procedure as in section 3.3.3.1 was used in collecting the data which involved a spectrum taken at a 15s interval for 3 min. This provides 12 data appoints for each concentration analyse. Peak at 1652cm^{-1} was used to extract the data which represent the C=N bonding in the imine species. The data collected was plotted to establish the relationship of the concentration and peak height.

3.3.4 Quantification of the Residence Time Distribution

The quantification of residence time distribution (RTD) in this study was based on the statistical moment method, and used the mean residence time (τ), distribution curve (E(t)), variance (σ) and skewness. These variables were transformed to their dimensionless forms (eq.3-1 to eq.3-5) to give a better comparison of the measurements with diferent process parameters.

Mean residence time: $\tau = \dfrac{\sum_i t_i C_i \Delta t_i}{\sum_i C_i \Delta t_i}$ eq. 3-1

Dimensionless time: $\theta = t_i/\tau$ eq. 3-2

Distribution curve: $E(\theta) = \tau E(t) = \tau(C_i/\sum_i(\Delta t_i C_i))$ eq. 3-3

Variance: $\sigma(\theta)^2 = \sigma(t)^2/\tau^2 = \sum_i [(t_i - \tau)^2 E(t)\Delta t_i]/\tau^2$ eq. 3-4

Skewness: $\gamma(\theta)^3 = \gamma(t)^3/\sigma(t)^3$

$= \sum_i [(t_i - \tau)^3 E(t)\Delta t_i]/(\sum_i (t_i - \tau)^2 E(t)\Delta t_i)^{3/2}$ eq. 3-5

….where C_i the existing tracer concentration at time t_i and Δt_i is the interval between two measurements.

The E(θ) curve shows the distribution of the tracer injected inside the system. This varies according to the flow behaviour, e.g. a narrow and symmetric distribution represents plug flow behaviour, whereas a monotonic decay with a long tail indicates mixing inside a reactor similar to that of a stirred tank. Variance (eq.3-4) and skewness (eq.3-5) parameters are used to characterize this E(θ) curve, e.g. $\sigma(\theta)^2$ and $\gamma(\theta)^3$ are zero when plug flow is achieved.

The tanks-in-series (N) model was used to represent the flow in mesoscale-OBR. The model is based on a fluid flowing through a series of perfectly mixed tanks. This model was used in this study with an assumption that the mixing in each baffle cavity was

similar and uniform. This validated the usage of the model for the mesoscale-OBR system. This method is simple and flexible yet effective in determining the plug flow behaviour of a reactor system because it describes the system in one parameter (number of N) (Levenspiel, 1999). The quantification for the model used the number of tank-in-series which is obtained from the RTD curve (eq.3-6). In order to approach a Gaussian RTD curve, which reflects plug flow behaviour, the number of tank-in-series (N) must be ≥10 (Figure 3-16) (Levenspiel, 1999; Phan *et al.*, 2011a).

$$E(\theta) = \tau E(t) = [N(N\theta)^{N-1}/(N-1)!]\, e^{-N\theta} \qquad \text{eq. 3-6}$$

The N was determined from the experimental data using an initial estimated N shown in eq.3-7. The RTD curve obtained from the experimental data (eq.3-3) and initial estimated value of N (eq.3-9) was compared in terms of shape, spread and height of the curve distribution until the best fit was obtained (Phan and Harvey, 2010; Phan *et al.*, 2011a).

$$\sigma(\theta)^2 = \sigma(t)^2/\tau^2 = \int_0^\infty (\theta-1)^2 E(\theta) d(\theta) = 1/N$$

$$N = 1/\sigma(t)^2 \qquad \text{eq. 3-7}$$

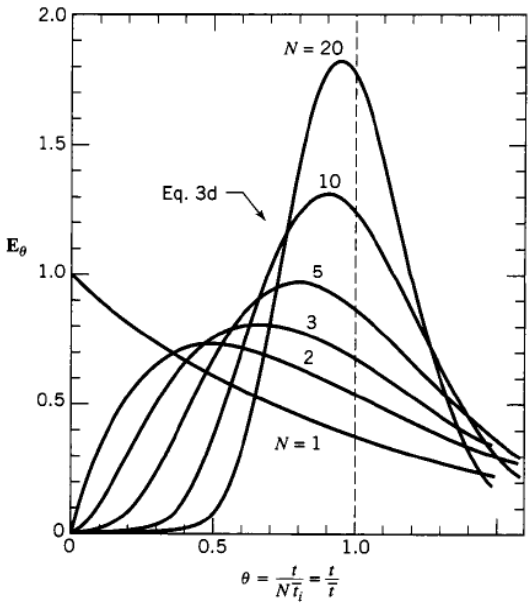

Figure 3-16: Residence time distribution curve for the tank-in-series model (Levenspiel, 1999)

3.4 Kinetic Modelling of Imine Synthesis

3.4.1 Expression of Reaction Rates

Generally, the chemical reaction path for the imine reaction process was represented through a reversible process, with (eq.3-8) (Jencks, 1959; Layer, 1963; Rotondo *et al.*, 1976) and with negligible formation of intermediates (eq.3-9) (Saggiomo and Lüning, 2009). Differences between the former and latter reaction expression are associated with the type of catalyst. The former was conducted in the presence of acid catalysts, whereas the latter was performed without acid catalysts. However, there is also available literature describing using a stoichiometric equation that contains an irreversible reaction with the negligible formation of the intermediates (eq.3-10) (Crowell and Peck, 1953; Cordes and Jencks, 1962; Guzen *et al.*, 2007). The reasons for these differences are due to many factors, such as the types of aldehyde and amine, solvents and catalyst used. This indicates that the mechanism of the reaction can vary. Due to the several different possibilities of the reaction mechanism, mathematical modelling was used to facilitate understanding the 1-butanamine, N-(phenylmethylene) reaction process in hexane, and to obtain its reaction kinetic parameters. With modelling, it is possible to validate easily different proposed mechanism paths. The validation was conducted through comparison with the experimental data. An example of four reaction mechanisms proposed are shown in eqs.3-8 to .3-10, below, which contain the reaction paths mention previously, but with the addition of the reaction path shown in eq.3-10. The addition reaction path (eq.3-10) was proposed to try to understand the effect of combining the irreversible reaction and the formation of intermediates. Although the tetrahedral intermediate was reported to be too unstable and reactive to detect via analytical instruments (Evans *et al.*, 2002; Iwasawa *et al.*, 2007), the reaction kinetics related to its formation can be predicted with the mathematical modelling method.

$$A + B \underset{k_{-1}}{\overset{k_1}{\leftrightarrow}} C \underset{k_{-2}}{\overset{k_2}{\leftrightarrow}} D + E \qquad \text{eq. 3-8}$$

$$A + B \underset{k_{-1}}{\overset{k_1}{\leftrightarrow}} C + D \qquad \text{eq. 3-9}$$

$$A + B \xrightarrow{k_1} C + D \qquad \text{eq. 3-10}$$

$$A + B \xrightarrow{k_1} C \xrightarrow{k_2} D + E \qquad \text{eq. 3-11}$$

…where A, B, C, D and E represent benzaldehyde, n-butylamine, intermediate, imine and water, respectively. k_1 and k_2 are the forward rate constants, and k_{-1} and k_{-2} the reverse rate constants.

The proposed reaction mechanisms were expressed as ordinary differential equations (ODEs). Here, each ODE is a derivative function that provides changing rate with respects to its independent variable. Typically, an initial or boundary value is needed to solve these types of functions. Also known as the hard-modelling method, the related kinetic parameters (rate constant and reaction order) were adjusted until they adequately fitted the experimental data within the error limits of the measurement. Below listed are the example of the ODEs for eq.3-14 reaction model (Table 3-5).

Table 3-5: Example of ordinary differential equations (ODE) for irreversible reaction with the formation of intermediates proposed for (1-butanamine, N-(phenylmethylene)) synthesis.

Reaction mechanism model	**Ordinary Differential Equations (ODE)**
$A + B \xrightarrow{k_1} C \xrightarrow{k_2} D + E$	$\frac{dA}{dt} = -k_1[A]^m[B]^n$ $\frac{dB}{dt} = -k_1[A]^m[B]^n$ $\frac{dC}{dt} = k_1[A]^m[B]^n - k_2[C]^o$ $\frac{dD}{dt} = k_2[C]^o$ $\frac{dE}{dt} = k_2[C]^o$

...where m, n, and o are reaction orders

3.4.2 Modelling Procedure

Kinetic parameters (reaction orders and rate constant) were modelled using MATLAB version R2011a following the procedure shown in Figure 3-17 (following page). The first step was to input the initial concentration for all species involved and initial kinetic parameter value (rate constant and reaction order), based on the proposed reaction mechanism. The present study used the rate constant and reaction orders at a molar ratio of 1:1 (stoichiometric ratio) obtained from experimental data using batch mesoscale-OBR. Then the ordinary differential equation (ODE) of the reaction model was solved numerically using an ODE45 function. The ODE45 is the standard MATLAB solver for the ODE. This function implements fourth and fifth order Runge-Kutta formulae with variable time-step. Generally, solving the ODE through the ODE45 function requires the determination of the mathematical function (right-hand side of eq. 3-12) and the initial condition ($x = x_o$ at time t_o). Comparison between experimental and modelling data was quantified via the sum of squares of errors (SSE) value (eq. 3-13), where the tolerance error was set to be at $\leq 1.0\%$. If multiple data fits gives SSE value $\leq 1.0\%$, the lowest SSE value should be taken as the best fits. Lastly, the reaction order and rate constant value were obtained from the simulated concentration time profile data to represent the chemical reaction.

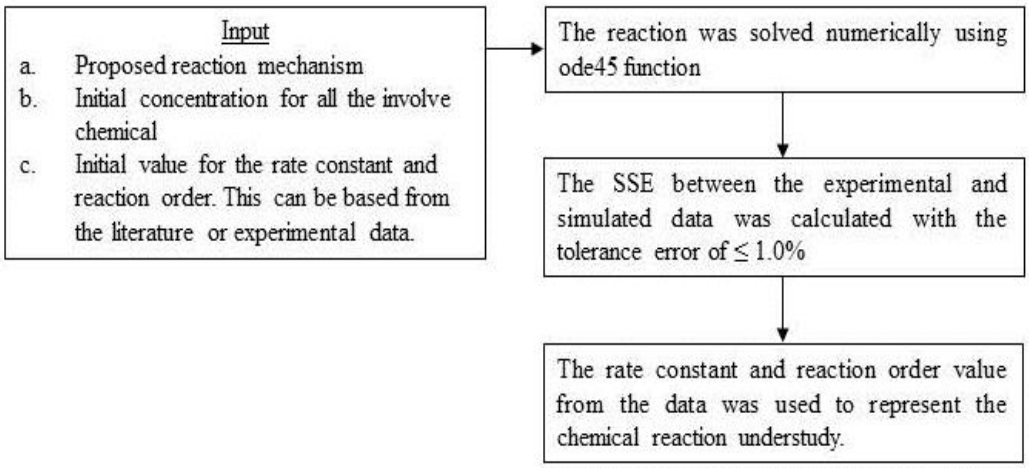

Figure 3-17: Process of obtaining the chemical kinetics parameter

$$\frac{dx}{dt} = f(t, x), \qquad x(t_o) = x_o$$ eq. 3-12

$$sse = \sum(Ci_e - Ci_m)^2 \; x \; 100$$ eq. 3-13

…where Ci_e the experimental concentration and Ci_m the simulated concentration at time *t*.

Chapter 4 Results and Discussions

4.1 Introduction

This chapter presents the results obtained from experiments using the centrally baffled mesoscale OBR, including characterization of the reactor, and imine synthesis with and without solvent in a continuous mode. The flexibility and advantages of continuous screening are discussed and compared with a conventional batch screening method. The kinetics for 1-butanamine, N-(phenylmethylene)- reaction from benzaldehyde and *n*-butylamine were also investigated numerically and experimentally.

4.2 Infrared Spectroscopy (IR)

4.2.1 Quantitative Analysis of Imine Synthesis Reagents

The quantitative infrared technique used in this study involved construction of a calibration curve for the absorption of a known reagent concentration (Beer's Law). It is important to monitor a suitable peak to avoid, for instance, overlapping peaks that will result in a false interpretation of a reaction profile. IR spectra of benzaldehyde and *n*-butylamine are presented in Figure 4-1, below:

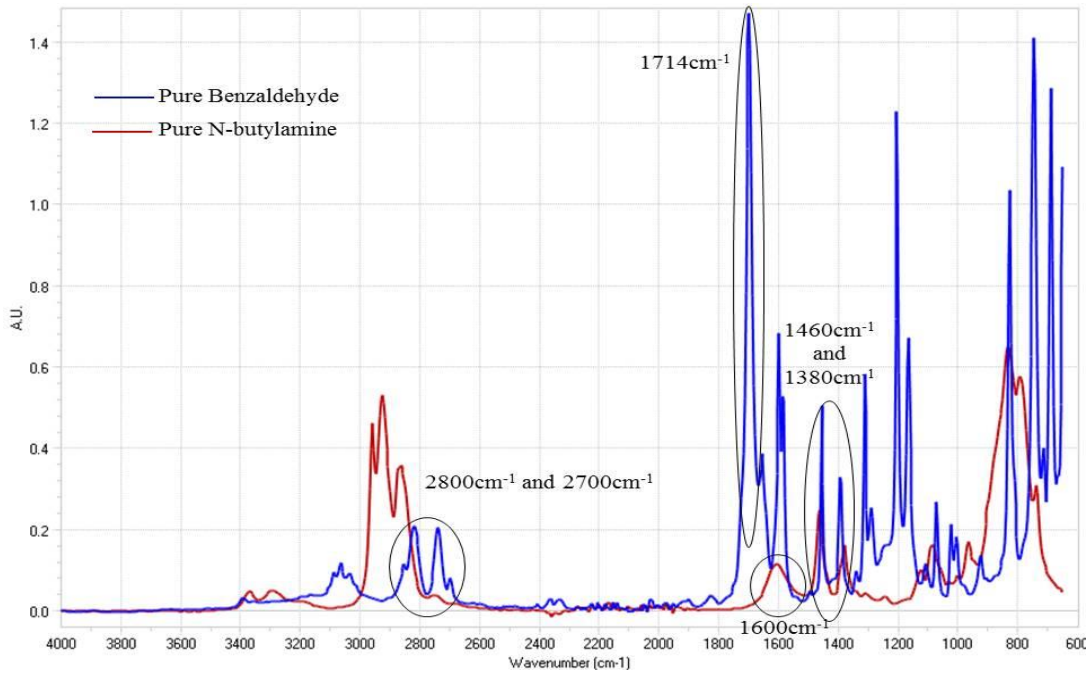

Figure 4-1: Infrared Spectra of benzaldehyde and n-butylamine.

The absorption band assignment at different wavenumbers for these chemicals are well known (Silverstein and Bassler, 1962; Conley, 1972; Morimoto *et al.*, 1974). It is clear that the strongest absorption band, which can be used to quantify the benzaldehyde, was at 1714cm^{-1} for the C=O stretching and the pair peaks at the regions of 2800cm^{-1} and 2700cm^{-1} for the C-H stretches. *N*-butylamine exhibits the NH_2 bending vibration at 1600cm^{-1} and the CH_2 bending vibration at 1460cm^{-1} and 1380cm^{-1}. The common indicative amino-containing substance at peaks at 3370cm^{-1} and 3280cm^{-1} were not evident in a dilute non-polar solution of *n*-butyalmine, although other work (Conley, 1972) showed a clear spectrum in those regions (Figure 4-2). Furthermore, the peaks of *n*-butylamine and benzaldehyde at 1600cm^{-1}, 1460cm^{-1} and 1380cm^{-1} overlapped (Figure 4-1 above) . Therefore, only the C=O peak at 1714cm^{-1} was chosen to monitor the imine synthesis *in situ* in this study.

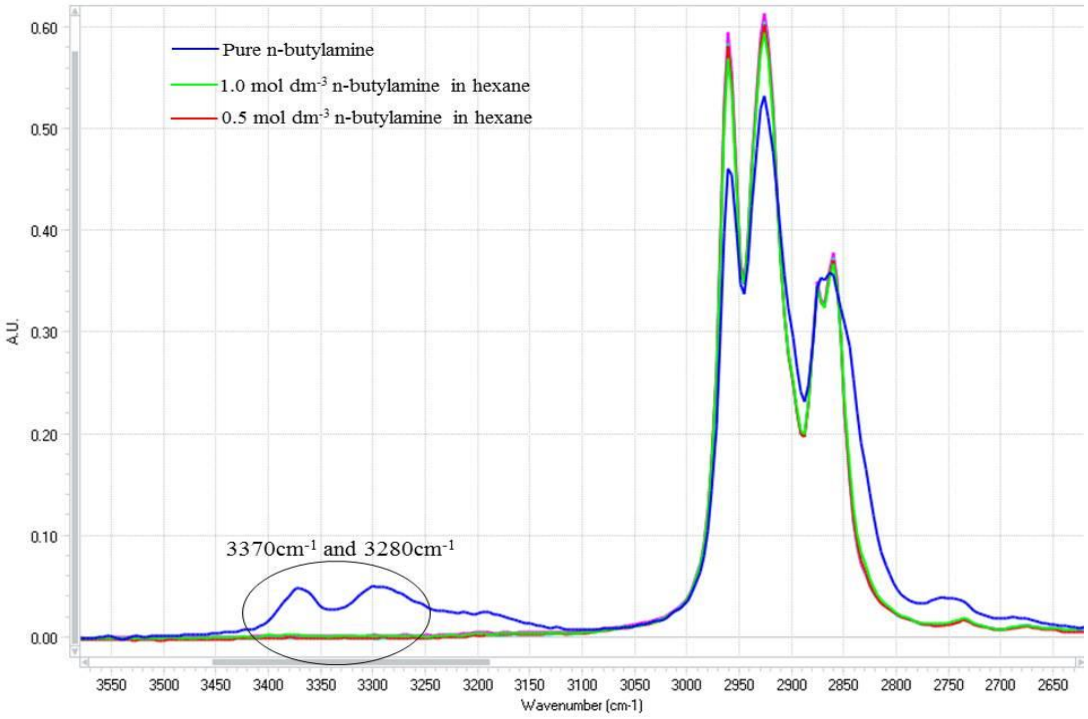

Figure 4-2: Infrared spectrum for *n*-butylamine for pure, 1 mol dm^{-3} and 0.5 mol dm-3 concentration

For *o*-tolualdehyde, *m*-tolualdehyde and *p*-tolualdehyde, a region around the C=O stretch at 1700-1740 cm^{-1} was also used to monitor the reaction. The peaks occurred at 1706cm^{-1} and 1711cm^{-1} as shown in Figure 4-3.

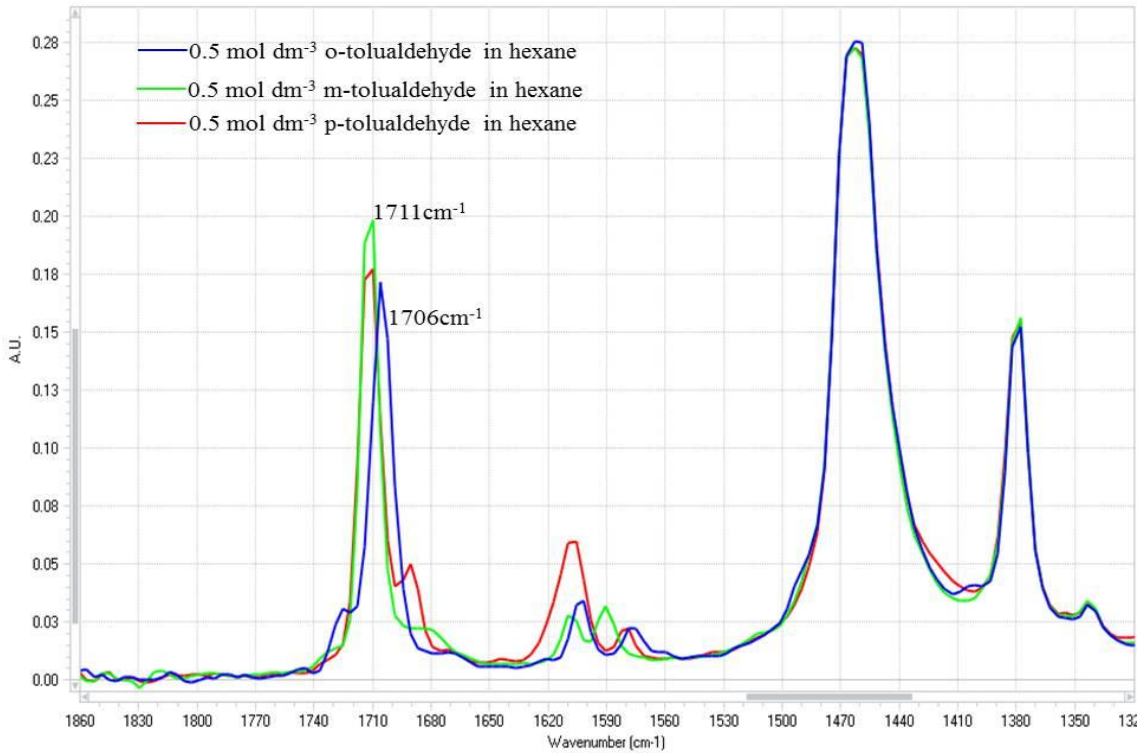

Figure 4-3: Infrared spectra of *o*-tolualdehyde, *m*-tolualdehyde and *p*-tolualdehyde at 0.5mol dm^{-3}

4.2.2 Solvent Effect on Infrared Spectra of Benzaldehyde

As mentioned in 4.2.1, the imine synthesis was monitored *in situ* via infrared spectroscopy (IR) by observing the benzaldehyde reduction at the 1714cm^{-1} peak representing the C=O stretch. This peak did not interfere with the peak from *n*-butylamine and therefore it was used to quantify the benzaldehyde concentration profile. However, the effect of the solvent was not taken into account. This section determines the effect of different solvents on the C=O strectching of benzaldehyde.

Generally, most of the chemical reactions in laboratories or industries are carried out in the liquid phase with the presence of solvents (Buncel *et al.*, 2003). There are many types of solvents available to cater for a wide range of reaction applications and/or synthesis. The interaction of a chemical with a solvent varies depending on its classification, i.e. non-polar, polar aprotic and polar protic solvents. Methanol, chloroform and hexane were used to determine the compatibility of benzaldehyde in this study (Rotondo *et al.*, 1976; Lee *et al.*, 2003; Shah and Shah, 2013).

As shown in Figure 4-4 below, the non-polar (hexane and chloroform) solvents gave strong peak intensities at 1714cm^{-1} compared to the polar-protic solvent (methanol).

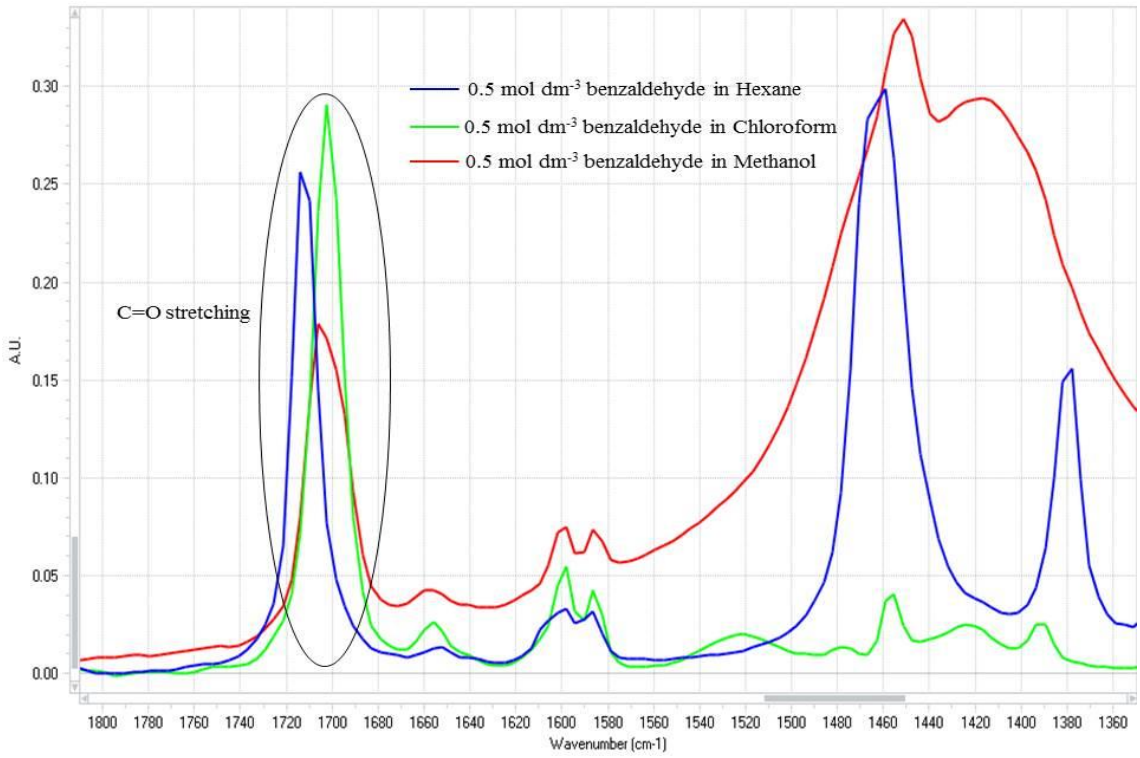

Figure 4-4: Effect of solvents on the C=O stretching in 0.5 mol dm^{-3}benzaldehyde .

This was because the effects of solute-solvent intermolecular interactions in non-polar solvents on the C=O structure were minimal (Conley, 1972; Reichardt, 2006). A homogenous solution in hexane can be achieved because of the compatibility of the carbon chain with the benzene ring of benzaldehyde, whereas in chloroform, the interaction of solute-solvent was between an active hydrogen atom of benzaldehyde and the highly electonegative chlorine atom in the chloroform (Li *et al.*, 2012). The shift in peak wavenumber from 1714cm^{-1} in hexane to 1710cm^{-1} in chloroform was due to hydrogen bond formation in the chloroform (Li *et al.*, 2012). Compared to the polar-protic solvents (e.g. methanol), the interaction of the O-H structure with the C=O was stronger than the interaction between the linear carbon chain of methanol and the benzene ring of benzaldehyde. This reduced the double-bond characteristic of the carbonyl group, leading to a reduction in the peak intensity. This agreed with the findings of Gonjo *et al.* (2011). Although the C=O intensity in methanol was lower than that in the non-polar solvents, the strength intensity for all the three solvents are suitable for the imine synthesis reaction with IR monitoring.

Choosing a solvent is restricted not only by the compatibility with the analytical method, but also the uniformity of the solute dispersion, carcinogenicity, reactivity of the solvent towards the reagent or product and the energetics of the reaction

(exothermic/endothermic). Chloroform was not used in the study due to its carcinogenicity according to International Agency for Research on Cancer (IARC). It was reported (Meadows and Darwent, 1952) that methanol reacted with aldehyde spontaneously to form hemiacetal (Figure 4-5), which reduced the benzaldehyde reactivity to n-butylamine to form imine. Therefore, hexane was chosen as the solvent for this study.

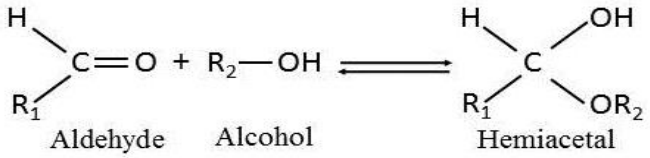

Figure 4-5: Mechanism of the formation of hemiacetal from aldehyde and alcohol

4.2.3 Aldehyde Calibration

A calibration curve of benzaldehyde in hexane was constructed to convert the peak height data collected from the IR into its corresponding concentration. This quantitative analysis would allow calculation of kinetic parameters, such as rate constants and reaction order. The calibration curve for benzaldehyde is shown in Figure 4-6 over a concentration range from 0 to 1.0 mol dm^{-3}. This range was chosen to cover all experiments concentration conducted for the screening work. The correlation coefficient obtained was at R^2=0.988. The fit was substantially non-linear for concentration between 0.1- 1.0 mol dm^{-3} with an average deviation of ~15%.

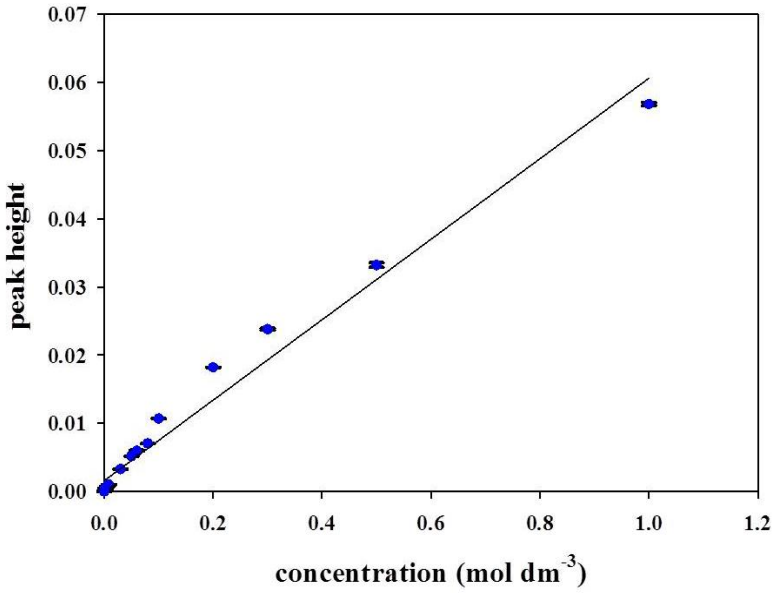

Figure 4-6: Benzaldehyde calibration curve analysis for concentration range from 0.0 to 1.0 mol dm^{-3}.

However, this calibration curve (Figure 4-6) generated negative concentrations, as shown in Figure 4-7. This indicated that the lowest region in the concentration range does not follow Beer-Lambert law.

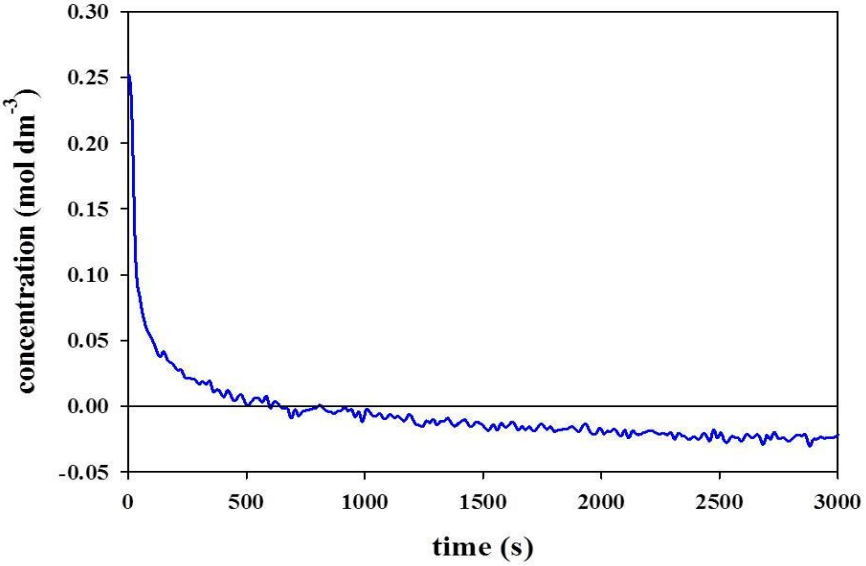

Figure 4-7: Benzaldehyde concentration reduction profile

This suggests that the calibration cannot be described by a simple linear curve, and instead needs to be segmented (see Figure 4-8). 3 different trends have been identified: 0.2-1.0 mol dm^{-3} (Figure 4-8(a)), 0.0018-0.2-mol dm^{-3} (in between the trends in Figure 4-8(a) and Figure 4-8 (b)) and 0.000-0.0018-mol dm^{-3} (Figure 4-8(b)).

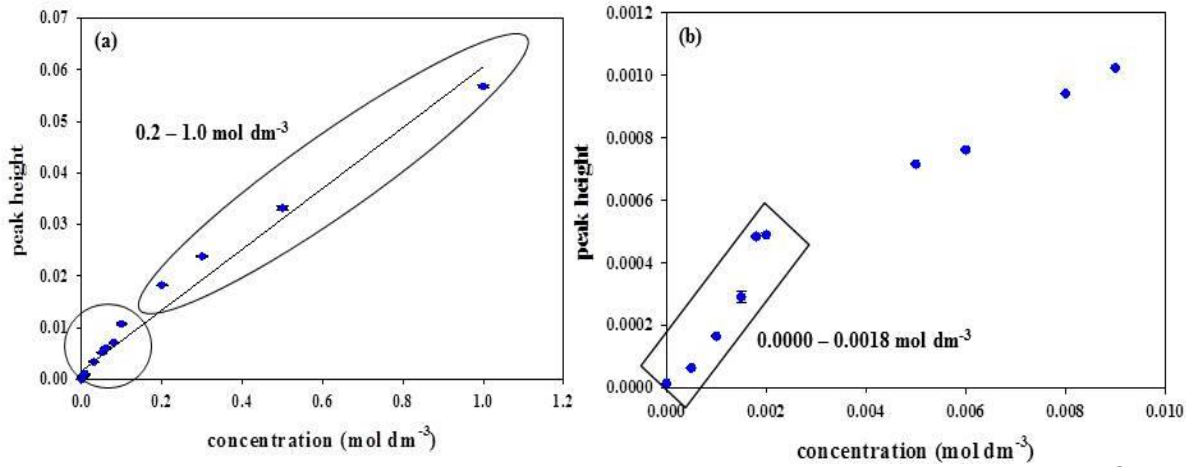

Figure 4-8: Segmented trends of benzaldehyde calibration curve at (a) 0.2-1.0 mol dm^{-3} and (b) 0.0000-0.0018 mol dm^{-3}

A linear relationship was only observed for the concentration ranges of 0.2-1.0 mol dm^{-3} (Figure 4-9(a)) and 0.0018-0.2 mol dm^{-3} (Figure 4-9(b)) with correlation coefficients of

R^2=0.9998 and 0.9964, respectively. For the concentration range of 0.000-0.0018 mol dm^{-3} (Figure 4-9(c)), an exponential relationship was observed with a correlation coefficient of R^2=0.9914.

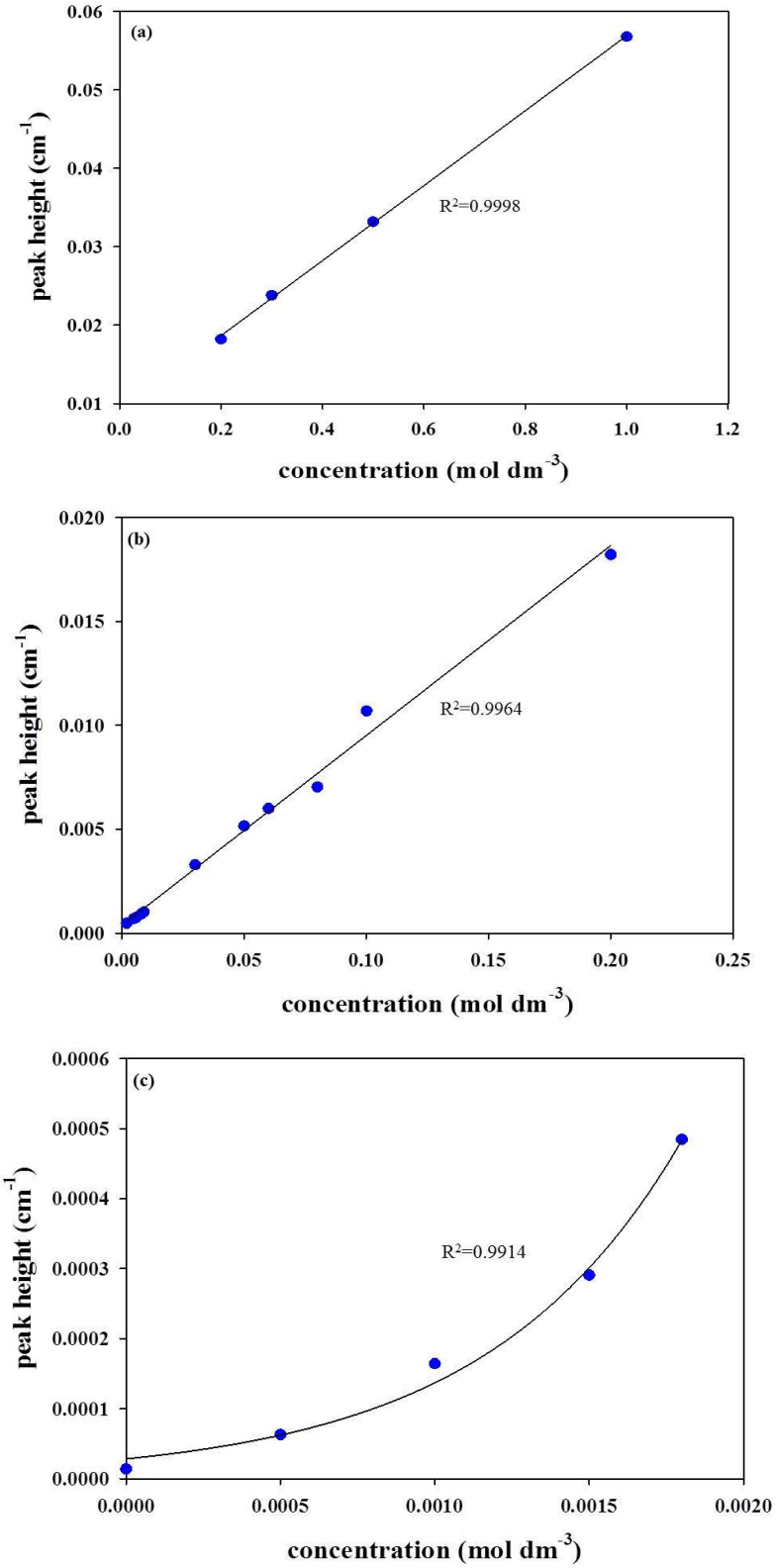

Figure 4-9: Benzaldehyde calibration curves at (a) 1.0-0.2 mol dm^{-3} , (b) 0.2-0.0018mol dm^{-3} and (c) 0.0018-0.000mol dm^{-3}.

With the new calibration curves, benzaldehyde concentration decreased to zero, as presented in Figure 4-10.

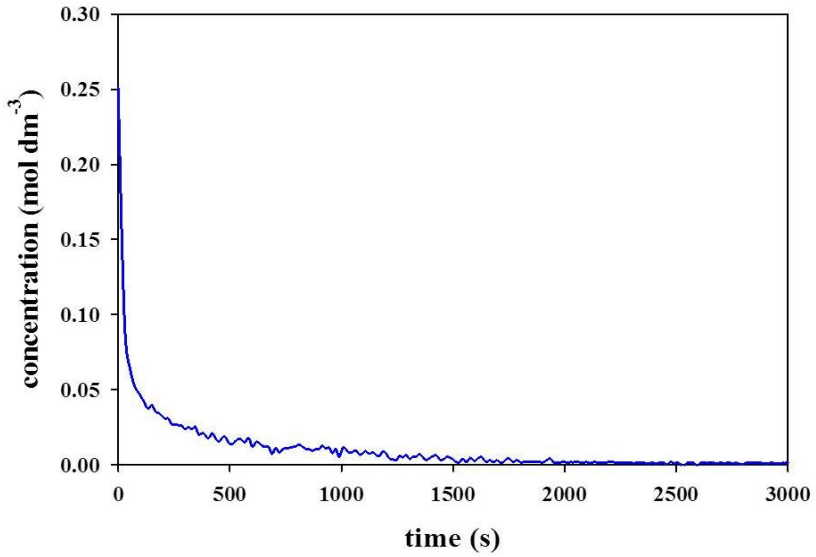

Figure 4-10: Benzaldehyde concentration reduction profile using the segmented concentration calibration curve

A similar segmented concentration analysis was also applied for the *o*-tolualdehyde (Figure 4-11), *m*-tolualdehyde (Figure 4-12) and *p*-tolualdehyde (Figure 4-13) calibration curves.

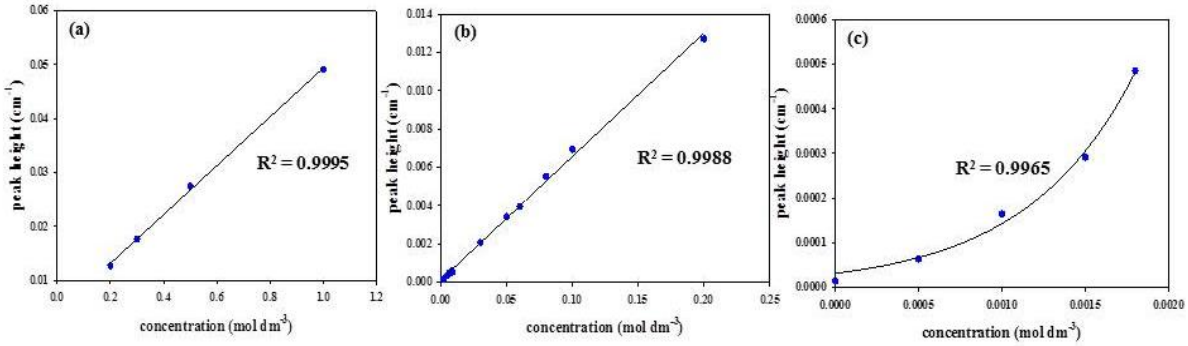

Figure 4-11: Calibration curves for *o*-tolualdehyde for (a) 1.0-0.2 mol dm^{-3}, (b) 0.2-0.0018 mol dm^{-3} and (c) 0.0018-0.000 mol dm^{-3} concentration range.

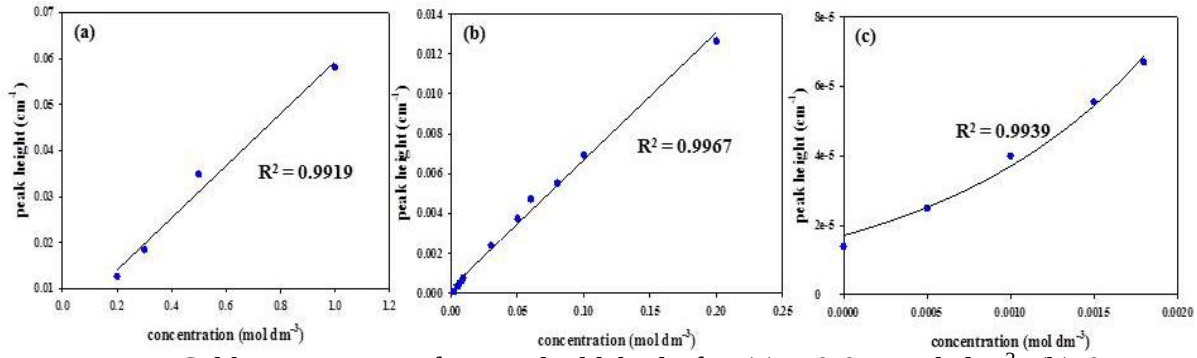

Figure 4-12: Calibration curves for *m*-tolualdehyde for (a) 1.0-0.2 mol dm^{-3}, (b) 0.2-0.0018mol dm^{-3} and (c) 0.0018-0.000mol dm^{-3} concentration range.

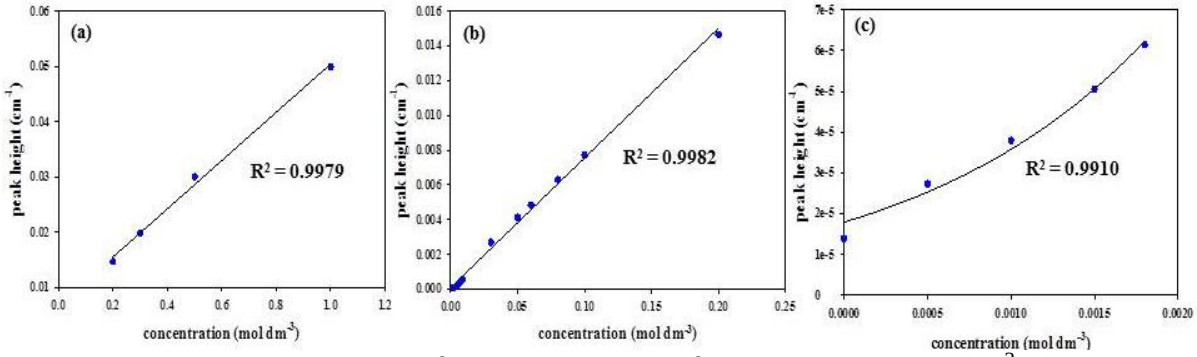

Figure 4-13: Calibration curves for *p*-tolualdehyde for (a) 1.0-0.2 mol dm^{-3}, (b) 0.2-0.0018mol dm^{-3} and (c) 0.0018-0.000mol dm^{-3} concentration range.

Deviation from Beer's law was observed at the lowest concentration range for all three types of aldehydes. At these conditions the noise in the signal becomes significant. The correlation coefficients (all R^2>0.99) for these reagents are listed in Table 4-1.

Table 4-1: Correlation coefficients for calibration curves of different types of aldehyde at various concentration ranges

	Types of Aldehyde		
Concentration range	**o-tolualdehyde**	**m-tolualdehyde**	**p-tolualdehyde**
1.0-0.2 mol dm^{-3}	0.9995	0.9919	0.9979
0.2-0.0018 mol dm^{-3}	0.9988	0.9967	0.9982
0.0018-0.000 mol dm^{-3}	0.9965	0.9939	0.9910

4.3 Characterisation of the modified central baffled mesoscale-OBR

A 350mm length, 5.0mm internal diameter of the central baffled (hexagonal stainless steel solid discs approximately 4mm diameter) mesoscale OBR was previously extensively characterized over a wide range of net flow Reynolds numbers (Re_n of 1-34)

at oscillatory Reynolds numbers of 10-500 (corresponding to amplitude x_o of 0.5-4mm and frequency *f* of 0.5-10Hz) (Phan and Harvey, 2010; Phan *et al.*, 2011a). However, due to the large IR probe size used in this study; the reactor was enlarged from 5mm to 20mm at the outlet to accommodate the 16mm diameter IR probe. This requires the reactor system to be characterised to determine the effect of the modified section on the flow behaviour.

Figure 4-14 shows the residence time distribution (RTD) profiles for the modified and unmodified mesoscale-OBR at an oscillation amplitude of 2.0mm and frequency of 3.0Hz and net flows of Re_n=6.4 and Re_n=7.2 respectively. For the unmodified mesoscale-OBR, the data was collected using a 4mm diameter 2-pole E61014 conductivity probe with water as the working fluid and KCl as a tracer (Phan and Harvey, 2010). As for the modified mesoscale-OBR, the IR probe with hexane as the working fluid and benzaldehyde as a tracer was used. The change with the tracer and working fluid system was to create and understand the similar reaction environment during the imine screening. It was found that the residence time distribution (RTD) curve of the modified mesoscale-OBR had a slightly right-tailed profile compared to the unmodified mesoscale-OBR (Figure 4-14). The variance and skewness of the RTD curve for the modified mesoscale-OBR RTD profile were 0.12 and 0.08 compared to 0.04 and 0.003 for the unmodified mesoscale-OBR

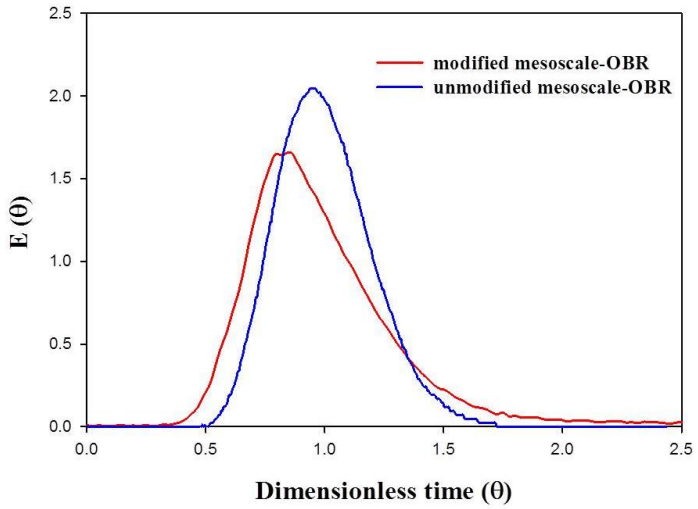

Figure 4-14: Residence time distribution (RTD) profiles for modified (Re_n=6.4) and unmodified (Re_n=7.2) mesoscale-OBR at amplitude, x_o=2.0mm and frequency, *f*=3.0Hz.

The difference in the RTD profiles in terms of the variance and skewness between the two reactors indicated that the broader area next to the probe had a substantial effect on

the flow behaviour. This could be due to the formation of stagnation zones at the corners of the modified section and/or backmixing (Figure 4-15). Therefore, the characterisation of the modified reactor was required to establish the effect of net flows (Re_n) and oscillation conditions (Re_o) on the flow behaviour.

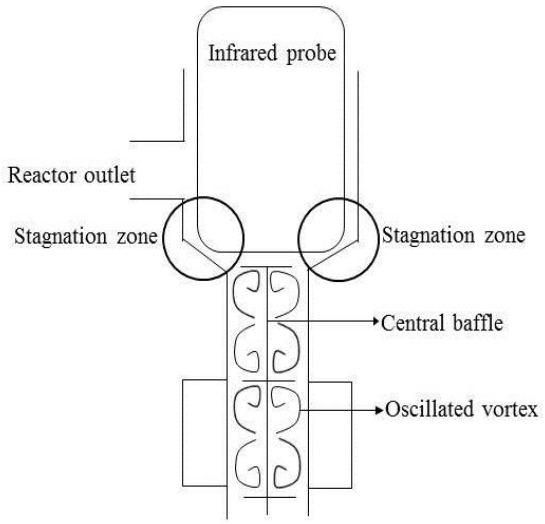

Figure 4-15: Diagram of possible stagnation zones at the outlet of the modified mesoscale-OBR

4.3.1 Effects of Oscillation and Net Flow Reynolds Number on modified mesoscale-OBR.

As the aim was to screen the imine reaction at different residence times (different flow rates), the effects of the net and oscillatory flows had to be studied to ensure conditions that provide good plug flow were used. A series of net flows of $6.0 \leq Re_n \leq 120$ with oscillation condition (Re_o) of 62, 185 and 246 were tested. Figure 4-16 shows the dependency of the number of tank-in-series (N) on Re_o at different Re_n.

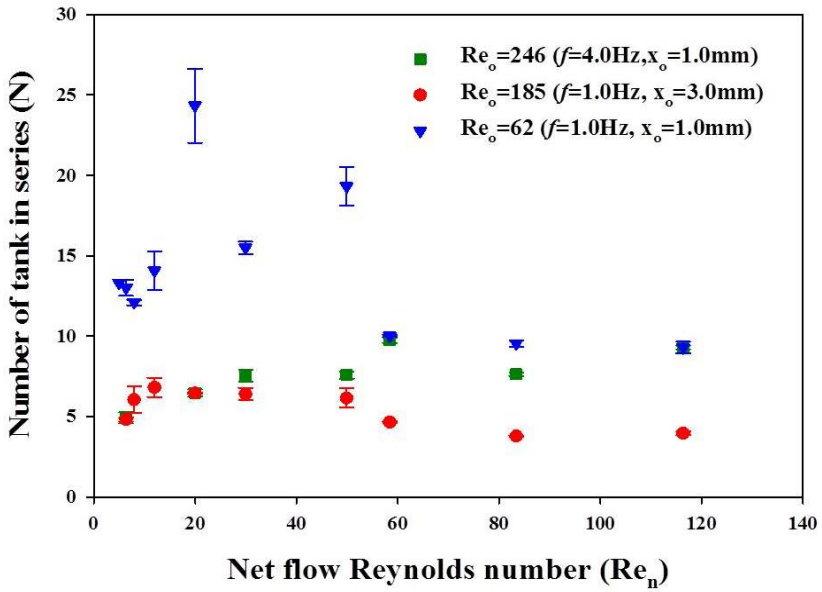

Figure 4-16: Number of tank- in-series obtained at various net flow Reynolds numbers (Re_n) at Re_o of 246, 185 and 65 in the modified central baffled mesoscale-OBR

Plug flow behaviour varied significantly over the range of the tested oscillatory conditions, e.g., N was below 10 at Re_o of 185 and 246 but ≥10 at Re_o of 62 in the range Re_n of 6.0 to 120. Therefore, it is crucial to choose the right oscillation condition to maintain the plug flow behaviour during the continuous screening of imine synthesis. The N must be ≥10 to denote the plug flow behaviour (Levenspiel, 1999).

Re_o is a function of both the frequency and amplitude, so various combinations of these factors produce similar values of Re_o. However, their effects on the flow behaviour differed. The oscillation amplitude directly relates to the lengths of vortices generated and the oscillation frequency relates to the intensity of mixing inside each of the baffle cavity (Roberts and Mackley, 1995). Therefore, the effects of individual factors on the flow behaviour were investigated to determine a suitable operating window for both factors (frequency and amplitude).

The oscillation amplitudes tested ranged from 0.5 – 4.0 mm, corresponding to Strouhal numbers (St) of 0.8 – 0.1 and oscillation frequencies from 0.5-5Hz were applied at a fixed net flow of Re_n=6.4. The Re_n of 6.4, corresponding to a residence time of approximately 600s was sufficient for completion of the reaction of the imine synthesis of benzaldehyde with *n*-butylamine. As shown in Figure 4-17, the number of tank-in-series, N, increases when increasing St (decreasing amplitude), which was similar to other studies at Re_n=7.2 (Phan and Harvey, 2010).

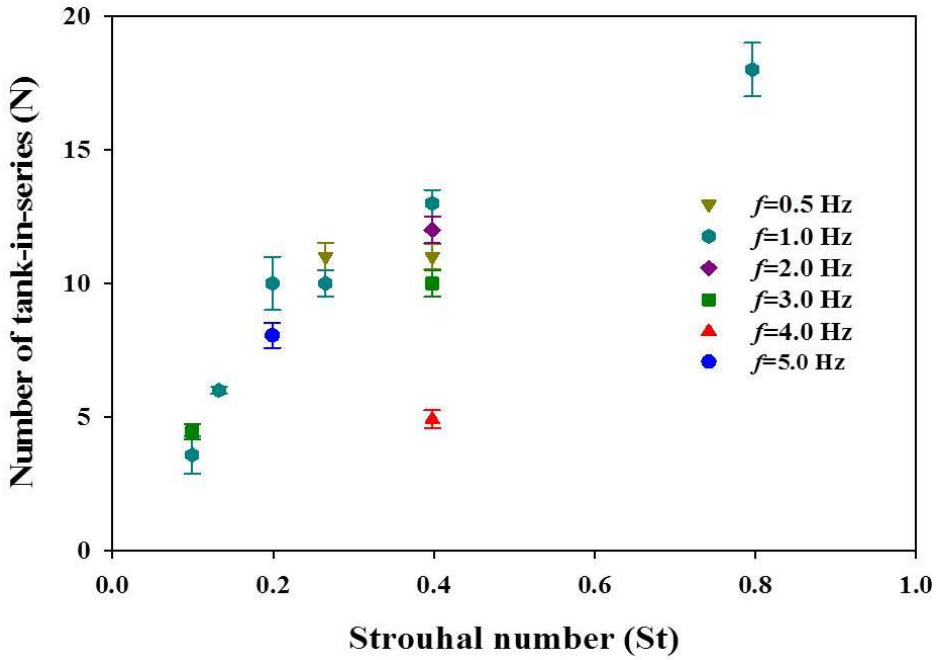

Figure 4-17: Number of tank- in-series obtained at various Strouhal number (St) and oscillation frequency at net flow Reynolds number Re_n of 6.4.

Plug flow behaviour inside the modified mesoscale-OBR was not observed at St<0.2 (amplitude ≥ 2.0m), as N was below 10. At this mixing condition, axial mixing dominated radial. According to Dickens *et al.* (1989), vortices formed at higher amplitudes travel too far toward the next baffle, thereby reducing the degree of plug flow as the baffle cavities behave less like individual units. At a given St of 0.40 (x_o=1.0mm), N was ≥10 for frequencies between 0.5 and 3.0Hz but decreased to 5 when the frequency increased to 4Hz. The plug flow deviation above 4Hz could be due to backmixing (Takriff and Masyithah, 2002), causing the tracer (benzaldehyde) from an upstream baffle of the flow to intermix with the feed from the downstream baffle of the flow.

In summary, plug flow behaviour in the modified central baffled mesoscale-OBR is dependent on both the frequency and amplitude of oscillation. This is in agreement with other findings using conventional OBRs (Stonestreet and Van Der Veeken, 1999) and mesoscale-OBR with different baffle designs (Phan and Harvey, 2010). However, the flow behaviour was more strongly affected by the oscillatory amplitude than the oscillation frequency. In order to maintain the plug flow behaviour for the modified central baffle mesoscale-OBR, the operating window for amplitude and frequency needs to be in the range of $0.5\text{mm} \leq x_o \leq 2.0\text{mm}$ and $1.0 \leq f \leq 3.0\text{Hz}$.

4.4 Imine Synthesis

4.4.1 Reaction mechanism

Imine synthesis is an addition-elimination reaction, comprising a nucleophilic attack by the amine species, followed by an elimination process producing a C=N bond. The reaction mechanism of benzaldehyde and *n*-butylamine reaction shown in Figure 4-18 starts with the attack of *n*-butylamine on the benzaldehyde carbonyl carbon. Due to the electronegativity of the oxygen atom in the carbonyl group, the electron is drawn away from the carbon centre thereby creating a polar bond for the C=O structure. This creates the environment for a nucleophilic addition to occur. The first step involves transferring the electron from the nitrogen nucleophile to the carbon electrophile (Step1), followed by proton transfer steps (steps 2 and 3) to form a tetrahedral intermediate known as a carbinolamine. Generally, steps 2 and 3 can be acid- or base-catalysed (Carey and Sundberg, 2007). However, in this study, no catalyst was used because *n*-butylamine is a strong nucleophile (Sayer *et al.* (1974)). The mechanism continues with the elimination process to complete the reaction (step 4) with the electron transfers to form a positively charged iminium ion. Then the iminium ion is de-protonated by the hydroxides and hydrogen to form the imine product, with the elimination of a water molecule (Anslyn and Dougherty, 2006).

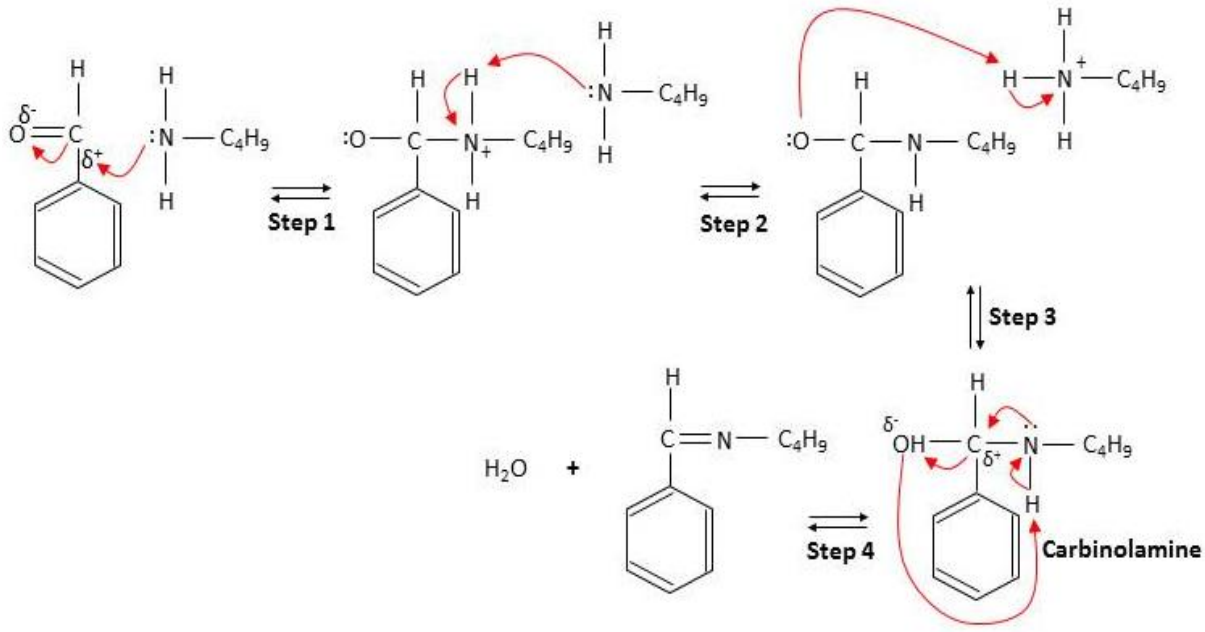

Figure 4-18: Reaction mechanisms of benzaldehyde and n-butylamine reaction.

In this study the IR spectra collected showed no evidence of a tetrahedral carbinolamine intermediate. Figure 4-19(a) exhibits no peak in the C-O region (1120-1080cm^{-1}) for

this intermediate. Similar findings were observed with the C-N-C stretching region (1190-1130cm^{-1}) (Figure 4-19(b)), which exhibited constant peak intensity from 0s-3600s indicating no formation of intermediate. The peak observed in the region 1190-1130cm^{-1} was assigned to the C-C of the aliphatic and aromatic structures of the benzaldehyde (the blue line). The lack of any absorption with this species was due to its unstable, reactive nature, resulting in negligible accumulation at any point in the reaction (Evans *et al.*, 2002; Iwasawa *et al.*, 2007) to be monitored using IR spectroscopy.

Figure 4-19: Peaks observed at (a) 1120-1180 cm^{-1} for the C-O stretching for alcohol and (b) 1190-1130cm^{-1} for the C-N-C of secondary amine in the formation of an intermediate in the synthesis of 1-butanamine, N-(phenylmethylene) from benzaldehyde and n-butylamine

However, the mass balance calculation from the benzaldehyde reduction and imine formation data indicated that about 20 wt % intermediate was formed but disappeared after approximately 200s reaction time as shown in Figure 4-20.

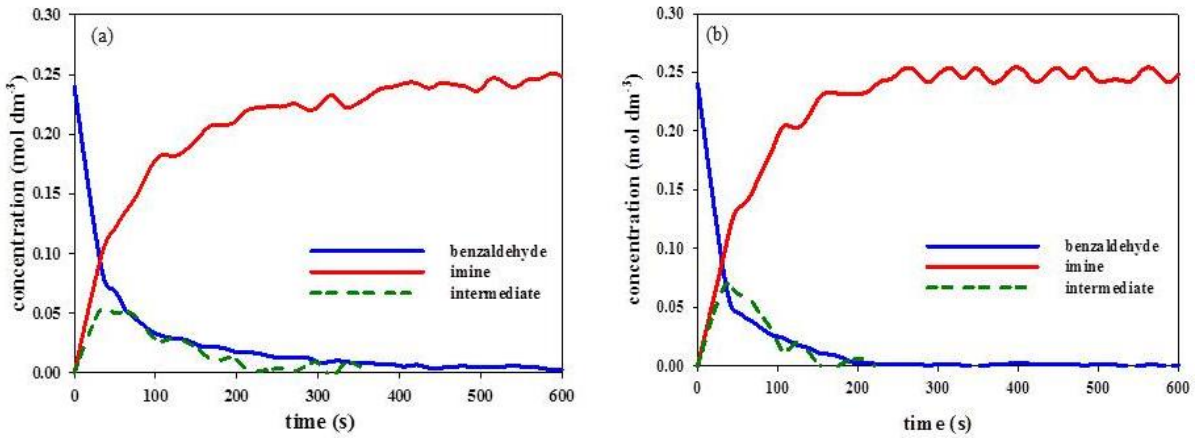

Figure 4-20: Imine synthesis profiles in hexane at (a) 1:1 molar ratio of benzaldehyde to n-butylamine and (b) 1:4 molar ratio of benzaldehyde to n-butylamine.

It was reported (Carey and Sundberg, 2007) that the elimination process to form the product was the rate limiting step in neutral and basic solution, resulting in delayed product formation due to the accumulation of carbinolamine intermediate in the solution. However, no delay in product formation (imine) was observed as product formation occurs as the benzaldehyde reactant diminishes, as shown in Figure 4-20. This was resulted due to the used of aromatic aldehyde and reactive amine which stated by (Layer, 1963) produces stable and quantitative imine products. The formation of the product 1-butanamine, N-(phenylmethylene)-, monitored and followed using the IR at 1652 cm^{-1}(C=N) (Conley, 1972; Socrates, 1994), also correlated with the decrease in the strong C=O carbonyl stretching vibration from 0 to 3600s (Figure 4-21(a)). The findings from the IR spectroscopy were confirmed by ^{1}H NMR analysis as shown in Figure 4-21(b). The proton NMR was performed on a 500 MHz instrument in deuterated chloroform ($CDCl_3$). The determination of the imine proton was achieved by integration of the peak at δ = 8.4 ppm, consistent with Habibi *et al.* (2006). Disappearance of the carbonyl proton was also observed at δ = 10.5 ppm indicating that the benzaldehyde completely reacted to form imine. As for the peaks in the ranges δ = 7.0-8.0 ppm and δ = 1.0-4.0 ppm, they were assigned to aromatic protons and the methyl/methylene protons of the hydrocarbon structure.

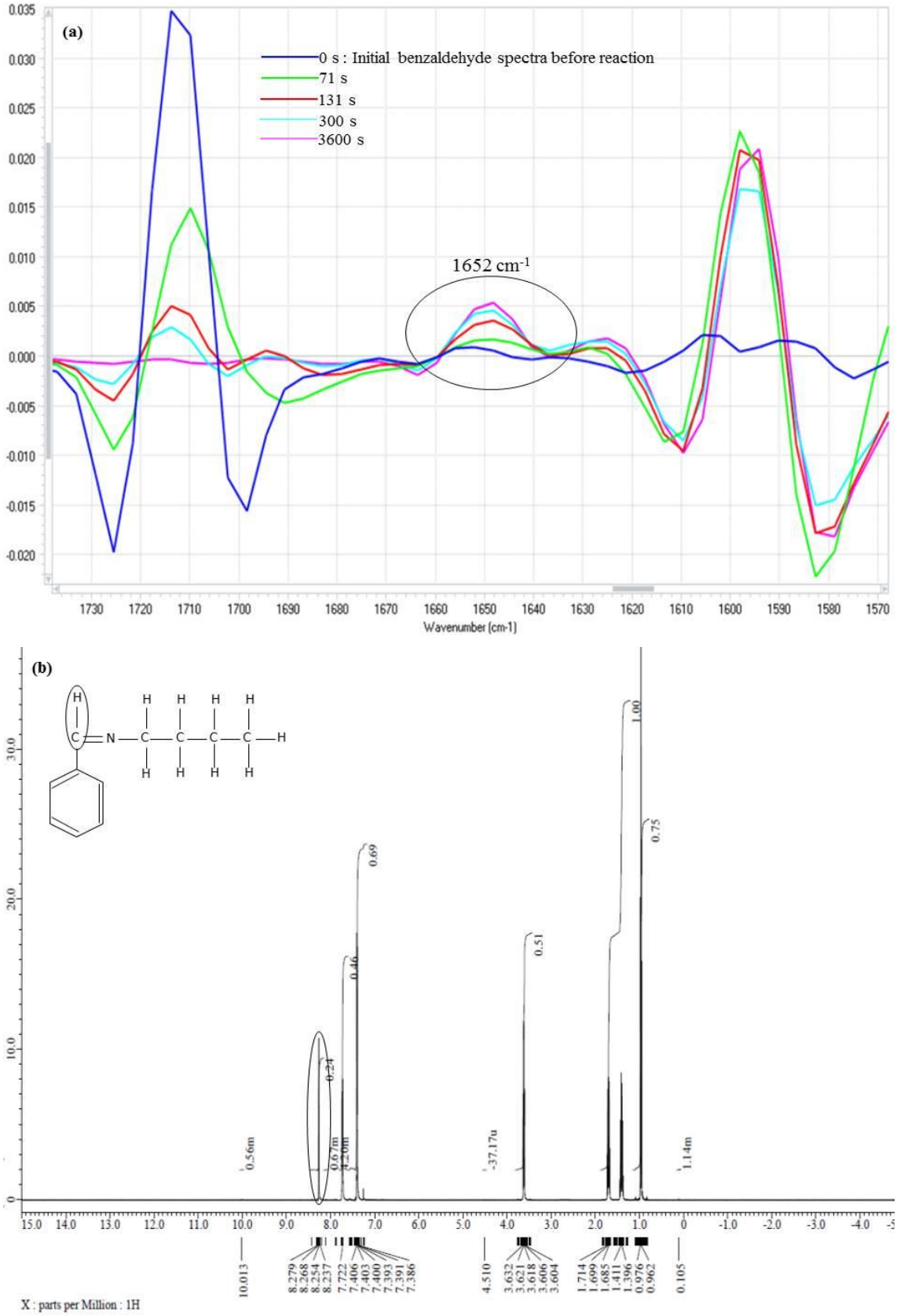

Figure 4-21: Evidence of the 1-butanamine,N-(phenylmethylene)- formation using (a) IR at the peak of 1652cm^{-1} (C=N) and (b) ^{H}NMR at 8.3ppm (H-C=N)

4.4.2 Batch screening

Batch screening processes are typically used in laboratories for compound and/or drug development and/or synthesis in chemical and pharmaceutical industry (Jas and Kirschning, 2003; Wiles and Watts, 2007). At this stage, all the possibilities involved with the chemistry route are tested to maximise yield and purity and to minimise waste. The rapidity with which reliable outcomes are determined at this stage is very important, especially for pharmaceuticals, as "time-to-market" can be critical (Wheeler *et al.*, 2007). With this general approach, batch screening was used as the benchmark to compare a continuous screening work conducted in this research.

In this study, batch reaction screening was conducted using a conventional 100mL glass beaker and a mesoscale-OBR in batch mode. Figure 4-22 shows the benzaldehyde concentration profile at a molar ratio of 1:1 of benzaldehyde and *n*-butylamine.

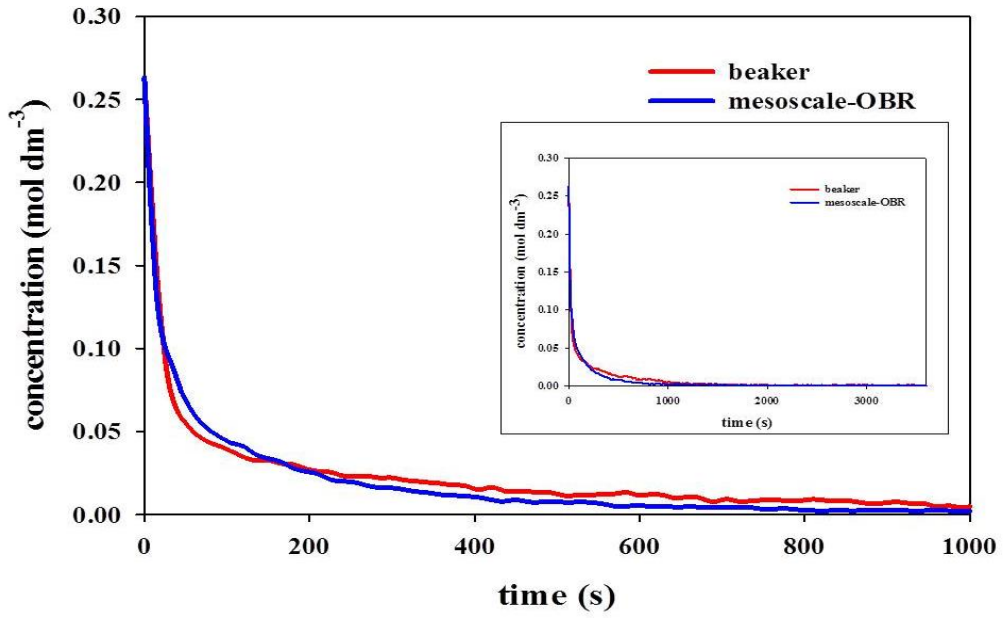

Figure 4-22: Batch reaction screening of benzaldehyde reduction profile at stoichiometric molar ratio of 1:1 using a batch beaker and a mesoscale-OBR

Generally, there was no significant difference between the two methods with the completion of the reaction occurring at approximately 1000s. However two phenomena were observed in the batch beaker experiments: benzaldehyde reductions were faster at reaction times below 200s, but slower at higher reaction times than those obtained in the mesoscale-OBR system. This was due to the method of adding reagent in general laboratory apparatus system such as beakers and volumetric flasks (Issa *et al.*, 2013; Jin *et al.*, 2013) and the effect of mixing. Typically, in beakers, the reagents were added at

the same time or one after the other in their full amount. This made it difficult to achieve rapid homogenous mixing due to the greater volume to area ratio (Houson, 2011). Moreover, localised mixing in the beaker occurred due to the absence of baffles to break up the flow, leading to higher uncertainty between results in the initial stages of the reaction, e.g. the uncertainty at 15s reaction time was 6.73×10^{-2} mol dm^{-3} and 7.49×10^{-3} mol dm^{-3} for beaker and mesoscale-OBR, respectively (Figure 4-23).

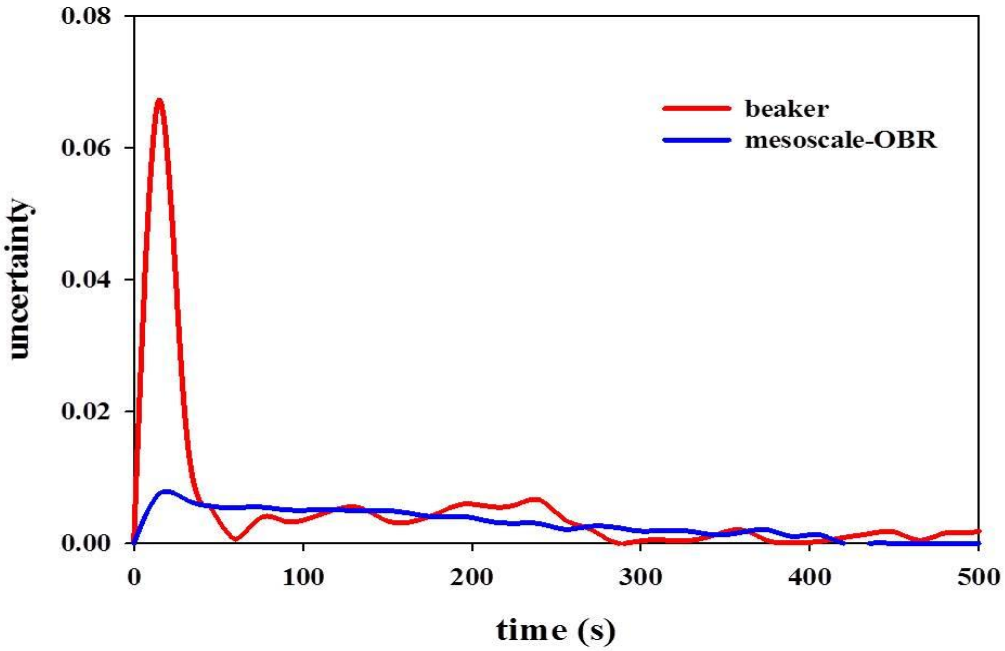

Figure 4-23: Uncertainty of batch reaction screening of benzaldehyde reduction profile at a stoichiometric molar ratio of 1:1 using a batch beaker and a mesoscale-OBR.

For the mesoscale-OBR, the reactants were fed in simultaneously. The vortices formed due to the combination of oscillatory flow and baffles provided good mixing in each baffle cavity (Howes *et al.*, 1991; Stephens and Mackley, 2002; Vilar *et al.*, 2008), thereby eliminating concentration gradients within baffle cavities. This resulted in a substantially lower uncertainty in the OBR at the initial stage of the reaction as shown in Figure 4-23 (above) than that in the beaker. Here the uncertainty study was conducted to shows the differences at the initial states of the mixing which reflected to limitation of the macromixing in the beaker system(Al-hengari, 2011). With that, it resulted to lower overall uncertainty (7.36×10^{-4} mol dm^{-3}) of the mesoscale-OBR. Apart from that, the mesoscale-OBR also was closer to a 100% conversion for the reaction of 1:1 ratio of benzaldehyde to *n*-butylamine which indicative of "better" (i.e. more uniform) mixing than the beaker system. However, the claims relate to the uncertainty measurements was only conducted based upon duplicates data.

4.4.2.1 Effect of mixing conditions on reduction rates of benzaldehyde for 1-butanamine, N-(phenylmethylene)- reaction.

Mixing conditions have significant effects on rates of reaction for competitive-consecutive and competitive-parallel reactions (Shah *et al.*, 2012). Figure 4-24 shows the benzaldehyde reduction profile for a batch beaker at different mixing speeds. In general, there was no significant difference between the benzaldehyde reduction profiles. However, the benzaldehyde reduction rate differed during the initial period of the reaction time ≤100s. At 15s reaction time (Figure 4-24), the concentration decreased with increasing mixing intensity, e.g., the concentration was 0.19 ± 0.03mol dm^{-3} for the speed of 229 rpm and 0.14± 0.02mol dm^{-3} for 1119 rpm. This was due to the molecular collisions occurring during mixing related to stretching and folding of material surfaces (Ottino, 1990). At lower speeds, this interaction is reduced, resulting in higher concentrations. It shows a mass transfer limitation within the reactor systems.

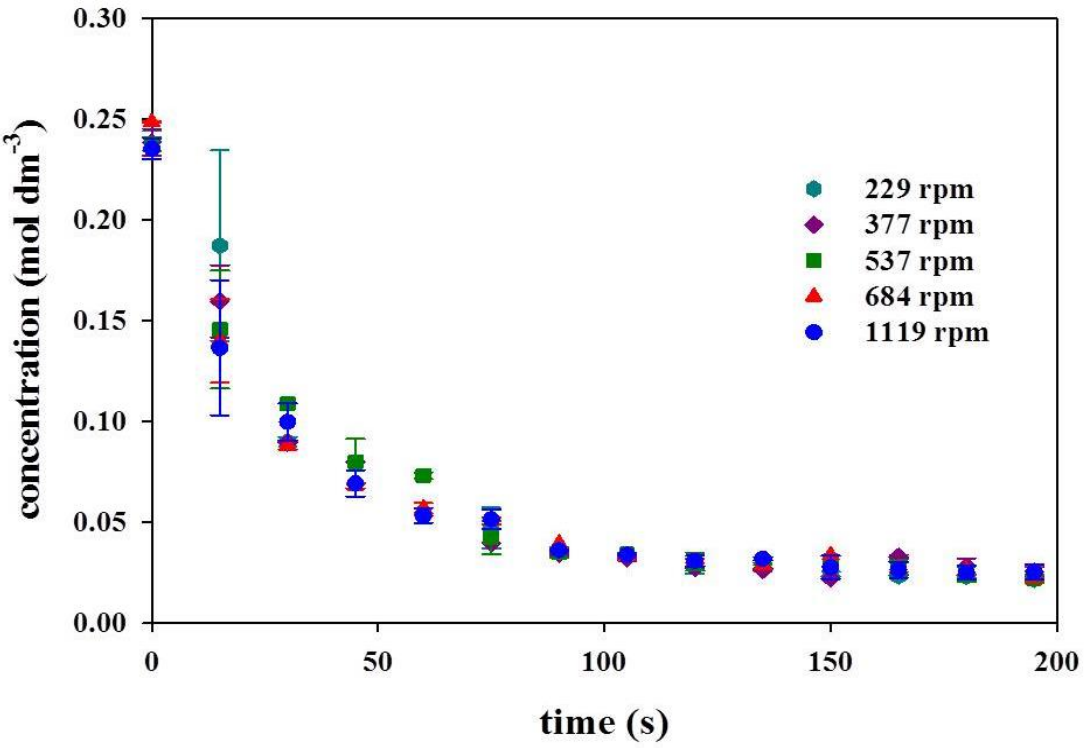

Figure 4-24: Effects of mixing intensity using a batch beaker for benzaldehyde reduction rate at reaction time below 200s.

A similar reaction completion (approximately zero value in concentration) at 1000s was obtained using a batch mesoscale-OBR (Figure 4-25). However, there was no significant difference in the benzaldehyde reduction over the initial period of <100s at different mixing intensity (different Re_o) (Figure 4-26) compared to the batch beaker reduction profile as shown previously.

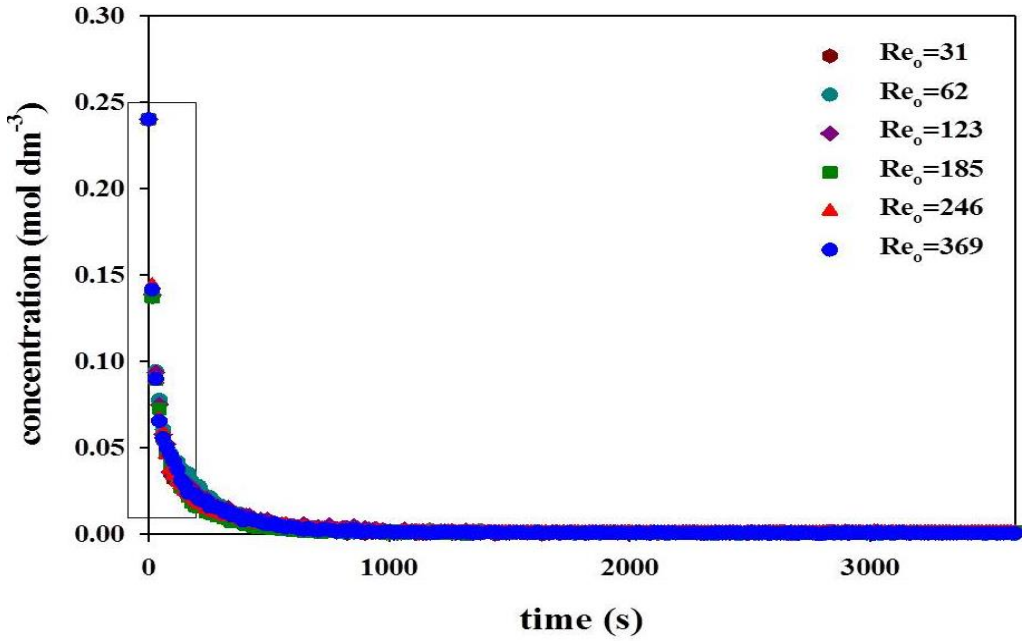

Figure 4-25: Benzaldehyde reduction profile for batch mesoscale-OBR at different oscillatory Reynolds number (Re_o)

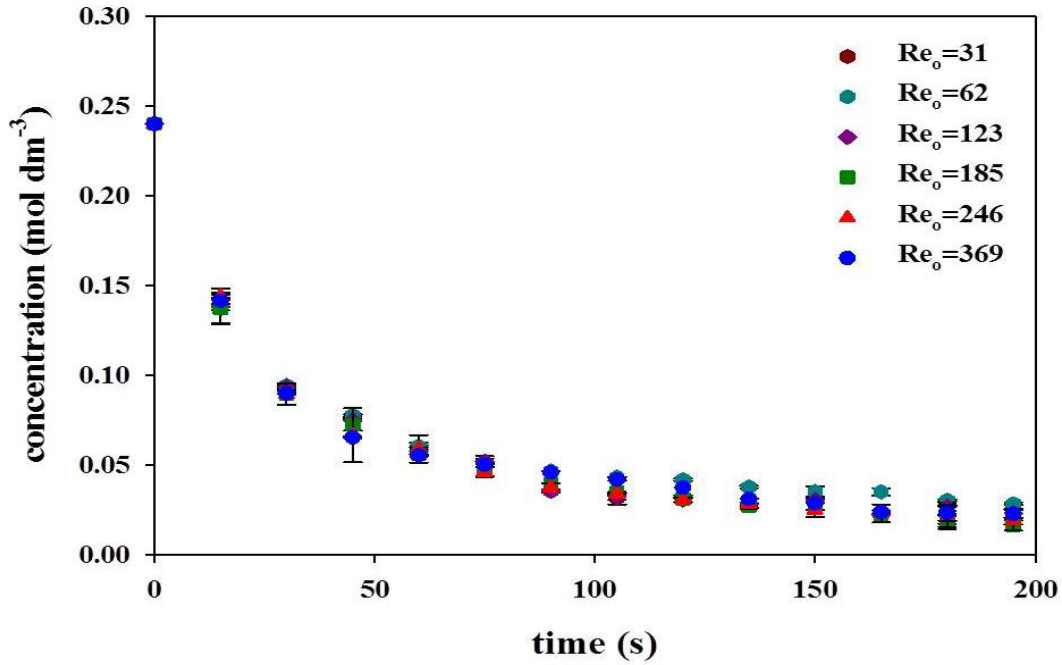

Figure 4-26: Effects of mixing intensity using batch mesoscale-OBR for benzaldehyde reduction rate at <100s reaction time.

As mentioned in section 4.4.2 both reagents (benzaldehyde and *n*-butylamine) were dispensed simultaneously during oscillatory mixing within the reactor. This provides very rapid homogeneous mixing between the reagents. The benzaldehyde concentration profile also exhibited low uncertainty throughout the reaction, regardless of the oscillatory Reynolds number (Re_o). The reaction kinetic parameters for the mesoscale-OBR and beaker were calculated, based on their respective profiles.

The apparent rate constants calculated through integration method were studied at a molar ratio of benzaldehyde and *n*-butylamine of 1:1 over a range of mixing conditions, Re_o of 30-350 for the mesoscale-OBR, and 200-1100 rpm for the 100mL beaker. As shown in Figure 4-27, the average rate constants determined were identical (k_1= 2.1 x $10^{-1}mol^{-0.9}L^{0.9}s^{-1}$) for both reactor systems. This implied that mixing had no effect on the apparent rate constant in both systems at the tested conditions. However, the mesoscale-OBR exhibited average error across all the data points at 3 times lower than for the beaker.

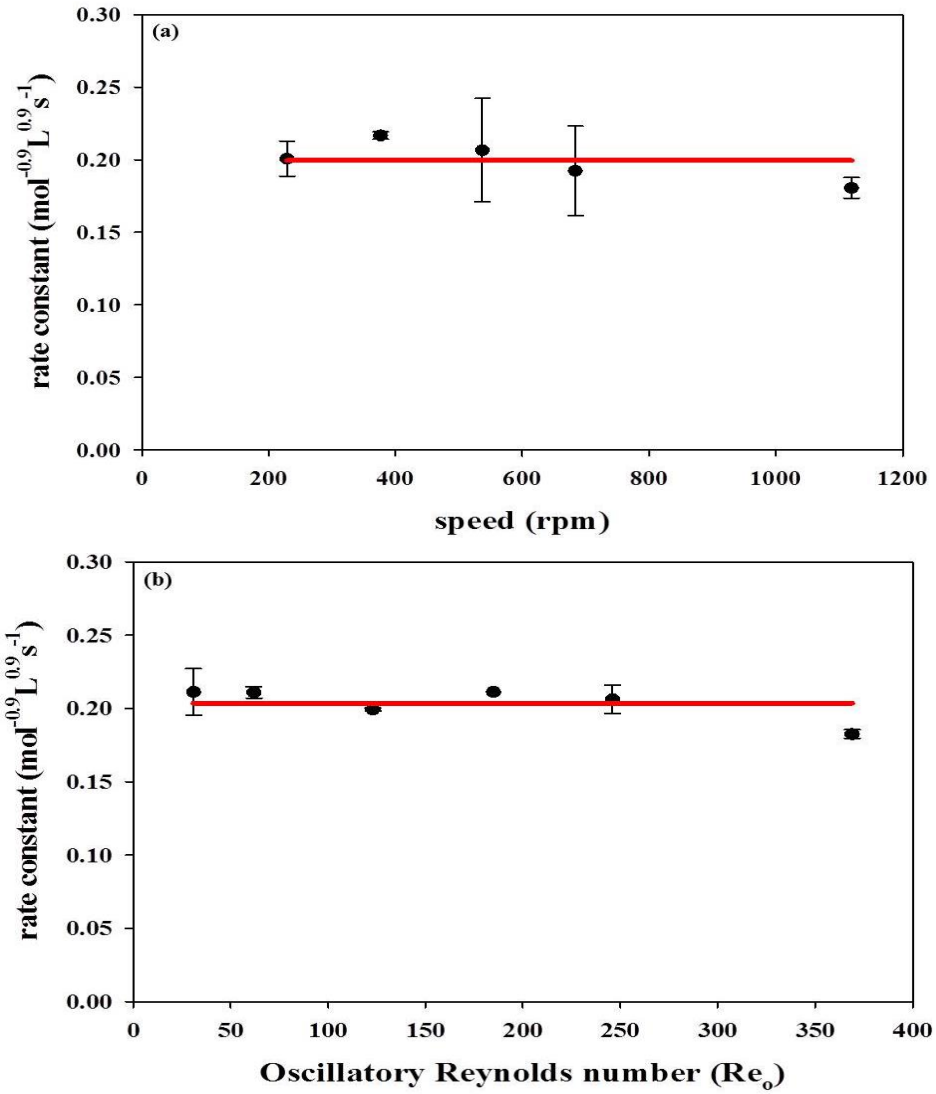

Figure 4-27: Rate constant of imine synthesis using (a) 100 mL beaker (b) centrally baffled mesoscale-OBR.

As presented in Table 4-2, an average uncertainty of the rate constant for the mesoscale OBR was 5.5 x 10^{-3} $mol^{-0.9}L^{0.9}s^{-1}$ compared to 1.8 x 10^{-2} $mol^{-0.9}L^{0.9}s^{-1}$for the beaker. In addition, the total volume of chemicals used in this screening was 75% lower in the

mesoscale-OBR than in the beaker, due to the much smaller volume of the mesoscale OBR (6 mL) than the beaker (80 mL). Smaller beaker volumes could not be used due to impracticality with the large IR probe size.

Table 4-2: Comparison of the uncertainty of rate constant using different reaction vessel.

Beaker		**Mesoscale-OBR**	
RPM	**Uncertainty level**	**Re_o**	**Uncertainty level**
229	1.2×10^{-2}	31	1.6×10^{-2}
337	2.5×10^{-3}	62	3.9×10^{-3}
537	3.6×10^{-2}	123	1.1×10^{-3}
684	3.1×10^{-2}	185	0.0
1119	7.1×10^{-3}	246	9.5×10^{-3}
		369	2.9×10^{-3}

4.4.3 Continuous screening

Continuous screening using the mesoscale-OBR has been conducted through "multi-steady state" and "dynamic screening" modes. The former refers to a process in which a sequence of different residence times was imposed sequentially, each for a desired period of time including attainment of a steady state. In the latter, the residence time was continuously varied.

4.4.3.1 Multi steady-state screening

Multi steady-state screening was conducted at different molar ratios of, e.g. 1:1, 1:1.5 and 1:2 over a range of residence times of 30s to 600s at an Re_o of 62. The continuous steady-state is referred to plateau states of the screening conditions. This was resulted from maintaining the desired screening conditions at a prescribe period of time. Nine consecutive residence times were imposed for the screening with each residence time maintained at approximately of 240s. A clear step change between residences times, regardless of the different ratios of benzaldehyde to *n*-butylamine, can be observed in Figure 4-28, below:

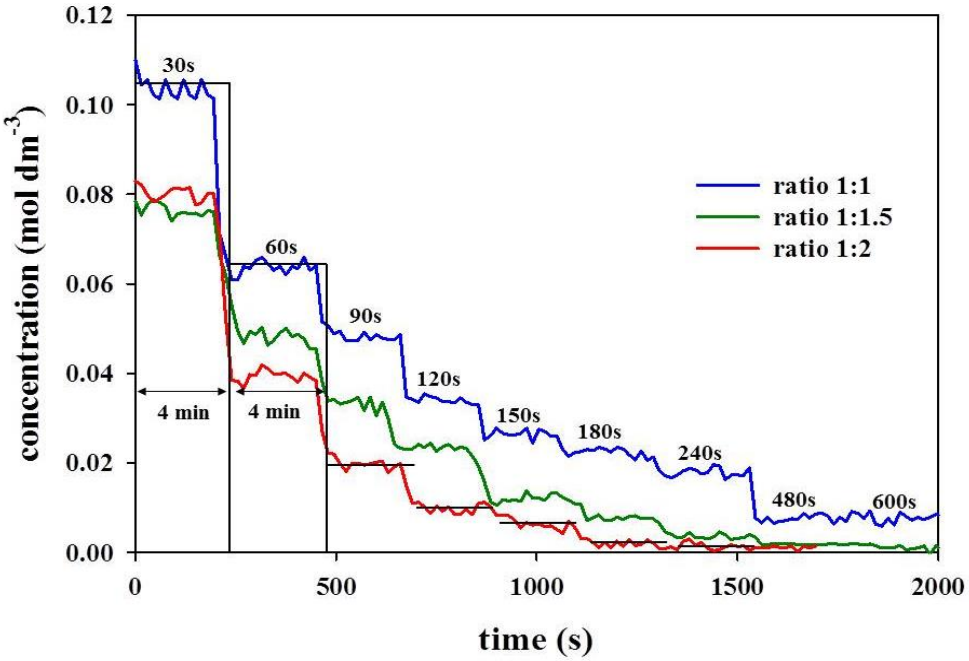

Figure 4-28: Multi steady- state step change of residence time for imine synthesis at a molar ratio of 1:1, 1:1.5 and 1:2 for benzaldehyde:n-butylamine at Re_o=62 using centrally baffled mesoscale-OBR.

A change in concentration was observed immediately after completing the steady-state condition (approximately 4 min for each residence time), e.g. from 0.11 mol dm^{-3} at 30s residence time to 0.06mol dm^{-3} at 60s for the reaction at ratio 1:1 of benzaldehyde to *n*-butylamine. The variability data at each plateau condition observed in these studies was at average uncertainty of $5x10^{-4}$ mol dm^{-3}($\leq$ 4.0%). The variability was not only affected due to the plug flow mixing behaviour inside the mesoscale-OBR but also with the analytical instrument used. However in this study, the consistency and accuracy of the spectrum/data collected was assured through maintaining the signal to noise ratio of the IR system at a suitable range of 2500-3500 (Toledo, 2010). This behaviour has also been observed in a multiphase reaction screening, e.g., biodiesel production at various ratios of methanol to rapeseed oil (Phan *et al.*, 2011). OBR results required a smaller volume of fluid (~20% less) per data point than in beaker batch screening. The average of a series of data points ($\sigma = 1.2x10^{-3}$ mol dm^{-3}) at each reaction time is more accurate than one data point conducted in batch. The consistency and the clear step change indicate that further processing advantages are possible, such as introducing additional or third reagent into the flow stream at precisely the time point to generate further reaction. This was a challenge when operating using a microreactor system on a segmented flow (Smith *et al.*, 2011). The series of short reaction plugs conducted in a constant stream of solvent only allowed the microreactor to briefly reach a steady-state

condition at a point of time. This was overcome by using an excess volume of the third reagent which resulted in a greater downstream purification duty.

As mentioned in section 4.4.2, there was no significant difference in the benzaldehyde concentration profile at 1:1 molar ratio between the batch beaker and the batch mesoscale-OBR reactor. On that note, examination of the multi steady-state concentration data was compared only to the data obtained from batch mesoscale-OBR. This eliminates differences due to reactor design and mixing pattern creates within the reactor system. Figure 4-29 shows the average results obtained from a continous multi steady-state and batch mode at different residence times for at different ratios of benzaldehyde to *n*-butylamine of 1:1, 1:1.5 and 1:2.

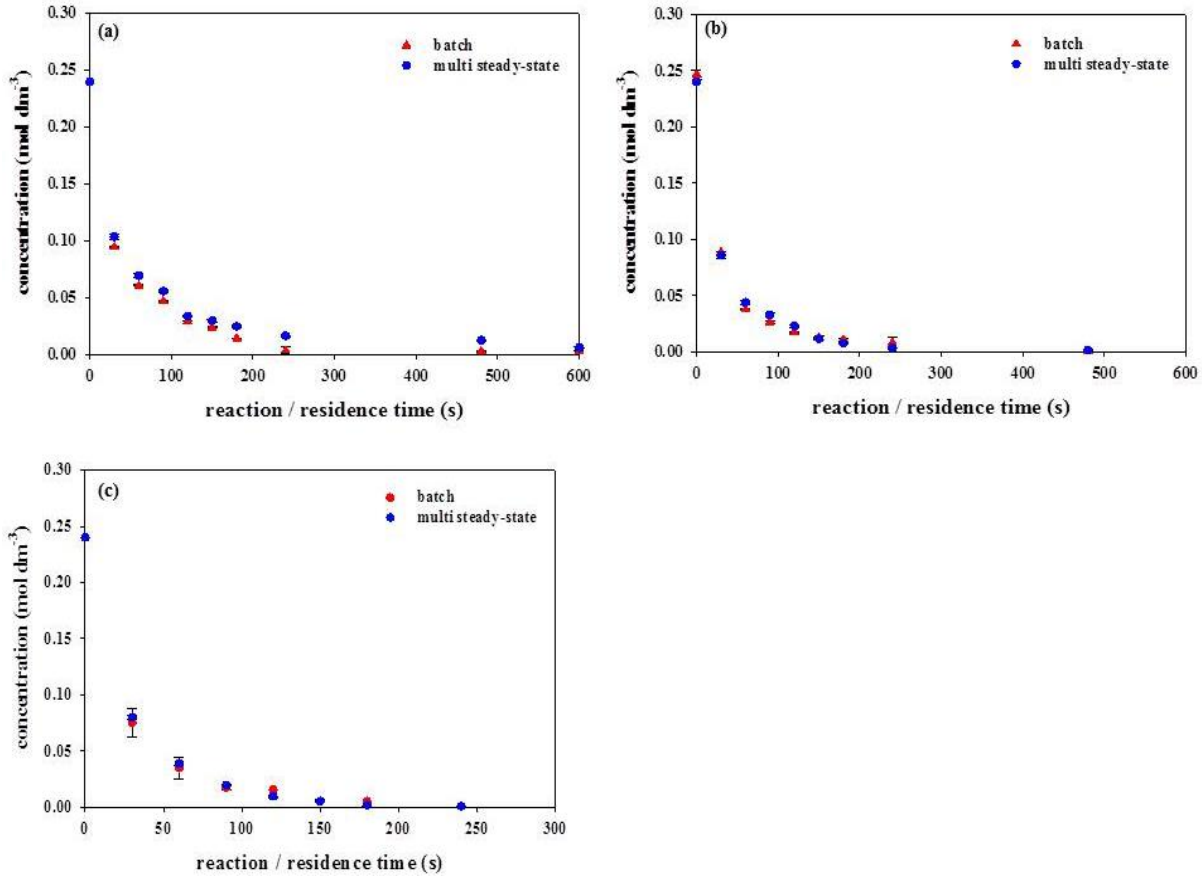

Figure 4-29: Comparison of benzaldehyde reduction profile through multi steady-state and batch screening using mesoscale-OBR at (a) 1:1, (b) 1:1.5 and (c) 1:2 ratio of benzaldehyde and n-butylamine

There was no significant difference in the benzaldehyde reduction profile between batch and multi steady-state method of screening regardless of the reaction ratio. This suggests that the mesoscale-OBR can be used as a tool for conducting continuous screening of chemical reactions. In the continuous mode the mesoscale-OBR provides

advantages in rapid, simple manipulation of the reaction parameters (e.g. different ratios). Apart from that, removal of the need for cleaning and refilling each time reduces the process development time by about 50% compared to the screening via batch using conventional glassware set-up.

4.4.3.2 Dynamic screening

Continuous dynamic screening refers to a process in which reactor inputs are continuously changed. This was conducted at different molar ratios of 1:1, 1:1.5 and 1:2 of benzaldehyde to *n*-butylamine over a range of residence times of 30s to 240s at an oscillation condition Re_o of 62. The screening started with similar condition as the multi steady-state to obtain the plateau profile at 30s residence time for 4 min (Figure 4-30). Next, the residence time was continuously increased at an interval of 5s until the plateau condition was again achieved at a 240s residence time. The plateaus were important as they acted as good markers of the initial and end points of the screening, and their agreement with the multi steady-state plateaus could be evaluated. Each residence time was only maintained for 15s residence time before it is changed to the other desired residence time.

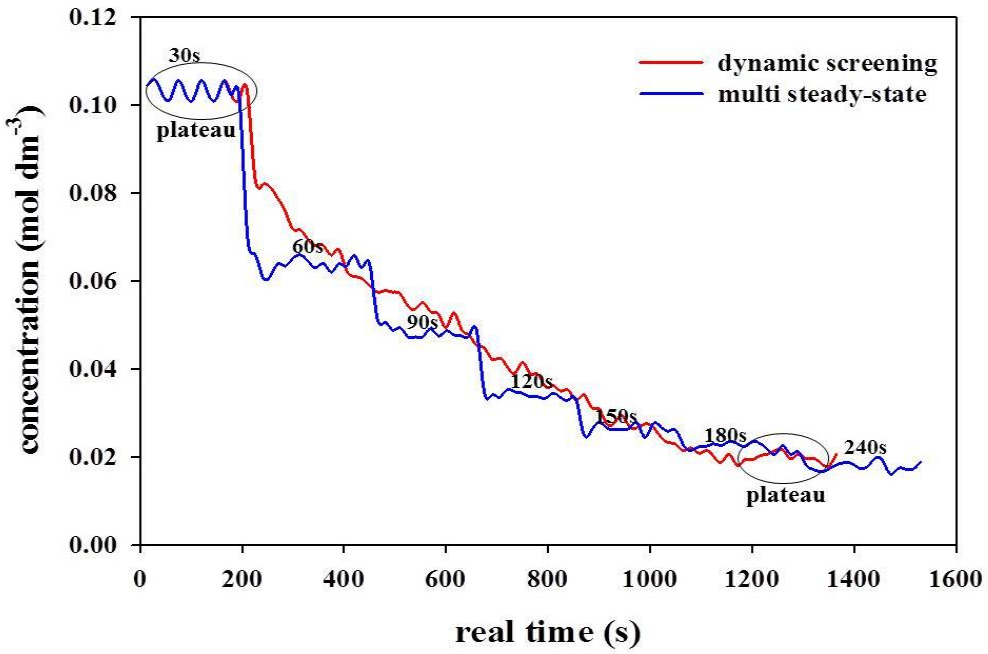

Figure 4-30: Comparison for dynamic and multi steady-state screening of benzaldehyde reduction profile at 1:1 ratio of benzaldehyde to n-butyalmine.

The rapid changes (~every 15s) for each residence time generated benzaldehyde reduction profiles similar to those achieved by screening in batch mode, as can be

observed in Figure 4-31. However, the dynamic screening produces more data (smaller interval data) than conventional batch screening.

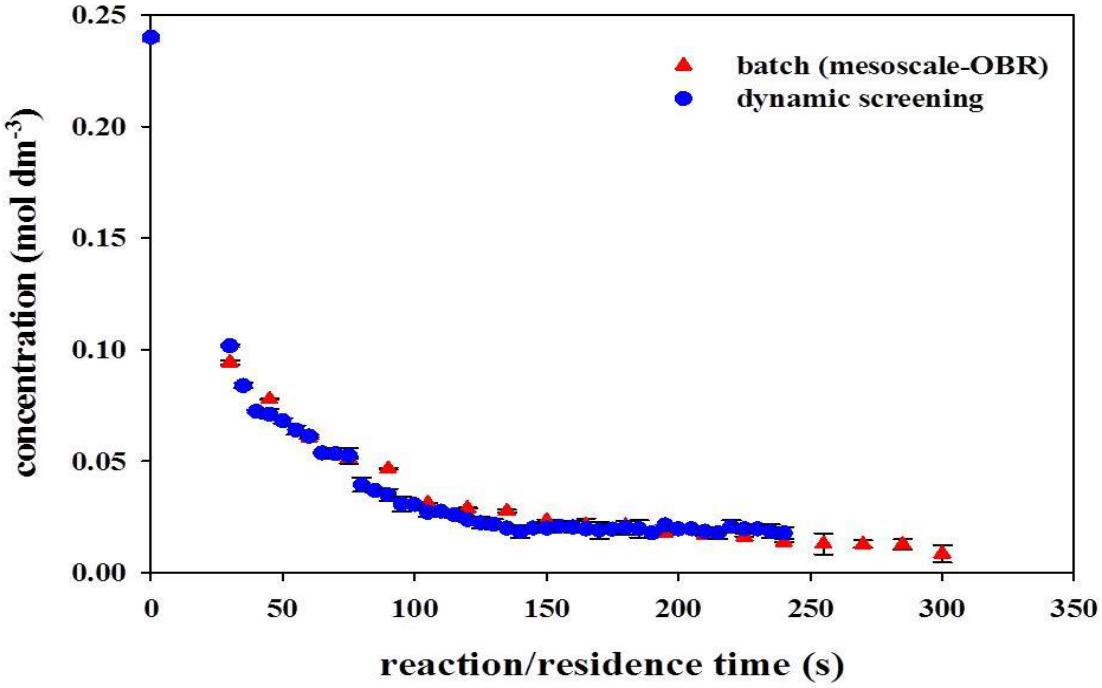

Figure 4-31: Comparison of benzaldehyde reduction profile through dynamic and batch screening using mesoscale-OBR at 1:1 ratio of benzaldehyde and n-butylamine

In dynamic screening, the data interval depends on the flow rate/residence time sequence (Table 4-3) which was varied accordingly to the desired residence times. However the frequency of the data collected still depends on the time resolution of the analytical instrument (IR).

Table 4-3: Comparison of data obtained through dynamic and batch screening using a mesoscale-OBR at 1:1 ratio of benzaldehyde and n-butylamine

Dynamic screening		**Batch screening**	
Time (s)	**Concentration (mol dm^{-3})**	**Time (s)**	**Concentration (mol dm^{-3})**
30	0.10	30	0.09
35	0.08	45	0.07
40	0.07	60	0.05
45	0.07		
50	0.07		
55	0.06		
60	0.06		

Even though the IR data was collected at 15s interval, the continuous system gives flexibility in changing the conditions once the data was collected (i.e. from 30s to 35s residence time). However this was not possible with the conventional batch screening. Due to that, batch screening data interval was restricted to the time resolution of the instrument. The data collected at the holding period (15s) was taken to represent the residence time screened (yellow boxes in Figure 4-32). Example of this statement is shown in Figure 4-32.

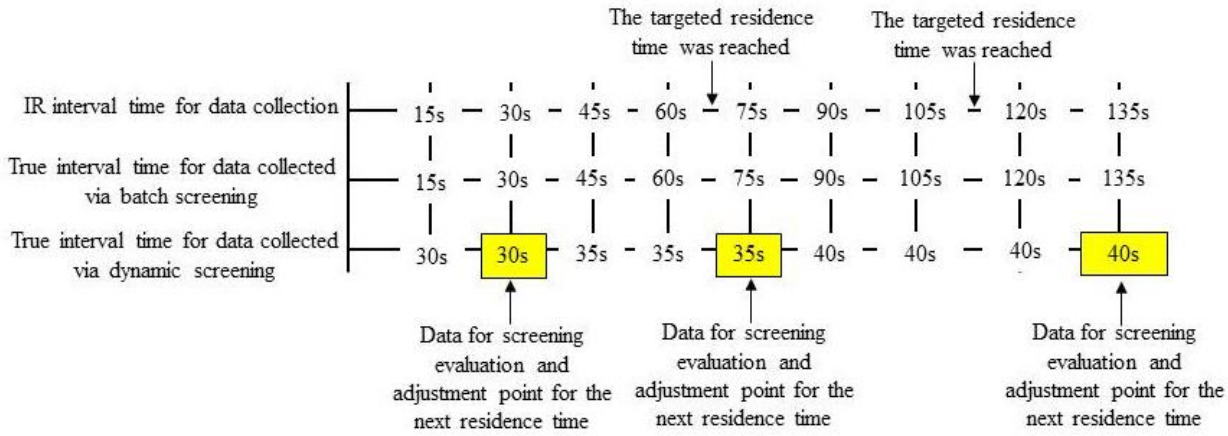

Figure 4-32: Comparison of the time interval for the IR system with the true interval time for data collected via batch and continuous dynamic screening.

Here it shows that the continuous screening (i.e. dynamic screening) gives more interval data points (smaller interval) than the batch screening. The extra data points provide more advantages in understanding the rate of a chemical reaction at smaller time interval. When comparing to the continuous multi steady-state screening, dynamic screening reduces the total reagent volume by approximately 50% and the process development time by 30%. This reduction was due to the elimination of the constant conditions maintained for approximately 4 min at each residence time with the multi steady-state screening. It therefore allows rapid replication of experiments and larger experimental matrices to be conducted more quickly and more economically.

Screening data shows that there is approximately 98% agreement between the different methods (batch, multi steady-state and dynamic screening). This can be observed in Figure 4-33 below, for data generated at different molar ratios of 1:1, 1:1.5 and 1:2 for benzaldehyde to *n*-butylamine. These results demonstrate that the mesoscale-OBR can

be used as a tool to obtain reaction data in a batch or continuous manner, and it generates data in a more rapid and economical manner for any reaction screening study.

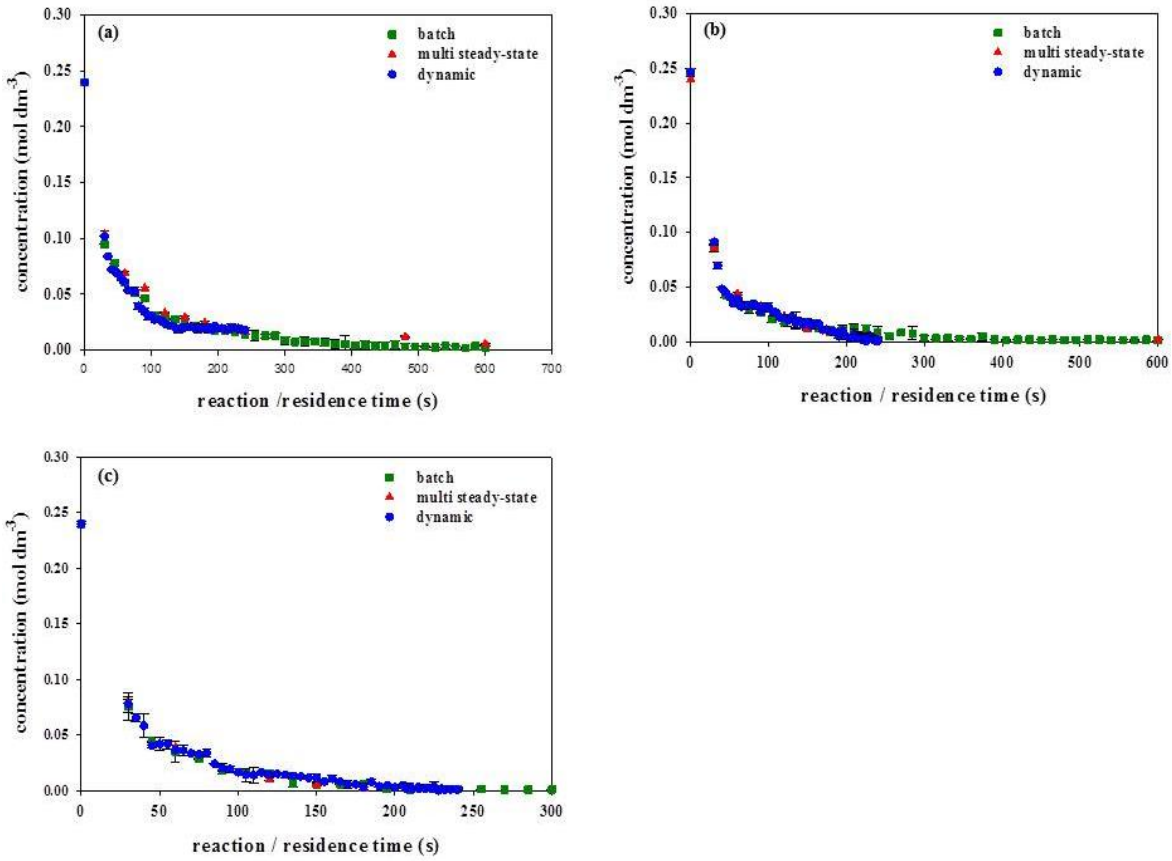

Figure 4-33: Comparison of different screening methods using mesoscale-OBR for (a) 1:1, (b) 1:1.5 and (c) 1:2 ratio of benzaldehyde to n-butylamine

4.4.3.3 Dynamic Multiple Variable Screening

The manipulation of variables, e.g. molar ratio, residence time and temperature, in organic synthesis or reaction kinetics studies is limited when screening in batch mode (Baxendale, 2013b). Changing experiment conditions and/or variables can only be done once the reaction is complete. Therefore, it is time-consuming and costly, especially when dealing with expensive reagents. However, through continuous screening, manipulation of the experimental variables can be conducted *in situ*. As mentioned previously, (multi steady-state in section 4.4.3.1 and dynamic screening in section 4.4.3.2) only one variable (residence time) was varied (Figure 4-34(a)). In multivariable dynamic screening, the aim was to manipulate two or more variables *in situ* simultaneously for each experiment (Figure 4-34(b)).

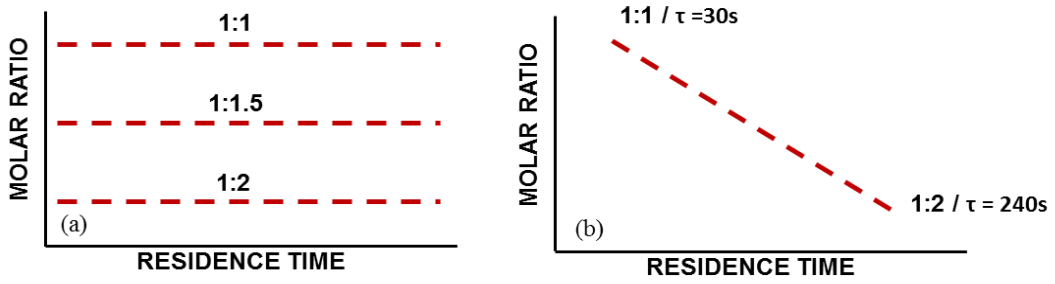

Figure 4-34: Manipulation of (a) single variable (residence time) and (b) multivariable (residence time and chemical ratio) for continuous screening using central baffled mesoscale-OBR.

Figure 4-35 shows the multivariable dynamic screening data and various steady-state experiments for residence time ranging from 30s to 240s and molar ratio of benzaldehyde to n-butylamine increasing gradually from 1:1 to 1:2. The multivariable data screened started with 0.10 mol dm^{-3} at 30s for 1:1 to 0.01mol dm^{-3} at 150s for 1:1.1 and ended at 0.00 mol dm^{-3} at 240s for 1:2 of benzaldehyde to n-butylamine ratio as shown in Table 4-4.

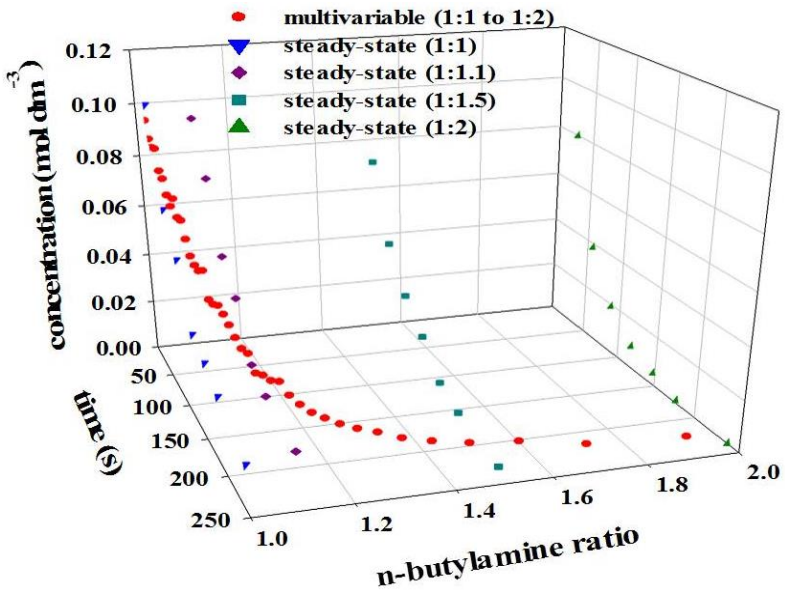

Figure 4-35: Comparison of multivariable dynamic screening with single variable data obtains from multi steady-state manner.

Table 4-4: Experimental conditions for dynamic multivariable screening

Residence time (s)	***N*-butylamine ratio**	**Concentration (mol dm^{-3})**	**Residence time (s)**	***N*-butylamine ratio**	**Concentration (mol dm^{-3})**
30	1.0	0.10	135	1.1	0.02
35	1.0	0.09	140	1.1	0.01
40	1.0	0.07	145	1.1	0.01
45	1.0	0.07	150	1.1	0.01
50	1.0	0.08	155	1.1	0.01
55	1.0	0.07	160	1.1	0.01
60	1.0	0.07	165	1.1	0.01
65	1.0	0.06	170	1.1	0.01
70	1.0	0.06	175	1.2	0.01
75	1.0	0.05	180	1.2	0.01
80	1.0	0.04	185	1.2	0.01
85	1.0	0.04	190	1.2	0.01
90	1.0	0.03	195	1.2	0.01
95	1.0	0.03	200	1.3	0.01
100	1.0	0.03	205	1.3	0.00
105	1.0	0.03	210	1.3	0.00
110	1.0	0.02	215	1.4	0.00
115	1.1	0.03	220	1.5	0.00
120	1.1	0.02	225	1.6	0.00
125	1.1	0.02	230	1.7	0.00
130	1.1	0.02	235	1.9	0.00
135	1.1	0.02	240	1.9	0.00

The concentration data obtained from the multivariable screening was compared individually to the corresponding residence time and molar ratio obtained through dynamic screening of each individual molar ratio of 1:1, 1:1.1, 1:1.5 and 1:2. The dynamic screening of molar ratio 1:1.1 was only conducted and discussed in this section for comparison with the multivariable screening process.

In Figure 4-36, the benzaldehyde concentration profile obtained was similar for both methods (multivariable and dynamic screening) with minor differences (~8%) for each individual concentration data at the first 75s of the reaction. For example, at a 1:1 molar ratio of benzaldehyde to n-butylamine, the data obtained at residence time 35s was 0.09 and 0.08 mol dm^{-3} for multivariable and dynamic screening respectively.

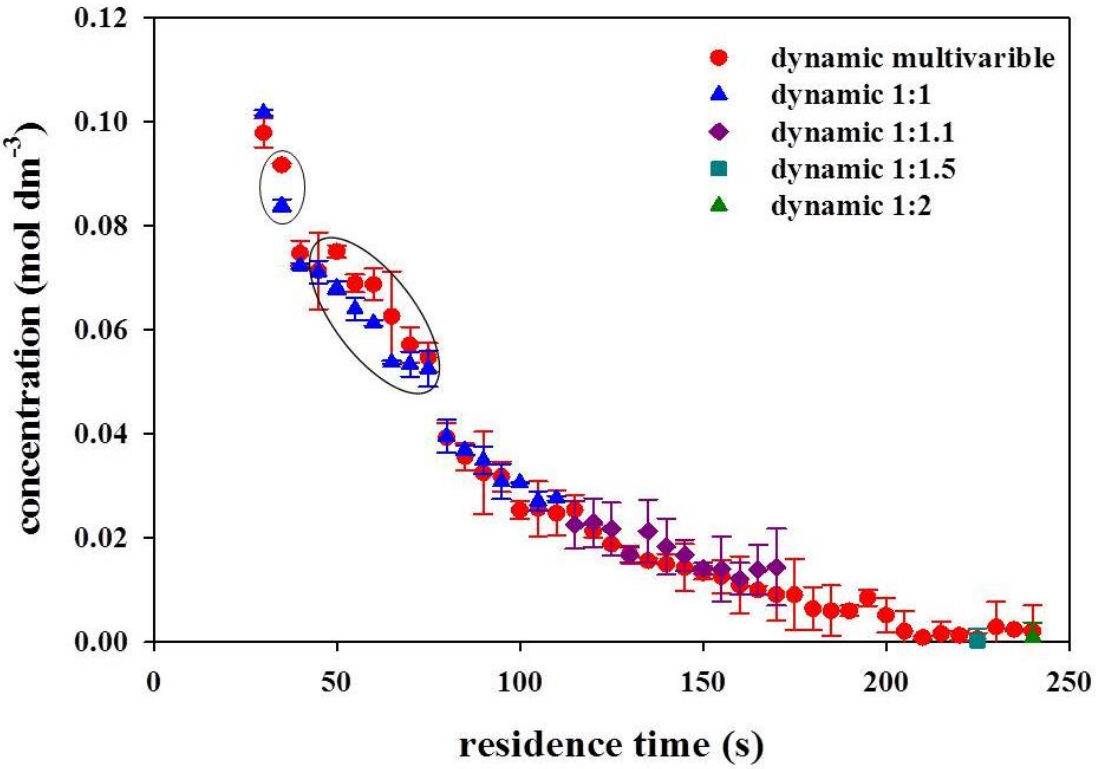

Figure 4-36: Comparison of concentration data obtained from multivariable screening molar ratios from 1:1 to 1:2 with one variable dynamic screening at molar ratios of 1:1, 1:1.1, 1:1.5 and 1:2 of.

Screening for residence times of 30s to 240s from ratios of 1:2 to 1:1 of benzaldehyde to *n*-butylamine was also conducted. This reverse manipulation of the chemical ratio from 1:2 to 1:1 was conducted to show the sensitivity of the screening in changes between different molar ratios. As illustrated in Figure 4-37, the benzaldehyde concentration increased from 0.00mol.dm^{-3} at a residence time of 195s to 0.01mol.dm^{-3}

at 220s. This corresponds to the molar ratio from 1:1.5 to 1:1.1 of benzaldehyde to *n*-butylamine. This was expected due to the different ratio of *n*-butylamine to react with the benzaldehyde. At higher ratios of n-butylamine, the reaction rate was higher, resulting in lower concentrations of benzaldehyde.

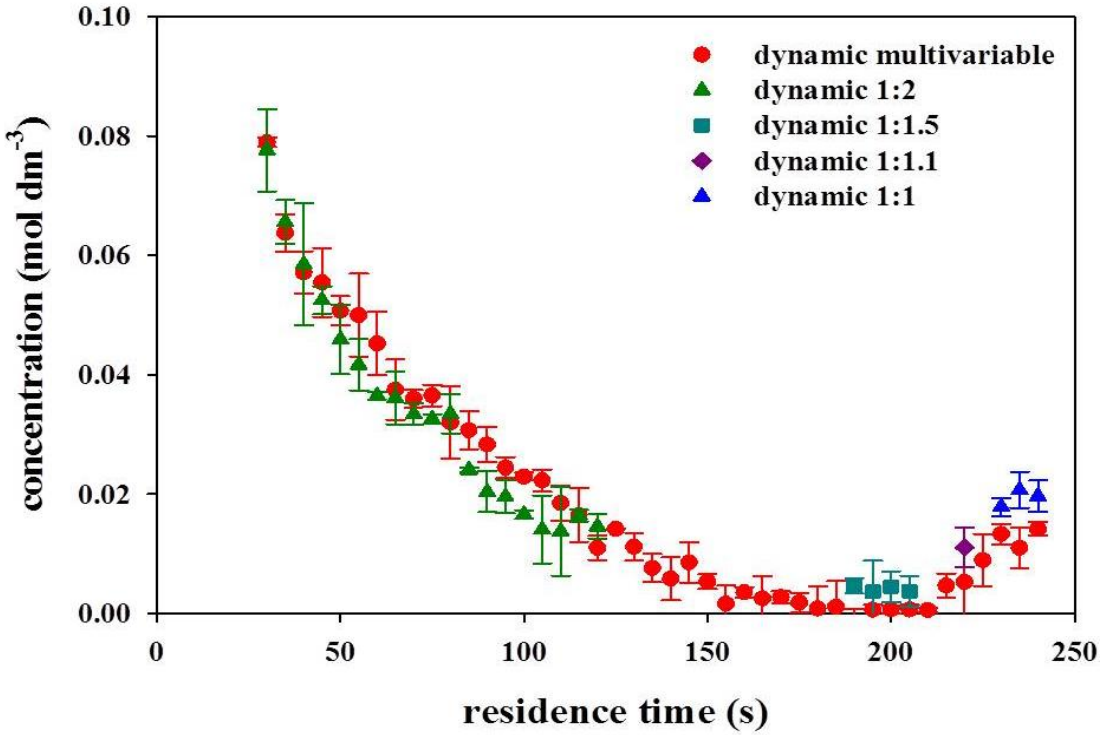

Figure 4-37: Comparison of concentration data obtained from multivariable screening from molar ratios of 1:2 to 1:1 with one variable dynamic screening at molar ratios of 1:1, 1:1.1, 1:1.5 and 1:2 .

A comparison of the dynamic screening for one variable (residence time at molar ratio of 1:1, 1:1.1, 1:1.5 and 1:2 for benzaldehyde to n-butylamine) and multivariable (1:1 to 1:2 and 1:2 to 1:1) exhibited good agreement (~90%). It also allows reactions to be evaluated at any condition rapidly and logically (Figure 4-38). However, the usefulness of this flexibility of the method will depend upon the aims and objectives of the study. Within chemical reaction screening, manipulation of the experimental space as shown in Figure 4-38(a) is useful. This allows rapid and easy parameter manipulations. However, if the aim is to study the reaction kinetics, the route in Figure 4-38(b) is more suitable. Even though only a single variable is changing in this method, the data collected can be applied to calculate various reaction kinetics parameters, such as the rate constant and reaction order. For example, data at different molar ratios can be used in calculating the reaction order via the initial rate method.

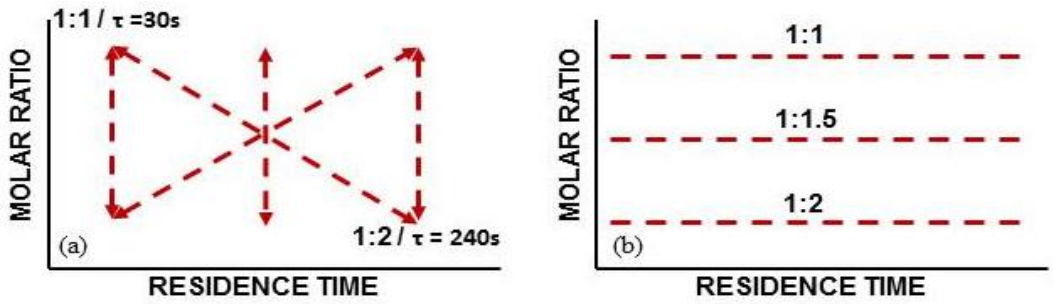

Figure 4-38: Manipulation of continuous screening, using central baffled mesoscale-OBR for (a) chemical reaction screening and (b) reaction kinetic study.

4.4.3.4 Dynamic screening of different imine synthesis

In this section, continuous screening of a series of imine synthesis reactions was investigated. *N*-butylamine was reacted with *o*-tolualdehyde, *m*-tolualdehyde and *p*-tolualdehyde. Batch screening of these reactions was also carried out for comparison. The concentration profiles obtained from the batch screening of different aldehydes with *n*-butylamine are shown in Figure 4-39.

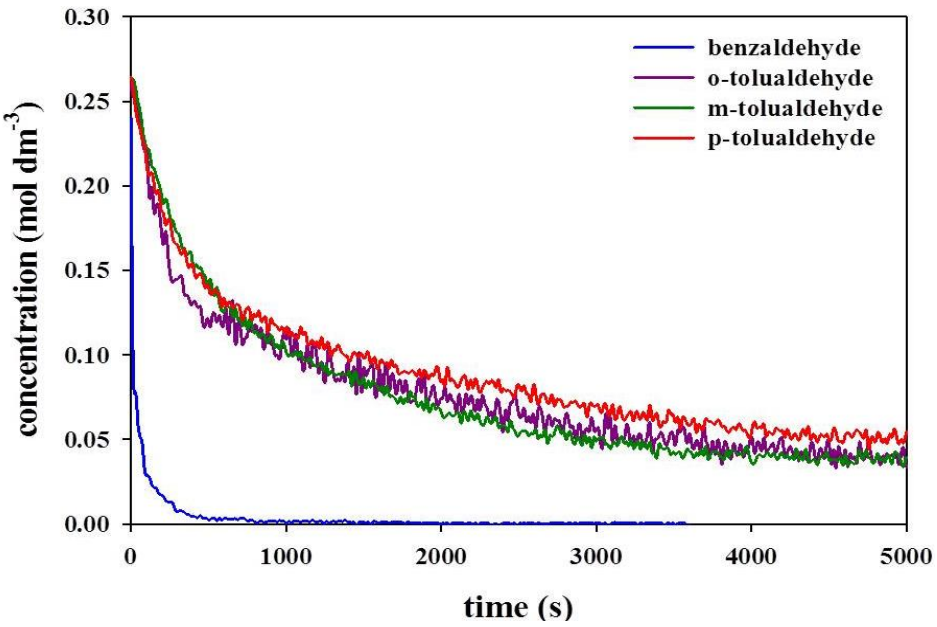

Figure 4-39: Aldehyde reduction profile from batch screening using a batch beaker for imine sysnthesis of benzaldehyde, *o*-, *m*-, and *p*-tolualdehyde with n-butylamine.

The reaction rate was significantly slower for *o*-, *m*- and *p*-tolualdehyde than that for benzaldehyde with *n*-butylamine. The differences in structure of the aldehyde (Figure 4-40) strongly affect the reaction rate. The presence of the methyl group on the *o*-, *m*- and *p*- position of the benzaldehyde increases the electron density of the benzene ring through resonance donating effects. This process stabilises the partial positive charge on

the carbon of the carbonyl group (Figure 4-41), thereby reducing the reactivity of this site with respect to amine attack.

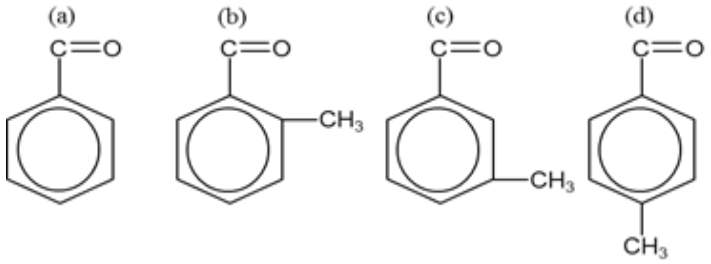

Figure 4-40: Different aldehyde structure of (a) benzaldehyde, (b) *o*-tolualdehyde, (c) *m*-tolualdehyde and (d) *p*-tolualdehyde

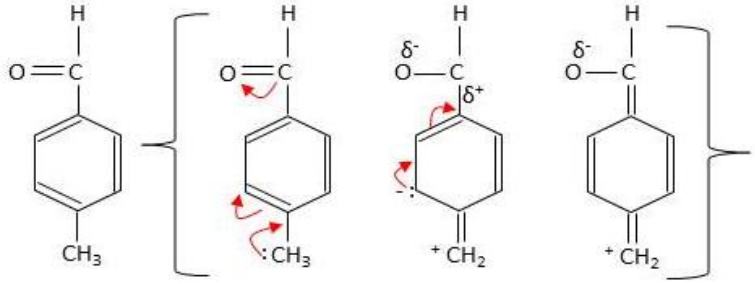

Figure 4-41: Methyl electron donating effects on benzene structure for *p*-tolualdehyde.

The reaction reached its equilibrium at approximately 4500s at a concentration of 0.05mol dm^{-3} (80% conversion). This was not observed with the reaction of benzaldehyde with *n*-butylamine, which exhibited 100% conversion at 1000s.

The concentration profile for a continuous screening of a set of aldehydes (*o*-tolualdehyde, *m*-tolualdehyde, *p*-tolualdehyde and benzaldehyde) with *n*-butylamine to form imine is shown in Figure 4-42.

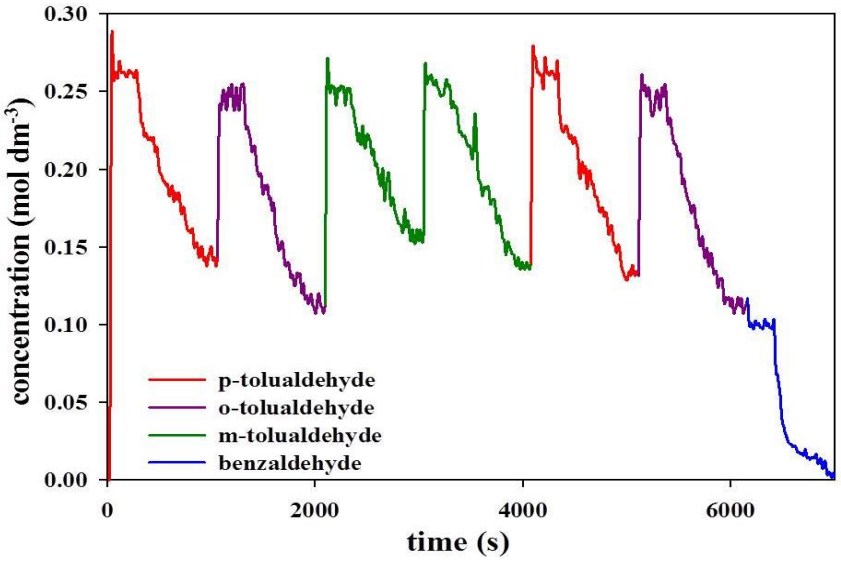

Figure 4-42: Aldehyde reduction profile obtained from multiple dynamic screening of different aldehydes (benzaldehyde, o-, m-, and p-tolualdehyde) with n-butylamine using a mesoscale-OBR.

The screening was conducted from residence times of 30s to 480s. The total processing time for the screening was approximately 2 hours to screen 4 different reactions, including repetitions. This multiple screening process is a good example of the advantages of conducting screening via a continuous method. Procedures that would interrupt the process; e.g. cleaning, refilling and measuring reagent volume were not involved, allowing data to be obtained faster than via batch methods, a ~50% reduction in process development time. Furthermore, with continuous screening using the mesoscale-OBR more data was collected than in the batch method.

Aldehyde reduction profiles of *o*-, *m*- and *p*-tolualdehyde comparison between batch and dynamic screening are presented in Figure 4-43. Good agreement (~98%) was observed between single variable and multiple variable screening methods.

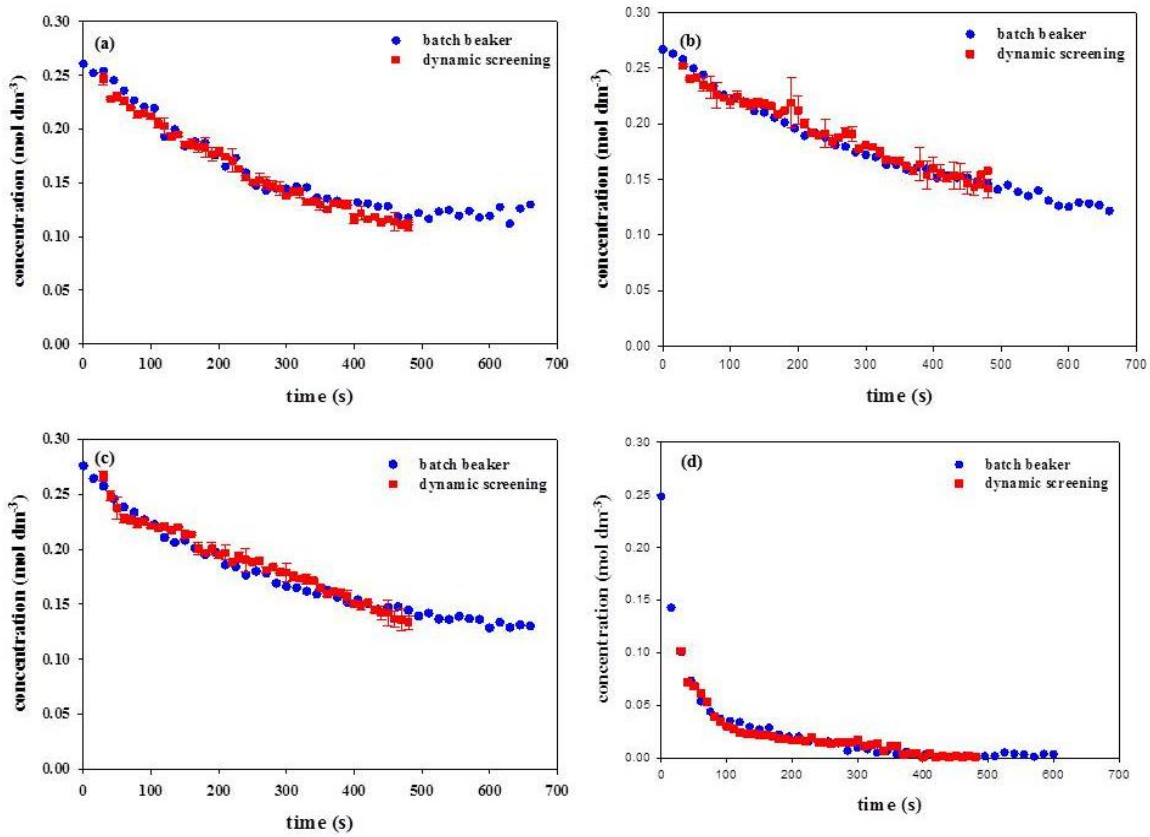

Figure 4-43: Aldehyde reduction profiles in a batch beaker and the mesoscale-OBR dynamic screening for (a) *o*-tolualdehyde, (b) *m*-tolualdehyde, (c) *p*-tolualdehyde and (d) benzaldehyde.

4.4.3.5 Summary of continuous screening

The mesoscale-OBR can be used as a tool for continuous screening of chemical reactions via multi steady-state or dynamic screening. Both methods have their own advantages depending on the objective and the aim of the research. The steady-state screening could be applied to multistep syntheses in which the desired concentration can easily be maintained, while different reagents are introduced into the reactor system. For example, as in Figure 4-44 below, if the best condition for reagent D to react with C is at *y* mol dm^{-3} equivalent to *z* residence time, this condition can easily be maintained at steady-state method to achieve high yields of E.

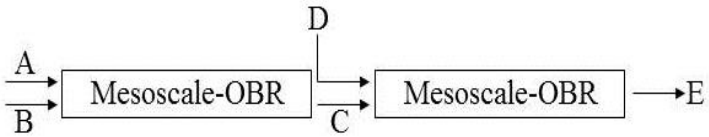

Figure 4-44: Multistep synthesis concepts using mesoscale-OBR steady-state screening

Dynamic screening can be used to optimise reaction conditions and screen catalysts etc, using significantly reduced amounts of reagents and waste generated and time (50% and

25% reduction in process development time compared to batch and multi steady-state method, respectively). Furthermore, the greater number of data points obtained, compared to the batch method, is advantageous for reaction kinetics studies, as they allow a higher degree of accuracy. Such studies can be conducted either in single or multiple variable screening (e.g. different ratios, residence time).

Continuous mesoscale-OBR screening has several advantages over a beaker. Firstly, the amount of reagents can be reduced to approximately 30%, and this increases the overall safety of the process when dealing with hazardous material, as it reduces the inventory used at any given point in time. Secondly, continuous screening provides flexibility for choosing the conditions of interest. It is difficult to change different screening conditions during batch methods i.e. the experiment must be completed or terminated before changing to other sets of screening condition. However with continuous screening this can be conducted *in situ* once the targeted result is achieved. Ideally, the mesoscale-OBR system can also be attached to a feedback controller system which will enhance the screening operation in finding the optimum condition in real time. Lastly, continuous screening also eliminates procedures that interrupt the screening process that necessarily occur in batch screening, e.g. measuring reagent volume and refilling the reactor for each different set of experiments.

The OBR system has also been shown to overcome some of the disadvantages of batch scale-up by easily maintaining the geometric parameter (baffle spacing and baffle open area) and dynamic factors (Re_o, Re_n, St and ψ) of the system. It was reported that scale-up of OBR reactor was linear from 24mm diameter laboratory scale to 150mm diameter pilot plant scale (Ni *et al.*, 2001b; Smith and Mackley, 2006). However, the method of scale-up from mesoscale upwards is as yet unproven, but scale-up must only be demonstrated from the meso to the 24mm diameter scale, as it is understood from this scale upwards.

4.4.4 Determination of reaction kinetic parameters

The data collected through continuous screening experiments of the imine synthesis produced from various aldehydes (benzaldehyde, *o*-tolueladehyde, *m*-tolualdehyde and *p*-tolualdehyde) with *n*-butylamine using the mesoscale-OBR was used to determine reaction kinetic parameters, i.e., reaction orders and rate constant. MATLAB modelling

was applied to predict reaction mechanisms and to obtain kinetic parameters and validated using experimental data.

4.4.4.1 Conventional experimental kinetics parameter determination

The initial rates and integration rate law methods were used to determine the reaction orders of individual reactants and rate constant of 1-butanamine, N-(phenylmethylene)- from benzaldehyde and *n*-butylamine experimentally. The proposed reaction mechanism for this reaction is shown in eq. 4-1 based on the benzaldehyde reduction profile obtained in Figure 4-20 (section 4.4.1). The reaction was completed (benzaldehyde profile reached zero) at reaction times above 600s and 300s for ratios of aldehyde to *n*-butylamine of 1:1 and 1:4. Therefore, the reverse rate constants (k_{-1} and k_{-2}) were assumed to be zero. The differential equations for the anticipated reaction mechanism are listed in eqs.4-2 to 4-6.

$$\mathrm{A} + \mathrm{B} \xrightarrow{k_1} \mathrm{C} \xrightarrow{k_2} \mathrm{D} + \mathrm{E} \qquad \text{eq. 4-1}$$

$$\frac{dA}{dt} = -k_1[A]^m[B]^n \qquad \text{eq. 4-2}$$

$$\frac{dB}{dt} = -k_1[A]^m[B]^n \qquad \text{eq. 4-3}$$

$$\frac{dC}{dt} = k_1[A]^m[B]^n - k_2[C]^o \qquad \text{eq. 4-4}$$

$$\frac{dD}{dt} = k_2[C]^o \qquad \text{eq. 4-5}$$

$$\frac{dE}{dt} = k_2[C]^o \qquad \text{eq. 4-6}$$

…where A, B, C, D and E represent benzaldehyde, *n*-butylamine, intermediate, imine and water, respectively. m, n and o are reaction orders for benzaldehyde, *n*-butylamine and intermediate respectively.

The calculated initial rates at various molar ratios of benzaldehyde to *n*-butylamine (1:1 to 1:4) are shown in Table 4-5. From these, the reaction order (n) for *n*-butylamine was calculated at an average of 0.22 (refer to Appendix D). At an equal initial concentration of benzaldehyde (A_o) and *n*-butylamine (B_o), the rate expression of benzaldehyde (eq.4-2) can be simplified as below (eq.4-7).

Table 4-5: Initial reaction rate of at various molar ratios of benzaldehyde to n-butylamine

Benzaldehyde concentration (mol dm^{-3})	**N-butylamine concentration (mol dm^{-3})**	**Initial rate (mol dm^{-3}/ s)**
0.25	0.25	7.00 x 10^{-3}
0.25	0.5	8.10 x 10^{-3}
0.25	1.00	9.10 x 10^{-3}
0.25	1.50	1.03 x 10^{-2}

$$\frac{dA}{dt} = -k_1[A]^{m+0.22} \qquad \text{eq. 4-7}$$

Integrating results from eq.4-7 displays a relationship between benzaldehyde concentration and reaction rate constant (k_1) as shown in eq.4-8:-

$$\frac{50}{(50m-39)[A]^{\frac{50m-39}{50}}} = \frac{50}{(50m-39)[A_o]^{\frac{50m-39}{50}}} + kt \qquad \text{eq. 4-8}$$

Graphical plots of eq.4-8 (refer to Appendix E) were used to determine the rate constant and reaction order through the slope and linearity value respectively. At various m values (1.0-2.0 with 0.1 interval), the highest coefficient R^2 value obtained was at m=1.7 (Table 4-6).

Table 4-6: Comparison of rate constant and benzaldehyde order according to the best fit of regression at equal molar ratio of benzaldehyde and *n*-butylamine.

Benzaldehyde order (m)	**Rate constant (mol $^{1-(m+n)}$. L $^{(m+n)-1}$. s^{-1})**	**R^2**
1.00	2.7 x 10^{-2}	0.9226
1.10	3.6 x 10^{-2}	0.9337
1.20	4.8 x 10^{-2}	0.9427
1.30	6.4 x 10^{-2}	0.9498
1.40	8.6 x 10^{-2}	0.9551
1.50	1.2 x 10^{-1}	0.9586
1.60	1.6 x 10^{-1}	0.9606
1.70	2.1 x 10^{-1}	0.9610
1.80	2.9 x 10^{-1}	0.9600
1.90	3.9 x 10-1	0.9578
2.00	5.3 x 10-1	0.9545

This resulted in a rate constant (k_1) of 2.1x10^{-1} $mol^{-0.9}L^{0.9}s^{-1}$ with the total reaction order of 1.9 (1.7 for benzaldehyde (m) and 0.22 for n-butylamine (n)). The total reaction order of 1.9 obtained for the reaction between benzaldehyde and *n*-butylamine in hexane agrees well with other researchers' findings (Crowell and Peck, 1953; Hill and Crowell, 1956; Santerre *et al.*, 1958). Their findings exhibited a reaction order of 2.0 which used the Schiff base reaction from an aromatic aldehydes or ketone with primary amines in polar solvents either with or without the present of acid catalyst. This reaction order determination was conducted through integration of pseudo first order rate law. However, their findings did not state the reaction order for each of the components (aldehyde and amine).

The integration method to determine the kinetic parameters becomes complex at unequal molar ratios. Therefore, numerical modelling method was used to determine the reaction kinetics parameter at unequal concentrations for comparison purposes to the results obtained from the equal concentration ratio condition of the benzaldehyde and *n*-butylamine. Furthermore, the modelling helps to understand and validate the propose reaction mechanisms of the chemical reaction studied.

4.4.4.2 Numerical method analysis through mathematical modelling

The benzaldehyde and *n*-butylamine imination reaction was modelled using the reaction mechanisms shown in eq.4-1 (above in section 4.4.4.1) using Matlab software (version R2011a). The reaction orders for individual reagents (m: benzaldehyde and n: n-butylamine) and rate constant (k_1) obtained from experiment using the integration method was used as the initial value for the model (Table 4-7). As for the rate constant (k_2) and reaction order of the intermediate (o), the value were listed in a range of 0.04-0.06 and 1-1.5 with 0.005 and 0.5 interval respectively (Table 4-7). These intervals were chosen to provide more intermediate value to increase the modelling data looping in determine the kinetic parameters data. Smaller intervals values can also be used, such as 0.01 for the intermediate (o) interval, but require longer simulation times (~1-2 hours). The model was run until a best fit (sum square of error (SSE) ≤1.0%) between experimental and modelling results was achieved. This process was applied to the different ratios of benzaldehyde to *n*-butylamine conditions (1:1 to 1:4) at various screening methods (batch, continuous steady-state and continuous dynamic).

Table 4-7: Kinetic parameters for benzaldehyde and *n*-butylamine imination used in modelling.

k_1	0.21
k_2	0.04-0.06 (at 0.005 interval)
m	1.7
n	0.22
o	1-1.5 (at 0.5 interval)

Table 4-8 shows the modelling kinetics parameters obtained at various molar ratios of benzaldehyde and *n*-butylamine. At k_2=0.045 and o=1, the best fit was observed in Figure 4-45. The results show that the rate constant (k_1) and reaction order (m and n) obtained from the experimental calculation are valid to fit the propose reaction mechanism (eq.4-1 in section 4.4.4.1) with benzaldehyde and imine SSE < 1%. Apart from that, through this modelling method it was possible to obtained the value for the rate constant (k_2) and reaction order of intermediate (o), which was impossible with the experimental integration method due to the intermediate (carbinolamine) not being detected (Evans *et al.*, 2002; Iwasawa *et al.*, 2007).

Table 4-8: Kinetic parameter obtained from modelling for batch screening using mesoscale-OBR at different ratio of benzaldehyde and n-butylamine.

Ratio	**1:1**	**1:2**	**1:4**
Benzaldehyde concentration (mol dm^{-3})	0.25	0.25	0.25
N-butylamine concentration (mol dm^{-3})	0.25	0.50	1.00
Rate constant (k_1) ($mol^{-0.9}L^{0.9}s^{-1}$)	0.21	0.21	0.21
Rate constant (k_2) ($mol^{-0.9}L^{0.9}s^{-1}$)	0.045	0.045	0.045
Benzaldehyde order (m)	1.7	1.7	1.7
N-butylamine order (n)	0.22	0.22	0.22
Intermediate order (o)	1	1	1
SSE error (%)			
Benzaldehyde concentration fit	0.02	0.02	0.01
Imine concentration fit	0.30	0.12	0.01

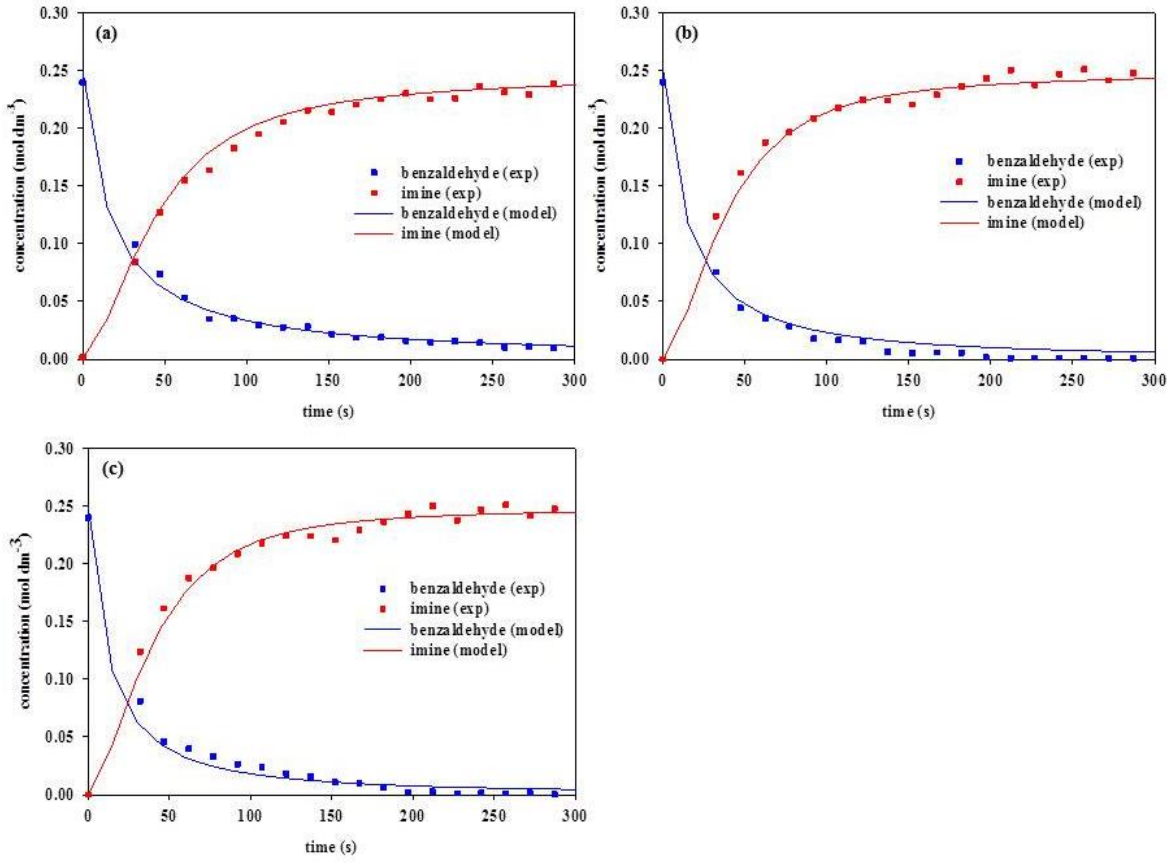

Figure 4-45: Concentration profiles obtained from modelling (solid lines) and experimental results (dotted lines) using the mesoscale OBR reactor for benzaldehyde reduction and imine formation at molar ratios of benzaldehyde: n-butylamine of (a) 1:1 (b) 1:2 (c) 1:4 screened via batch manner.

A good fit (SSE < 1%) between experimental data collected via a continuous method and modelling results was also observed regardless the ratio of the benzaldehyde to n-

butylamine (1:1 and 1:2) or screening manner (steady-state and dynamic as shown in Figure 4-46 and Figure 4-47 respectively). Similar reaction mechanisms (eq.4-1) shown in section 4.4.4.1 were used to obtain concentration profiles. Summary of the reaction kinetics parameter for these fits was illustrated in Table 4-9 (following).

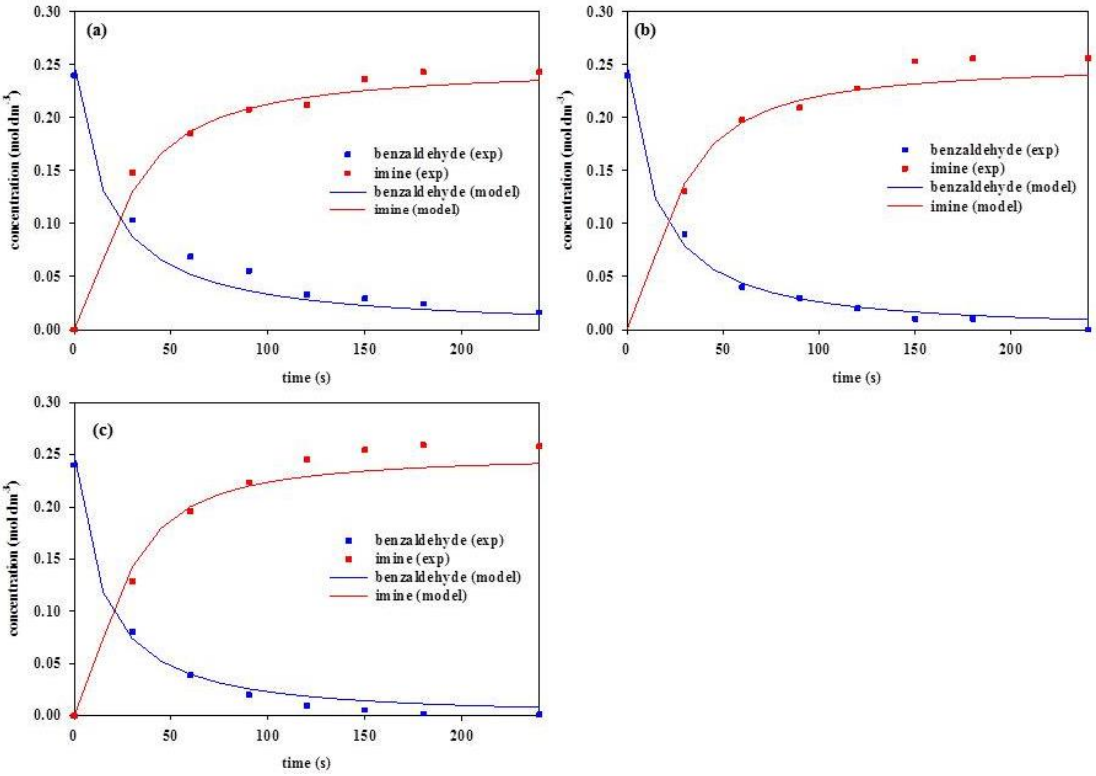

Figure 4-46: Concentration profiles obtained from Matlab modelling (solid lines) and experimental results (dotted lines) using continuous steady-state screening of the mesoscale reactor for benzaldehyde reduction and imine formation at molar ratios (a) 1:1 (b) 1:1.5 (c) 1:2 of benzaldehyde: n-butylamine.

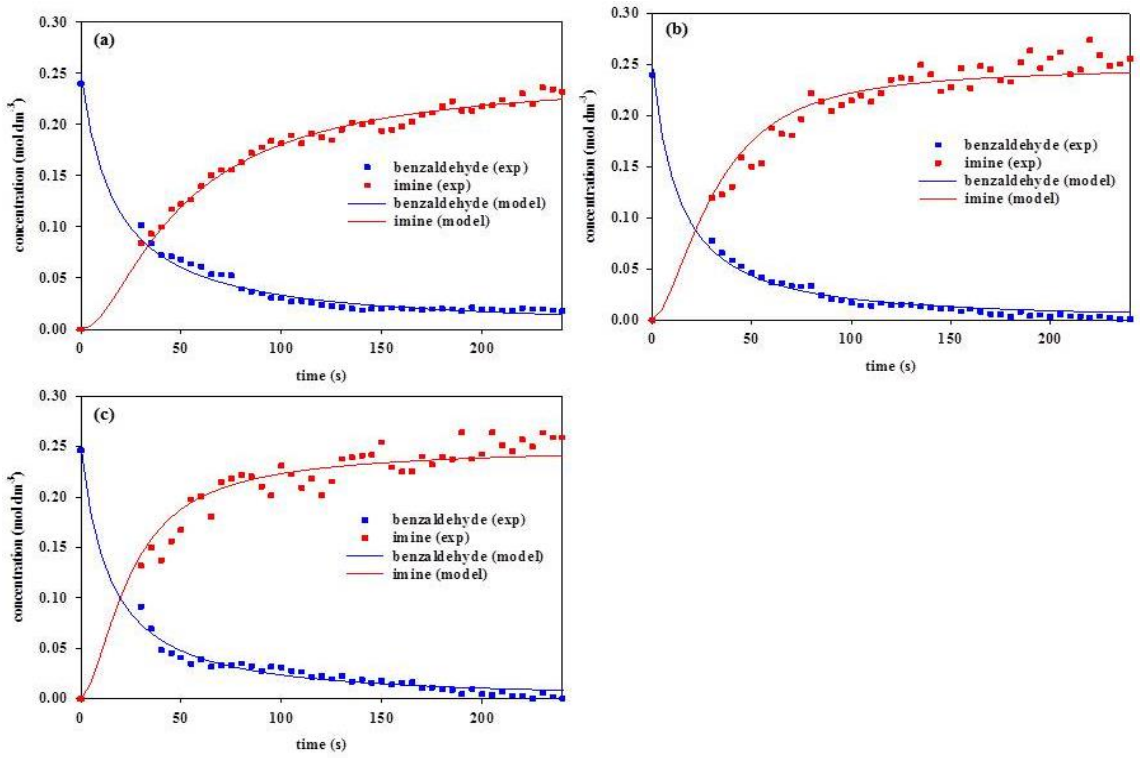

Figure 4-47: Concentration profiles obtained from Matlab modelling (solid lines) and experimental results (dotted line) using continuous dynamic screening of the mesoscale reactor for benzaldehyde reduction and imine formation at molar ratios (a) 1:1 (b) 1:1.5 (c) 1:2 of benzaldehyde: n-butylamine.

Table 4-9: Kinetic parameters obtained from modelling for continous screening (steady-state and dynamic manner) using mesoscale-OBR at different ratio of benzaldehyde and n-butylamine.

	Steady-state screening			**Dynamic screening**		
Ratio	1:1	1:1.5	1:2	1:1	1:1.5	1:2
Benzaldehyde concentration (mol dm^{-3})	0.25	0.25	0.25	0.25	0.25	0.25
N-butylamine concentration (mol dm^{-3})	0.25	0.38	0.50	0.25	0.38	0.50
Rate constant (k_1) ($mol^{-0.9}L^{0.9}s^{-1}$)	0.21	0.21	0.21	0.23	0.23	0.23
Rate constant (k_2) ($mol^{-0.9}L^{0.9}s^{-1}$)	0.045	0.045	0.045	0.055	0.055	0.055
Benzaldehyde order (m)	1.7	1.7	1.7	1.7	1.7	1.7
N-butylamine order (n)	0.22	0.22	0.22	0.22	0.22	0.22
Intermediate order (o)	1	1	1	1	1	1
SSE error (%)						
Benzaldehyde concentration fit	0.37	0.05	0.19	0.21	0.10	0.66
Imine concentration fit	0.11	0.38	0.70	0.13	0.00	0.33

The kinetic parameters (k_1, k_2, m, n, and o value) for the steady-state continuous screening as shown in Table 4-9 were similar to those obtained via batch screening which fits between the experimental and modelling data at SSE <1%. In order to achieve good fits (SSE < 1.0%) between the experimental and modelling data for the dynamic screening, adjustment on the k_1 and k_2 value were conducted to $2.3x10^{-1}$ $mol^{-0.9}L^{0.9}s^{-1}$ and $5.5x10^{-2}$ $mol^{-0.9}L^{0.9}s^{-1}$ with differences of 7% and 15% respectively than the value used for the data collected via batch screening data. This was resulted due to the frequency of the data interval at 5s compared to the 15s via the dynamic and batch screening respectively. However, the differences were not significant.

For other aldehyde reactions (*o*-tolualdehyde, *m*-tolualdehyde and *p*–tolualdehyde) with *n*-butylamine, the initial rates and integration rate law used with the benzaldehyde reaction could not be implemented due to the limitation of the screening data collected (experiments was only conducted at the ratio of 1:1 of aldehyde to n-butylamine). This is because the aim was only to demonstrate the flexibility of the mesoscale-OBR in conducting multiple screening of different reactions continuously. However, the reaction kinetics was determined using the modelling method. Different reaction mechanisms from benzaldehyde and *n*-butylamine reaction were proposed according to the aldehydes (*o*-tolualdehyde, *m*-tolualdehyde and *p*–tolualdehyde) concentration profiles shown in Figure 4-39 (section 4.4.3.4). The profiles show a limiting equilibrium concentration value greater than zero. This resulted with a significant opposing reaction (k_{-1} and k_{-2}) which was not present with the benzaldehyde and *n*-butylamine reaction (E.S.Swinbourne, 1971). With that, the reaction mechanism in eq.4-9 was proposed which includes the reversible rate constants (k_{-1} and k_{-2}). The initial reaction parameters were shown in Table 4-10.

$$A + B \underset{k_{-1}}{\overset{k_1}{\leftrightarrow}} C \underset{k_{-2}}{\overset{k_2}{\leftrightarrow}} D + E \qquad \text{eq. 4-9}$$

…where A, B, C, D and E represent benzaldehyde, *n*-butylamine, intermediate, imine and water, respectively. m.n,o,p and q are reaction orders for benzaldehyde, *n*-butylamine, intermediate, imine and water, respectively.

Table 4-10: Kinetic parameters used in modelling for different aldehyde (*o*-tolualdehyde, *m*-tolualdehyde and *p*–tolualdehyde) with *n*-butylamine at molar ratio of 1:1.

k_1	0.001-0.09
k_2	0.001-0.09
k_{-1}	0.0001-0.01
k_{-2}	0.0001-0.01
m	1.0-3.0
n	0.1-1.0
o	1.0-2.0
p	1-1.5
q	1-1.5

The proposed mechanism delivered good agreement (SSE <1.0%) between the experimental and modelling data as shown in Figure 4-48 for the different aldehydes (*o*-tolualdehyde, *m*-tolualdehyde and *p*–tolualdehyde) with *n*-butylamine. Detailed kinetic parameter results are shown in Table 4-11.

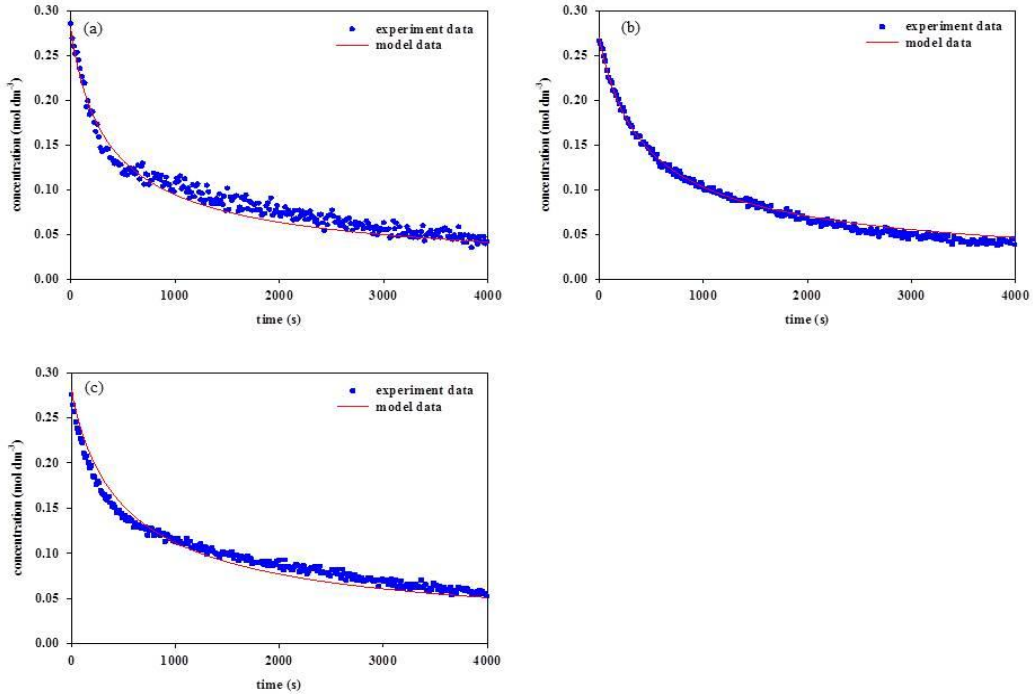

Figure 4-48: (a) *o*-tolualdehyde (b) *m*-tolualdehyde and (c) *p*-tolualdehyde reduction concentration profiles obtained from Matlab modelling (solid lines) and experimental results (dotted square) using mesoscale-OBR via batch screening.

Table 4-11: Reaction kinetics data obtained for reaction of *o*-tolualdehyde, *m*-tolualdehyde and *p*-tolualdehyde with *n*-butylamine at molar ratio 1:1.

	***o*-tolualdehyde**	***m*-tolualdehyde**	***p*-tolualdehyde**
Aldehyde and N-butylamine ratio	1:1	1:1	1:1
Rate constant (k_1) ($mol^{-1.5}L^{1.5}s^{-1}$)	0.018	0.015	0.013
Rate constant (k_{-1}) ($mol^{-1.5}L^{1.5}s^{-1}$)	0.0004	0.0004	0.0004
Rate constant (k_2) ($mol^{-1.5}L^{1.5}s^{-1}$)	0.04	0.04	0.04
Rate constant (k_{-2}) ($mol^{-1.5}L^{1.5}s^{-1}$)	0.0004	0.0004	0.0004
aldehyde order (m)	2.2	2.2	2.2
N-butylamine order (n)	0.28	0.28	0.28
Intermediate order (o)	2	2	2
Imine order (p)	1	1	1
Water order (q)	1	1	1
SSE error (%)			
Benzaldehyde concentration fit	0.79	0.06	0.35

Regardless of the aldehydes, the reaction order for each of the reagent and product was similar at 2.2, 0.28, 2, 1 and 1 for aldehyde, *n*-butylamine, intermediate, imine and water respectively. Similar findings were also observed for rate constant value of k_{-1}, k_2 and k_{-2}. Differences were only observed with the rate constant (k_1) value. It shows value increased from $1.3x10^{-2}$ to $1.5x10^{-2}$ followed with $1.8x10^{-2}$ $mol^{-1.5}L^{1.5}s^{-1}$ for *p*-tolualdehyde, *m*-tolualdehyde and *o*-tolualdehyde respectively. The presence of the methyl group increases the electron density of the benzene ring, but the effects of stabilising the partial positive charge on the carbon of the carbonyl group decreases with the following trend: ortho- < meta- < para-.

4.4.5 Solvent-free imine synthesis in mesoscale-OBR reactors

Solvents are commonly used in chemical reactions both in laboratory and industry. The role of a solvent varies depending on the nature of the chemical reactions. Its role can be to dissolve solid substances to remove mass transfer limitations or to reduce the effect of exothermic reactions.

The reaction between benzaldehyde and *n*-butyalmine is exothermic. By using hexane as solvent, the increase in temperature at the initial stage of the reaction (~100s) was only 2^{o}C difference, as shown in Figure 4-49, below.

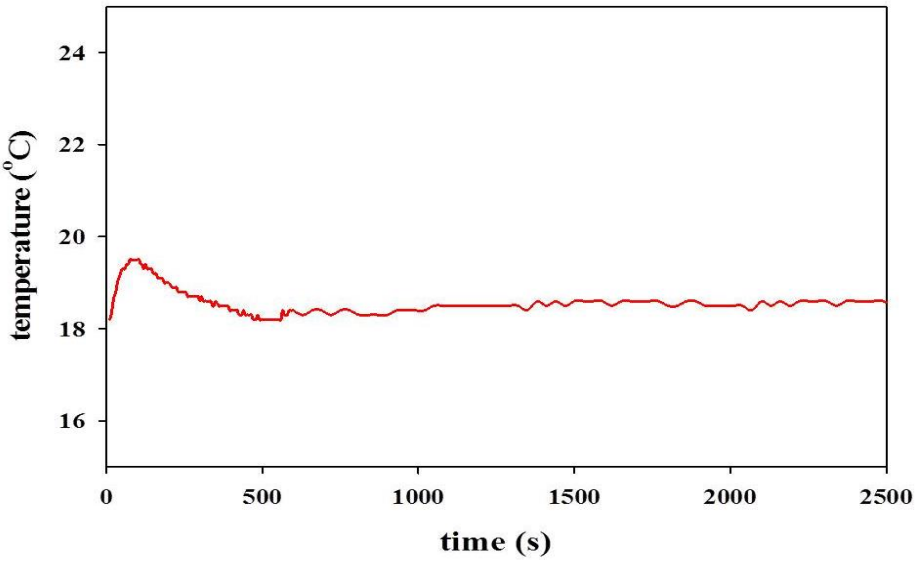

Figure 4-49: Temperature profile for 1:1 ratio of benzaldehyde to *n*-butylamine in hexane using a beaker via batch screening.

However, without solvent, the temperature of the reaction mixture increased rapidly to 90^{o}C, which is above the boiling point of *n*-butylamine (77-79^{o}C), at 50s reaction time and slowly decreased to 30^{o}C and 20^{o}C for the non-jacketed and for jacketed beaker system (water as the cooling fluid) respectively (Figure 4-50). This would lead to significant difficulties in performing this reaction in a conventional batch reactor, predominantly safety issues.

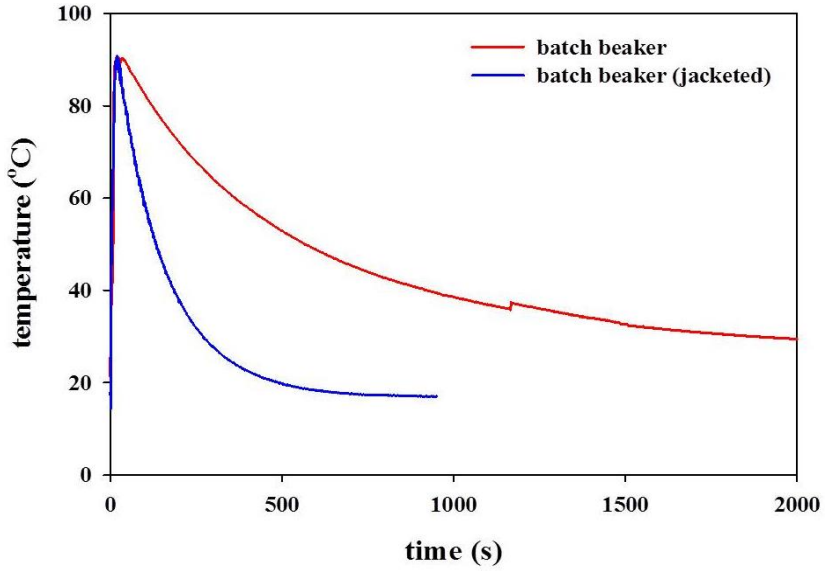

Figure 4-50: Temperature profile for 1:1 ratio of benzaldehyde to *n*-butylamine with solvent-free system using non-jacketed and jacketed beaker via batch screening.

However, by conducting the solvent-free reaction in the mesoscale-OBR (either batch or continuous mode), the hazard is reduced due to the small volume of reagents in the system and the higher surface area to volume ratio, which allows more effective heat transfer.

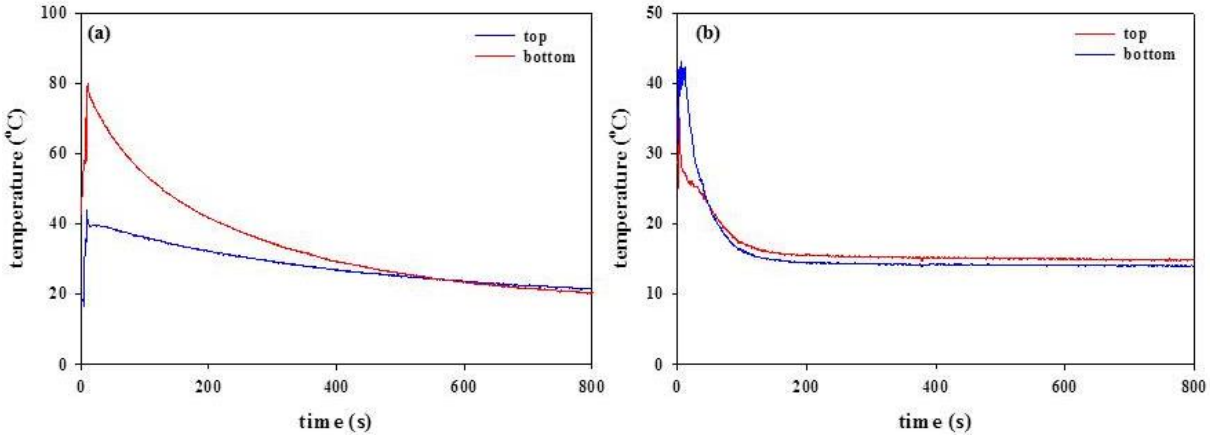

Figure 4-51: Temperature profiles for solvent-free reaction of benzaldehyde with n-butylamine at a molar ratio of 1:1 using (a) non-jacketed and (b) jacketed batch mesoscale-OBR.

As shown in Figure 4-51, the temperature was measured along the length of the mesoscale-OBR at 10cm (top) and 28cm (bottom) from the outlet. With the non-jacketed mesoscale-OBR (Figure 4-51(a)), the highest temperature was 80°C at 10s after which it slowly decreased to 20°C at ~500s. This was much shorter than the time required (2000s) for a non-jacketed beaker to reach the same minimum temperature (~20°C) (Figure 4-50). One reason for this was the higher surface area to volume ratio

for the mesoscale-OBR than the beaker system (10:1), allowing the heat generated to be more easily distributed to the surroundings. However, isothermal operation along the non-jacketed mesoscale-OBR was not achieved at the beginning of the reaction (<400s). The temperature difference was significant, at an average of 40^{o}C, and decreased with time. By using water as cooling fluid, the initial temperature along the jacketed mesoscale-OBR became much more uniform, with around 5^{o}C difference between the two points (Figure 4-51(b)) after ~20s reaction time. The isothermal temperature (20^{o}C) was reached at 50s. This decreased further to ~15^{o}C at 100s. This resulted in a lower temperature during the screening, thereby reducing the hazards of the solvent-free reaction.

To examine the effect of temperature on the reaction rate of a chemical reaction, the concentration profiles of benzaldehyde obtained from the batch non-jacketed and jacketed beaker and mesoscale-OBR are shown in Figure 4-52.

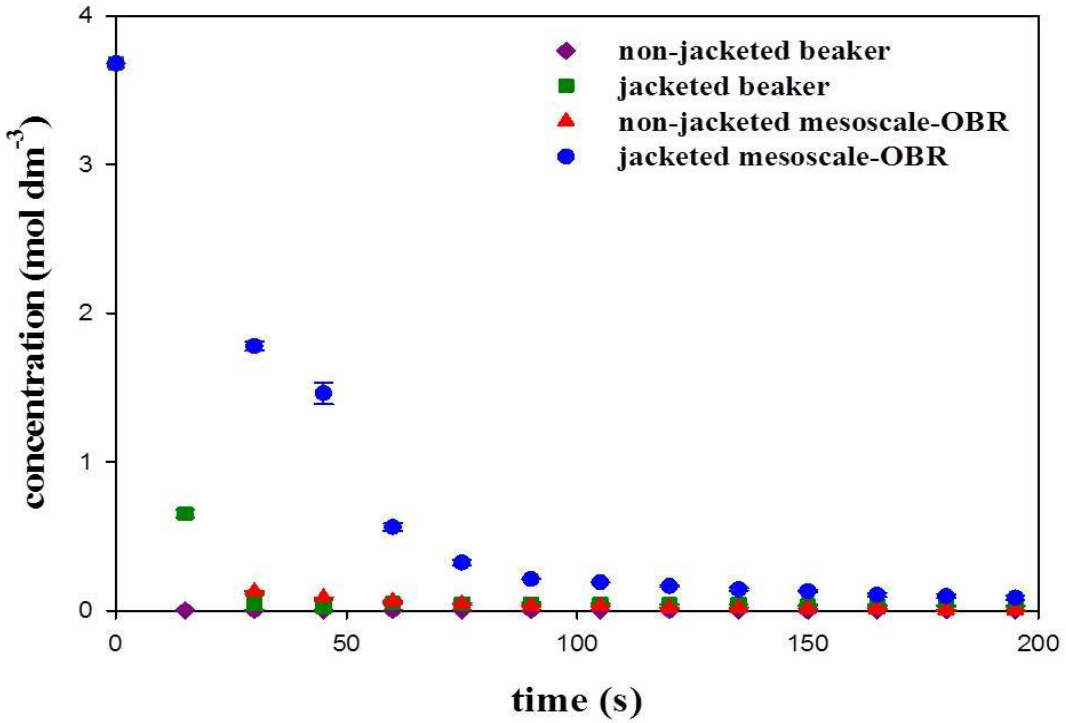

Figure 4-52: Benzaldehyde concentration profiles at 1:1 molar ratio of benzaldehyde to n-butylamine in batch using non-jacketed and jacketed beaker and mesoscale-OBR.

As observed in Figure 4-52, the benzaldehyde reduction rate obtained in the non-jacketed beaker was higher than that in the non-jacketed mesoscale-OBR (approximately 4%). The same trend was also observed for the jacketed reactors. For example, the benzaldehyde reduction rate at 30s was 0.12 M s^{-1} and 0.06 M s^{-1} for

jacketed beaker and jacketed mesoscale-OBR respectively. This was expected due to the higher temperatures in the beaker system than in the mesoscale OBR during the initial period of the reaction.

With the temperature established and concentration profile for solvent-free batch screening using the mesoscale-OBR, the system was used for continuous multi-steady screening method. This allowed temperature profiles to be determined at different conditions to assess the uniformity of temperature along the reactor. The screening was conducted at residence times of 30s, 60s, 90s, 120s and 600s. Temperature profiles for continuous screening for the non-jacketed mesoscale-OBR system and jacketed mesoscale-OBR are illustrated in Figure 4-53 and in Figure 4-54 respectively.

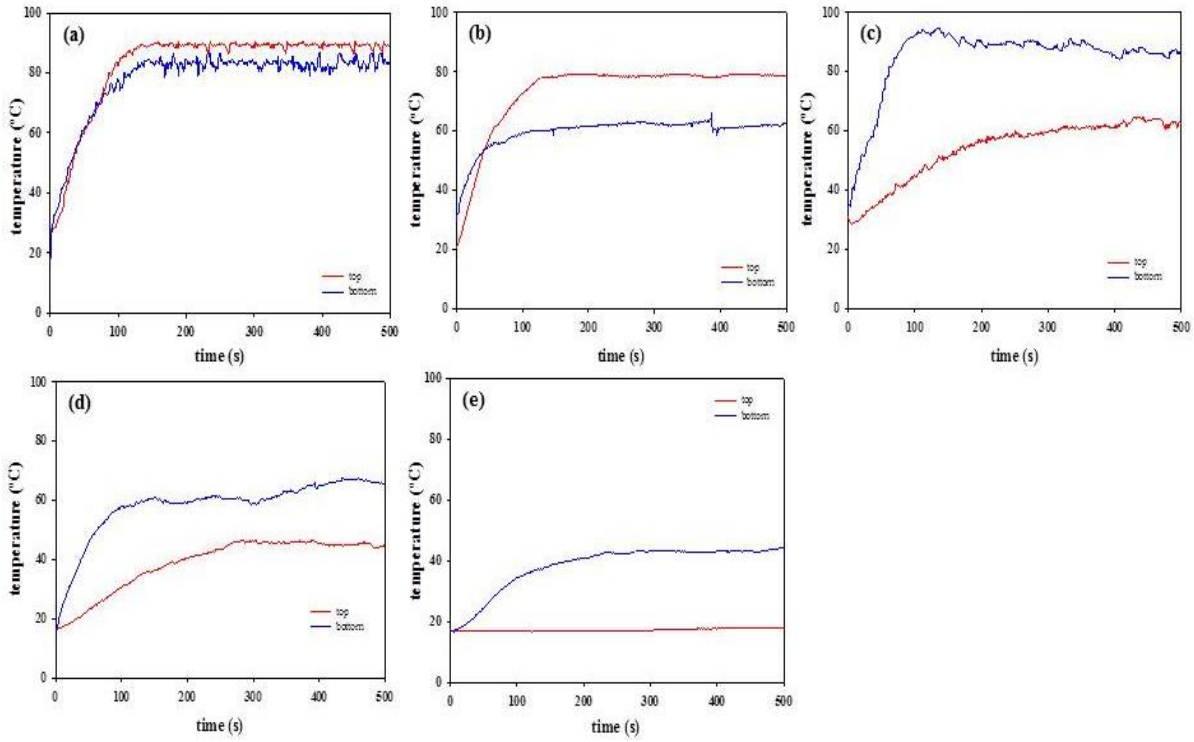

Figure 4-53: Temperature profiles for solvent-free reaction of benzaldehyde with *n*-butylamine at 1:1 molar ratio using the non-jacketed mesoscale-OBR at (a) 30s, (b) 60s, (c) 90s, (d) 120s and (e) 600s.

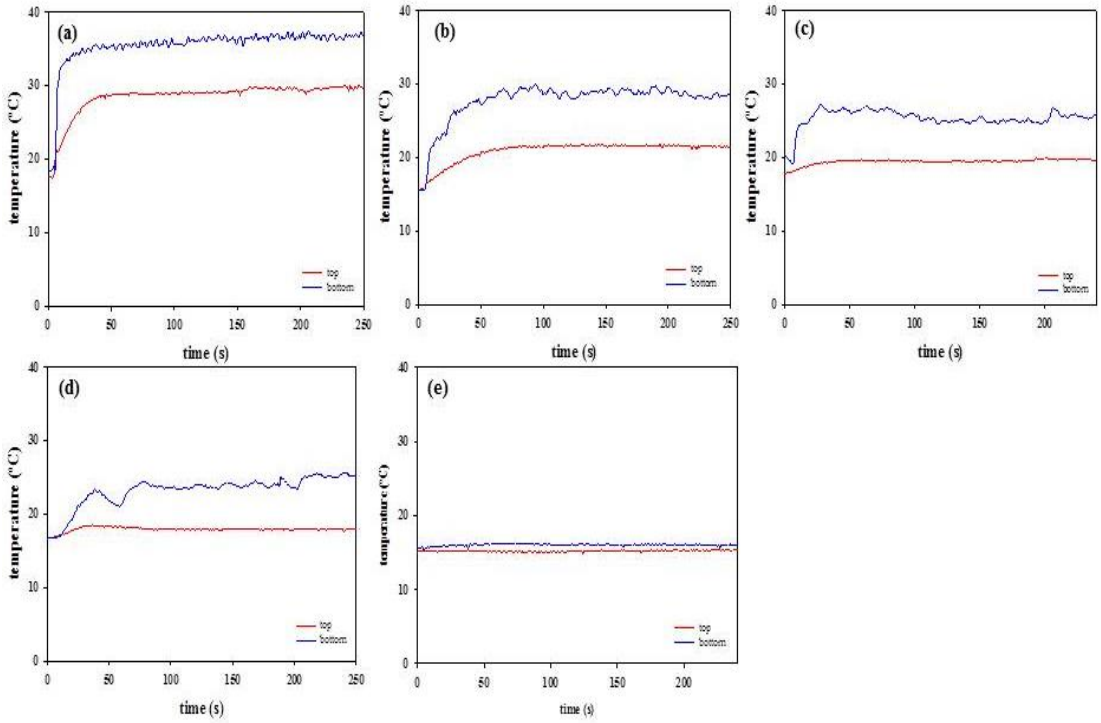

Figure 4-54: Temperature profiles for solvent-free reaction of benzaldehyde with *n*-butylamine at 1:1 molar ratio using the jacketed mesoscale-OBR at (a) 30s, (b) 60s, (c) 90s, (d) 120s and (e) 600s.

Regardless of the position (top or bottom), the temperature reached its steady state at approximately 100s for the non-jacketed mesoscale-OBR and 50s for the jacketed mesoscale-OBR at all tested residence times. Isothermality was not established in either case. The temperature difference between the top and the bottom varied between 17°C and 27°C for residence times of 60-600s for the non-jacketed mesoscale-OBR (Table 4-12).

Table 4-12: Temperature differences between top and bottom positions inside the non-jacketed and jacketed mesoscale-OBR

Residence time (s)	**Non-jacketed mesoscale-OBR (°C)**	**Jacketed mesoscale-OBR (°C)**
30	6.0 ± 0.52	7.0 ± 0.62
60	17.0 ± 0.80	7.0 ± 0.30
90	27.0 ± 1.20	6.0 ± 0.63
120	18.0 ± 1.30	6.0 ± 0.60
600	26.0 ± 0.87	0.8 ± 0.52

The temperature difference in the non-jacketed mesoscale-OBR was higher than that in the jacketed mesoscale-OBR. For example, at 60s, the temperature difference between the top and the bottom was 17.0 ± 0.80^{o}C for the non-jacketed mesoscale-OBR but only 7.0 ± 0.30^{o}C for the jacketed mesoscale-OBR. The large difference in the non-jacketed system was due to the heat generated at the initial mixing point of reactor (bottom temperature). With the jacketed system, this heat was more effectively removed by the cooling fluid (water).

Benzaldehyde concentration profiles obtained from the continuous screenings using the jacketed and non-jacketed mesoscale-OBR are shown in Figure 4-55 Figure 4-56, below:

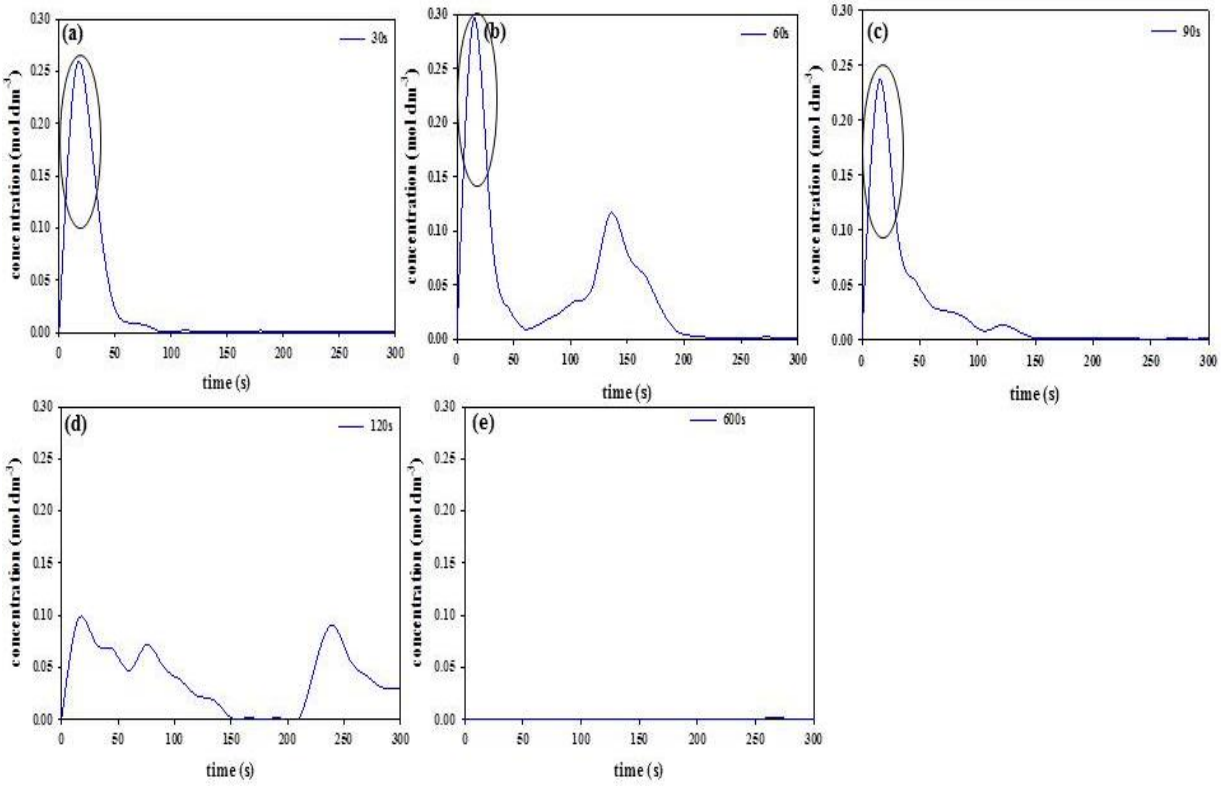

Figure 4-55: Benzaldehyde concentration profiles obtained in solvent-free reaction of benzaldehyde with n-butylamine at 1:1 molar ratio using the non-jacketed mesoscale-OBR screened at (a) 30s, (b) 60s, (c) 90s, (d) 120s and (e) 600s.

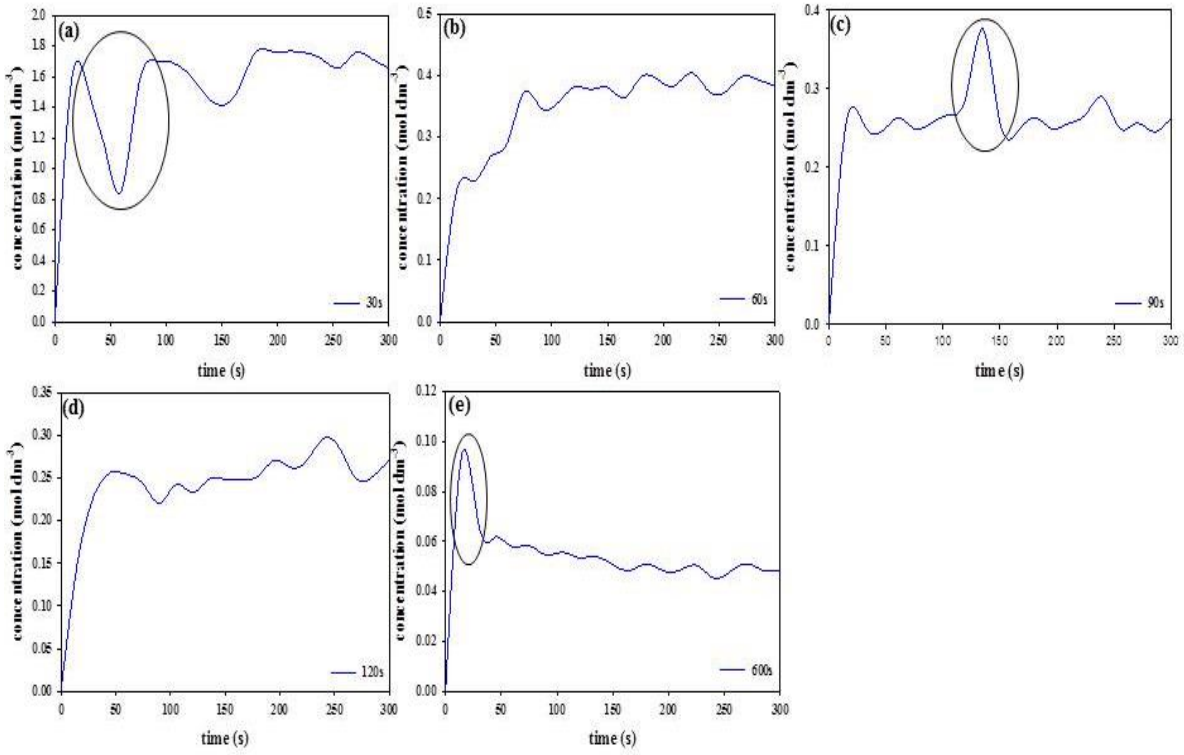

Figure 4-56: Benzaldehyde concentration profiles obtained in solvent-free reaction of benzaldehyde with n-butylamine at 1:1 molar ratio using the jacketed mesoscale-OBR screened at (a) 30s, (b) 60s, (c) 90s, (d) 120s and (e) 600s.

As mentioned in Figure 4-53 (above), the temperature profile for the non-jacketed system took ~100s to reach it steady-state condition. Due to this, the benzaldehyde went through a peak before diminishing as shown in Figure 4-55 (a), (b) & (c). Steady-state readings were only observed in the jacketed mesoscale-OBR as shown in Figure 4-56. Higher temperatures (~80^{o}C), above the boiling point of *n*-butylamine, obtained during screening using the non-jacketed mesoscale-OBR caused the formation of bubbles which disturbed the IR measurement and the plug flow condition. For example, the temperature at the bottom location reached 80^{o}C for screening at 30s and 90s residence times. Entrapment of bubbles under the IR sensor reduces the accuracy of data collection during the screening process. The effects of bubble entrapment can be observed in the concentration profiles using the jacketed mesoscale-OBR shown in Figure 4-56(a), (c) and (e). Once the bubbles were removed, the concentration profile returned to its appropriate value corresponding to the screening condition. Bubble formation using the jacketed mesoscale-OBR was due to the area at the inlet of the reactor system (Figure 4-57) that was not jacketed. Clearly at this point the heat generated at the mixing point reached the boiling point of *n*-butylamine.

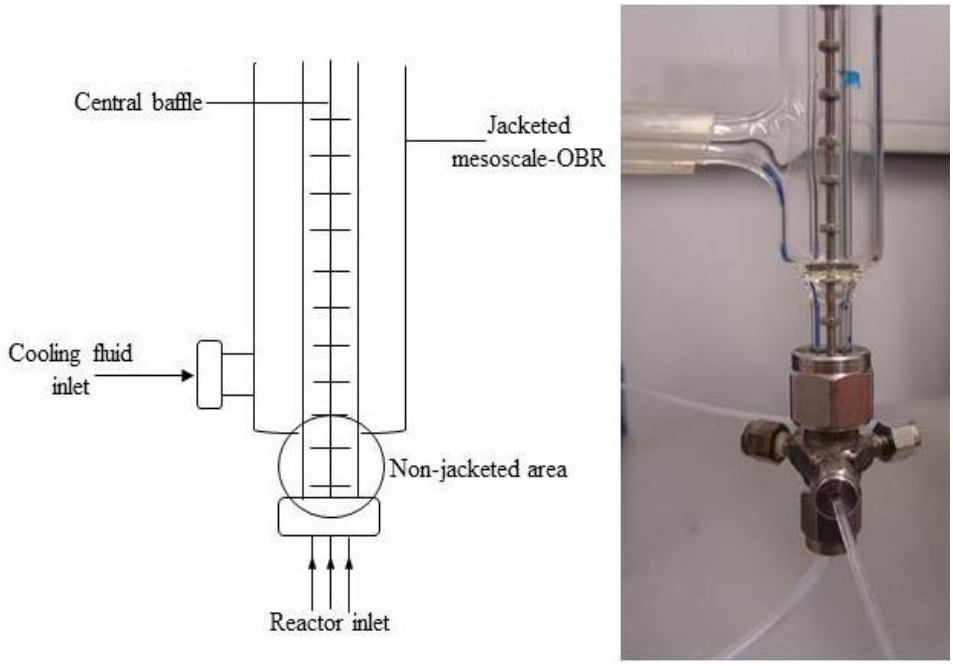

Figure 4-57: The non-jacketed area on the jacketed mesoscale-OBR system.

The benzaldehyde concentrations obtained using the jacketed mesoscale-OBR in the continuous screening was comparable to those in the batch mode due to the similarity in the temperature profile in both methods. There was good agreement (~95%) as shown in Figure 4-58.

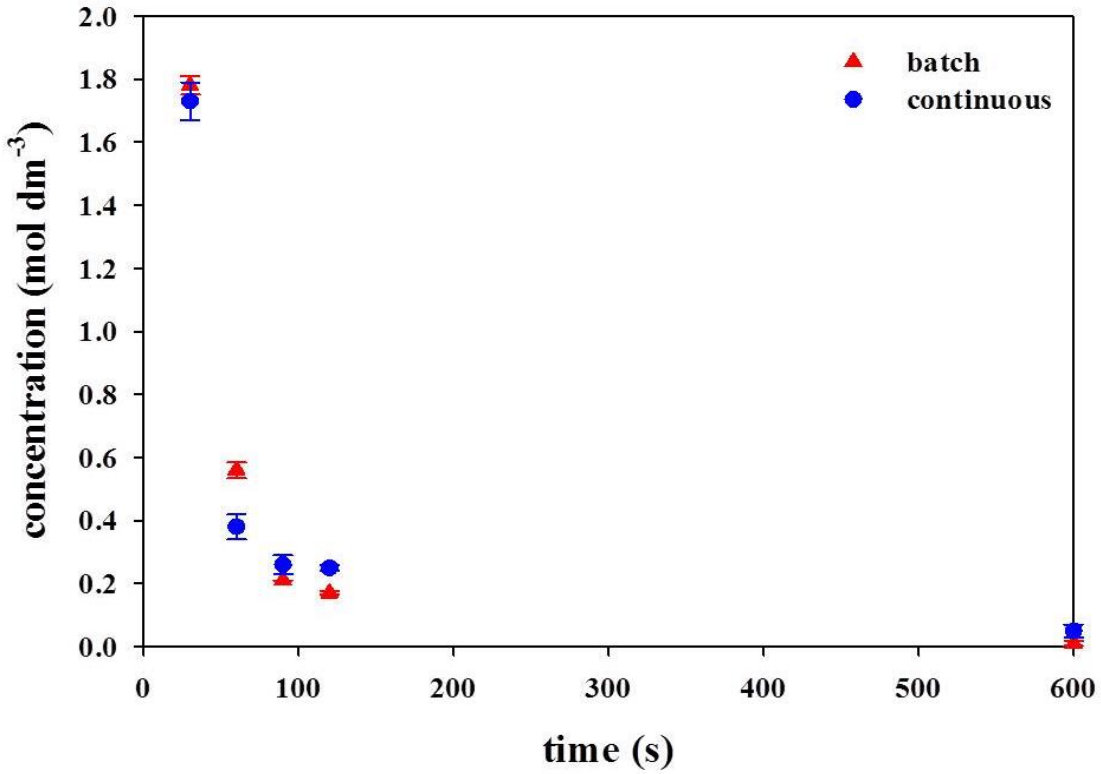

Figure 4-58: Benzaldehyde concentrations obtained in batch and continuous screening for solvent-free reaction at 1:1 molar ratio of benzaldehyde to n-butylamine conducted using the jacketed mesoscale-OBR.

In summary, the mesoscale-OBR is a better platform in terms of safety, temperature control and heat transfer in conducting screening for exothermic reactions, e.g. a solvent-free reaction of benzaldehyde with *n*-butylamine, than the batch beaker. Due to its small volume, the inventory of material in a hazardous state is reduced when using the mesoscale-OBR. Furthermore, the mesoscale OBR also had better heat transfer performance than the beaker system. The reaction temperature was reduced to 40^{o}C when using the batch jacketed mesoscale-OBR, compared to 90^{o}C using the batch jacketed beaker. Although isothermality was not obtained along the length of the jacketed mesoscale-OBR, the temperature difference was small, around 6-7^{o}C.

To improve the temperature control and to obtain highly isothermal condition along the mesoscale-OBR, a heat pipe-based design was developed. Heat pipe designs are used in many applications, such as spacecraft (Swanson and Birur, 2003), solar cells (Armijo and Carey, 2013), chemical reactors (Parent *et al.*, 1983; Richardson *et al.*, 1988), heat exchangers (Vasiliev, 2005) and electronics cooling activities (Reay and Kew, 2006). The concept was to design a passive heat pipe jacketed system to isothermalise the reactor, by "spreading out" the heat generated along the reactor.

4.4.6 Thermosyphon mesoscale-OBR reactor

A mesoscale-OBR system was incorporated within a thermosyphon. A thermosyphon system was chosen due to the simplicity of its structure and because it could easily be coupled to the existing vertical orientation of the mesoscale-OBR. The aim was to design and fabricate the first OBR longitudinally isothermalised using a heat pipe.

4.4.6.1 Operation mechanism of the thermosyphon mesoscale-OBR

The thermosyphon reactor system was a copper tube of 360mm length, consisting of two main units: a 20mm outer diameter thermosyphon tube and a 5mm inner diameter mesoscale-OBR reactor as shown in Figure 4-59.

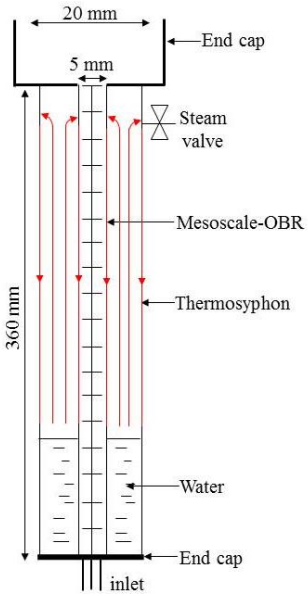

Figure 4-59: Diagram of the thermosyphon mesoscale-OBR with the evaporation-condensation cycle.

The mode of operation of the thermosyphon mesoscale-OBR is evaporation and condensation outside the wall of the mesoscale-OBR, and oscillatory mixing within (Figure 4-59). The evaporation-condensation cycles begin when the liquid at the evaporator side is heated (bottom end) due to the exothermic reaction. This causes the liquid to vaporize and move to the cold end of the thermosyphon (top end). The condensate then returns to the hot end (evaporator side) by flowing down the walls by gravity. Repeating this cycle created an isothermal condition along the length of the mesoscale-OBR. The high thermal conductivity of copper also enhanced the heat transfer from the mesoscale-OBR to the thermosyphon side. Prior to the evaporation-condensation cycles, oscillatory mixing was imposed on the net flow of reagents inside the reactor. To obtain a sufficient length for the evaporator, adiabatic and condenser region, the diameter of the thermosyphon must be correct. In this preliminary study, a 20mm diameter tube with 360mm in length was chosen, providing 100mL volume for the evaporation-condensation cycles to occur. However, further investigations need to be performed to determine an optimum diameter for the system: this was the very first example of this type of reactor.

4.4.6.2 Evaluation of the thermosyphon mesoscale-OBR reactor system

The isothermality achieved using an aluminium heat pipe system obtained from Thermacore (Europe) was tested for comparison to the thermosyphon mesoscale-OBR system. The heat pipe tube was 15cm in length and 0.5cm in diameter. It was tested by immersing in hot water (~80^{o}C) and the temperature was measured at 2 locations: 1cm and 10cm from the top. The temperature profiles showed that the isothermal condition was reached within 20s with a temperature difference between the top and bottom of approximately 1^{o}C (Figure 4-60). The temperature measured in the tube was 5^{o}C different to that of the heat source. This showed that good temperature control and rapid isothermal conductance was obtained along the length of the system. The thermosyphon mesoscale-OBR was evaluated, with a view to achieving similar levels of isothermalisation.

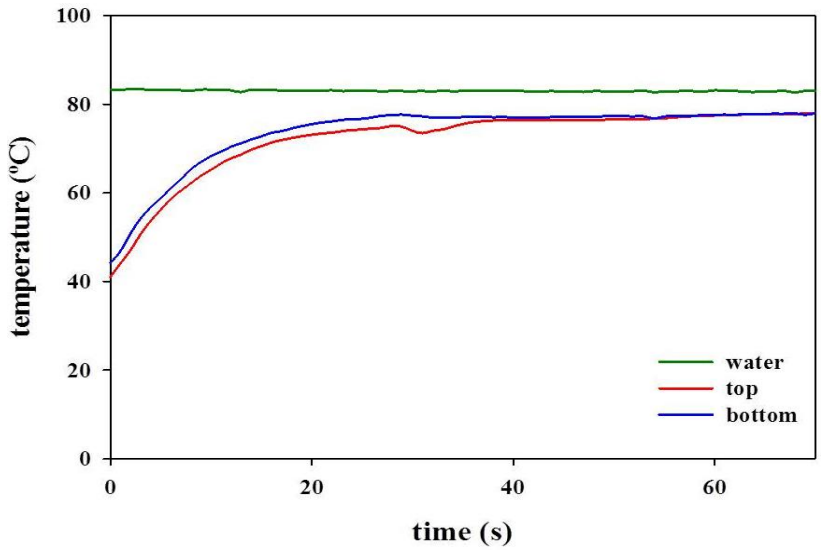

Figure 4-60 : Tested isothermal temperature profiles of heat pipe obtained from Thermacore (Europe) Ltd (top: 1cm from the top; bottom: 10cm from the top of the tube).

It is essential that all connections between the thermosyphon and the mesoscale-OBR are leak-free. Several joining methods were tested such as (i) using adhesive material, (ii) welding and (iii) brazing.

For the first method, the end caps of the thermosyphon mesoscale-OBR tube were glued together using an adhesive material (Loctite) that could withstand high temperatures (>150^{o}C) and high pressures (25MPa). Once both systems were joined, outgassing was carried out to release trapped gas inside the vapour space of the thermosyphon tube

system (Reay and Kew, 2006). This is to avoid any gas disturbance during the circulation of evaporate-condensate inside the thermosyphon chamber. Two methods of the outgassing were used as listed in section 3.2.3.2.1.1.

As shown in Figure 4-61, an isothermal condition was not obtained using outgassing method A.

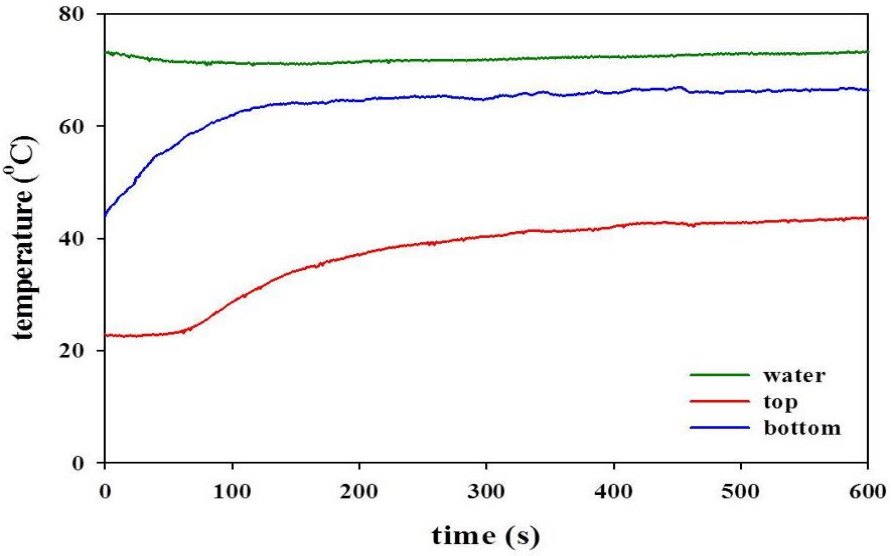

Figure 4-61: Temperature profiles obtained from thermosyphon mesoscale-OBR system with 70% filling ratio.

The lack of isothermality could be due to a high initial filling ratio of the working fluid. The 30mL water left inside the themosyphon system after the outgassing was equivalent to approximately 70% of the evaporator volume. As the system was heated, the liquid pool expanded from the evaporator towards the condenser region (El-Genk and Saber, 1999). This resulted in surface blockage and limited the condensation process (Reay and Kew, 2006). There are several suggestions related to an optimum filling ratio of the thermosyphon system. Bezrodnyi and Alekssenko (1977) proposed that a filling ratio should be at a maximum of 50% of the evaporator volume while Feldman and Srinivasan (1984) proposed the range of 18-20%. Due to this, the process was repeated at approximately 50% filling ratio (20ml water left inside the thermosyphon system) but the non-isothermal profile persisted, as shown in Figure 4-62.

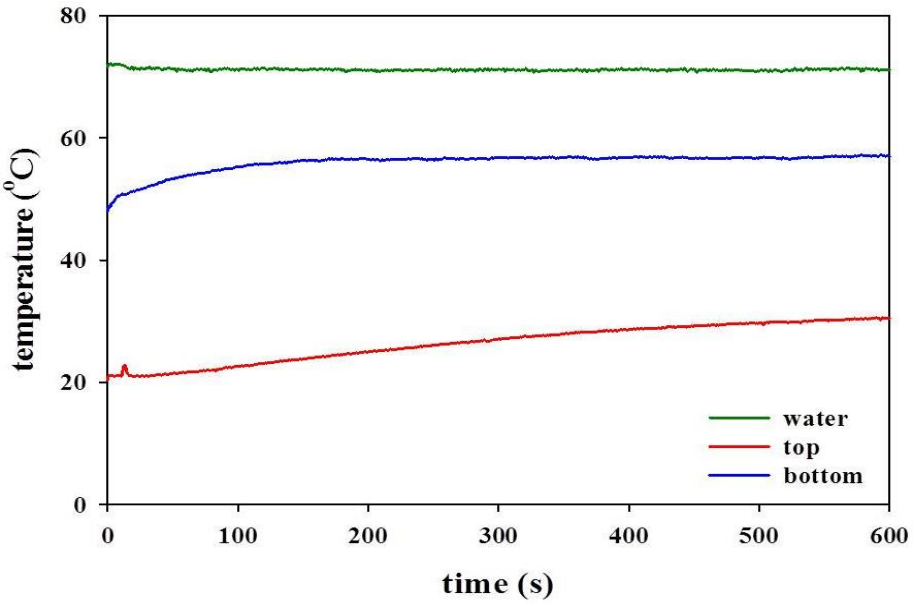

Figure 4-62: Temperature profiles obtained from the thermosyphon mesoscale-OBR system with 50% filling ratio.

Therefore, it can be concluded that the outgassing process using method A could not remove completely gas trapped inside the system. For the outgassing method B, the system could be guaranteed to release the air trapped due to high pressure built up inside the close system by heating water to its boiling temperature. However, water leakages were observed at the bottom fittings during the outgassing process. It indicated that the system was not fitted tightly, leading to a poor performance of the system, e.g. non-isothermal condition. It was concluded that the adhesive method was not suitable for fitting the thermosyphon mesoscale-OBR system.

A welding process was required, but copper cannot withstand high temperatures of the welding process. The brazing method, which involves melting and then cooling down metal filler between two fittings parts, was used. The system was outgassed using the methods mentioned in section 3.2.3.2.1.1 with a filling ratio of 70%. A non-isothermal profile was observed using outgassing method A (Figure 4-63(a)), whilst a good isothermal condition was obtained using outgassing method B (Figure 4-63(b))

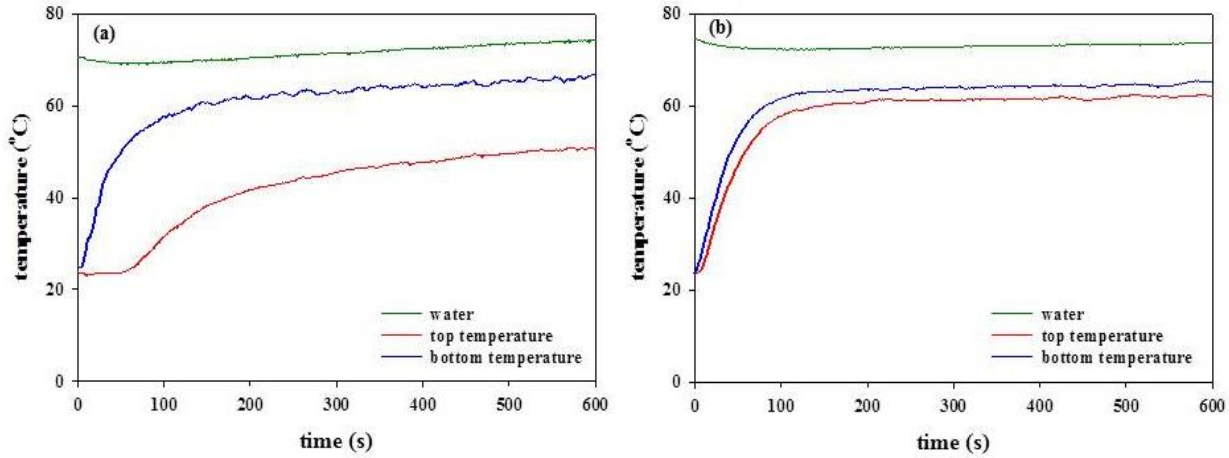

Figure 4-63: Outside wall temperature profiles at the top (5cm) and bottom (28cm) of the thermosyphon mesoscale-OBR reactor system using the outgassing procedure (a) method A and (b) method B with 70% filling ratio of the evaporator volume

The difference in temperature between the top and bottom with the outgassing method B was small, approximately 3°C, which was similar to that in a heat pipe system obtained and tested from Thermacore (Europe) Ltd. (Figure 4-60). This suggests that the outgassing method B can release completely the gas/air trapped inside the system, allowing evaporation and condensation circulation to occur effectively.

4.4.6.3 Solvent-free imine synthesis using the thermosyphon mesoscale-OBR

When the achievement of isothermality was demonstrated to be achievable in the thermosyphon mesoscale-OBR, the system was used to screen a solvent-free imine synthesis. This was conducted continuously via a steady-state method at residence times of 30s, 60s, 90s, 120s and 600s. The temperature inside the mesoscale-OBR was measured at 10 cm (top) and 28 cm from the reactor outlet (bottom). The temperature profiles obtained in the system are shown in Figure 4-64.

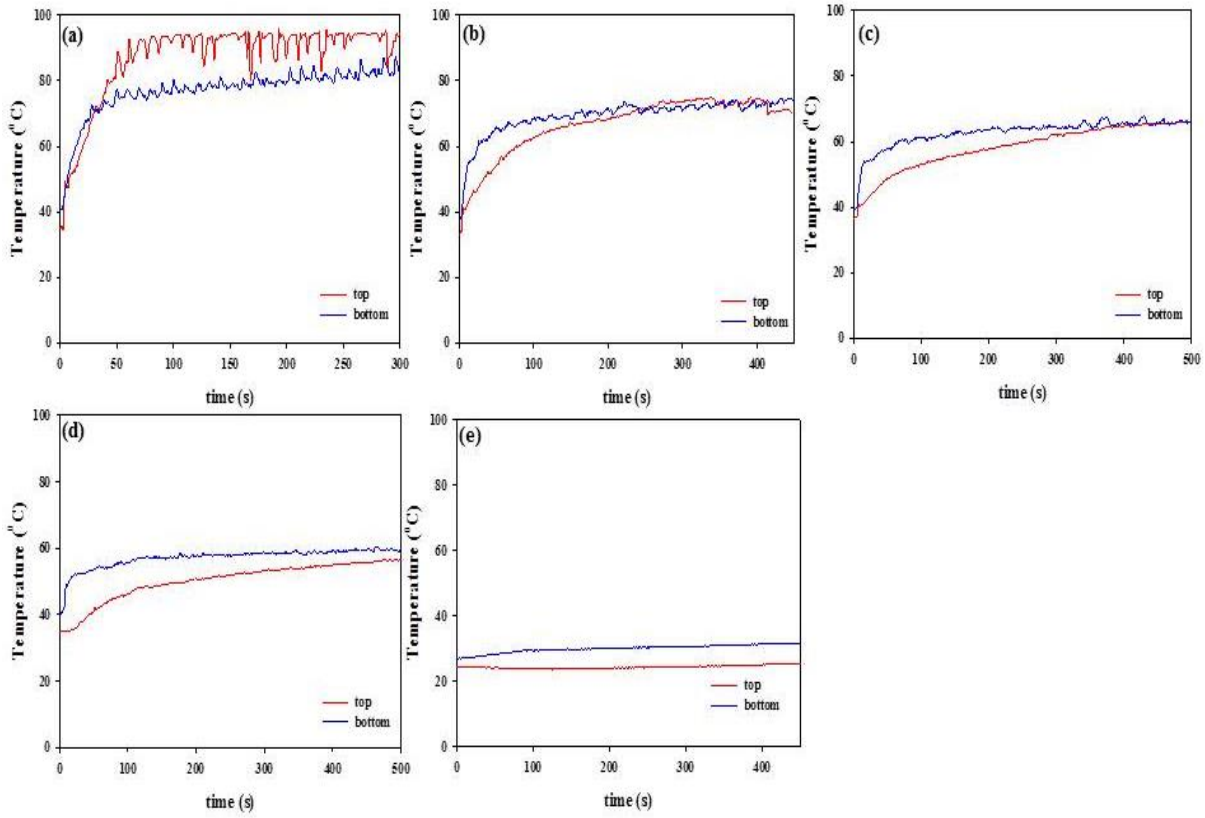

Figure 4-64: Temperature profiles for solvent-free reaction of benzaldehyde with n-butylamine at 1:1 molar ratio using the thermosyphon mesoscale-OBR system screened at (a) 30s, (b) 60s, (c) 90s, (d) 120s and (e) 600s residence time via continuous multi steady-state manner .

The difference in temperature between the top and bottom positions was below 5°C for residence times from 60s to 600s. It suggested that 70% filling ratio of the evaporator volume was a viable level to obtain a good temperature control along the reactor during the imine synthesis reaction. The highest exotherm occurs during the initial reaction time (i.e. when the reagents initially come into contact). Here, the temperature measured at the bottom position was always higher than that at the top position, as expected at residence time 60s (Figure 4-64(b)) ,90s (Figure 4-64(c)) ,120s (Figure 4-64(d)) and 600s (Figure 4-64(e)). However, this behaviour was not observed at the 30s residence time temperature profile (Figure 4-64(a)). This indicates that at the highest flow rate (at the shortest residence time of 30s), the exotherm is moved away from the evaporator section (inlet). This results in high heat input at the condensation side, which reduces the rate of liquid returning from the condenser section (El-Genk and Saber, 1999). Due to this "dry-out" phenomenon, the performance of the thermosyphon mesoscale-OBR was reduced. Hence, the top temperature was higher than the bottom temperature and resulted in no isothermal profile observed at this screening condition (τ=30s). The

isothermal condition along the reactor was only observed at residence times of 60s and 90s after 250s and 400s respectively. This isothermality was not observed with the jacketed mesoscale-OBR at any tested residence time conditions. The isothermality achieved with the thermosyphon mesoscale-OBR system was due to the fixed heating duty along the length of the reactor. This shows that the 70% filling ratio was suitable to absorb and circulate the heat generated from the exothermic reaction during these screening conditions (60s and 90s residence times), resulting in a high degree of isothermalisation along the reactor. Isothermality clearly depends upon screening time. The isothermal condition might occur if the screening time were increased (>500s). The difference for the temperature profiles between the top and bottom decreased with time; e.g. the difference was 10^{o}C at 200s, decreasing to 4^{o}C at 500s. With screening at 600s residence time, constant temperature profiles at the top and bottom positions were observed with temperature of 25^{o}C and 30^{o}C respectively.

A non-steady state condition was observed for the benzaldehyde concentration profiles as shown in Figure 4-65.

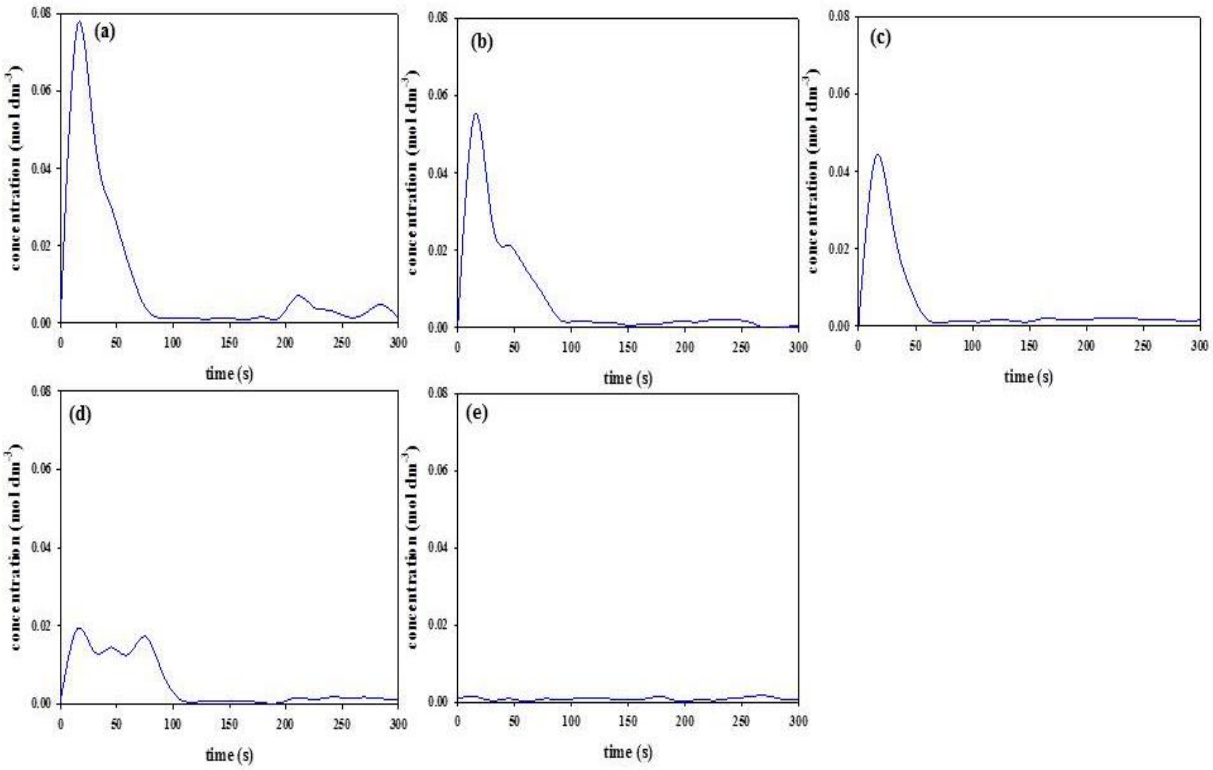

Figure 4-65: Benzaldehyde concentration profiles for solvent-free reaction of benzaldehyde with n-butylamine at 1:1 molar ratio using the thermosyphon mesoscale-OBR screened at residence times of (a) 30s, (b) 60s, (c) 90s, (d) 120s and (e) 600s.

This non steady-state benzaldehyde profile was similar to the data collected via continuous screening for the solvent-free reaction using the non-jacketed mesoscale-OBR. The steady-state was not observed due to the reaction temperature reaching the boiling temperature for *n*-butylamine, causing the formation of bubbles that disturbed the plug flow behaviour. Moreover, the copper material reacted with *n*-butylamine (Figure 4-66) which was evident in the blue colour of the outflowing reaction mixture. This indicates that the *n*-butylamine reacts with the copper to form copper hydroxide ($Cu(OH)_2$).

Figure 4-66: Pale blue precipitation observed from the outflow of the solvent-free reaction of benzaldehyde and n-butylamine conducted using the thermosyphon mesoscale-OBR

The effects of copper reduce the rate of loss of benzaldehyde by approximately 60% as shown in Figure 4-67.

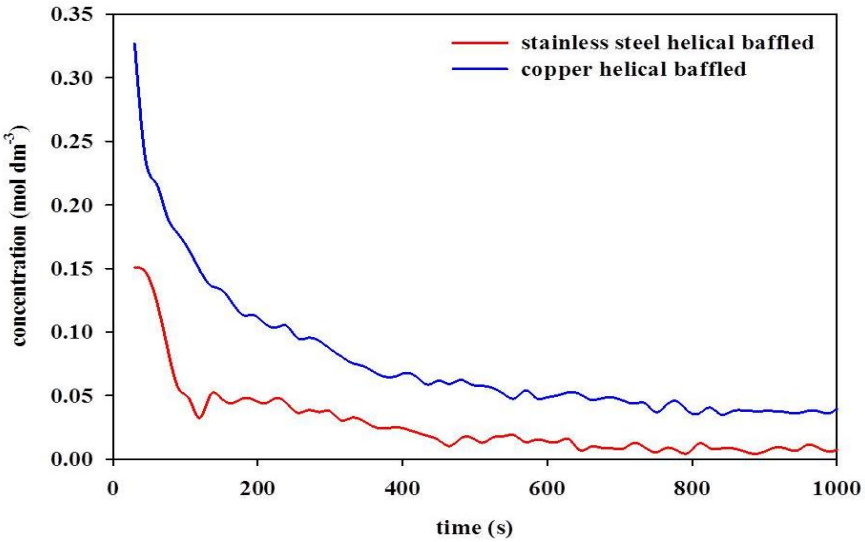

Figure 4-67: Comparison of benzaldehyde reduction profile via batch manner using stainless steel and copper helical baffled mesoscale-OBR.

Clearly the use of copper will have to be changed in future designs. The reactor will be constructed from a material that does not react with the reagents. However, the aim of this investigation was to obtain good temperature control and an isothermal condition along the length of a reactor by inserting a reactor inside a heat pipe, and copper was chosen because of its thermal conductivity. This was proven with the summary temperature differences between the top and bottom positions for various designs as shown in Figure 4-68. The average temperature for the thermosyphon mesoscale-OBR was as low as ~4^{o}C.

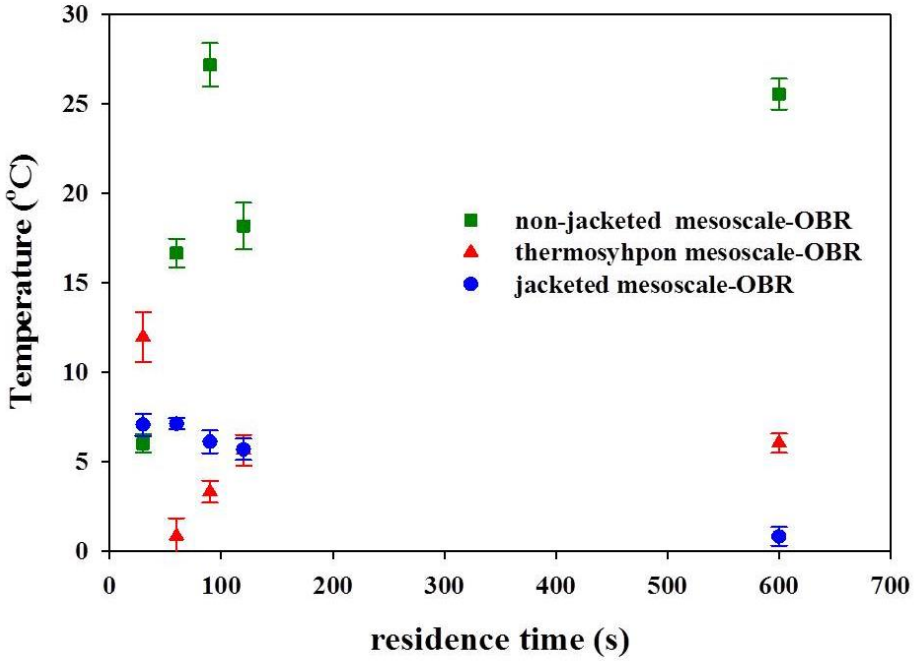

Figure 4-68: Temperature difference between top and bottom positions

4.4.6.4 Summary of themosyphon mesoscale-OBR reactor

Generally, the thermosyphon mesoscale-OBR system behaviour is comparable to the jacketed mesoscale-OBR. However, further studies need to be conducted to determine the optimum filling ratio and diameter of the thermosyphon system. Otherwise, understanding the efficiency of the evaporator and condenser section is important, as the heat input into the system for screening a chemical reaction is generated along the reactor length. The thermosyphon mesoscale-OBR is a compact design because it acts as a passive jacketed reactor, which eliminates the need for additional pumps to circulate cooling fluids inside the jacketed system. This reduces the footprint of the device.

Chapter 5 Conclusions and Future works

5.1 Conclusions

The reaction of several aldehydes (benzaldehyde, *o*-tolualdehyde, *m*-tolualdehyde and *p*-tolualdehyde) with *n*-butylamine to form imine was chosen as a case study to demonstrate the ability of the continuous "mesoscale" Oscillatory Baffled Reactor ("OBR") to rapidly screen process conditions. The reactor was coupled to online FTIR, to determine kinetic data (rate constants and reaction orders). The mesoscale-OBR was operated in 3 different modes:

- Batch operation.
- "Multi-steady state" mode, in which a sequence of different residence times was imposed, each for a prescribed period of time.
- "Dynamic" mode in which the residence time was continuously varied.

5.1.1 Comparison of batch screening between mesoscale-OBR and conventional beaker system

The comparison was conducted only with the reaction of benzaldehyde with n-butylamine at the ratio of 1:1 respectively to forms 1-butanamine, N-(phenylmethylene)-. The results show that:-

- A batch beaker exhibited a higher uncertainty (6.73×10^{-2} mol dm^{-3}) than the batch mesoscale-OBR (7.49×10^{-3} mol $dm^{-3)}$ at the initial stages (~<200s) of the benzaldehyde reduction profile.

- Regardless of the mixing intensity ($31 < Re_o < 369$), a similar reaction rate value (~0.007M/s at 15s reaction time) was observed in the mesoscale-OBR. This indicates that over this range of conditions there were no mass transfer limitations within the reactor system.

- The mesoscale OBR exhibited a higher degree of consistency in experimental results: the uncertainty in the rate constant for benzaldehyde and *n*-butylamine imination, at 5.5×10^{-3} $mol^{-0.9}L^{0.9}s^{-1}$, was approximately three times lower than

that (1.8×10^{-2} $mol^{-0.9}L^{0.9}s^{-1}$) determined using a conventional batch beaker method.

- The amount of reagents required for reaction screening was reduced by 75% using the mesoscale-OBR compared to standard laboratory glassware (beaker).

5.1.2 Advantages of the continous screening in "multi-steady state" and "dynamic screening" modes

Continuous screening using the mesoscale-OBR has been proven in the "multi steady-state" and "dynamic" modes of operation. Both methods have their own advantages. It was demonstrated that:-

- A clear step change between residences times regardless the different ratios of benzaldehyde to *n*-butylamine (1:1, 1:1.5 and 1:2) was observed through "multi steady-state" screening. This indicates that further processing advantages, such as the use of staged addition generate further reactions/products, are possible.

- More data is produced per volume of reactants than in batch mode (mesoscale-OBR or beaker).

- At "multi steady-state" each data point at a given steady state was equivalent to one batch reaction. This equates to a much smaller (~20% less) volume of fluid per data point than in batch screening. Furthermore it produced a series of data (average = 1.2×10^{-3} mol dm^{-3}) at each reaction time rather than one data point per batch screening experiment.

- In dynamic screening, it gives flexibility in rapidly changing the conditions (e.g. flow rate) as the data was collected. Hence the frequency of the data collection was increased.

- The process development time when using continuous dynamic screening was 50% lower than that required for batch screening using a batch reactor, and 25% lower than that required when using "multi steady-state" method.

- The single variable and multivariable dynamic screening agree well (~8% difference), implying that this method, multivariable screening, can reliably be used to screen rapidly experimental space or parameter. The method also shows good sensitivity to concentration changes between different molar ratios

- The continuous screening mode allows *in situ* manipulation of the reaction parameter (e.g. chemical ratio, residence time and temperature) which was not possible with the batch screening mode, which only allows changes once the reaction was completed.

Despite the differences between the three different screening methods (batch, multi steady-state and dynamic screening), screening data shows approximately ~98% degree of agreement between the methods. These results indicate that the mesoscale OBR can be used as a tool to obtain reaction data rapidly and reproducibly either in batch or continuous manner.

5.1.3 Non-solvent reaction using jacketed, non-jacketed and thermosyphon mesoscale-OBR

The higher area to volume ratio of the mesoscale-OBR than the beaker system allows the exothermic solvent free 1-butanamine, N-(phenylmethylene)- reaction to be screened more safely:

- A lower initial temperature of ~40^{o}C in the jacketed mesoscale-OBR, compared to ~90^{o}C with the jacketed beaker. This indicates that the mesoscale-OBR had better heat transfer performance than the beaker.

- The high temperature within the beaker increased the reduction rate of the benzaldehyde by ~50%.

- Better temperature control was observed when using the jacketed (~7^{o}C temperature different) rather than the non-jacketed (~20^{o}C) mesoscale-OBR along the reactor system at residence time of 30-600s. However, isothermality was not obtained in either system.

- An improvement in the temperature control was demonstrated using thermosyphon mesoscale-OBR. The temperature difference between the top and bottom of the reactor was below 5^{o}C, at residence times in the range 60-600s.

- The thermosyphon mesoscale-OBR can act as a passive jacketed reactor system, eliminating the need for additional pumps to circulate cooling fluids inside the jacketed system. This reduces the footprint, surrounding infrastructure required and energy consumption of the laboratory device.

5.1.4 Determination of reaction kinetics parameter (rate constants and reaction order)

The reaction kinetic parameters (reaction order and rate constant) were calculated and determined through the conventional experimental analysis (method of initial rates and integration rate law). This resulted in the following data for the 1-butanamine, N-(phenylmethylene) reaction:

- Rate constant (k_1) at $2.1x10^{-1}$ $mol^{-0.9}L^{0.9}s^{-1}$.

- Total reaction order of 1.9 with benzaldehyde order and *n*-butylamine at 1.7 and 0.22 respectively.

These results were modelled using MATLAB, resulting in:-

- Good fits (SSE $\leq$ 1.0%) between the experimental and modelling concentration profile for benzaldehyde and imine. These were observed at different molar ratio of benzaldehyde to *n*-butylamine condition (1:1 to 1:4) at various screening method (batch, continuous steady-state and continuous dynamic).

- A reaction mechanism of $A + B \overset{k_1}{\rightarrow} C \overset{k_2}{\rightarrow} D + E$ for benzaldehyde and *n*-butylamine reaction was consistent with the experimental data.

- The rate constant (k_2) and reaction order (o=intermediate) at $4.5x10^{-2}$ $mol^{-0.9}L^{0.9}s^{-1}$ and 1.0 respectively were found.

The results for different aldehydes (*o*-tolualdehyde, *m*-tolualdehyde and *p*–tolualdehyde) with *n*-butylamine based on the MATLAB modelling shows:-

- The reaction mechanism of $A + B \underset{k_{-1}}{\overset{k_1}{\leftrightarrow}} C \underset{k_{-2}}{\overset{k_2}{\leftrightarrow}} D + E$ was proposed based on the aldehyde's reduction profile, including the back rate constants (k_{-1} and k_{-2})The proposed mechanism led to good agreement (SSE <1.0%) between the experimental and modelling data for all the aldehydes (*o*-tolualdehyde, *m*-tolualdehyde and *p*–tolualdehyde) with *n*-butylamine.

- The rate constant (k_1) increased from $1.3x10^{-2}$ to $1.5x10^{-2}$ to $1.8x10^{-2}$ $mol^{-1.5}L^{1.5}s^{-1}$ for *p*-tolualdehyde, *m*-tolualdehyde and *o*-tolualdehyde respectively. This order was as expected due to the various methyl group positions' effects on the electron density of the benzene ring.

- Regardless of the aldehydes, the reaction order for each of the reagents and products was similar at 2.2, 0.28, 2, 1 and 1 for aldehyde, *n*-butylamine, intermediate, imine and water respectively.

5.2 Future Work

Continuous screening using the mesoscale-OBR has been shown to reduce the process development time and reagent usage. However, it is recommended that further work be conducted in the following areas:

i. **Improvement to the mesoscale-OBR system.** The current procedure only allows 2 thermocouples (0.5mm OD probe each) to be inserted inside the reactor (ID=5mm) due to the size of the baffle (4mm OD). The thermocouple channel port should be design along the reactor system for easier monitoring of the temperature along the system. This provides more data at different positions along the reactor length for better temperature determination. This will also reduce difficulties during the insertion of the thermocouples from the outlet of reactor.

ii. **Improvement to the thermosyphon mesoscale-OBR system.** The system has been proven to provide a high level of isothermality during the continuous screening of an imine reaction. However, further studies need to be performed to understand the effects of filling ratios and different diameters of the thermosyphon system. This relates to the understanding of the efficiency of the evaporator and condenser sections as the heat input into the system for screening a chemical reaction is generated along the reactor. The reactor material also needs to be changed in order to avoid any interference between reactor materials and reagents, but the good heat transfer between the mesoscale-OBR reactor and thermosyphon system must be maintained.

iii. **Improvement to the modelling.** This can be achieved by incorporating determination of initial rate constant values through modelling with the assistant from the curve fitting MatLab toolbox. This allows rates (i.e. dA/dt) value to be obtained and combining the concentration value leads to the initial rate constant determination.

iv. **Reduce the size of the infrared probe.** The 16mm IR probe used in this study causes bubble entrapment under the IR sensor that reduces the accuracy in data collection during the screening process. Release of the bubbles was possible for

the glass reactor, but is more difficult if different reactor materials are used (stainless steel or copper). A smaller probe diameter (<6mm) should be used to avoid any difficulties in data collection during the screening.

REFERENCES

A. L. Woodhead, F.J.H.a.J.S.C. (1997) 'Assessment Of The Chlorination of Wool by Infrared Spectroscopy. Part I: The Classical Approach', *The internet journal of vibrational spectroscopy*, 1(3).

Abbott, M.S.R., Valente Perez, G., Harvey, A.P. and Theodorou, M.K. (2014) 'Reduced power consumption compared to a traditional stirred tank reactor (STR) for enzymatic saccharification of alpha-cellulose using oscillatory baffled reactor (OBR) technology', *Chemical Engineering Research and Design*.

Abdallah, L.A.M. (2010) 'Determination of the rate constant for a consecutive second order irreversible chemical reaction using MATLAB toolbox', *Wuropean Journal of Scientific Research*, 41(3), pp. 412-419.

Ahmed, B., Barrow, D. and Wirth, T. (2006) 'Enhancement of reaction rates by segmented fluid flow in capillary scale reactors', *Advanced Synthesis and Catalysis*, 348(9), pp. 1043-1048.

Al-hengari, S. (2011) *Process Intensification: A study of micromixing and Residence Time Distribution characteristics in the Spinning Disc Reactor*. Newcastle University.

Anderson, B.M. and Jencks, W.P. (1960) 'The effect of structure on reactivity in semicarbazone formation', *Journal of the American Chemical Society*, 82(7), pp. 1773-1777.

Anslyn, E.V. and Dougherty, D.A. (2006) *Modern Physical Organic Chemistry*. United State of America: University Science Book.

Armijo, K.M. and Carey, V.P. (2013) 'Gravity-assisted heat pipe with strong marangoni fluid for waste heat management of single and dual-junction solar cells', *Journal of Solar Energy Engineering, Transactions of the ASME*, 135(2).

Baird, M.H.I. and Stonestreet, P. (1995) 'Energy dissipation in oscillatory flow within a baffled tube', *Chemical Engineering Research and Design*, 73(A5), pp. 503-511.

Baxendale, I.R. (2013a) 'The integration of flow reactors into synthetic organic chemistry', *Journal of Chemical Technology and Biotechnology*, 88(4), pp. 519-552.

Baxendale, I.R. (2013b) 'The integration of flow reactors into synthetic organic chemistry', *Journal of Chemical Technology & Biotechnology*, 88(4), pp. 519-552.

Benito-Lopez, F., Verboom, W., Kakuta, M., Gardeniers, J.G.E., Egberink, R.J.M., Oosterbroek, E.R., van den Berg, A. and Reinhoudt, D.N. (2005) 'Optical fiber-based on-line UV/Vis spectroscopic monitoring of chemical reaction kinetics under high pressure in a capillary microreactor', *Chemical Communications*, 0(22), pp. 2857-2859.

Betteridge, D. and Hallam, H.E. (1972) *Modern analytical methods*. London, The Chemical Society

References

Bezrodnyi, M.K. and Alekssenko, D.B. (1977) 'Investigation of the critical region of heat and mass transfer in low-temperature wickless heat pipes', *High Temperature*, 15(2), pp. 309-313.

Binnie, A.M. (1945) 'A double-refraction method of detecting turbulence in liquids', *Proceedings of the Physical Society*, 57(5), pp. 390-402.

Bottausci, F., Cardonne, C., Meinhart, C. and Mezić, I. (2007) 'An ultrashort mixing length micromixer: The shear superposition micromixer', *Lab on a Chip - Miniaturisation for Chemistry and Biology*, 7(3), pp. 396-398.

Brunold, C.R., Hunns, J.C.B., Mackley, M.R. and Thompson, J.W. (1989) 'Experimental observations on flow patterns and energy losses for oscillatory flow in ducts containing sharp edges', *Chemical Engineering Science*, 44(5), pp. 1227-1244.

Buncel, E., Stairs, R. and Wilson, H. (2003) *The Role of the Solvent in Chemical Reactions*. Great Britain: Oxford University Press.

Calabrese, G.S. and Pissavini, S. (2011) 'From batch to continuous flow processing in chemicals manufacturing', *AIChE Journal*, 57(4), pp. 828-834.

Capellos, C. and Bielski, B.H.J. (1980) *Kinetic Systems: Mathematical description of chemical kinetics in solution*. United States of America: John Wiley & Sons Inc.

Carey, F.A. and Sundberg, R.J. (2007) *Advanced Organic Chemistry: Structure and Mechanisms Pt. A* 5th edn. Springer-Verlag New York Inc.

Chen, D.L. and Ismagilov, R.F. (2006) 'Microfluidic cartridges preloaded with nanoliter plugs of reagents: an alternative to 96-well plates for screening', *Current Opinion in Chemical Biology*, 10(3), pp. 226-231.

Chu, G. and Li, C. (2010) 'Convenient and clean synthesis of imines from primary benzylamines', *Organic and Biomolecular Chemistry*, 8(20), pp. 4716-4719.

Conley, R.T. (1972) *Infrared Spectroscopy*. 2nd edn. Boston, Massachusetts: Allyn and Bacon.

Cordes, E.H. and Jencks, W.P. (1962) 'Nucleophilic catalysis of semicarbazone formation by anilines', *Journal of the American Chemical Society*, 84(5), pp. 826-831.

Cordes, E.H. and Jencks, W.P. (1963) 'The Mechanism of Hydrolysis of Schiff Bases Derived from Aliphatic Amines', *Journal of the American Chemical Society*, 85(18), pp. 2843-2848.

Crowell, T.I. and Peck, D.W. (1953) 'Kinetic evidence for a Schiff base intermediate in the knoevenagel condensation', *Journal of the American Chemical Society*, 75(5), pp. 1075-1077.

References

De Carvalho Alcântara, A.F., Piló-Veloso, D. and Nelson, D.L. (1996) 'A study of the formation and stability of N-alkylbutanimines by 1H-NMR spectroscopy', *Journal of the Brazilian Chemical Society*, 7(4), pp. 225-232.

de Juan, A., Maeder, M., Martínez, M. and Tauler, R. (2000) 'Combining hard- and soft-modelling to solve kinetic problems', *Chemometrics and Intelligent Laboratory Systems*, 54(2), pp. 123-141.

E.S.Swinbourne (1971) *Analysis of kinetic data*. Appleton Century Crofts.

Ehly, M., Gemperline, P.J., Nordon, A., Littlejohn, D., Basford, J.K. and De Cecco, M. (2007) 'Scale-up of batch kinetic models', *Analytica Chimica Acta*, 595(1–2), pp. 80-88.

Ehrich, H., Linke, D., Morgenschweis, K., Baerns, M. and Jähnisch, K. (2002) 'Application of microstructured reactor technology for the photochemical chlorination of alkylaromatics', *Chimia*, 56(11), pp. 647-653.

El-Genk, M.S. and Saber, H.H. (1999) 'Determination of operation envelopes for closed, two-phase thermosyphons', *International Journal of Heat and Mass Transfer*, 42(5), pp. 889-903.

Evans, D.A., Borg, G. and Scheidt, K.A. (2002) 'Remarkably stable tetrahedral intermediates: Carbinols from nucleophilic additions to N-acylpyrroles', *Angewandte Chemie - International Edition*, 41(17), pp. 3188-3191.

Eze, V.C., Phan, A.N., Pirez, C., Harvey, A.P., Lee, A.F. and Wilson, K. (2013) 'Heterogeneous catalysis in an oscillatory baffled flow reactor', *Catalysis Science and Technology*, 3(9), pp. 2373-2379.

Fabiyi, M.E. and Skelton, R.L. (1999) 'The application of oscillatory flow mixing to photocatalytic wet oxidation', *Journal of Photochemistry and Photobiology A: Chemistry*, 129(1-2), pp. 17-24.

Feldman, K.T. and Srinivasan, R. (1984) 'Investigation of heat transfer limits in two-phase closed thermosyphons'.

Feth, H., Pothof, F., Thoma, F., Schmidt, T., Mueller, C., Goldschmidtboeing, F. and Woias, P. (2013) 'Design, fabrication and characterization of a piezoelectrically actuated bidirectional polymer micropump', *Microsystem Technologies*, pp. 1-12.

Gaidhani, H.K., McNeil, B. and Ni, X.-W. (2003) 'Production of pullulan using an oscillatory baffled bioreactor', *Journal of Chemical Technology & Biotechnology*, 78(2-3), pp. 260-264.

Geyer, K., Codée, J.D.C. and Seeberger, P.H. (2006) 'Microreactors as tools for synthetic Chemists - The chemists' round-bottomed flask of the 21st century?', *Chemistry - A European Journal*, 12(33), pp. 8434-8442.

References

Ghazi, A.T.M., Resul, M.G., Yunus, R. and Yaw, T.S. (2008) 'Preliminary design of oscillatory flow biodiesel reactor for continuous biodiesel production from jatropha triglycerides', *Journal of Engineering Science and Technology*, 3(2), pp. 138-145.

Godoy-Alcántar, C., Yatsimirsky, A.K. and Lehn, J.M. (2005) 'Structure-stability correlations for imine formation in aqueous solution', *Journal of Physical Organic Chemistry*, 18(10), pp. 979-985.

Gonjo, T., Futami, Y., Morisawa, Y., Wojcik, M.J. and Ozaki, Y. (2011) 'Hydrogen Bonding Effects on the Wavenumbers and Absorption Intensities of the OH Fundamental and the First, Second, and Third Overtones of Phenol and 2,6-Dihalogenated Phenols Studied by Visible/Near-Infrared/Infrared Spectroscopy', *The Journal of Physical Chemistry A*, 115(35), pp. 9845-9853.

Goodell, J.R., McMullen, J.P., Zaborenko, N., Maloney, J.R., Ho, C.-X., Jensen, K.F., Porco, J.A. and Beeler, A.B. (2009) 'Development of an Automated Microfluidic Reaction Platform for Multidimensional Screening: Reaction Discovery Employing Bicyclo[3.2.1]octanoid Scaffolds', *The Journal of Organic Chemistry*, 74(16), pp. 6169-6180.

Guzen, K.P., Guarezemini, A.S., Órfão, A.T.G., Cella, R., Pereira, C.M.P. and Stefani, H.A. (2007) 'Eco-friendly synthesis of imines by ultrasound irradiation', *Tetrahedron Letters*, 48(10), pp. 1845-1848.

Habibi, M.H., Montazerozohori, M., Lalegani, A., Harrington, R.W. and Clegg, W. (2006) 'Synthesis, structural and spectroscopic properties of a new Schiff base ligand N,N′-bis(trifluoromethylbenzylidene)ethylenediamine', *Journal of Fluorine Chemistry*, 127(6), pp. 769-773.

Halász, G., Gyüre, B., Jánosi, I.M., Szabó, K.G. and Tél, T. (2007) 'Vortex flow generated by a magnetic stirrer', *American Journal of Physics*, 75(12), pp. 1092-1098.

Hall, J.F., Barigou, M., Simmons, M.J.H. and Stitt, E.H. (2005) 'Just Because It's Small Doesn't Mean It's Well Mixed: Ensuring Good Mixing in Mesoscale Reactors', *Industrial & Engineering Chemistry Research*, 44(25), pp. 9695-9704.

Hartman, R.L., McMullen, J.P. and Jensen, K.F. (2011) 'Deciding whether to go with the flow: Evaluating the merits of flow reactors for synthesis', *Angewandte Chemie - International Edition*, 50(33), pp. 7502-7519.

Harvey, A.P., Mackley, M.R. and Stonestreet, P. (2001) 'Operation and Optimization of an Oscillatory Flow Continuous Reactor', *Industrial & Engineering Chemistry Research*, 40(23), pp. 5371-5377.

Hessel, V., Löwe, H. and Schönfeld, F. (2005) 'Micromixers—a review on passive and active mixing principles', *Chemical Engineering Science*, 60(8–9), pp. 2479-2501.

Hill, R.L. and Crowell, T.I. (1956) 'Structural effects in the reactivity of primary amines with piperonal', *Journal of the American Chemical Society*, 78(10), pp. 2284-2286.

References

Hisham, M. (2012) *Use of Microfluidic Technology for Cell Separation*.

Holsey (2006) *Imine Synthesis*. Available at: http://usefulchem.wikispaces.com/Chapter+4+-+Imine+Synthesis.

Houson, I. (2011) *Process Understanding: For Scale-Up and Manufacture of Active Ingredients*. Wiley-VCH.

Howes, T. and Mackley, M.R. (1990) 'Experimental axial dispersion for oscillatory flow through a baffled tube', *Chemical Engineering Science*, 45(5), pp. 1349-1358.

Howes, T., Mackley, M.R. and Roberts, E.P.L. (1991) 'The simulation of chaotic mixing and dispersion for periodic flows in baffled channels', *Chemical Engineering Science*, 46(7), pp. 1669-1677.

Imlinger, N.C., Blattner, C., Krell, M. and Buchmeiser, M.R. (2008) 'Hard-modeling of reaction kinetics by combining online spectroscopy and calorimetry', *Journal of Chemometrics*, 22(11-12), pp. 758-767.

Imlinger, N.C., Krell, M. and Buchmeiser, M.R. (2007) 'Modeling the Kinetics of Hydrosilylation Based Polyaddition', *Monatshefte für Chemie / Chemical Monthly*, 138(4), pp. 285-291.

International, A. (2002) *Standard practice for general techniques for obtaining infrared spectra for qualitative analysis*. United State.

Issa, M.M., Nejem, R.a.M., Shanab, A.M.A. and Shaat, N.T. (2013) 'Kinetic spectrophotometric H-point standard addition method for the simultaneous determination of diloxanide furoate and metronidazole in binary mixtures and biological fluids', *Spectrochimica Acta Part A: Molecular and Biomolecular Spectroscopy*, 114(0), pp. 592-598.

Iwasawa, T., Hooley, R.J. and Rebek Jr, J. (2007) 'Stabilization of labile carbonyl addition intermediates by a synthetic receptor', *Science*, 317(5837), pp. 493-496.

Jas, G. and Kirschning, A. (2003) 'Continuous Flow Techniques in Organic Synthesis', *Chemistry – A European Journal*, 9(23), pp. 5708-5723.

Jencks, W.P. (1959) 'Studies on the Mechanism of Oxime and Semicarbazone Formation[1]', *Journal of the American Chemical Society*, 81(2), pp. 475-481.

Jian, H. and Ni, X. (2005) 'A Numerical Study on the Scale-Up Behaviour in Oscillatory Baffled Columns', *Chemical Engineering Research and Design*, 83(10), pp. 1163-1170.

Jin, J.-j., Wang, D.-c., Niu, H.-y., Wu, S., Qu, G.-r., Zhang, Z.-b. and Guo, H.-m. (2013) 'Brønsted acid catalyzed synthesis of 1,3-di(2-quinolyl)propane derivatives via tandem C(sp3)–H functionalization', *Tetrahedron*, 69(32), pp. 6579-6584.

References

Junkers, M. (2014) 'Continuous Flow Synthesis in Microstructured Reactors — A New Way of Thinking Chemical Synthesis', *ChemFiles*, 9(4).

K. Laqua, W.H.M.a.M.Z. (1988) 'Molecular absorption spectroscopy, ultraviolet and visible (UV/VIS)', *Pure and Applied Chemistry*, 60(9), pp. 1449-1460.

Kang, S.W., Tsai, M.C., Hsieh, C.S. and Chen, J.Y. (2010) 'Thermal performance of a loop thermosyphon', *Tamkang Journal of Science and Engineering*, 13(3), pp. 281-288.

Laidler, K.J. (1987) *Chemical Kinetics*. Third Edition edn. Harper Collins.

Lawton, S., Steele, G., Shering, P., Zhao, L., Laird, I. and Ni, X.-W. (2009) 'Continuous Crystallization of Pharmaceuticals Using a Continuous Oscillatory Baffled Crystallizer', *Organic Process Research & Development*, 13(6), pp. 1357-1363.

Layer, R.W. (1963) 'The chemistry of imines', *Chemical Reviews*, 63, pp. 489-510.

Lee, M., Kim, H., Rhee, H. and Choo, J. (2003) 'Reaction monitoring of imine synthesis using Raman spectroscopy', *Bulletin of the Korean Chemical Society*, 24(2), pp. 205-208.

Levenspiel, O. (1999) *Chemical Reaction Engineering (3rd Edition)*. John Wiley & Sons.

Li, Y., Zhang, H. and Liu, Q. (2012) 'FT-IR spectroscopy and DFT calculation study on the solvent effects of benzaldehyde in organic solvents', *Spectrochimica Acta - Part A: Molecular and Biomolecular Spectroscopy*, 86, pp. 51-55.

Liu, B., Fan, Y., Lv, X., Liu, X., Yang, Y. and Jia, Y. (2013) 'Generation and reactions of heteroaromatic lithium compounds by using in-line mixer in a continuous flow microreactor system at mild conditions', *Organic Process Research and Development*, 17(1), pp. 133-137.

Lu, Y., Zhang, L. and Lin, H. (2014) 'The Use of a Microreactor for Rapid Screening of the Reaction Conditions and Investigation of the Photoluminescence Mechanism of Carbon Dots', *Chemistry – A European Journal*, 20(15), pp. 4246-4250.

Mackley, M.R. (1991) 'Process innovation using oscillatory flow within baffled tubes', *Chemical Engineering Research and Design*, 69(3), pp. 197-199.

Mackley, M.R. and Ni, X. (1991) 'Mixing and dispersion in a baffled tube for steady laminar and pulsatile flow', *Chemical Engineering Science*, 46(12), pp. 3139-3151.

Mackley, M.R. and Ni, X. (1993) 'Experimental fluid dispersion measurements in periodic baffled tube arrays', *Chemical Engineering Science*, 48(18), pp. 3293-3305.

References

Mackley, M.R. and Stonestreet, P. (1995) 'Heat transfer and associated energy dissipation for oscillatory flow in baffled tubes', *Chemical Engineering Science*, 50(14), pp. 2211-2224.

McMullen, J.P. and Jensen, K.F. 3 (2010) 'Integrated microreactors for reaction automation: New approaches to reaction development'. pp. 19-42. Available at: http://www.scopus.com/inward/record.url?eid=2-s2.0-77958171527&partnerID=40&md5=fa7df291a3d8cb5d95a07d91ba71f16a.

Meadows, G.W. and Darwent, B.D.B. (1952) 'The kinetics of the reactions of acetaldehyde with methanol', *Transactions of the Faraday Society*, 48, pp. 1015-1023.

Mettler, M.S., Stefanidis, G.D. and Vlachos, D.G. (2010) 'Scale-out of microreactor stacks for portable and distributed processing: Coupling of exothermic and endothermic processes for syngas production', *Industrial and Engineering Chemistry Research*, 49(21), pp. 10942-10955.

Mohd Rasdi, F.R., Phan, A.N. and Harvey, A.P. (2013) 'Rapid determination of reaction order and rate constants of an imine synthesis reaction using a mesoscale oscillatory baffled reactor', *Chemical Engineering Journal*, 222(0), pp. 282-291.

Morimoto, T., Imai, J. and Nagao, M. (1974) 'Infrared spectra of butylamine adsorbed on silica-alumina', *The Journal of Physical Chemistry*, 78(7), pp. 704-708.

Mukhopadhyay, S., Roy, S.S., Mathur, A., Tweedie, M. and McLaughlin, J.A. (2010) 'Experimental study on capillary flow through polymer microchannel bends for microfluidic applications', *Journal of Micromechanics and Microengineering*, 20(5).

Murugesan, A., Vidhyadevi, T., Kalaivani, S.S., Premkumar, M.P., Ravikumar, L. and Sivanesan, S. (2012) 'Kinetic and thermodynamic studies on the removal of Zn2+ and Ni2+ from their aqueous solution using poly(phenylthiourea)imine', *Chemical Engineering Journal*, 197(0), pp. 368-378.

Naef, O., Roch, M. and Chappuis, T. (2010) 'Reaction Screening Using a Microreactor', *CHIMIA International Journal for Chemistry*, 64(12), pp. 889-891.

Namli, H. and Turhan, O. (2006) 'Background defining during the imine formation reaction in FT-IR liquid cell', *Spectrochimica Acta Part A: Molecular and Biomolecular Spectroscopy*, 64(1), pp. 93-100.

Namli, H. and Turhan, O. (2007) 'Simultaneous observation of reagent consumption and product formation with the kinetics of benzaldehyde and aniline reaction in FTIR liquid cell', *Vibrational Spectroscopy*, 43(2), pp. 274-283.

Naqvi, A., Shahnawaaz, M., Rao, A.V., Seth, D.S. and Sharma, N.K. (2009) 'Synthesis of Schiff Bases via Environmentally Benign and Energy-Efficient Greener Methodologies', *E-Journal of Chemistry*, 6(S1), pp. S75-S78.

References

Ni, X.-W., Valentine, A., Liao, A., Sermage, S.B.C., Thomson, G.B. and Roberts, K.J. (2004) 'On the Crystal Polymorphic Forms of l-Glutamic Acid Following Temperature Programmed Crystallization in a Batch Oscillatory Baffled Crystallizer', *Crystal Growth & Design*, 4(6), pp. 1129-1135.

Ni, X., Brogan, G., Struthers, A., Bennett, D.C. and Wilson, S.F. (1998) 'A Systematic Study of the Effect of Geometrical Parameters on Mixing Time in Oscillatory Baffled Columns', *Chemical Engineering Research and Design*, 76(5), pp. 635-642.

Ni, X., Cosgrove, J.A., Cumming, R.H., Greated, C.A., Murray, K.R. and Norman, P. (2001a) 'Experimental Study of Flocculation of Bentonite and Alcaligenes Eutrophus in a Batch Oscillatory Baffled Flocculator', *Chemical Engineering Research and Design*, 79(1), pp. 33-40.

Ni, X., De Gélicourt, Y.S., Baird, M.H.I. and Rama Rao, N.V. (2001b) 'Scale-up of single phase axial dispersion coefficients in batch and continuous oscillatory baffled tubes', *Canadian Journal of Chemical Engineering*, 79(3), pp. 444-448.

Ni, X., Gao, S., Cumming, R.H. and Pritchard, D.W. (1995) 'A comparative study of mass transfer in yeast for a batch pulsed baffled bioreactor and a stirred tank fermenter', *Chemical Engineering Science*, 50(13), pp. 2127-2136.

Ni, X. and Gough, P. (1997) 'On the discussion of the dimensionless groups governing oscillatory flow in a baffled tube', *Chemical Engineering Science*, 52(18), pp. 3209-3212.

Ni, X. and Mackley, M.R. (1993) 'Chemical reaction in batch pulsatile flow and stirred tank reactors', *The Chemical Engineering Journal*, 52(3), pp. 107-114.

Ni, X., Mackley, M.R., Harvey, A.P., Stonestreet, P., Baird, M.H.I. and Rama Rao, N.V. (2003) 'Mixing Through Oscillations and Pulsations--A Guide to Achieving Process Enhancements in the Chemical and Process Industries', *Chemical Engineering Research and Design*, 81(3), pp. 373-383.

Ni, X. and Stevenson, C.C. (1999) 'On the effect of gap size between baffle outer diameter and tube inner diameter on the mixing characteristics in an oscillatory-baffled column', *Journal of Chemical Technology and Biotechnology*, 74(6), pp. 587-593.

Ni, X., Zhang, Y. and Mustafa, I. (1999) 'Correlation of polymer particle size with droplet size in suspension polymerisation of methylmethacrylate in a batch oscillatory-baffled reactor', *Chemical Engineering Science*, 54(6), pp. 841-850.

Noie, S.H. (2005) 'Heat transfer characteristics of a two-phase closed thermosyphon', *Applied Thermal Engineering*, 25(4), pp. 495-506.

Ottino, J.M. (1990) 'Mixing, chaotic advection, and turbulence', *Annual Review of Fluid Mechanics*, 22(1), pp. 207-253.

Page, M.I. (1983) *The Chemistry of enzyme action*. Elsevier Science. Available at: http://NCL.eblib.com/patron/FullRecord.aspx?p=405490.

Paquin, L., Hamelin, J. and Texier-Boullet, F. (2006) 'Efficient microwave-assisted solvent-free synthesis of N-substituted aldimines', *Synthesis*, (10), pp. 1652-1656.

Parent, Y.O., Caram, H.S. and Coughlin, R.W. (1983) 'Tube-Wall catalytic reactor cooled by an annular heat pipe ', *AIChE Journal*, 29(3), pp. 443-451.

Parton, T., Elvassore, N., Bertucco, A. and Bertoloni, G. (2007) 'High pressure CO2 inactivation of food: A multi-batch reactor system for inactivation kinetic determination', *Journal of Supercritical Fluids*, 40(3), pp. 490-496.

Phan, A.N. and Harvey, A. 'Development and evaluation of novel designs of continuous mesoscale oscillatory baffled reactors', *Chemical Engineering Journal*, 159(1-3), pp. 212-219.

Phan, A.N. and Harvey, A. (2010) 'Development and evaluation of novel designs of continuous mesoscale oscillatory baffled reactors', *Chemical Engineering Journal*, 159(1-3), pp. 212-219.

Phan, A.N., Harvey, A. and Lavender, J. (2011a) 'Characterisation of fluid mixing in novel designs of mesoscale oscillatory baffled reactors operating at low flow rates (0.3-0.6 ml/min)', *Chemical Engineering and Processing: Process Intensification*, 50(3), pp. 254-263.

Phan, A.N. and Harvey, A.P. (2011b) 'Effect of geometrical parameters on fluid mixing in novel mesoscale oscillatory helical baffled designs', *Chemical Engineering Journal*, 169(1-3), pp. 339-347.

Phan, A.N. and Harvey, A.P. (2012) 'Characterisation of mesoscale oscillatory helical baffled reactor—Experimental approach', *Chemical Engineering Journal*, 180(0), pp. 229-236.

Phan, A.N., Harvey, A.P. and Eze, V. (2012) 'Rapid Production of Biodiesel in Mesoscale Oscillatory Baffled Reactors', *Chemical Engineering and Technology*, 35(7), pp. 1214-1220.

Phan, A.N., Harvey, A.P. and Rawcliffe, M. (2011) 'Continuous screening of base-catalysed biodiesel production using New designs of mesoscale oscillatory baffled reactors', *Fuel Processing Technology*, 92(8), pp. 1560-1567.

Pierce, M.M. and Wehling, R.L. (1994) 'Comparison of sample handling and data treatment methods for determining moisture and fat in cheddar cheese by near-infrared spectroscopy', *Journal of Agricultural and Food Chemistry*, 42(12), pp. 2830-2835.

Pintar, A., Batista, J. and Levec, J. (2002) 'In situ Fourier transform infrared spectroscopy as an efficient tool for determination of reaction kinetics', *Analyst*, 127(11), pp. 1535-1540.

Raju, R., Balachandar, S., Hill, D.F. and Adrian, R.J. (2005) 'Reynolds number scaling of flow in a stirred tank with Rushton turbine. Part II - Eigen decomposition of fluctuation', *Chemical Engineering Science*, 60(12), pp. 3185-3198.

Raposo, F., Borja, R., Martín, M.A., Martín, A., de la Rubia, M.A. and Rincón, B. (2009) 'Influence of inoculum-substrate ratio on the anaerobic digestion of sunflower oil cake in batch mode: Process stability and kinetic evaluation', *Chemical Engineering Journal*, 149(1-3), pp. 70-77.

Reay, D. and Kew, P. (2006) *Heat Pipes: Theory, Design and Applications*. Fifth edn. Butterworth-Heinemann.

Reichardt, C. (2006) *Solvents and Solvent Effects in Organic Chemistry*. Wiley. Available at: http://NCL.eblib.com/patron/FullRecord.aspx?p=482243.

Reis, N., Gonçalves, C., Aguedo, M., Gomes, N., Teixeira, J. and Vicente, A. (2006a) 'Application of a Novel Oscillatory Flow Micro-bioreactor to the Production of γ-decalactone in a Two Immiscible Liquid Phase Medium', *Biotechnology Letters*, 28(7), pp. 485-490.

Reis, N., Gonçalves, C.N., Vicente, A.A. and Teixeira, J.A. (2006b) 'Proof-of-concept of a novel micro-bioreactor for fast development of industrial bioprocesses', *Biotechnology and Bioengineering*, 95(4), pp. 744-753.

Reis, N., Harvey, A.P., Mackley, M.R., Vicente, A.A. and Teixeira, J.A. (2005) 'Fluid Mechanics and Design Aspects of a Novel Oscillatory Flow Screening Mesoreactor', *Chemical Engineering Research and Design*, 83(4), pp. 357-371.

Reis, N., Mena, P.C., Vicente, A.A., Teixeira, J.A. and Rocha, F.A. (2007) 'The intensification of gas-liquid flows with a periodic, constricted oscillatory-meso tube', *Chemical Engineering Science*, 62(24), pp. 7454-7462.

Reis, N., Pereira, R.N., Vicente, A.A. and Teixeira, J.A. (2008) 'Enhanced gas-liquid mass transfer of an oscillatory constricted-tubular reactor', *Industrial and Engineering Chemistry Research*, 47(19), pp. 7190-7201.

Reis, N., Vicente, A.A. and Teixeira, J.A. (2010) 'Liquid backmixing in oscillatory flow through a periodically constricted meso-tube', *Chemical Engineering and Processing: Process Intensification*, 49(7), pp. 793-803.

Reis, N., Vicente, A.A., Teixeira, J.A. and Mackley, M.R. (2004) 'Residence times and mixing of a novel continuous oscillatory flow screening reactor', *Chemical Engineering Science*, 59(22-23), pp. 4967-4974.

Reusch, W. (1999) *Virtual Textbook of Organic Chemistry*. Available at: http://www2.chemistry.msu.edu/faculty/reusch/VirtTxtJml/intro1.htm.

Richardson, J.T., Paripatyadar, S.A. and Shen, J.C. (1988) 'Dynamics of a sodium heat pipe reforming reactor ', *AIChE Journal*, 34(5), pp. 743-752.

References

Rieppo, L., Saarakkala, S., Närhi, T., Helminen, H.J., Jurvelin, J.S. and Rieppo, J. (2012) 'Application of second derivative spectroscopy for increasing molecular specificity of fourier transform infrared spectroscopic imaging of articular cartilage', *Osteoarthritis and Cartilage*, 20(5), pp. 451-459.

Roberts, E.P.L. and Mackley, M.R. (1995) 'The simulation of stretch rates for the quantitative prediction and mapping of mixing within a channel flow', *Chemical Engineering Science*, 50(23), pp. 3727-3746.

Rotondo, E., Pietropaolo, R., Tresoldi, G., Faraone, F. and Cusmano, F. (1976) 'Mechanism of formation of Schiff base complexes. Part. I. Reaction of Ni(bis-salicylaldehyde) with primary amines', *Inorganica Chimica Acta*, 17, pp. 181-191.

Saggiomo, V. and Lüning, U. (2009) 'On the formation of imines in water-a comparison', *Tetrahedron Letters*, 50(32), pp. 4663-4665.

Santerre, G.M., Hansrote Jr, C.J. and Crowell, T.I. (1958) 'The reaction of aromatic aldehydes with n-butylamine. Acid catalysis and substituent effects', *Journal of the American Chemical Society*, 80(5), pp. 1254-1257.

Sayer, J.M., Pinsky, B., Schonbrunn, A. and Washtien, W. (1974) 'Mechanism of carbinolamine formation', *Journal of the American Chemical Society*, 96(26), pp. 7998-8009.

Seoud, A.L.A. and Abdallah, L.A.M. (2010) 'Two optimization methods to determine the rate constants of a complex chemical reaction using FORTRAN and MATLAB', *American Journal of Applied Sciences*, 7(4), pp. 509-517.

Shah, A. and Shah, A.A. (2013) 'Spectroscopic studies and keto-enol tautomeric effect of newer schiff bases of ortho-hydroxybenzaldehyde/ naphthaldehyde with 1,2-phenylenediamine and 4-aminophenyl ether', *Asian Journal of Chemistry*, 25(8), pp. 4215-4218.

Shah, S.I.A., Kostiuk, L.W. and Kresta, S.M. (2012) 'The Effects of Mixing, Reaction Rates, and Stoichiometry on Yield for Mixing Sensitive Reactions-Part I: Model Development', *International Journal of Chemical Engineering*, 2012, p. 16.

Silverstein, R.M. and Bassler, G.C. (1962) 'Spectrometric identification of organic compounds', *Journal of Chemical Education*, 39(11), pp. 546-null.

Simion, A., Simion, C., Kanda, T., Nagashima, S., Mitoma, Y., Yamada, T., Mimura, K. and Tashiro, M. (2001) 'Synthesis of imines, diimines and macrocyclic diimines as possible ligands, in aqueous solution', *Journal of the Chemical Society, Perkin Transactions 1*, (17), pp. 2071-2078.

Smith, C.J., Smith, C.D., Nikbin, N., Ley, S.V. and Baxendale, I.R. (2011) 'Flow synthesis of organic azides and the multistep synthesis of imines and amines using a new monolithic triphenylphosphine reagent', *Organic & Biomolecular Chemistry*, 9(6), pp. 1927-1937.

Smith, K.B. and Mackley, M.R. (2006) 'An Experimental Investigation into the Scale-up of Oscillatory Flow Mixing in Baffled Tubes', *Chemical Engineering Research and Design*, 84(11), pp. 1001-1011.

Snyder, D.A., Noti, C., Seeberger, P.H., Schael, F., Bieber, T., Rimmel, G. and Ehrfeld, W. (2005) 'Modular microreaction systems for homogeneously and heterogeneously catalyzed chemical synthesis', *Helvetica Chimica Acta*, 88(1), pp. 1-9.

Socrates, G. (1994) *Infrared Characteristic Group Frequencies*. John Wiley & Sons.

Solano, J.P., Herrero, R., Espín, S., Phan, A.N. and Harvey, A.P. (2012) 'Numerical study of the flow pattern and heat transfer enhancement in oscillatory baffled reactors with helical coil inserts', *Chemical Engineering Research and Design*, 90(6), pp. 732-742.

Stephens, G.G. and Mackley, M.R. (2002) 'Heat transfer performance for batch oscillatory flow mixing', *Experimental Thermal and Fluid Science*, 25(8), pp. 583-594.

Stojkovič, G. and Žnidaršič-Plazl, P. (2012) 'Continuous synthesis of l-malic acid using whole-cell microreactor', *Process Biochemistry*, 47(7), pp. 1102-1107.

Stonestreet, P. and Harvey, A.P. (2002) 'A Mixing-Based Design Methodology for Continuous Oscillatory Flow Reactors', *Chemical Engineering Research and Design*, 80(1), pp. 31-44.

Stonestreet, P. and Van Der Veeken, P.M.J. (1999) 'The Effects of Oscillatory Flow and Bulk Flow Components on Residence Time Distribution in Baffled Tube Reactors', *Chemical Engineering Research and Design*, 77(8), pp. 671-684.

Swanson, T.D. and Birur, G.C. (2003) 'NASA thermal control technologies for robotic spacecraft', *Applied Thermal Engineering*, 23(9), pp. 1055-1065.

Toledo, M. (2010) *ReactIR and iC IR Product Documentation Portfolio Manual*. Mettler Toledo.

Varma, R.S. and Dahiya, R. (1997) 'Microwave-Assisted Facile Synthesis of Imines and Enamines using Envirocat EPZGR as a Catalyst', *Synlett*, 1997(11), pp. 1245-1246.

Vasiliev, L.L. (2005) 'Heat pipes in modern heat exchangers', *Applied Thermal Engineering*, 25(1), pp. 1-19.

Vilar, G., Williams, R.A., Wang, M. and Tweedie, R.J. (2008) 'On line analysis of structure of dispersions in an oscillatory baffled reactor using electrical impedance tomography', *Chemical Engineering Journal*, 141(1-3), pp. 58-66.

Watts, P. (2010) 'Scale out of chemical synthesis in flow reactors' Chemtrix *Chemtrix* 7/10/2010. The Netherlands. Available at: http://www.chemtrix.com/downloads.

Wen, Z., Yu, X., Tu, S.-T., Yan, J. and Dahlquist, E. (2009) 'Intensification of biodiesel synthesis using zigzag micro-channel reactors', *Bioresource Technology*, 100(12), pp. 3054-3060.

Westlund, G. and Weller, D. (2011) *Aromatic Imine Compounds For Use As Sulfide Scavengers*.

Wheeler, R.C., Benali, O., Deal, M., Farrant, E., MacDonald, S.J.F. and Warrington, B.H. (2007) 'Mesoscale flow chemistry: A plug-flow approach to reaction optimisation', *Organic Process Research and Development*, 11(4), pp. 704-710.

Wiles, C. and Watts, P. (2007) 'Improving chemical synthesis using flow reactors', *Expert Opinion on Drug Discovery*, 2(11), pp. 1487-1503.

Wiles, C. and Watts, P. (2012) 'Continuous flow reactors: a perspective', *Green Chemistry*, 14(1), pp. 38-54.

Wilson, B., Sherrington, D.C. and Ni, X. (2005) 'Butylation of Phenylacetonitrile in an Oscillatory Baffled Reactor', *Industrial & Engineering Chemistry Research*, 44(23), pp. 8663-8670.

Wirth, T. (2008) *Microreactors in Organic Synthesis and Catalysis*. Wiley-VCH.

Wright, M.R. (2004) *An Introduction to Chemical Kinetics*. John Wiley & Sons.

Zhang, J.S., Lu, Y.C., Jin, Q.R., Wang, K. and Luo, G.S. (2012a) 'Determination of kinetic parameters of dehydrochlorination of dichloropropanol in a microreactor', *Chemical Engineering Journal*, 203, pp. 142-147.

Zhang, L., Geng, M., Teng, P., Zhao, D., Lu, X. and Li, J.-X. (2012b) 'Ultrasound-promoted intramolecular direct arylation in a capillary flow microreactor', *Ultrasonics Sonochemistry*, 19(2), pp. 250-256.

Zhang, Z., Szita, N., Boccazzi, P., Sinskey, A.J. and Jensen, K.F. (2006) 'A well-mixed, polymer-based microbioreactor with integrated optical measurements', *Biotechnology and Bioengineering*, 93(2), pp. 286-296.

Zheng, M. and Mackley, M. (2008) 'The axial dispersion performance of an oscillatory flow meso-reactor with relevance to continuous flow operation', *Chemical Engineering Science*, 63(7), pp. 1788-1799.

Zheng, M., Skelton, R.L. and Mackley, M.R. (2007) 'Biodiesel Reaction Screening Using Oscillatory Flow Meso Reactors', *Process Safety and Environmental Protection*, 85(5), pp. 365-371.

APPENDIX

Appendix A MATLAB® coding

```
global k1 k2 m n o

C =[];
K1 =[];
K2 =[];
M=[];
N=[];
J =[];
X=[];

for k1 =0.21;%initial value for rate constant.
    for k2 =0.001;%initial value for rate constant.
        for m =1.7;%initial value for reaction order
            for n = 0.22;%initial value for reaction order

    tspan =[0:15:300];%time range
    c0=[0.25 0.25 0 0];%initial concentration of the reaction
    [t,c] = ode45(@firstequ,tspan,c0);
    C =[C,c];
    K1 =[K1,k1];
    K2 =[K2,k2];
    M=[M,m];
    N=[N,n];
    O=[O,o];
    P=[P,p];

    end
    end
    end
    end
    end
    end

num_cols=size(C,2);
for i=1:4:num_cols; %aldehyde concentration data
j=C(:,i);
J=[J,j];
end
for w=3:4:num_cols; %imine concentration data
    x=C(:,w);
    X=[X,x];
end
```

```
function cp=firstequ(t,c)

global k1 k2 m n o


%differential equations of the propose reaction mechanism

c1=-k1*(c(1)^m)*(c(2)^n);

c2= -k1*(c(1)^m)*(c(2)^n);

c3=(k1*(c(1)^m)*(c(2)^n))-(k2*(c(3)^o));

c4=k2*(c(3)^o);

c5=k2*(c(3)^o);


cp=[c1;c2;c3;c4;c5];
```

Appendix B Amplitude and frequency command for the Eurodyne Ltd pump system

a) Frequency command

Frequency *f* (Hz)	Amplitude, x_o (mm) 0.25	0.5	1.0	1.5	2.0	3.0	4.0
0.5			140	202	266	390	520
1	161	292 /170	290	430	570	830	232
2	363	672/370	670	1000	1315	365 / 2030	467
3	642	1192/650	1300	1850	410 / 3000	563	723
4	1033	2845/1100	2800	450	565	785	1017
5	950	530/2300	325	586	738	1050	1373
6		860	450	750	950	1350	1902
7		239	870	934	1170	1820	
8	230	328	999	1121	1500		
9	242	410	747				
10	334	520	950				
11	420	671					
12	550	870					
13	700						
14	915						

Key	Syringe
	0.5ml
	1.0ml
	5.0ml
	5.0ml (alternative pump)

b) Amplitude command

Computer command (A)	Syringe volume		
amplitude (x_o)	0.5ml	1.0ml	5.0ml
0.25	A30A	A15A	A3A
0.5	A60A	A30A	A6A
1.0	A120A	A60A	A12A
1.5	A180A	A90A	A18A
2.0	A240A	A120A	A24A
3.0	A360A	A180A	A36A
4.0	A480A	A240A	A48A

Appendix C List of command for Eurodyne Ltd. Synringe pump

List of common commands used for a syringe pump in dynamic screening of imine synthesis

Function	Command
Pump initialize	/1ZR
Oscillation	/1ZS1L2Ov1000V738c2700gOA24A0GR
Batch flow	/1IV5800A3000OA0G3R
Steady state / dynamic flow	/gIV5800A3000OV370A0G2gIV5800A3000OV37A0GR
Stop	/1T
Tracer flow	/1IV5800A1500OA0G3R

Each of the letters and numbers has its own function. For example, command: [/1IV5800A3000OV370A0G2R] moves a valve of pump 1 to the input position with a maximum speed of 5800 and a piston position at 3000 (the bottom of the syringe). The outflow from the syringe was at the rate of 370 (corresponding to a flow rate of 222 mL/hr) and this process repeats 2 cycles before stopping.

The letters/numbers functions list used for Eurodyne syringe pump command.

Command List	Functions
A	Defines the piston position. It can varies from 0 to 3000
c	Defines the final speed in Hz. The value can range between 50 to 2700
G	To repeat a command sequence
g	Marks the beginning of a repetition sequence
I	It move the valve into the input position
L	Defines the speed ramp of the pump movement
O	It move the valve into the output position
R	Executes a command
S	Defines the pump speed
T	Termination of the pump command
V	Defines the maximum pump speed. It can be in the range of 5 to 5800.
v	Defines the initial speed in Hz. The value can range between 50 to 1000

Appendix

The number used in the command such as the maximum speed (V), piston position (A) and number of repeated sequence (G) can be changed to the desired value, from a flow rate and the volume of the syringe (eq.AC-1 and AC-2).

$$V = (3000 \times Q \times 10^6) \times 2 \qquad \text{eq. AC-1}$$

$$G = Q \times 10^6 \times t_s \times 60 \qquad \text{eq. AC-2}$$

…where Q (m^3/s) is the flow rate; t_s (s) is the time required to maintain the flow rate condition.

Appendix D Reaction order calculation using initial rate method

Initial reaction rate of at various molar ratios of benzaldehyde to n-butylamine

Remarks	Benzaldehyde concentration (mol dm^{-3})	N-butylamine concentration (mol dm^{-3})	Initial rate (mol dm^{-3}/ s)
A	0.25	0.25 (A)	7.00 x 10^{-3}
B	0.25	0.50 (B)	8.10 x 10^{-3}
C	0.25	1.00 (C)	9.10 x 10^{-3}
D	0.25	1.50 (D)	1.03 x 10^{-2}

Example of calculation:-

$$\frac{8.1\text{x}10^{-3}}{7.0\text{x}10^{-3}} = \frac{0.25^{m}0.50^{n}}{0.25^{m}0.25^{n}}$$

$$\mathbf{1.157 = 2.0^{n}}$$

$$\log 1.157 = n \log 2.0$$

$$n = \frac{\log 1.157}{\log 2.0}$$

$$n = 0.21$$

$$\text{Average } n = \frac{0.21 + 0.19 + 0.22 + 0.17 + 0.22 + 0.30}{6}$$

$$\text{Average } n = 0.22$$

*The 6 reaction order data were obtained through the calculation of all possible pairs of the concentration (i.e. B/A, C/A, D/A, C/B, D/B and D/C) from the initial reaction rate data.

Appendix E Graphical plots for rate constant determination

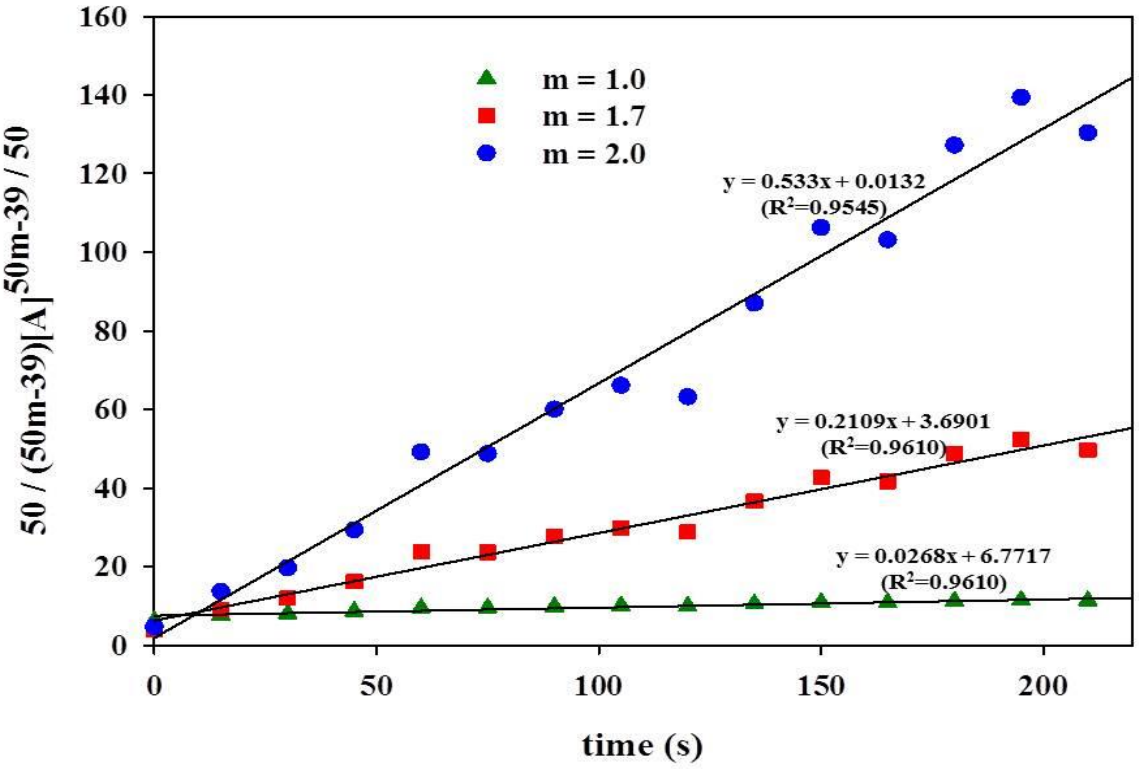

Appendix F Calibration curves for 1-butanamine, N-(phenylmethylene) from benzaldehyde and n-butylamine

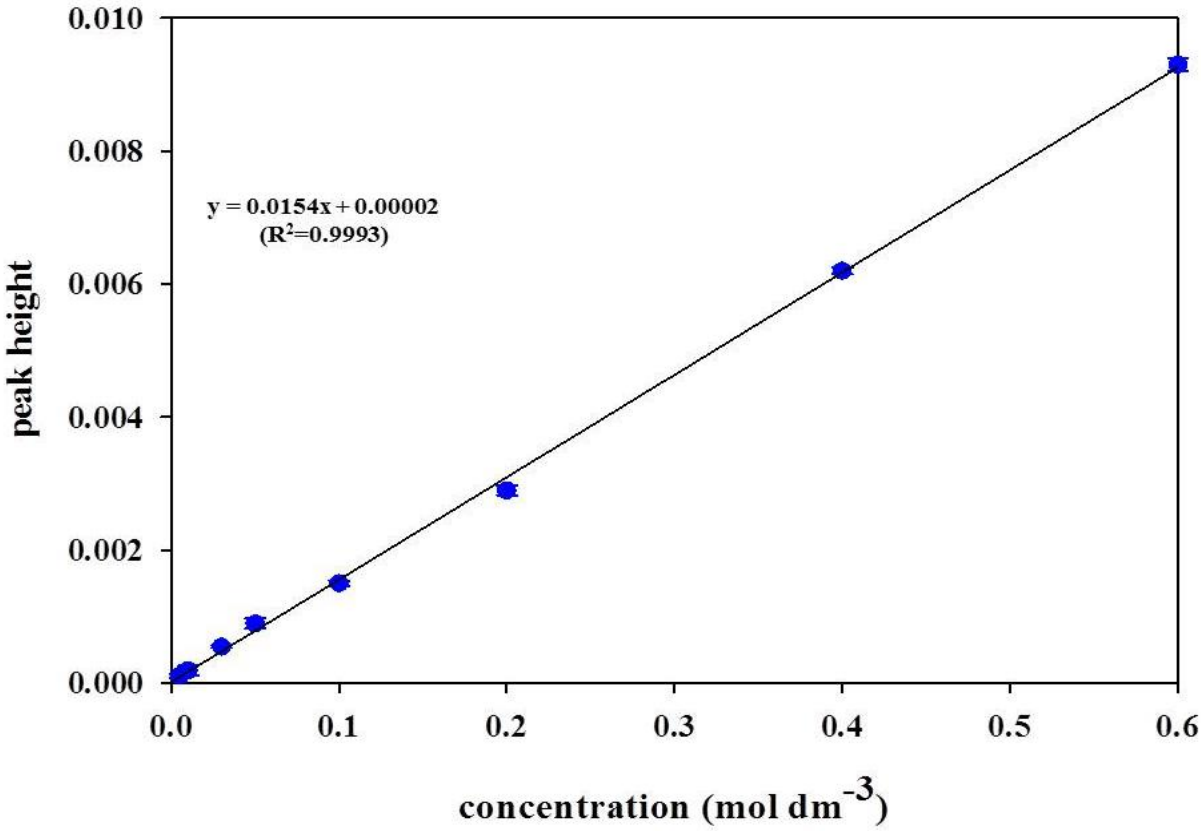

Appendix G Characterisation of a multi-tube meso-OBR

A multi-pass OBR (length of 1.4m) was characterised at low flow rates ($Re_n \leq 5.0$) to demonstrate its operational flexibility and to determine its mixing behaviour during long reactions (residence times up to hours). Three different baffled designs, namely the integral, central and helically baffled designs, were tested to determine the operating windows for high degrees of plug flow.

Effect of net flow (Re_n) for different baffle designs

The effects of Re_n on residence time distribution (E(θ)) curve for different baffled designs are shown in Figure . Re_n was varied from 1.56 to 4.39 at a fixed oscillation condition Re_o of 126 (x_o=1mm, *f*=4 Hz) for the central and integral baffled designs and at Re_o=314 (x_o=2mm, *f*=5 Hz) for the helical baffled designs. It showed that the fluid mixing behavior for these three baffled designs were similar. The E(θ) curve became narrower and less skewed when increasing net flows. For example, the variance was 0.047 at Re_n=1.56 but decreased to 0.036 at Re_n=3.11 (Table) for the integral baffled design. The narrower E(θ) curve was obtained when increasing the net flows due to reduced back mixing at high net flows. The trend of these findings was similar to those obtained in a 23mm internal diameter (id.) baffled tube and 0.7m long conventional OBR conducted by Stonestreet and Van Der Veeken (1999).

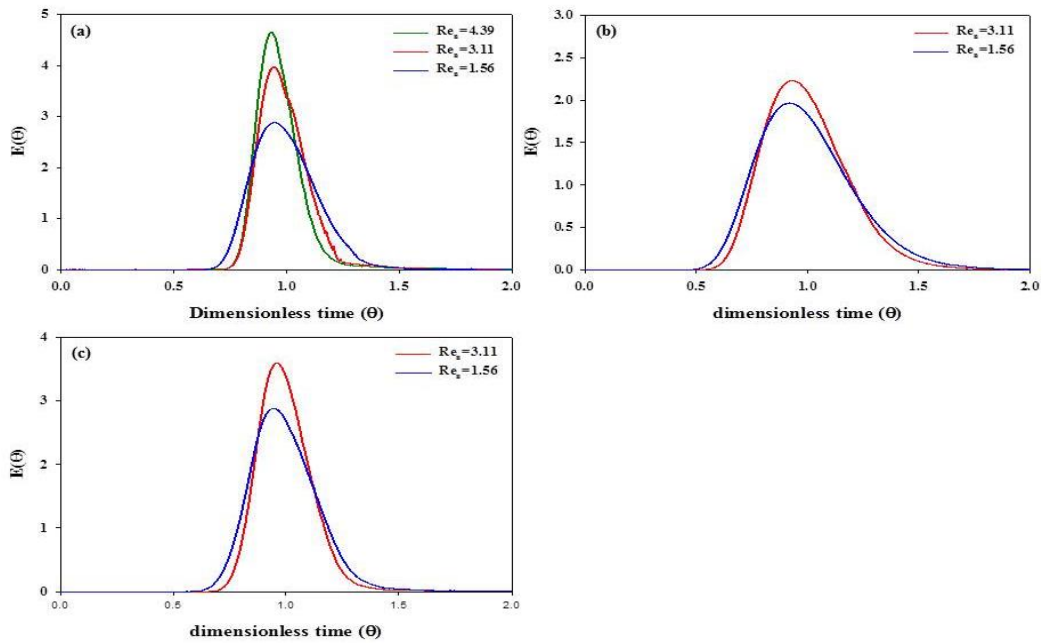

Figure AF-1: Effect of Re_n at a fixed Re_o of 126 for (a) central baffles, (b) integral baffles) and (c) helical baffles at Re_o=314.

Appendix

Table AF-1: Effect of Re_n on variance and skewness at a oscillatory condition Re_o of 126

Design	Net-flow (Re_n)	Variance	Skewness
Integral Baffle	1.56	0.047	0.003
	3.11	0.036	-0.006

Mean residence time, which is calculated using the exiting tracer concentration was higher than the hydraulic residence time (a ratio of the volume of the reactor and flow rate ($\tau = V/Q$)), for all tested designs as shown in Table . The prolonged mean residence time could be due to the formation of the vortices within the baffles cavities (Reis *et al.*, 2005) and was reported in literature (Reis *et al.*, 2004; Phan and Harvey, 2010).

Table AF-2: Mean residence time and hydraulic residence time obtained in three baffled designs over various Ren

Baffle Designs	Net flow Reynolds number (Re_n)	Oscillatory Reynolds number (Re_o)	Mean residence time (min)	Hydraulic residence time (min)
Integral (volume=22ml)	1.56	126	79	60
	3.11	126	41	30
Central (volume=24ml)	1.56	126	86	84
	3.11	126	45	42
	4.39	126	32	30
Helical (volume=24 ml)	1.56	314	68	65
	3.11	314	34	33

Effect of oscillation conditions (Re_o) on different baffle designs

a) Central baffled design

Figure shows the dependency of the number of tanks-in-series on the oscillation condition (Re_o) over a range of Re_n ($1.5 \leq Re_n \leq 4.7$). The number of tank-in-series (N) was above 10 for all tested Re_n. At Re_n=4.39, the highest N (44) was obtained at an Re_o of 190. At Re_n=2.19, N=50 was achieved at Re_o=120 and decreased to 25 at Re_o=190. This suggests that at Re_n<3, the optimum region for the Re_o is in the range Re_o=100-

130. At Re_n>4, the Re_o needed to be above 150 to obtain the highest N≈40. The trend in this study was similar to a single pass system (Phan and Harvey; Phan *et al.*, 2011a).

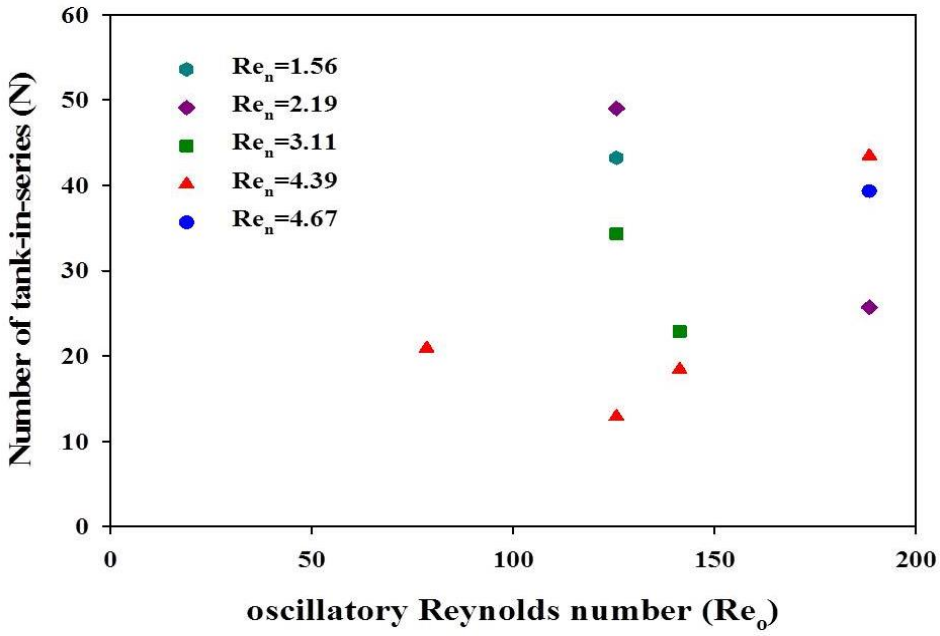

Figure AF-2: Dependence of RTD performances on oscillatory Reynolds number (Re_o) for the central baffled design

The multi-pass system had 4 times more tanks-in-series (N) (Figure (a)) than a single pass system (Figure (b)) at the same operating conditions, e.g. velocity ratio (ψ) of 40 and Re_n=4.3. This suggests that connecting more series of "CSTRs" together i.e. increasing the length of a mesoscale-OBR, increased the degree of plug flow.

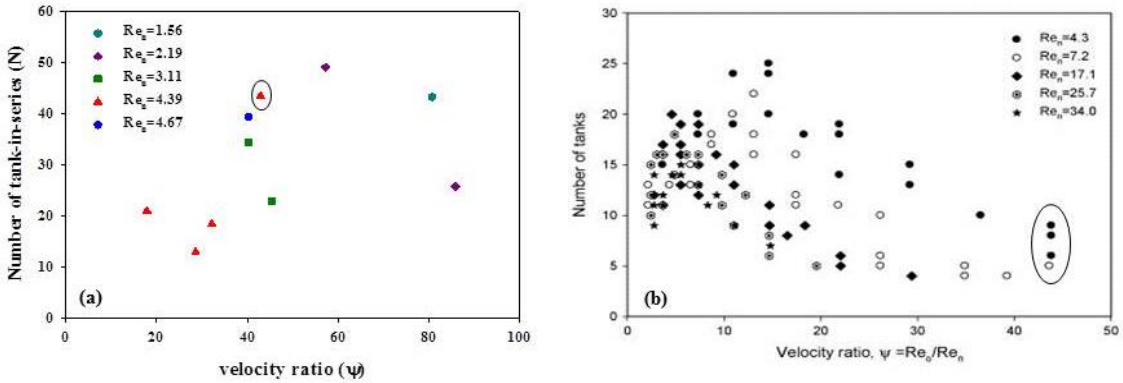

Figure AF-3: Dependence of RTD performance on velocity ratio for the central baffled design at (a) multi-tube system and (b) single tube system (Phan and Harvey, 2010)

Another advantage of increasing the length of the mesoscale system was observed at different Strouhal numbers (St) (Table).

Table AF-3: Effect of oscillation on the variance of the RTD profile for the multi-tube and single-tube configuration of central baffles design

Strouhal Number (St)	**Oscillatory Reynolds Number (Re_o)**	**Multi-tube**		**Single-tube**	
		Net flow (Re_n)	**Variance**	**Net flow (Re_n)**	**Variance**
0.2	188.4	4.39	0.05	4.30	0.14
0.4	125.6		0.08		0.08
0.8	78.5		0.02		0.08

An approximately 60% higher degree of plug flow (higher N) was obtained for the multi-pass configuration than for a single-pass in terms of variance. The limitation of applying oscillation amplitudes at St=0.2 (x_o=2.0mm) as reported with single-pass system (Phan and Harvey, 2010) was not observed in the multi-pass system. Its behavious was always close to ideal plug flow condition in the multi-system, with a variance of 0.05. Although large eddies radius were generated at these conditions (x_o=2.0mm)(Phan and Harvey, 2010), the greater length provided more space for uniform mixing to occur.

b) Integral baffled design

The trend in the number of tanks in series with various Re_o conditions with Re_n from 1.5 to 4.7 for the integral baffled design was different to that in the central baffled design. As shown in Figure , the number of tank-in-series, N, decreased with an increase in oscillation condition regardless of the net flow. For example, at Re_n=1.56, N decreased from 20 at Re_o=125 to 10 at Re_o of 180. The Strouhal number (St) also had an effect on the degree of plug flow. N decreased with decreasing St. For example, at Re_n=3.11, N was 27 for St=0.8 (x_o=0.5mm) and decreased to 15 for St=0.2 (x_o=2mm).

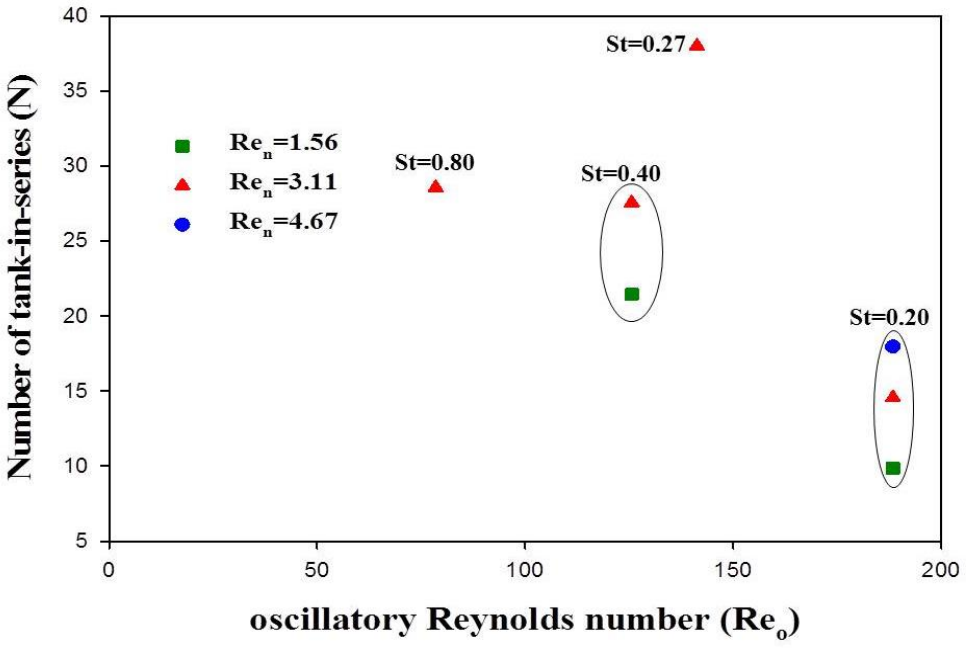

Figure AF-4: Dependence of number of tanks-in-series at various Strouhal number (St=0.2-0.8) for multi-tube integral baffled design

This trend was not observed in a single-tube system, where N remained between 5 and 10 at $1.59 \leq St \leq 0.4$ and $St \leq 0.2$ for $Re_n \leq 5$ (Figure) (Phan *et al.*, 2011a).

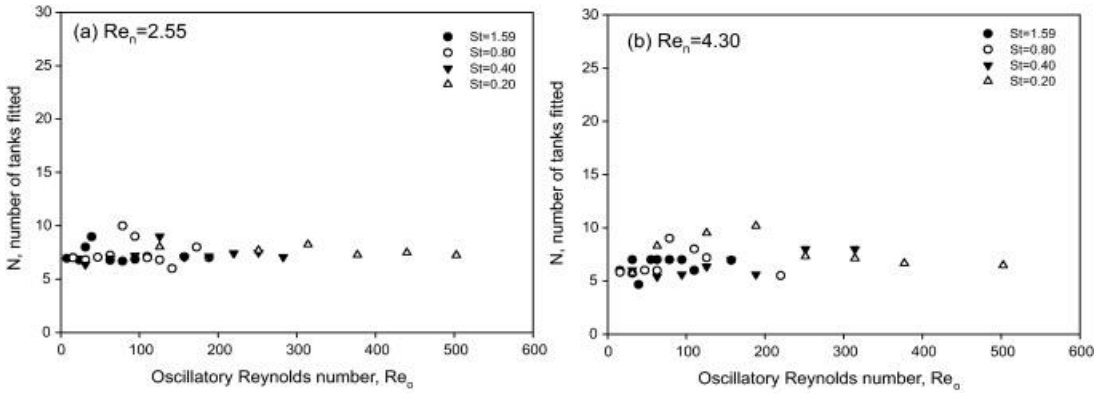

Figure AF-5: Dependence of N on oscillation conditions with (a) Re_n = 2.55 and (b) Re_n = 4.30 for single-tube pass of integral baffled design. (Phan *et al.*, 2011a)

The different trend observed between the two configurations (single and multi-tube) could be due to the length of the system. As mentioned in section a), increasing the length increased the number of baffle cavities, enhancing the degree of plug flow. This can be observed in the variance achieved in the RTDs in both systems, as shown in Table . Re_n=3.13 for the multi-tube system was the closest value to the Re_n of 2.55 used in the single-tube system, hence these two are compared. The variance obtained at similar Re_o was lower with the multi-tube compared to the single-tube; i.e. at Re_o=126, the variance obtained was 0.04 and 0.17 for the multi-tube and single-tube respectively.

The effect of different amplitudes was clearly observed in the multi-tube system (Figure (above)). A St of 0.2 (x_o=2mm) gave the lowest N (~N=15) for all tested Re_n. However the the N was still maintained above 10 at all conditions, indicating that a high degree of plug flow behaviour was achieved.

Table AF-4: Effect of oscillation on the variance of the RTD profile for the multi-tube and single-tube configuration of integral baffles design

Strouhal Number (St)	**Oscillatory Reynolds Number (Re_o)**	**Multi-tube**		**Single-tube**	
		Net-flow (Re_n)	**Variance**	**Net-flow (Re_n)**	**Variance**
0.2	188.4	3.11	0.07	2.55	0.10
0.4	125.6		0.04		0.17
0.8	78.5		0.04		0.13

c) Helical Baffled design

The mixing behaviour in the helical baffled design was substantially different to the central and integral designs, as a high degree of plug flow behaviour was achieved at oscillation amplitudes of 2-4mm for Re_n=7.2 (Phan and Harvey, 2010). Simulation work by Solano *et al.* (2012) proposed that the interaction between helical baffles and oscillation flow produced a swirling motion *and* vortex formation. Also, the helical pitch had a strong influence on the flow behaviour (Phan and Harvey, 2011b). However this study focused on one helical baffled design of pitch/tube diameter ratio of 1.5.

In this study only mixing conditions for Re_n at 1.56 and 3.11 were evaluated , corresponding to residence time of 2hrs at Re_o= 350-700 (to demonstrate that plug flow behaviour can be achieved at these low net flows). At Re_n=1.56 (Figure), the number of tanks-in-series, N, in the multi-pass system remained constant at an average of 45 regardless of the values of St and Re_o. However, at Re_n=3.11, N reached a maximum (N=60) at Re_o=300 and decreased to 30 at Re_o=650.

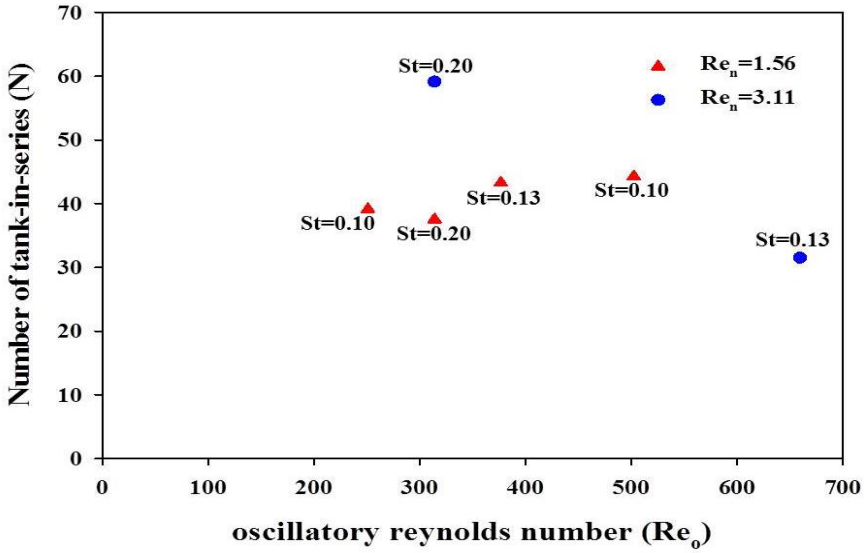

Figure AF-6: Dependence of number of tanks-in-series (N) on oscillation Reynolds number (Re_o) for the helical baffled design

Appendix H Publications

a) Mohd Rasdi, F.R., Phan, A.N. and Harvey, A.P. (2013) 'Rapid determination of reaction order and rate constants of an imine synthesis reaction using a mesoscale oscillatory baffled reactor', *Chemical Engineering Journal*, 222(0), pp. 282-291.

b) Rasdi, F.R.M., Phan, A.N. and Harvey, A.P. (2012) 'Rapid Determination of the Reaction Kinetics of an n-Butylbenzaldimine Synthesis Using a Novel Mesoscale Oscillatory Baffled Reactor', *Procedia Engineering*, 42(0), pp. 1527-1539.